

Role of Additives in Enhancing the Kinetics of Gas Hydrate Formation and Dissociation: Application in Gas Separation and Storage

Thesis Submitted to AcSIR For the Award of
the Degree of
DOCTOR OF PHILOSOPHY
In Engineering Sciences



By
Gaurav Bhattacharjee
20EE13A26053

Under the guidance of
Dr. Rajnish Kumar (Supervisor)
Dr. Sanjay P. Kamble (Co-Supervisor)

CSIR-National Chemical Laboratory, Pune (INDIA)

Abstract

Gas hydrates have come a long way from being viewed as a nuisance for the oil and gas industry to becoming one of the foremost options as a fuel of the future and an alternative route for a variety of technological options such as methane and hydrogen storage, carbon dioxide capture and separation, carbon dioxide sequestration and seawater desalination. Since gas hydrate formation, by itself, is a gradual and time consuming process, in order to make the hydrate based technologies for the above mentioned applications industrially relevant, it is required to make some modifications or tweaks to the systems which would figuratively act as catalysts for the hydrate formation process. It is the same story with regards to hydrate dissociation. The current methods of gas hydrate dissociation all pose teething problems (one of them being the slow kinetics of hydrate dissociation) which need to be overcome to ensure commercial production of natural gas from its hydrate reserves. A possible technique of enhancing the kinetics of gas hydrate formation or dissociation is to introduce certain additives to the system which may act specifically as hydrate formation promoters or hydrate dissociation promoters.

The objective of this dissertation is to study the role of additives in enhancing the kinetics of gas hydrate formation and dissociation with a special focus on applications such as gas separation and storage and this has been executed with the use of experiments at the engineering (macroscopic) level.

The effect of various additives on the kinetics of methane hydrate formation was investigated with a focus on rapid hydrate formation kinetics for methane storage in the hydrate form. This includes mixtures of surfactants capable of forming micelles at hydrate forming temperatures and bio based additives such as biosurfactants and amino acids.

The problem of foam generation usually encountered when using surfactants as kinetic hydrate promoters was tackled by mixing the commonly used anionic surfactant Sodium Dodecyl Sulfate with a silicone based surfactant that acts as antifoam. Efficient foam suppression was obtained while at the same time keeping the kinetics of methane hydrate formation intact.

Separation of gas mixtures using hydrate based gas separation was studied for a low concentration coal bed methane gas mixture containing CH_4 and N_2 and an equimolar CO_2 - CH_4 natural gas mixture representative of biogas or landfill gas. Additives capable of enhancing both the kinetics and the separation efficiency of the hydrate based gas separation process for the concerned gas mixture were identified and used.

CO_2 sequestration through hydrate formation in natural and synthetic siliceous porous media was studied for mid to long term storage of CO_2 with a focus on enhancing the kinetics of CO_2 hydrate formation.

The effect of using benign environment friendly additives in significantly low concentrations on the dissociation kinetics of natural gas hydrate was studied and a process for dissociation of natural gas hydrates was developed by combining the injection of the identified additives with depressurization and thermal stimulation, the two major conventional hydrate dissociation processes.

Certificate

This is to certify that the work incorporated in this Ph.D. thesis entitled “***Role of Additives in Enhancing the Kinetics of Gas Hydrate Formation and Dissociation: Application in Gas Separation and Storage***” submitted by ***Mr. Gaurav Bhattacharjee*** to Academy of Scientific and Innovative Research (AcSIR) in fulfillment of the requirements for the award of the Degree of ***Doctor of Philosophy in Engineering Sciences***, embodies original research work under our supervision/guidance. We further certify that this work has not been submitted to any other University or Institution in part or full for the award of any degree or diploma. Research material obtained from other sources has been duly acknowledged in the thesis. Any text, illustration, table etc., used in the thesis from other sources, have been duly cited and acknowledged.



(Student)

Mr. Gaurav Bhattacharjee
CEPD Division,
CSIR-NCL, Pune



(Supervisor)

Dr. Rajnish Kumar
Associate Professor,
Chemical Engineering
Department,
IIT Madras, Chennai



(Co-Supervisor)

Dr. Sanjay P. Kamble
Senior Scientist,
CEPD Division,
CSIR-NCL, Pune

Declaration by Research Scholar

I hereby declare that the thesis “*Role of Additives in Enhancing the Kinetics of Gas Hydrate Formation and Dissociation: Application in Gas Separation and Storage*” submitted for the degree of Doctor of Philosophy to the AcSIR has been carried out by me at the Chemical Engineering and Process Development Division, CSIR-National Chemical Laboratory, Pune – 411 008, India, under the supervision of *Dr. Rajnish Kumar and Dr. Sanjay P. Kamble*. Research material obtained from other sources has been duly acknowledged in the thesis. I declare that the present work has not been submitted to any other University for the award of any other degree or diploma.



Mr. Gaurav Bhattacharjee

Senior Research Fellow,

Chemical Engineering and Process Development Division,

CSIR-National Chemical Laboratory,

Dr. Homi Bhabha Road, Pune-411 008, Maharashtra, India

& Academy of Scientific & Innovative Research (AcSIR)-CSIR, India

Table of Contents

Cover Page	i
Abstract	iii
Certificate	v
Declaration by Research Scholar	vii
Table of Contents	ix
List of Tables	xiv
List of Figures	xvi
Acknowledgements	xxiii
Dedication	xxv

Chapter 1

1. Introduction	1
1.1. The world energy scenario	2
1.2. Fundamentals of gas hydrates	5
1.2.1. Gas hydrate structures	5
1.2.2. The gas hydrate timeline	8
1.3. Technological applications of gas hydrates and the need to enhance gas hydrate formation and dissociation kinetics	11
1.3.1. Kinetics of hydrate formation: rate limiting factors and techniques for enhancement	14
1.3.2. Surface active agents (Surfactants) and their role in gas hydrate studies	16
1.3.3. Surfactants as kinetic hydrate promoters	18
1.3.4. Amino Acids and their role in gas hydrate studies	22
1.3.4.1. L-leucine as a kinetic promoter for methane hydrate formation	22
1.3.4.2. Morphology of methane hydrate formation in presence of L-leucine	23
1.3.5. Fundamentals of hydrate dissociation and the various gas hydrate production methods	24
1.4. Research Objectives	26
1.5. Organization of the thesis	27
1.6. References	29

Chapter 2

2. Effects of Micellization on Growth Kinetics of Methane Hydrate	35
2.1. Introduction	36
2.2. Experimental Section	39
2.2.1. Materials	39

ix

2.2.2.	Procedure followed for carrying out Dynamic Light Scattering (DLS) studies	39
2.2.3.	Apparatus used and procedure followed for carrying out solubility measurements	40
2.2.4.	Apparatus used and procedure followed for hydrate formation experiments	41
2.2.5.	Procedure used for analysing the composition of the gas phase	43
2.2.6.	Calculation of the solubility of gas in aqueous solution	43
2.2.7.	Calculation of the amount of gas consumed during hydrate formation	44
2.2.8.	Calculation of the Split Fraction and Separation Factor from gas phase analysis	45
2.3.	Results and Discussions	45
2.3.1.	Determination of the presence of surfactant micelles at hydrate forming temperature using dynamic light scattering experiments (DLS)	45
2.3.2.	Enhancement in solubility of methane in micellar solutions of surfactants	48
2.3.3.	Hydrate formation kinetics in presence of surfactants	50
2.3.3.1.	Hydrate formation in stirred tank reactor	53
2.3.3.2.	Hydrate formation in fixed bed reactor using Stainless Steel Packing and low concentration CBM gas in presence of surfactants	56
2.3.4.	Gas phase analysis: split fraction of CH ₄ in hydrate gas and separation factor	59
2.4.	Conclusions	60
2.5.	References	61

Chapter 3

3.	Kinetic promotion of methane hydrate formation by combining anionic and silicone surfactants: scalability promise of methane storage due to prevention of foam formation	66
3.1.	Introduction	67
3.2.	Experimental Section	69
3.2.1.	Materials	69
3.2.2.	Procedure followed for making the SDS-Silicone complex	69
3.2.3.	Apparatus and procedure for hydrate formation experiment	70
3.2.4.	Apparatus and procedure for morphology study	71
3.2.5.	Calculation of the amount of gas consumed during the Hydrate Formation Experiments	73
3.2.6.	Calculation of the rate of hydrate formation	73
3.3.	Results and Discussions	73
3.3.1.	Methane hydrate formation in the presence of Antifoam-A: promotion in hydrate formation kinetics and reduction in induction time	75

3.3.2.	Suppression in foam formation in the presence of Antifoam-A	81
3.3.3.	Morphology of methane hydrate formation and dissociation in presence of Antifoam-A	82
3.4.	Conclusions	85
3.5.	References	87

Chapter 4

4.	Bio based additives as kinetic promoters for methane hydrate formation	90
4.1.	Introduction	91
4.2.	The biosurfactant Surfactin as a kinetic promoter for methane hydrate formation	92
4.2.1.	Introduction	92
4.2.2.	Experimental Section	93
4.2.2.1.	Materials	93
4.2.2.2.	Procedure followed for the production of Surfactin	93
4.2.2.3.	Procedure followed for hydrate formation experiments	93
4.2.3.	Results and Discussions	94
4.2.3.1.	Screening for the presence of Surfactin	94
4.2.3.2.	Effect of Surfactin on Methane Hydrate formation kinetics	95
4.2.4.	Conclusions	97
4.3.	Effect of the amino acid L-histidine on methane hydrate growth kinetics	98
4.3.1.	Introduction	98
4.3.2.	Experimental Section	101
4.3.2.1.	Materials	101
4.3.2.2.	Apparatus and procedure for hydrate formation experiments	102
4.3.2.3.	Calculation of the amount of gas consumed during the hydrate formation experiments	103
4.3.2.4.	Calculation of the rate of hydrate formation	103
4.3.3.	Results and Discussions	104
4.3.3.1.	Methane Hydrate formation kinetics in presence of L-Histidine	104
4.3.3.2.	Rate of hydrate formation	108
4.3.3.3.	Final gas consumption in presence of L-histidine and comparison with SDS	110
4.3.3.4.	Ease of handling L-histidine as compared to SDS with regards to foam generation	111
4.3.4.	Conclusions	112
4.4.	Comparison between the different synthetic and bio based additives used as kinetic hydrate promoters for methane hydrate formation	114
4.5	References	118

Chapter 5

5.	CH₄-CO₂ gas separation using clathrate hydrate formation in presence of selective hydrate promoters	124
5.1.	Introduction	125
5.2.	Experimental Section	128
5.2.1.	Materials	128
5.2.2.	Apparatus used and procedure followed for hydrate formation	129
5.2.3.	Procedure used for analysing the composition of the gas phase	131
5.2.4.	Calculation of the amount of gas consumed during hydrate formation	131
5.2.5.	Calculation of the rate of hydrate formation	131
5.2.6.	Calculation of the split fraction and separation factor from gas phase analysis	132
5.3.	Results and Discussions	133
5.3.1.	Hydrate formation in fixed bed reactor using Brass packing and in the presence of various additives	133
5.3.2.	Induction time for hydrate formation from a 50% CO ₂ -50% CH ₄ gas mixture in the presence of additives	139
5.3.3.	Gas separation analysis	140
5.4.	Conclusions	142
5.5.	References	145

Chapter 6

6.	Carbon Dioxide Sequestration in simulated sub sea sediment	149
6.1.	Introduction	150
6.2.	Experimental Section	152
6.2.1.	Materials	152
6.2.2.	Calculation of the water retention capacities of the different materials studied	153
6.2.3.	Apparatus and procedure for hydrate formation experiments	154
6.2.4.	Calculation of the amount of gas consumed during the hydrate formation experiments	155
6.2.5.	Calculation of the water to hydrate conversion	156
6.2.6.	Calculation of the CO ₂ to hydrate conversion	156
6.2.7.	Calculation of the hydrate saturation	156
6.2.8.	Calculation of the rate of hydrate formation	157
6.3.	Results and Discussions	157
6.3.1.	Gas hydrate formation in various porous media with constant volume of	162

6.3.2.	Effect of particle size and water saturation on gas hydrate formation kinetics	165
6.3.3.	Effect of bed height on gas hydrate formation kinetics	169
6.3.4.	Hydrate Saturation	171
6.4.	Conclusions	172
6.5.	References	173

Chapter 7

7.	Enhancement of hydrate dissociation kinetics using benign additives in low concentrations	178
7.1.	Introduction	179
7.1.1.	Hydrate dissociation by depressurization	179
7.1.2.	Hydrate dissociation by thermal stimulation	181
7.1.3.	Hydrate dissociation by inhibitor injection method	182
7.2.	Methane recovery using benign additives	183
7.2.1.	Identification of benign additives	183
7.2.1.1.	Preliminary identification of additives	183
7.2.1.2.	Brief individual description of the different additives studied	185
7.3.	Enhanced hydrate dissociation kinetics in presence of low concentrations of benign additives	188
7.3.1.	Experimental Setups	188
7.3.2.	Testing of additives in the dedicated reactor setup for additive selection	191
7.3.3.	Injection of additives to enhance hydrate dissociation kinetics: Continuous flow loop circulating apparatus	195
7.3.4.	Energy and Efficiency Analysis in the presence of low concentrations of additives (injection)	200
7.4.	Conclusions	203
7.5	References	204

Chapter 8

8.	Summary of Conclusions, Contribution to Knowledge and Recommendations for Future Work	206
8.1.	Summary of Conclusions	207
8.2.	Contribution to Knowledge	210
8.3.	Recommendations for Future Work	211
9.	Appendix A	213
10.	Appendix B	223
11.	Appendix C	228
12.	Cirriculum Vitae	232

List of Tables

1.1.	Size ratio for CH ₄ , CO ₂ and N ₂ .	7
2.1.	Solubility (Henry's Constant) of methane in pure water and in the different surfactant solutions used in the present study.	50
2.2.	Summary of all the experiments conducted with pure methane gas. Relevant data such as the sample state, initial hydrate formation pressure, run time of each experiment, amount of gas consumed at the end of each experiment (mol of gas consumed/ mol of water) and the induction time for hydrate formation in each experiment have been reported. The hydrate formation temperature was kept constant (275.15K) for all the systems.	51
2.3.	Summary of all the experiments conducted with the CBM gas mixture. Relevant data such as the sample state, initial hydrate formation pressure, run time of each experiment, amount of gas consumed at the end of each experiment (mol of gas consumed/ mol of water) and the induction time for hydrate formation in each experiment have been reported. The hydrate formation temperature was kept constant (275.15K) for all the systems if not otherwise denoted by *.	52
2.4.	Split Fraction (%) of CH ₄ in hydrate phase and Separation Factor obtained via gas phase analysis.	60
3.1.	Summary of all the experiments conducted in the course of this study. Relevant data such as the sample state, initial hydrate formation pressure, run time of each experiment, amount of gas consumed at the end of each experiment (mol of gas consumed/ mol of water) and the induction time for hydrate formation in each experiment have been reported.	74
4.1.	Summary of all the experiments conducted. Gas consumption is reported for a set time of 3 hours after nucleation. A fixed volume of water (140 ml) was used for all the experiments.	105
5.1.	Summary of all the experiments conducted in this study-50% CO ₂ -50 % CH ₄ gas mixture was used for all the experiments. Relevant data such as the sample state, initial hydrate formation pressure, run time of each experiment, amount of gas consumed at the end of each experiment (mol of gas consumed/ mol of water), water to hydrate conversion (mol %) at the end of each experiment and the induction time (h) for hydrate formation in each experiment have been reported. The hydrate formation temperature was kept constant (274 K) for all the systems.	136
5.2.	Mole fractions of CO ₂ and CH ₄ in hydrate phase, Split Fraction (%) of CO ₂ and CH ₄ in hydrate phase and CO ₂ and CH ₄ Separation Factors obtained via gas phase analysis.	142
6.1.	Volume of water required to completely fill the void spaces between the particles of the different size fractions of porous media used.	153
6.2.	Summary of all experiments conducted with constant volume of water (24 ml).	158
6.3.	Summary of all experiments conducted with constant bed height (3 cm).	160
6.4.	Pumice: Effect of bed height: Summary of all experiments conducted.	161

6.5.	Average hydrate saturation for different systems studied (Pumice and FHRC).	171
7.1.	List of the additives identified for use as hydrate dissociation promoters in the present study.	185
7.2.	Energy and efficiency analysis for the various systems studied (injection of additives)	202
A1.	Initial apparent rates of hydrate formation (mol of gas consumed/h) for the different systems considered during the course of the work reported in Chapter 2 of the thesis.	214
A2.	Initial apparent rates of hydrate formation (mol of gas consumed/h) for the different systems considered during the course of the work reported in Chapter 3 of the thesis.	215
A3.	Initial apparent rates of hydrate formation (mol of gas consumed/h) for the different systems considered during the course of the first study reported in Chapter 4 of the thesis.	216
A4.	Initial apparent rates of hydrate formation (mol of gas consumed/h) for the different systems considered during the course of the second study reported in Chapter 4 of the thesis.	217
A5..	Initial apparent rates of hydrate formation (mol of gas consumed/h) for the different systems considered during the course of the work reported in Chapter 5 of the thesis.	219
A6.	Initial apparent rates of hydrate formation (mol of gas consumed/h) for the different systems considered during the course of the work reported in Chapter 6 of the thesis.	222
B1.	Comparison of the separation efficiencies of the HBGS process and other conventional gas separation processes for the separation of a CO ₂ -CH ₄ gas mixture. The determining factor here is the CO ₂ /CH ₄ selectivity or CO ₂ partition coefficient as given by equation C1. Additionally, for the sake of comparison, the separation efficiency of the HBGS process for other gas mixtures has also been given using some representative studies.	225

List of Figures

1.1.	World energy balance.	3
1.2.	The different structures of gas hydrates	7
1.3.	The various applications of gas hydrates.	14
1.4.	A typical gas uptake curve along with temperature profile during hydrate formation showing the gas dissolution, nucleation and hydrate growth phases.	15
1.5.	Different classes of surfactants and their corresponding structures.	17
1.6.	Morphology of methane hydrate formation in the presence of Leucine.	24
1.7.	Principles of gas hydrate dissociation.	25
1.8.	Mechanism of the simultaneous recovery of methane along with sequestration of CO ₂ .	26
2.1.	Schematic of the solubility setup.	40
2.2.	Detailed schematic of the stirred tank reactor setup for hydrate formation	42
2.3.	Detailed schematic of the fixed bed reactor setup for hydrate formation	43
2.4. (a)	Micelle formation in mixed SDS-CAPB surfactant system at 298 K.	46
and (b)	Micelle formation occurs even for pure SDS solution at 298 K. The size of the micelles increases with increase in concentration of CAPB.	
2.5. (a)	Micelle formation in mixed SDS-CAPB surfactant system at 275 K. No micelle formation for pure SDS solution. Micelles begin to form when SDS and CAPB are mixed in volumetric ratio 7:3. The size of the micelles increases with increase in concentration of CAPB.	47
and (b)		
2.6.	Solubility of methane in distilled water at 33 °C using the current method and comparison with literature data	49
2.7.	Comparison of solubility of methane in different micellar solutions of surfactants and in pure water at 33 °C.	49
2.8.	Comparison of the gas uptake obtained for pure methane gas with different surfactant solutions and pure water. Gas uptake has been shown for one hour from the start of hydrate formation. STR configuration was used.	54
2.9.	Comparison of the gas uptake obtained for CBM gas mixture with different surfactant solutions in conjunction with THF and with pure water (without the presence of any additives in the system. Gas uptake has been shown for thirty minutes from the start of hydrate formation. STR configuration was used.	56
2.10.	Comparison of the gas uptake obtained for CBM gas mixture with different surfactant solutions in conjunction with THF and with only THF. Gas uptake has been shown for a fixed time of thirty minutes from the start of hydrate formation. FBR configuration was used. No nucleation of hydrates could be observed with pure water and CBM gas, i.e. without the presence of any additives.	58
2.11.	Comparison of final gas uptake (mol of gas consumed/ mol of water)	58

obtained in present study with data already reported in literature for different CBM gas mixtures. Only the maximum values obtained in each of these studies have been compared.

3.1.	Detailed schematic of the stirred tank reactor setup for hydrate formation	71
3.2.	Detailed schematic of the reactor setup for morphology study of hydrate formation and dissociation.	72
3.3.	Comparison of the gas uptake for the different systems studied (fresh runs) with average and standard deviation.	76
3.4.	Average rate of gas uptake for the different systems studied (fresh runs) with standard deviation.	77
3.5.	Comparison of the gas uptake for the different systems studied (memory runs) with average and standard deviation. Memory runs could not be performed with the pure SDS system due to excessive foam generation.	78
3.6.	Average rate of gas uptake for the different systems studied (memory runs) with standard deviation.	79
3.7.	Comparison of the average induction times for the different systems studied (fresh runs) with standard deviation.	80
3.8.	Comparison of the average induction times for the different systems studied (memory runs) with standard deviation.	81
3.9.	Foam Suppression in presence of Silicone based surfactant.	82
3.10.	Morphology of formation of methane hydrate for the different systems studied.	84
3.11.	Morphology of dissociation of methane hydrate for the different systems studied.	84
4.1.	Comparison of average gas uptake during methane hydrate formation from different hydrate forming solutions: pure water, nutrient broth and cell free Surfactin containing supernatant.	95
4.2.	Comparison of average gas uptake during methane hydrate formation individually with pure water, NaCl, Beef Extract and Peptone (the different components present in the Nutrient Broth).	96
4.3.	Comparison of average gas uptake during methane hydrate formation with cell free supernatant containing the biosurfactant Surfactin and with 1 wt% SDS.	97
4.4.	Schematic of the structure of L-histidine.	101
4.5.	Detailed schematic of the experimental setup.	103
4.6.	Comparison of the gas uptake for the different systems studied (fresh runs) with average and standard deviation.	106
4.7.	Average induction times for the different systems studied (fresh and memory runs) with standard deviation.	107
4.8.	Hydrate growth (milimoles of gas consumed per mole of water) for the individual fresh runs of all three systems studied.	107
4.9.	Hydrate growth (milimoles of gas consumed per mole of water) for the individual memory runs of all three systems studied.	108

4.10.	Average rate of gas uptake for the different systems studied (fresh runs) with standard deviation.	109
4.11.	Linear fit of the first 20 minutes (0.334h) of hydrate growth for the different systems studied: Average of fresh runs.	110
4.12.	Average final gas consumption (milimoles of gas consumed/ mol of water) after 5 hours for the different systems studied (fresh runs) with standard deviation. Similar final gas consumption can be observed for both L-histidine (1 wt %) and SDS (1 wt %) systems.	111
4.13.	Ease of handling of l-histidine as compared to SDS: Vial A (1 wt % SDS) shows the generation of a large amount of foam whereas no foam generation can be seen in Vial B (1 wt % L-histidine).	112
5.1.	Chemical structures of (a) Propylene Carbonate (PC), (b) Sulfolane and (c) Tryptophan.	129
5.2.	Detailed schematic of the fixed bed reactor setup for hydrate formation.	130
5.3.	Comparison of the average gas uptake (moles of gas consumed/ mole of water) for the different systems studied (fresh runs).	137
5.4.	Comparison of the average water to hydrate conversion (mole %) for the different systems studied (fresh runs).	137
5.5.	Comparison of the average final gas consumption (moles of gas consumed/ mol of water) after 10 hours of hydrate formation for the different systems studied (fresh runs).	138
5.6.	Comparison of the average rates of gas uptake (moles of gas consumed/ mole of water/ hour) for the different systems studied (fresh runs).	138
5.7.	Comparison of the average induction times for the different systems studied (fresh runs). The induction times for the PC and Sulfolane systems could not be plotted here as no discernible nucleation point could be identified for these systems owing to the exceedingly slow hydrate formation kinetics.	140
6.1.	Schematic of the experimental apparatus.	155
6.2.	Comparison of the gas uptake and water to hydrate conversion in presence of the different porous media used for the case of the constant volume of water experiments: Sand: Average and standard deviation of experiment numbers 1, 3 and 5, Quartz: Average and standard deviation of experiment numbers 8 and 11, Pumice: Average and standard deviation of experiment numbers 20, 23 and 25 and FHRC: Average and standard deviation of experiment numbers 32, 35 and 37.	163
6.3.	Comparison of the gas uptake and water to hydrate conversion in presence of the different porous media used for the case of the constant bed height experiments: Sand: Average and standard deviation of experiment numbers 1, 3 and 5, Quartz: Average and standard deviation of experiment numbers 38 ad 41, Pumice: Average and standard deviation of experiment numbers 44, 47 and 50 and FHRC: Average and standard deviation of experiment numbers 51, 53 and 55.	163

- 6.4.** Comparison of the rates of gas uptake and water to hydrate conversion in presence of the different porous media used for the case of the constant volume of water experiments: Sand: Average and standard deviation of experiment numbers 1, 3 and 5, Quartz: Average and standard deviation of experiment numbers 8 and 11, Pumice: Average and standard deviation of experiment numbers 20, 23 and 25 and FHRC: Average and standard deviation of experiment numbers 32, 35 and 37. 164
- 6.5.** Comparison of the rates of gas uptake and water to hydrate conversion in presence of the different porous media used for the case of the constant bed height experiments: Sand: Average and standard deviation of experiment numbers 1, 3 and 5, Quartz: Average and standard deviation of experiment numbers 38 ad 41, Pumice: Average and standard deviation of experiment numbers 44, 47 and 50 and FHRC: Average and standard deviation of experiment numbers 51, 53 and 55. 164
- 6.6.** Effect of particle size of Pumice on hydrate formation kinetics. Pumice: > 420 micron: Experiment number 14, Pumice: 210-420 micron: Experiment number 17, Pumice: < 210 micron: Average of experiment numbers 20, 23 and 25. 166
- 6.7.** Effect of particle size of FHRC on hydrate formation kinetics. FHRC: > 420 micron: Experiment number 26, FHRC: 210-420 micron: Experiment number 29, FHRC: < 210 micron: Average of experiment numbers 32, 35 and 37. 166
- 6.8.** Mechanism of hydrate formation in systems having different particle size fractions (a) Large particle size fraction: no interaction between the hydrates and the surface of the particles. (b) Small particle size fraction: hydrates form in large masses almost completely enveloping the particles themselves. (Maroon: Sediment particles/grains, Blue:Water, White:Hydrates) 167
- 6.9.** Comparison of the rates of gas uptake for the different particle size fractions of pumice: Pumice: > 420 micron: Experiment number 14, Pumice: 210-420 micron: Experiment number 17, Pumice: < 210 micron: Average of experiment numbers 20, 23 and 25. 168
- 6.10.** Comparison of the rates of gas uptake for the different particle size fractions of FHRC: FHRC: > 420 micron: Experiment number 26, FHRC: 210-420 micron: Experiment number 29, FHRC: < 210 micron: Average of experiment numbers 32, 35 and 37. 168
- 6.11.** Effect of bed height on hydrate formation kinetics using Pumice as the porous medium: Pumice: 2.7 cm bed: Average and standard deviation of experiment numbers 20, 23 and 25 and Pumice: 5.5 cm bed: Average and standard deviation of experiment numbers 57, 60 and 62. 170
Inset: The different bed heights considered for the study and the corresponding change in volume of the gaseous phase; (a) Bed height: 2.7 cm and (b) Bed height: 5.5 cm.

6.12.	Comparison of rates of gas uptake for the two bed heights considered for pumice: Pumice: 2.7 cm bed: Average and standard deviation of experiment numbers 20, 23 and 25 and Pumice: 5.5 cm bed: Average and standard deviation of experiment numbers 57, 60 and 62.	170
7.1.	Concept of pressure reduction and methane hydrate dissociation induced by depressurisation method.	180
7.2.	Temperature reduction due to of methane hydrate dissociation by the depressurisation method.	180
7.3.	Overview of variety of thermal methods.	181
7.4.	Stirred tank reactor setup with optical window for additive selection.	189
7.5.	Schematic of the bench scale methane recovery setup.	190
7.6.	High pressure continuous setup for studying methane hydrate decomposition kinetics in sub-sea environments.	191
7.7.	Normalised moles of gas released vs. Time (h) for all the additives studied: Dissociation at 293 K. Fresh runs. Concentration of all the additives: 1 wt %.	192
7.8.	Dissociation of methane hydrates in presence of different additives at 293 K: % Methane recovery after 18 minutes.	193
7.9.	Normalised moles of gas released vs. Time (h) for all the additives studied: Dissociation at 283 K. Fresh runs. Concentration of all the additives: 1 wt %.	194
7.10.	Dissociation of methane hydrates in presence of different additives at 283 K: % Methane recovery after 18 minutes.	194
7.11.	Normalised moles of gas released vs. Time (h) for all the additives studied: Dissociation at 293 K. Memory runs. Concentration of all the additives: 1 wt%.	195
7.12.	Hydrate bearing sediment before formation and after dissociation of methane hydrates: (a) Hydrate formation sediment prior to the start of the experiment. (b) Hydrate bearing sediment after water flooding. (c) Presence of gas bubbles indicating release of gas as a result of dissociation of gas hydrates.	196
7.13.	% Methane recovery vs time (min) for hydrate dissociation effected by the injection of benign additive-water mixtures into the large scale continuous apparatus (0.1 wt % and 10 ml/ min).	198
7.14.	% Methane recovery vs time (min) for hydrate dissociation effected by the injection of benign additive-water mixtures into the large scale continuous apparatus (0.1 wt % and 30 ml/ min).	199
7.15.	% Methane recovery vs time (min) for hydrate dissociation effected by the injection of benign additive-water mixtures into the large scale continuous apparatus (1 wt % and 30 ml/ min).	200
A1.	Linear fit of the first 20 minutes (0.334h) of hydrate growth for pure methane gas with different surfactant solutions and pure water. STR	213

	configuration was used.	
A2.	Linear fit of the first 20 minutes (0.334h) of hydrate growth for CBM gas mixture with different surfactant solutions in conjunction with THF and with pure water (without the presence of any additives in the system. STR Configuration was used.	213
A3.	Linear fit of the first 20 minutes (0.334h) of hydrate growth for CBM gas mixture with different surfactant solutions in conjunction with THF and with only THF. FBR Configuration was used.	214
A4.	Linear fit of the first 20 minutes (0.334h) of hydrate growth (both fresh and memory runs) for pure methane gas with different surfactant/surfactant-antifoam solutions and pure water.	215
A5.	Linear fit of the first 20 minutes (0.334h) of hydrate growth for pure methane gas with different surfactant solutions (Bio-Surfactant/ Synthetic Surfactant) and pure water.	216
A6.	Linear fit of the first 20 minutes (0.334h) of hydrate growth (both fresh and memory runs) for pure methane with the various amino acid/ surfactant systems studied.	217
A7.	Linear fit of the first 10 minutes (0.167h) of hydrate formation for an equimolar CO ₂ -CH ₄ gas mixture in presence of the different selective hydrate promoters and varying hydrate formation pressures.	218
A8.	Linear fit of the first 20 minutes (0.334h) of hydrate formation for an equimolar CO ₂ -CH ₄ gas mixture in presence of the different selective hydrate promoters and varying hydrate formation pressures.	218
A9.	Linear fit of the first 20 minutes (0.334h) of hydrate formation for pure CO ₂ gas in presence of the different porous media used for the case of the constant volume of water experiments.	220
A10.	Linear fit of the first 20 minutes (0.334h) of hydrate formation for pure CO ₂ gas in presence of the different porous media used for the case of the constant bed height experiments.	220
A11.	Linear fit of the first 20 minutes (0.334h) of hydrate formation for pure CO ₂ gas using different particle size fractions of pumice as the porous medium.	221
A12.	Linear fit of the first 20 minutes (0.334h) of hydrate formation for pure CO ₂ gas using different particle size fractions of FHRC as the porous medium.	221
A13.	Linear fit of the first 20 minutes (0.334h) of hydrate formation for pure CO ₂ gas using pumice (particle size < 210 micron) as the porous medium and varying the bed height.	222
C1.	Comparison of the gas uptake and water to hydrate conversion in presence of the different porous media used for the case of the constant volume of water experiments. Sand: Experiment number 3, Quartz: Experiment number 9, Pumice: Experiment number 23 and FHRC: Experiment number 37. Gas uptake has been shown for the entire duration of the	228

	experiments.	
C2.	Comparison of the average induction times along with standard deviation for the different porous media used.	229
C3.	Comparison of the gas uptake and water to hydrate conversion in presence of the different porous media used for the case of the constant volume of water experiments: Sand: Average and standard deviation of experiment numbers 2, 4, 6 and 7, Quartz: Average and standard deviation of experiment numbers 9, 10, 12 and 13, Pumice: Average and standard deviation of experiment numbers 21, 22 and 24 and FHRC: Average and standard deviation of experiment numbers 33, 34 and 36.	229
C4.	Comparison of the gas uptake and water to hydrate conversion in presence of the different porous media used for the case of the constant bed height experiments: Sand: Average and standard deviation of experiment numbers 2, 4, 6 and 7, Quartz: Average and standard deviation of experiment numbers 39, 40, 42 and 43, Pumice: Average and standard deviation of experiment numbers 45, 46, 48 and 49 and FHRC: Average and standard deviation of experiment numbers 52, 54 and 56.	230
C5.	Effect of particle size of pumice on hydrate formation kinetics: Pumice: > 420 micron: Average of experiment numbers 15 and 16, Pumice: 210-420 micron: Average of experiment numbers 18 and 19, Pumice: < 210 micron: Average of experiment numbers 21, 22 and 24.	230
C6.	Effect of particle size of FHRC on hydrate formation kinetics: FHRC: > 420 micron: Average of experiment numbers 27 and 28, FHRC: 210-420 micron: Average of experiment numbers 30 and 31, FHRC: < 210 micron: Average of experiment numbers 33, 34 and 36.	231
C7.	Effect of bed height on gas hydrate formation kinetics using pumice as the fixed bed medium: Pumice: 2.7 cm bed: Average and standard deviation of experiment numbers 21, 22 and 24 and Pumice: 5.5 cm bed: Average and standard deviation of experiment numbers 58, 59 and 61.	231

Acknowledgements

It gives me the deepest of pleasures to extend my warm and humble appreciation to all those who helped and supported me in the testing time that is one's PhD tenure. Let it be known that the efforts of these individuals are no less than my own in the successful completion of this thesis.

First and foremost, I would like to take this opportunity to express my deepest sense of appreciation and reverence towards my research supervisor **Dr. Rajnish Kumar** for effortlessly guiding me throughout the course of this work. His experience and expertise helped me stand in this field. I would also like to express my sincerest gratitude to my co-research supervisor **Dr. Sanjay Kamble** for always motivating me, for the stimulating scientific discussions and for constantly keeping me on my toes to ensure that I see it through seamlessly.

I am grateful to **Dr. Sourav Pal** and **Dr. Ashwini Kumar Nangia**, Directors, CSIR-NCL, Pune for allowing me to carry out my research work in India's most prestigious, well-equipped and biggest chemical laboratory. I would like to acknowledge the members of my Doctoral Advisory Committee (DAC), **Dr. Vinay Bhandari**, **Dr. V Ravi Kumar** and **Dr. Shashank Gaikwad** for their sincere comments, suggestions and constant support.

To my parents, **Dr. Santanu Bhattacharjee** and **Sumita Bhattacharjee**, thank you for your support and encouragement throughout the years, and for providing the basic foundations which have enabled my success. They say genes maketh the man! Perhaps doing this PhD was just one of the things to be ticked off the list for me. I am truly indebted. I find this an exceptional opportunity to acknowledge my brother **Saurav Bhattacharjee** for always being my biggest supporter and competitor. We bring out the best in each other. You know it, bro!

I am indebted to many present and past colleagues at NCL: Asheesh, Omkar, Tushar, Nilesh, Vivek, Muzammil, Anuj, Saeed, Aneesh, Abhijeet, Vyom, Rajesh, Darshan, Rajat, Amruta and Ajay for providing a stimulating and fun environment in which to learn and grow. I am grateful to my dear friends Sayan, Chinmay, Akshay, Sayantan, Gunwant and Deepanjan for their constant encouragement and for always being there with me in my difficult times.

I would like to acknowledge our collaborators across the globe, **Drs. Suman Chakravarty**, **Syed Dastager**, **Pushpendra Kumar** and **Chandrajit Balomajumder** for their timely help, provocative ideas and encouraging suggestions towards the improvement of the thesis.

I would also like to thank the Council of Scientific and Industrial Research (CSIR) and Gas Authority of India Limited (GAIL) for providing funding for the various projects.

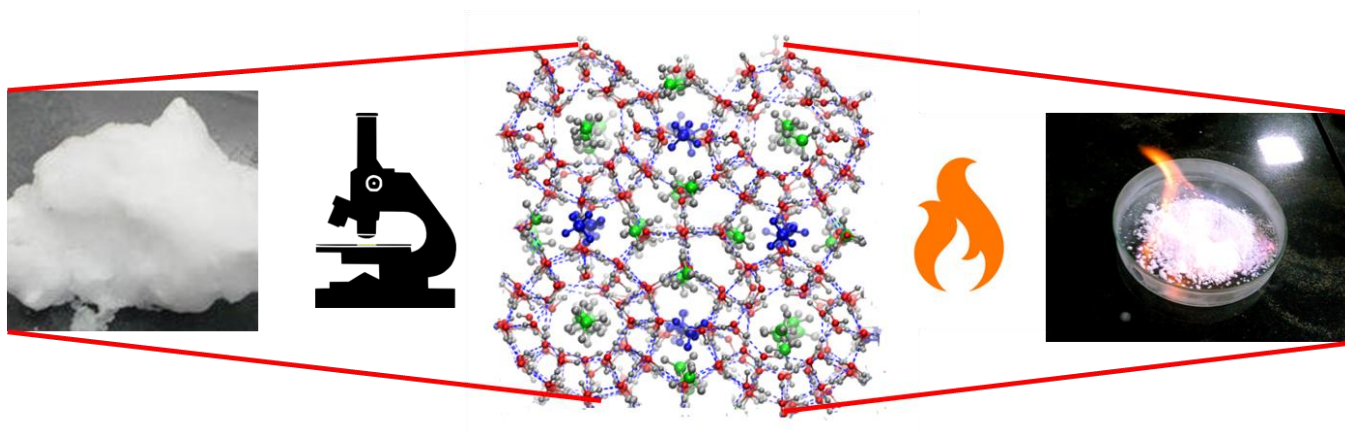
Gaurav Bhattacharjee

To those who inspired it and will not read it ...

My parents and my brother

Chapter 1

Introduction



1. Introduction¹

¹A version of this chapter has been published

Kumar, A.; Bhattacharjee, G.; Kulkarni, B. D.; Kumar, R. Role of surfactants in promoting gas hydrate formation. *Ind. Eng. Chem. Res.* **2015**, *54*, 12217-12232.

1.1.The World Energy Scenario

Population growth is connected with increase in energy demand in a nonlinear manner. Efforts to accommodate the ever increasing population within a finite space call for technological intervention; life style continuously gets updated and there is an ever growing pressure on increasing productivity leading to more and more energy consumption. This phenomenon may be put in the right perspective through the fact that in the past hundred years world population crossed 6.2 billion while energy demand rose by an order from 0.9×10^9 tons of oil equivalent(TOE) to 1.02×10^{10} TOE.(B.P. Statistical Review of World Energy, 2005).

Since the advent of time, the human race has relied on the sun to fulfill its energy needs and turned to burning resources such as wood, straw and dried dung when the sun failed them. Transportation needs were met with by the muscle of horses and the power of wind in our sails. Animals were employed to do jobs that couldn't be accomplished by manual labor. Water and wind energy was used to drive simple machines that met our day to day needs for food and water.

The growth rate of modern civilization depends on a large number of factors and perhaps on none more than on the production and consumption of energy. The threat of an acute energy crisis looms larger than ever before and new efforts are being made every day in order to prevent such a catastrophe. Fig. 1.1 shows the distribution of the different energy sources and their changes over time (Makogon et al., 2007).

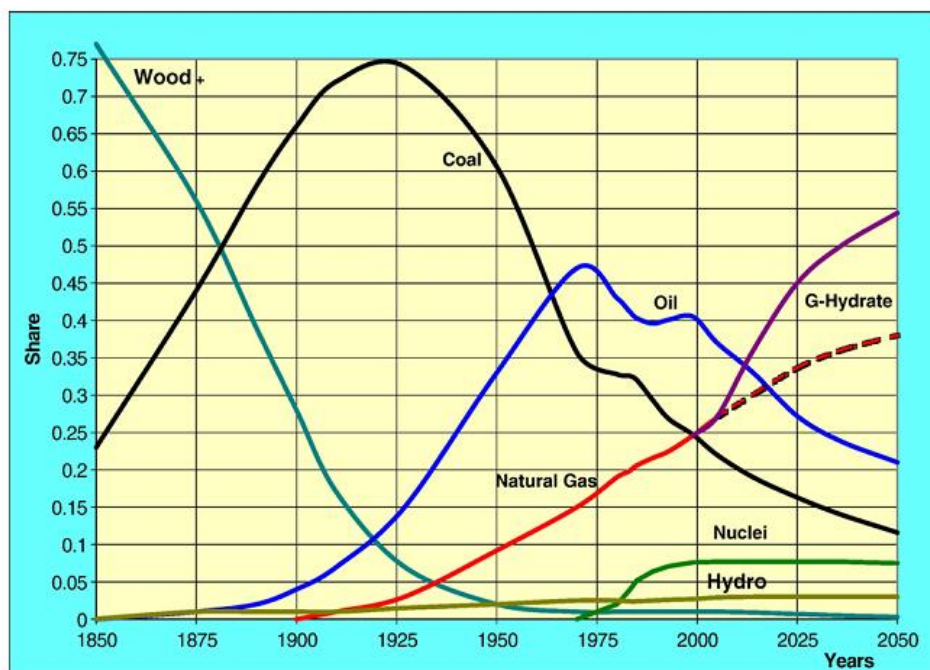


Fig. 1.1: World energy balance (adopted from Makogon et.al, 2007).

In 2015(B.P. Statistical Review of World Energy, 2016):

- Global primary energy consumption increased by just 1%, way below the ten year average of 1.9 %.
- Emerging economies account for 58.1 % of global energy consumption.
- Oil continued to be the fuel of choice and contributed to 32.9% of the global energy consumption.
- Global oil consumption grew by 1.9 million barrels per day (b/d), or 1.9% which is nearly double the recent historical average.
- Global oil production recorded a strongest ever growth in 2004, rising by 2.8 million barrels per day (b/d) or 3.2 %.
- World natural gas consumption grew by 1.7 %, below the ten year average of 2.3 %.
- Global natural gas production at 2.2 % grew more rapidly than its consumption.
- Global coal consumption fell by 1.8 % in 2015 whereas production of the same fell by 4 %. Coal's share of global primary energy consumption fell to 29.2 %, the lowest ever recorded since 2005.
- Global nuclear output increased by 1.3 %. Nuclear energy contributed to 4.4 % of the global primary energy consumption.
- Global hydroelectric output grew by 1%, well below the ten year average of 3 %.

- Hydroelectric energy contributed to 6.8 % of the global primary energy consumption.
- Renewable energy sources (wind, solar, biofuels etc.) contributed to 2.8 % of the global energy consumption, a significant increase from 0.8 % a decade ago.

These figures go on to show that for the foreseeable future, oil and gas will remain as our primary energy sources. According to BP (2016), as of 1 January 2016, the proven hydrocarbon reserves are 239.4 thousand million tonnes of oil and 186.9 trillion cubic metres of natural gas. At the current level of consumption, these reserves are sufficient to meet roughly 55.3 years and 55.0 years of global consumption for oil and natural gas respectively. However, if one takes the world population growth into consideration, at the current population growth rate of 1.12 % per year, the sufficiency of the earth's presently proven hydrocarbon reserves goes down to roughly 36-37 years for both oil and natural gas.

The standard of living of different countries in the modern world varies hugely and in part is determined by each entity's (country) location and its energy consumption. For example, USA houses only about 5% of the world's population but its share in the annual global primary energy consumption is a staggering 18 % (International Energy Outlook, 2016, U.S. EIA). On the other hand, India, one of the world's fastest developing countries is home to 18 % of the world's population but uses only 6 % of the world's primary energy (India Energy Outlook, 2015, IEA).

It is no secret that the world's readily accessible energy reserves are getting depleted at an alarmingly fast rate. As a result an unconventional energy resource which is a solid composite of gas and water has emerged as a potential future energy source which are known as clathrates of natural gas — commonly called gas hydrates.

Gas hydrate deposits hold a substantial amount of hydrocarbons. Estimates vary over several orders of magnitude but the volume of gas contained in gas hydrate accumulations is thought to be more than that in all the world's gas resources. A widely believed estimate puts the volume of natural gas stored in the form of gas hydrates deposits at 20,000 trillion cubic metres (TCM).

These accumulations often occur in parts of the world that lack in conventional reserves thus establishing a certain degree of self sufficiency to countries that rely on imported oil and natural gas. The promise of this untapped energy source is such that it has prompted many government and industry groups to set up national gas hydrate programs with countries like the USA, Russia, Japan, India, China and Korea largely in the mix.

1.2. Fundamentals of Gas Hydrates

Gas hydrates are non stoichiometric ice-like crystalline compounds that are formed when water and gas molecules interact under conditions of low temperature and high pressure. The gas (guest) molecules get trapped inside hydrogen bonded cages formed by the water (host) molecules and help stabilize these cages. Although generally referred to as gas hydrates (common gas molecules which act as guests include methane, carbon dioxide and hydrogen), there are also a few hydrocarbons having similar sizes as the aforementioned gas molecules with the ability to form clathrates (ex: tetrahydrofuran (THF) and neohexane (NH)). The incipient low temperature and high pressure conditions required to form gas hydrates are frequently encountered in deep-ocean (marine) and permafrost settings thus resulting in the presence of highly concentrated gas hydrate deposits on the continental shelves and in permafrost, formed over a period of millions and millions of years (Boswell and Collett, 2011; Sloan, 2003).

1.2.1. Gas Hydrate Structures

The structure of a gas hydrate is explicitly dependent on the size/s and chemical properties of the guest molecule/s. Different polyhedral cage structures can be formed depending on the sizes and the chemical properties of the guest molecules which further recombine to form well defined unit cells of gas hydrates. There are three major types of gas hydrate structures which occur in nature, namely the cubic Structures I and II and the hexagonal Structure H. While Structures I and II are frequently encountered in nature, natural occurrences of Structure H are rather rare.

Structure I (the most common type of gas hydrate structure) consists of two different types of cavities. The first cavity, known as a pentagonal dodecahedron and represented as 5^{12} is formed when water molecules come together through hydrogen bonding to build a structure having twelve pentagonal faces. This specific cavity or cage is present in all the three gas hydrate structures mentioned above (sI, sII and sH). Pentagonal dodecahedron cages may link together by sharing vertices to form the second cavity present in sI hydrates which is a polyhedron with twelve pentagonal and two hexagonal faces, known as a tetrakaidecahedron, larger than a pentagonal dodecahedron and represented as $5^{12}6^2$. A unit cell of sI hydrate comprises two 5^{12} cages and six $5^{12}6^2$ cages formed by 46 water molecules and each cage occupied by a single guest molecule. Guest molecules for sI hydrate typically have sizes

(diameter) between 4 and 6 Å (ex- methane, ethane, carbon dioxide, hydrogen sulfide etc). There are, however some exceptions to this rule. Nitrogen and other small molecules such as hydrogen ($d < 4.2$ Å) form structure II hydrates with each cage having either single or multiple occupancy of guest molecules (Sloan and Koh, 2008). When instead of vertices sharing, pentagonal dodecahedron cages link together through face sharing, they form the cavity which together with the 5^{12} cavity makes up the sII hydrate. On linking together by sharing faces, pentagonal dodecahedra cages form a polyhedron containing twelve pentagonal and four hexagonal faces. This cavity is known as a hexakaidecahedron, represented as $5^{12}6^4$ and is larger than the large ($5^{12}6^2$) cavity in sI hydrate owing to bending in the hydrogen bonds formed between water molecules. A unit cell of sII hydrate comprises sixteen 5^{12} and eight $5^{12}6^4$ cages made up by 136 water molecules. Guest molecules for sII hydrates have diameters below 4.2 Å or above 6 Å up to 7 Å (ex-nitrogen, hydrogen, propane etc).

Discovered in 1987 at the National Research Council in Canada (Ripmeester et.al, 1987), structure H is made up of three different types of crystal cages. It is similar to structures I and II in that it too contains the basic 5^{12} cage, however, it is unique in the fact that molecules of two different size ranges are required to stabilize this structure. Apart from the 5^{12} cage, the two other cavities which make up a sH hydrate are a $4^35^66^3$ cage which is a small cage and a $5^{12}6^8$ cage which is a large cage. The $4^35^66^3$ cage has three fairly strained square faces, six pentagonal faces and three hexagonal faces whereas the $5^{12}6^8$ cage consists of twelve pentagonal and eight hexagonal faces, the latter incidentally being the largest cavity present in any of the hydrate structures and capable of hosting guest molecules having diameters as large as 9 Å (Ripmeester et.al, 1994). A unit cell of sH hydrate consists of three 5^{12} cages, two $4^35^66^3$ cages and a single $5^{12}6^8$ cage. Small molecules such as methane or xenon act as help guests during the formation of sH hydrates and occupy the small 5^{12} and $4^35^66^3$ cages while intermediate sized hydrocarbons such as neohexane and cycloheptane are required to fill the large $5^{12}6^8$ cavities. Figure 1.2 shows the shapes of all the cavities present in the three hydrate structures discussed. The size ratio of the guest molecule to the cavity determines whether the guest can form a stable hydrate structure. In order to form a stable hydrate structure, this ratio needs to be approximately 0.9. If the ratio is far removed from unity, the guest molecules in question would not be possible to form stable hydrates. The molecular diameter to cavity diameter ratios for the gases relevant to this work (methane, carbon dioxide and nitrogen) is given in Table 1.1.

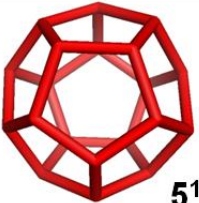

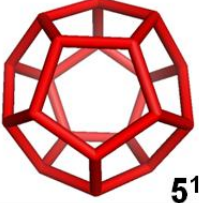

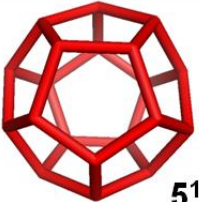
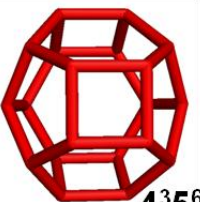
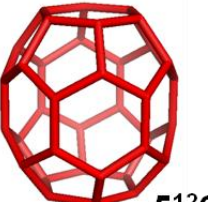
Small (S)	Medium (M)	Large (L)	Structure (Formula)
 5^{12}		 $5^{12}6^2$	Structure I (sI) $2S.6L.46H_2O$
 5^{12}		 $5^{12}6^4$	Structure II (sII) $16S.8L.136H_2O$
 5^{12}	 $4^3 5^6 6^3$	 $5^{12}6^8$	Structure H (sH) $3S.2M.1L.34H_2O$

Fig. 1.2: The different structures of gas hydrates.

Table 1.1: Size ratio for CH_4 , CO_2 and N_2 (data adopted from Sloan and Koh, 2008).

	Cavity Type	Structure I		Structure II	
		5^{12}	$5^{12}6^2$	5^{12}	$5^{12}6^4$
Molecule	Guest diameter (Å)	Guest diameter (Å)/ Actual cavity diameter (Å)*			
Methane	4.360	0.855	0.744	0.808	0.655
Carbon dioxide	5.120	1.000	0.830	1.020	0.769
Nitrogen	4.100	0.804	0.700	0.817	0.616

*Actual cavity diameter = Cavity diameter – Diameter of water (2.8) [All values in Å]

1.2.2. The Gas Hydrate Timeline (modified from Makogon et.al, 2007)

1778: Gas Hydrates first obtained by Priestly by bubbling SO₂ through water at 0°C and atmospheric pressure.

1811: Cl₂ clathrate crystals obtained by Davy who termed them as “hydrates of gas.”

1778-1934: Period of purely academic studies on Gas Hydrates. Only 56 papers from 16 authors were published.

1934: Hammerschmidt noted that the inspection of gas pipes of the USA was complicated by the formation of solid plugs in the wintertime. Through laboratory research, Hammerschmidt showed that as opposed to the belief that the plugs consisted of ice, they actually consisted of hydrates of the transported gas. There was a sudden urge to study the conditions of formation of such gas hydrates and hence develop an effective remedy to prevent their formation in places such as pipes and thus eradicate the problem of plugging. 144 papers on gas hydrates were published between 1934 and 1965.

1952: Studies by von Stackelberg and coworkers led to the discovery of two hydrate crystal structures (sI and sII) (Sloan and Koh, 2008).

1963: The Markhinskaya well drilled in Yakutiya to a depth of 1800m revealed a section of rock at 0 °C temperature at the 1450 m depth, with permafrost ending at approximately 1200 m depth.

1965: Comparing the conditions of that section of rock with hydrate formation conditions, Makogon formulated the idea of the possibility of the existence of gas-hydrate accumulations in the cooled layers. The idea was met with much skepticism in scientific circles.

1966: Hydrates of natural gas were formed in a laboratory in 1966 in porous media and in real core samples at the Gubkin Oil Institute in Moscow.

1969: After a comprehensive international examination, the discovery of natural hydrates was recorded in the USSR State Register of scientific discoveries (Moscow, 1969) as №75 with the following formulation: “Experimentally established was the previously unknown property of natural gases to form deposit in the solid gas-hydrate state in the earth's crust at specific thermodynamic conditions”

1970-71: A group of young geologists named Sapir, Ben'yaminovich and Beznosikov found the first gas-hydrate deposit in the Messoyakha field in the Transarctic, on the eastern border of West Siberia. Gas production was also started from the Messoyakha gas-hydrate deposit.

1982: The U.S. Geological Survey (USGS) and the Department of Energy National Energy Technology Laboratory conducted extensive research between 1982 and 1992, revealing that methane hydrate deposits could be found in offshore sediments as well. This was the first R&D Natural gas hydrate program of the USA.

1987: Discovery of hydrate crystal structure sH by Ripmeester and co-workers at the National Research Council in Canada (Ripmeester et.al, 1987).

1995: First natural gas-hydrate program of Japan (\$10 M).

1997: Government of India formulated a National Gas Hydrate Programme (NGHP) in 1997 for exploration and development of gas hydrates resources of the country (\$5 M).

1999: First natural gas-hydrate program of Korea (\$5 M).

2000: Following reconstitution of the NGHP (India) in the year 2000 by MOP&NG, a new sense of urgency was imparted to the programme and it was put on a fast track implementation.

2001: Japan's Methane Hydrate R&D Program was organized from a medium- to long-term viewpoint of aspiring to find solutions to various issues regarding the economical extraction and utilization of methane gas from methane hydrate-bearing layers (\$200M).

2001: Second natural gas-hydrate program of the USA (\$50 M).

2002: Mallik Gas Hydrate Production Research Well Program. Involved 5 different participating countries. Objectives were to quantify the production response of a gas hydrate reservoir to pressure stimulation, thermal stimulation and the development of a multidisciplinary science program for detailed engineering and reservoir simulation modeling. Full scale gas hydrate production was undertaken using the thermal stimulation route achieving rather reserved flows.

2004: China started its national gas hydrate program (\$50 M).

2004: Second natural gas-hydrate program of India. A total budget of \$56 M over 5 years.

2005: Second natural gas-hydrate program of Korea (\$83 M).

2005: Third natural gas-hydrate program of the USA (\$155 M) over 5 years.

2005: The Gulf of Mexico Gas Hydrate Joint Industry Project Leg I was undertaken.

2006: Expedition NGHP-01 began at 0600 hr 28 April 2006 with the arrival of the drill ship in Mumbai, India, and ended 113.5 days later in Chennai, India with the last line away North

Quay at 1912 hr 19 August 2006. Ultimately twenty one sites were occupied with five sites re-occupied at least once. Thirty nine holes were drilled. Of these, twelve holes were LWD/MWD drilled, twenty two holes were cored, and four holes were drilled as dedicated wireline logging holes. Thirteen holes were wireline logged and temperature gradients were established in eleven holes.

2008: Results of the Indian Natural Gas Hydrate Program were released.

2009: The Gulf of Mexico Gas Hydrate Joint Industry Project Leg II was undertaken.

2012: Field testing in the Prudhoe Bay gas hydrate site, Alaska by ConocoPhillips in association with JOGMEC and US, DOE. The feasibility of the CO₂-CH₄ exchange process in gas hydrate reservoirs was tested. A CO₂-N₂ mixture was used to displace methane from its formed hydrates. Continuous flow of gas was obtained for about 21 days before final lock-in.

2013: JOGMEC conducted the first offshore methane hydrate production test in the eastern Nankai Trough, Japan. The depressurization method was used to produce methane from the deepwater hydrate sediments. The test lasted for 6 days with an average daily gas production of about 20,000 cubic metres. Production had to be terminated due to an unprecedented increase in the sand production (Fire in the Ice, 2013, Vol. 13, Issue 2).

2013: The China Geological Survey, part of the Ministry of Land and Resources (MLR), has embarked on the research programme, costing 10 billion Yuan (US\$1.63 billion), while the Guangzhou Marine Geological Survey, also linked with the ministry, is to start working in seas 400 km south of Hong Kong.

2015: The Indian National Gas Hydrate Program Expedition 02 (NGHP 02) was carried out from 3 March, 2015 to 28 July, 2015 off the eastern coast of India. The primary goal of the expedition was the exploration and discovery of highly saturated gas hydrate occurrences in sandy reservoirs. These would serve as the sites for future production testing. This was the most comprehensive dedicated gas hydrate expedition ever carried out in the world with five months of continuous field operations.

2017: Japan and China, individually, for the first time, managed to produce a steady flow of gas from naturally existing hydrate reserves in the Nankai Trough and the Shenhu area in the South China Sea respectively.

1.3. Technological applications of gas hydrates and the need to enhance gas hydrate formation and dissociation kinetics

Apart from the obvious prospect as a future energy source, gas hydrates also find immense potential in a number of technological applications such as methane and hydrogen storage, carbon dioxide capture and separation, carbon dioxide sequestration and desalination. Fig. 1.3 lists the various applications of gas hydrates in different fields of research.

Since gas hydrate formation is an inherently gradual process, it would not make much sense to utilize resources in developing a technology that would progress at a rather slow rate. This creates the need to enhance the kinetics of gas hydrate formation which can be a result of subtle tweaks to the system (changing the reactor configuration) or the addition of certain catalyst-like chemicals to the same. These approaches may significantly bolster the rate of gas hydrate formation and would ideally be applicable to all the hydrate based technological applications. Of the various applications listed above, a few have been chosen to be studied in detail through the course of this thesis. Brief descriptions of these applications have been given below with special emphasis put on the specific individual goals of the hydrate based processes for each application and the corresponding challenges encountered for each.

- **Methane Storage**

Methane storage is one of the primary technological applications of gas storage, both in terms of importance of the application and technology readiness. This involves forming solid hydrates of methane which remain stable for long periods of time so that the methane gas can be stored in solid form at atmospheric pressure and low temperatures; ~ 253 K or even around 273 K (the latter by employing particular techniques) and may also be transported from one place to another. The gas storage capacity of said hydrates is also not unreasonable; 1 cm³ of methane hydrate can store approximately 172 cm³ of methane at standard conditions of temperature and pressure. By comparison, LNG (Liquified Natural Gas) has a much higher energy density but it must be stored at extremely low temperatures (113 K). The huge energy penalty that can be avoided by opting for the solid hydrate route to store methane/ natural gas is thus a major plus point in favor of this yet rather nascent technology at least in terms of public awareness. However, the development of the hydrate based technology has been somewhat hindered due to slow crystallization kinetics. The kinetics of hydrate formation, in this case pure methane hydrate is one aspect that can be improved upon endlessly and the

same is the motivation behind various studies discussed in the upcoming chapters of the thesis while also looking at improving the ease of operation of the process.

- **Gas Separation**

Gas separation using hydrate formation or as it is more formally known, the Hydrate Based Gas Separation (HBGS) process is an interesting application that actually holds a plethora of exciting opportunities, given the various different gas mixtures that can be subjected to this approach. The HBGS process is essentially a multistage hydrate formation and dissociation cycle which separates gases based on their feasibility to form hydrates, i.e. at a given temperature, one gas forms hydrates at moderate pressures than the other which results in the former gas getting trapped in the hydrate phase while the latter is now rich in the gaseous phase. Some of the different gas mixtures that have been separated using the HBGS process include $\text{CO}_2\text{-N}_2$ (flue gas), $\text{CO}_2\text{-H}_2$ (fuel gas), $\text{CH}_4\text{-N}_2$ (coal mine methane) and $\text{CH}_4\text{-CO}_2$ (unconventional sources of natural gas such as biogas), albeit with varying degrees of success. With regards to the HBGS process, the usual challenges faced are common with those discussed in the section for methane storage (requirement of rapid hydrate formation kinetics and high final gas uptake in conjunction with each of operation). However, the separation efficiency of the process also becomes important here with some gas mixtures better suited for separation using hydrate formation as compared to others. Thus in addition to enhancing the kinetics of the hydrate formation process, one also needs to look for suitable approaches to increase the separation efficiency of the same. This may or may not be achieved using certain specific additives as has been discussed in some of the upcoming chapters of the thesis. There is still a lot left to be desired as far as technology readiness goes for the HBGS process with each gas mixture posing its own set of requirements and challenges thus rendering the need to identify specific solutions for each. In the current thesis, the HBGS process has been studied for two of the gas mixtures mentioned earlier in this section with the objective being to enhance the kinetics and separation efficiency of the process for the individual systems while also keeping an eye on refining the process' ease of operation.

- **Carbon dioxide Sequestration**

Carbon dioxide sequestration in geological formations usually entails sequestration of anthropogenic CO_2 in depleted oil and gas reservoirs, saline aquifers, unmineable coal beds and deep sea beds. As all of these approaches come along with their fair share of disadvantages, a possible way out can be CO_2 sequestration in the form of solid hydrates in

suitable underground/ underwater geological formations. This idea is appealing as 1m^3 of CO_2 hydrate can store $120\text{-}160\text{ m}^3$ of CO_2 gas at STP. It can be easily understood that the kinetics of CO_2 hydrate formation pertaining to this application would need to be rather fast while the gas uptake would also not be far removed from the theoretical limit. A part of the current thesis would look into making this technology for CO_2 sequestration through hydrate formation viable from an Indian perspective.

To better understand the various factors at play, the upcoming sections discuss the major rate limiting issues for hydrate formation and what measures may be taken to overcome these hurdles. Special emphasis has been given to the use of additives (hydrate promoters) to enhance the kinetics of hydrate formation.

Gas hydrates are also frequently encountered in oil and gas pipelines, especially in cold countries and trans-continental pipelines where they may form as massive plugs and prevent the flow of hydrocarbons thus causing huge losses to the oil and gas industry. This calls into action preventive measures which may delay the formation of hydrate plus or if once, formed, aid in rapidly dissociating the same. It is still not possible to recover natural gas from gas hydrate reserves on an industrial scale as the three current major methods for dissociating gas hydrates (thermal stimulation, depressurization and chemical inhibitor injection) all have their own drawbacks. While thermal stimulation requires the use of huge amounts of energy and is quite expensive, depressurization is highly time consuming and the use of toxic chemical inhibitors in large quantities poses immense threat to the natural marine environment. It is widely believed that the way forward for recovery of natural gas from gas hydrates is a hybrid approach combining all the three basic hydrate dissociation methods although as far as field trials go, depressurization has so far been the hydrate dissociation method of choice owing to its ease of operation. Thus there is a real need to develop techniques which would allow us to dissociate hydrates as quickly as possible and at minimal cost. Faster production rate is one of the key requirements for commercial exploitation of natural gas hydrate resource.

It is abundantly clear that whatever the hydrate based technological application be in question, rapid hydrate formation kinetics and high gas uptake are a must for the technology to be relevant on a commercial scale. The same holds true for the kinetics of hydrate dissociation concerning the recovery of natural gas from hydrate deposits. This drives the motivation for the current thesis in which additives in low concentrations have been used to enhance hydrate formation and dissociation kinetics. Technological applications of gas hydrates such as methane storage, gas separation and carbon dioxide sequestration have been explored in

addition to methane recovery from marine gas hydrates. In the coming sections, the techniques to enhance gas hydrate formation and dissociation kinetics have been discussed in detail.

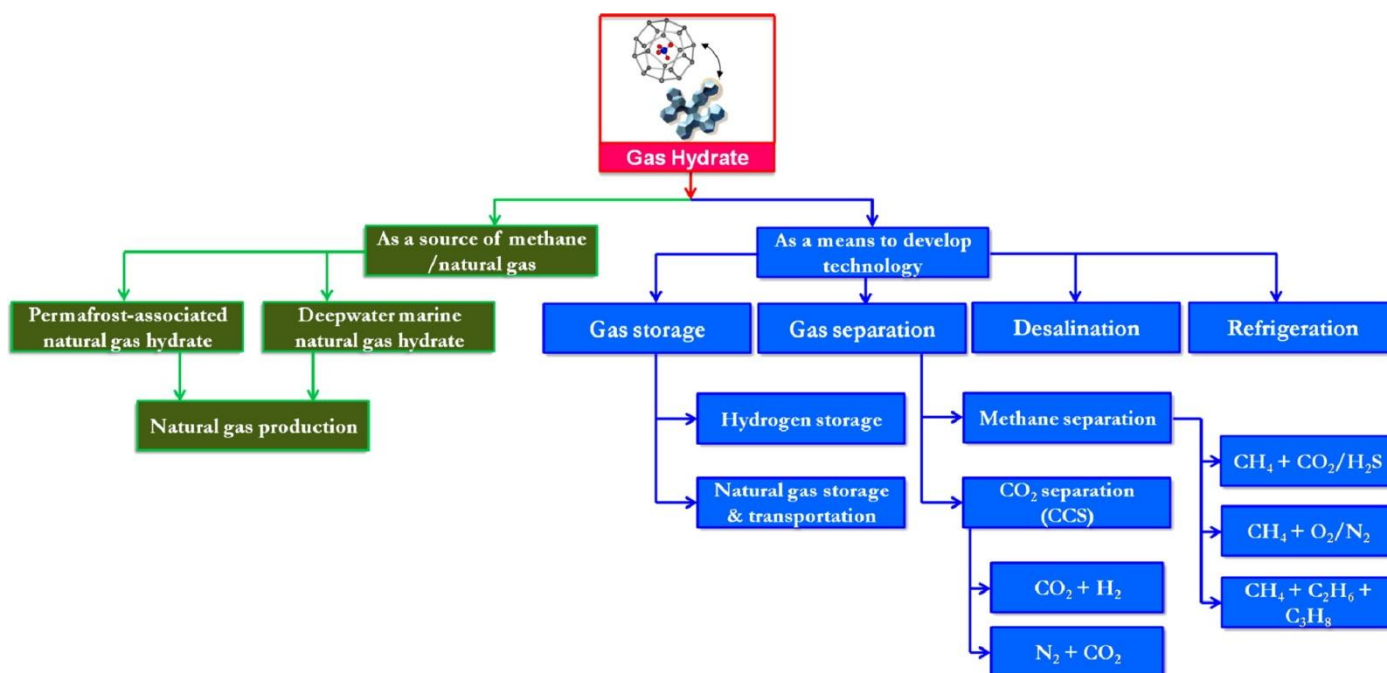


Fig. 1.3: The various applications of gas hydrates (adopted from Kumar et.al, 2015a).

1.3.1. Kinetics of hydrate formation: rate limiting factors and techniques for enhancement

Hydrate formation, which is basically a crystallization process, proceeds in three steps. The first step is known as dissolution in which the gas gets dissolved into the aqueous medium. Gas dissolution results in a gradual drop in pressure in the reactor. This is followed by induction or nucleation which is defined as the point in time of the formation of the first critically sized stable hydrate nucleus. Nucleation is characterized by a sudden drop in the pressure of the reactor accompanied by a sudden spike in the temperature profile of the same, the latter owing to the exothermic nature of hydrate formation. Subsequent to nucleation is the growth phase of hydrates where hydrate crystals continue to grow until the system reaches saturation, i.e. there isn't enough driving force left in the system to sustain hydrate formation. Figure 1.4 shows a typical hydrate formation (gas uptake) curve along with the corresponding temperature profile and induction time.

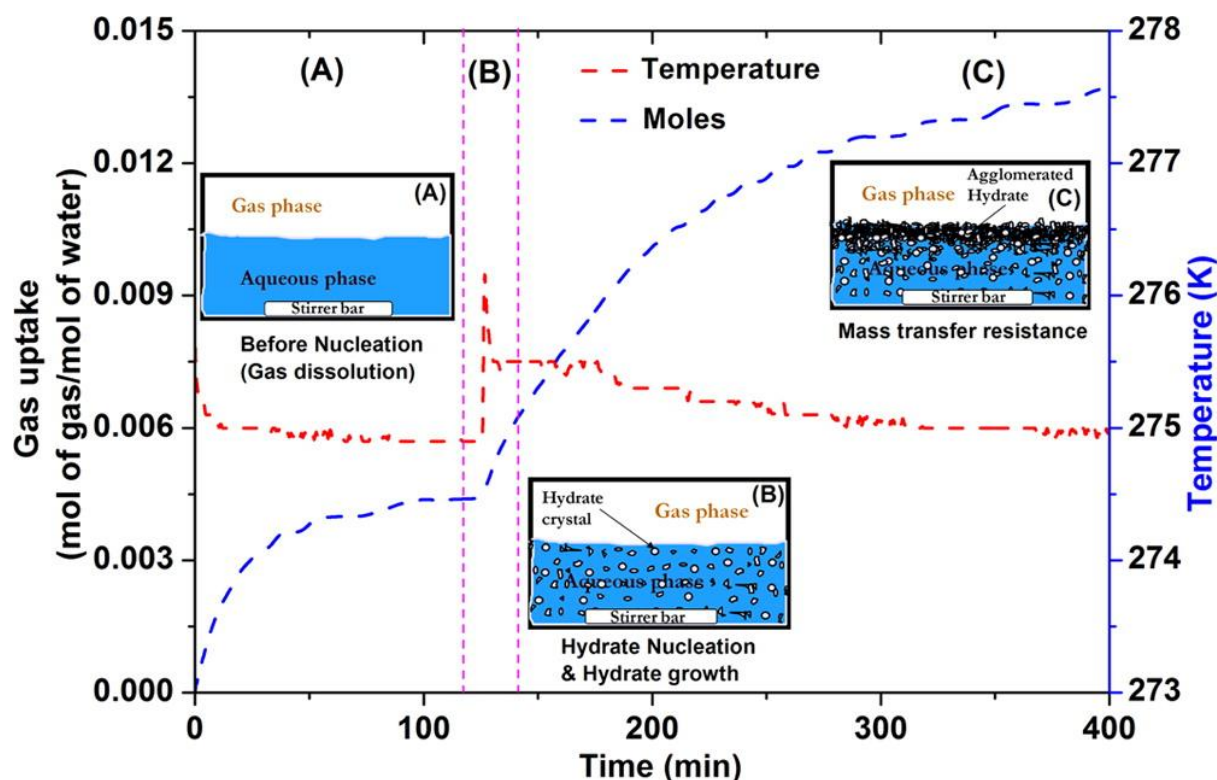


Fig. 1.4: A typical gas uptake curve along with temperature profile during hydrate formation showing the gas dissolution, nucleation and hydrate growth phases (adopted from Kumar et.al, 2015a).

It is well understood that nucleation occurs at the gas-water interface and upon successful nucleation, a thin hydrate layer forms on the interface which limits further gas-water contact (Gayet et.al, 2005). Different reactor configurations such as stirred tank and fixed bed reactors that ensure maximum gas-water contact were thus developed to tackle the problem of mass transfer resistance. Such reactors not only provide a larger contact area for the gas and water but also ensure higher solubility of the hydrate forming gas in aqueous solution (Mori et.al, 2003; Linga et.al, 2012). The use of metallic packing as the fixed bed medium can also help another common issue associated with the generally slow rate of gas hydrate formation, that of efficient heat dissipation. Hydrate formation is an exothermic reaction and efficient heat dissipation in a fixed bed medium is a known challenge which if left unattended considerably slows down the rate of hydrate formation by lowering the driving force for the same (Kumar et.al, 2016).

The use of certain additives (chemicals) to promote hydrate formation has also been long experimented with. These additives are known generally as hydrate promoters. Hydrate

promoters can be further categorized into two groups; thermodynamic and kinetic promoters. While thermodynamic promoters shift the hydrate equilibrium boundary to much milder conditions, kinetic promoters improve the kinetics of hydrate formation by either reducing the induction time or enhancing and subsequently sustaining the rate of hydrate growth for a long period of time or both. Since thermodynamic promoters specifically lower the hydrate equilibrium pressure for a certain gas/ gas mixture at a given temperature, determining the efficacy of a thermodynamic promoter requires hydrate equilibrium studies. On the other hand, a kinetic hydrate promoter is expected to reduce the induction time and or enhance and sustain the rate of hydrate growth; thus a classical gas uptake experiment and the ensuing gas uptake curve can be used to test the efficacy of a kinetic hydrate promoter. The rapid hydrate formation kinetics obtained as a result of adopting all these measures can then be utilized for a number of technological applications such as gas separation and storage, already mentioned above.

Kalogerakis et.al first suggested the addition of surfactants to water to enhance the kinetics of gas hydrate formation without having any effect on the hydrate equilibrium conditions (Kalogerakis et.al, 1993). Since then surfactants have gone on to become the most common class of kinetic hydrate promoters. The other major class of compounds that has found major importance as kinetic hydrate promoters is amino acids. The use of amino acids as kinetic hydrate promoters is a rather recent development and the subject still requires extensive research activity. Detailed discussions about the use of both surfactants and amino acids as kinetic hydrate promoters are provided in the upcoming sections.

1.3.2. Surface active agents (Surfactants) and their role in gas hydrate studies

Surface active agents (Surfactants) are compounds, whose molecules contain both lipophilic (hydrophobic) and hydrophilic moieties, i.e., they are amphiphilic (exhibit affinity for both polar and non-polar substances (Fig 3(a)). The lipophilic and hydrophilic groups, characteristic of each surfactant are the property determining factors. Surfactants can diffuse from the bulk phase to an interface, altering the surface or interfacial tension, modifying the contact angle between the phases and wettability of solid surfaces, and thus changing surface charge & surface viscosity (Shah, 1997). At suitable concentrations, the surfactant molecules in water aggregate to form various kinds of structures (called micelles) with diverse shapes and orientations (spherical, rod-like micelles, multilayer structures etc) (Fig 3(b)) (Vogtle, 1991; Fuhrhop and Koning, 1994). Surfactants can mainly be classified into three categories depending on the moieties they contain, namely anionic, cationic and non-ionic surfactants.

Zwitterionic surfactants are another major class which is distinguished from others as these compounds contain both cationic and anionic centers attached to the same molecule (Fig 1.5).

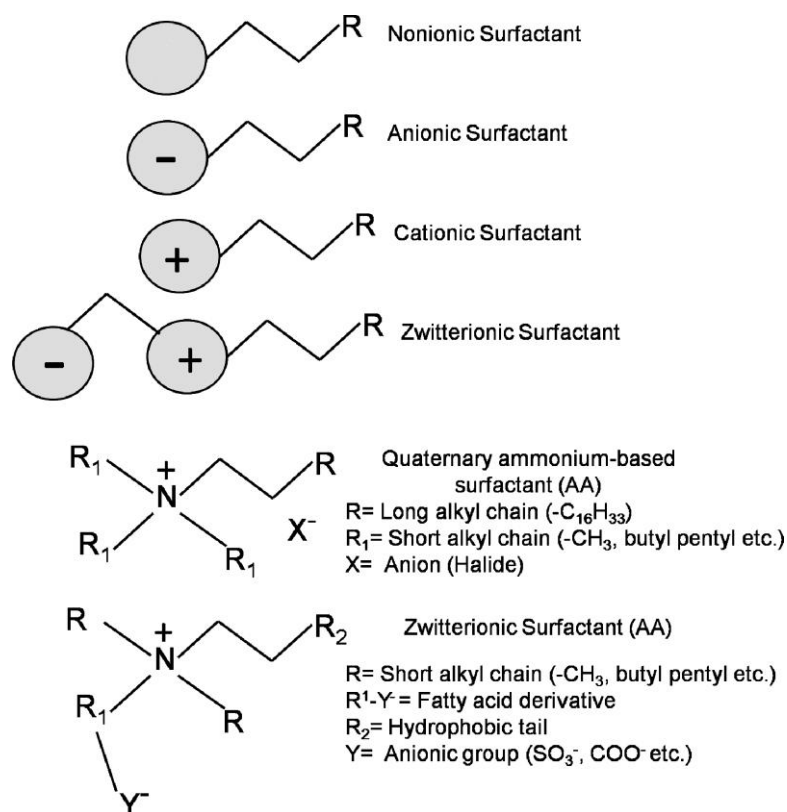


Fig. 1.5: Different classes of surfactants and their corresponding structures (adopted from Kumar et.al, 2015a).

Surfactants find application in a number of industries including petroleum and food. Addition of surfactants to a multiphase system enhances surface activity which favorably affects the spreadability, wetting, foaming, detergency etc of the system. In industries where micelle formation is one of the requirements, surfactants play a significant role (Suradkar and Bhagwat, 2006). Use of surfactants in gas hydrate related studies has been ongoing since the early 90s (Kalogerakis et.al, 1993; Kutergin et.al, 1992; Leporcher et.al, 1998). A thorough search of relevant literature clearly shows that use of surfactants greatly enhances the kinetics of hydrate formation and they have been widely used in different lab scale studies. However, there is still a lot of ambiguity as to which surfactant is going to work favorably for a particular system. It has been reported that efficacy of these surfactants for enhanced kinetics are system specific (Lim et.al, 2013; Kumar et.al, 2015(b)). Literature suggests that the gas mixture being used for hydrate formation plays a role as does the presence/absence of any

other additive such as a thermodynamic promoter. To provide a proper understanding of the effect of surfactants on gas hydrate formation kinetics, the immediately upcoming section extensively reviews the work that has been conducted so far using surfactants as an additive during gas hydrate formation. Different mechanisms by which such surfactants may enhance hydrate formation rate have been talked about and how certain combinations of surfactants help in improving the gas hydrate growth has been discussed.

1.3.3. Surfactants as kinetic hydrate promoters

The mechanism through which surfactants enhance hydrate formation kinetics is still up for debate although a few different theories have been put forward regarding the same. These include (a) significantly reducing the surface tension of the liquid solution, resulting in better diffusion of the gas in the liquid as well as significant altering of the morphology of gas hydrate, (b) forming an immobile surfactant–water phase, thus helping hydrates to nucleate faster, and (c) promoting hydrate nucleation due to formation of surfactant micelles or surfactant aggregates.

Karaaslan and Parlaktuna used three different types of surfactants (anionic, cationic and nonionic); they reported that hydrate formation kinetics was significantly better in the presence of the anionic surfactant as compared to a system without any surfactant. The effect of the nonionic surfactant was less pronounced while the cationic surfactant showed two different behaviours at low and high concentrations. At low concentrations, the cationic surfactant proved to be an effective kinetic hydrate promoter whereas at high concentrations of the same, no appreciable change in the rate of hydrate formation was observed (Karaaslan and Parlaktuna, 2000; Karaaslan and Parlaktuna, 2002 (a)). In a different work, Karaaslan and Parlaktuna studied the effect of three non-ionic surfactants, polyoxyethylene (5) nonylphenyl ether (IGEPAL-520), Brij-58 and Tween-40. The authors concluded that IGEPAL-520 is the most effective hydrate formation promoter among the three. An amount of 1 wt % IGEPAL-520 accelerates the methane hydrate formation rate by a factor of 2.4 compared to methane hydrate formation rate in pure water (Karaaslan and Parlaktuna, 2002 (b)).

Okutani et al. studied the effects of three homologues anionic surfactants (sodium dodecyl sulfate (SDS), sodium tetradecyl sulfate (STS), sodium hexadecyl sulfate (SHS)) on methane hydrate formation. At concentrations of ~1000 ppm or above, SDS was found to be very

effective in increasing both, the rate of pure methane hydrate formation and the final water-to-hydrate conversion. However, equivalent promotion effect was seen with STS at a much lower concentration, say ~ 100 ppm. It was concluded that, STS is more favorable than SDS as far as methane hydrate formation is concerned. SHS was found to be less effective compared to SDS and STS (Okutani et.al, 2008). According to Yoslim et al. the addition of SDS (concentration range between 242 to 2200 ppm) increases the gas uptake rate for mixed hydrate of methane /propane ($\text{CH}_4/\text{C}_3\text{H}_8$) by 14 times as compared to that for pure water. At SDS concentrations of 2200 ppm and 645 ppm, drop in the reactor pressure which relate to the extent of water to hydrate conversion was found to be maximum. They suggest that in presence of the surfactant (SDS), liquid-gas interface does not get covered with an impermeable solid hydrate film, rather hydrate grows as porous surface allowing efficient water to gas contact for better conversion. Hydrate growth was also seen on the walls of the reactor suggesting better water to gas contact by capillary effect (Yoslim et.al, 2010).

Kumar et al., studied the three types of surfactants (anionic, anionic and nonionic) for CO_2 hydrate formation kinetics; anionic surfactant (SDS) was found to be most effective in enhancing the rate of hydrate formation as well as reducing the induction time. Non-ionic surfactant (Tween-80) was found to be better than the cationic surfactant DTACl (Kumar et.al, 2013). Veluswamy et al. have also used cationic and nonionic surfactants (DTACl and Tween-20 respectively) but for mixed hydrogen/tetrahydrofuran (THF) and methane/THF hydrate formation. They observed a marginal improvement in hydrogen THF hydrate formation rates while a reduction in the hydrate formation rate of Methane/THF mixed hydrate was observed. Thus the effect of surfactants depends upon the guest gas and the system (Veluswanmy et.al, 2015). Han et al. in their study on natural gas hydrates concluded that the maximum gas hydrate formation for natural gas was achieved at 300 ppm concentration of SDS (Han et.al, 2002). Link et al., tested a large selection of surfactants in order to gauge their kinetic promoting properties on methane hydrate formation. The authors have that out of all the surfactants tested, SDS was the best surfactant for promoting methane hydrate formation (Link et.al, 2003). Zhang et al. working with methane hydrate reported that the use of SDS reduces the induction time; however a systematic trend could not be observed between induction times and SDS concentrations when the concentration of SDS was varied from 260 to 10000 ppm (Zhang et.al, 2007). Much earlier in a similar study done on ethane hydrate, Zhong and Rogers have found that by adding about 284 ppm of SDS to an ethane-water system, the rate of hydrate formation increased by a factor greater than about 700 as

compared to a system having only pure water. They have also reported good reproducibility of the induction time in the surfactant solution compared with no surfactant experiment. Furthermore, it was suggested that the formation of micelles in presence of surfactants not only enhanced ethane solubility but the micelles themselves acted as nucleating sites for faster hydrate growth (Zhong and Rogers, 2000). The authors report that the CMC value of SDS-water solution decreases with pressure from 2725 ppm (at atmospheric pressure and room temperature) to 242 ppm (at hydrate forming conditions). At 242 ppm concentration of SDS, there was a significant change in the hydrate induction time, which was used to define the CMC. Kang et al. through their experimental work concluded that the use of an optimum concentration of SDS acts as a promoter but an excess amount of the same can inhibit hydrate growth. In the presence of SDS, initial hydrate formation rates were found to increase the gas consumption resulting in faster hydrate growth (Kang et.al, 2010). It is important to note that micellization tendency of surfactant mixtures are completely different from those of pure species and mixed surfactants show superior performance as compared to individual surfactants (Suradkar and Bhagwat, 2006). Mandal and Laik studied the effects of anionic surfactant (SDS: 300 and 500 ppm) on ethane hydrate formation, dissociation and storage capacity in a static system. They concluded that in the presence of SDS, hydrates grow as very fine particles with enhanced gas consumption and storage capacities. They measured the hydrate dissociation rate and showed that the presence of SDS lowers the self-preservation effect and increases the dissociation rate. However their finding that presence of SDS shows a thermodynamic effect on hydrate formation resulting in shift in formation temperature (at a given pressure, compared to pure water) contradicts other work in the literature (Mandal and Laik, 2008). A critical commentary on this contradictory claim was provided by Y.H. Mori. Mori pointed out the doubtful experimental data provided in the paper discussed above (Mandal and Laik, 2008) and also argued that there was no evidence obtained to support the surfactant micelle hypothesis as claimed by Mandal and Laik (Mori, 2008). In light of such contradicting reports regarding faster hydrate nucleation in presence of micelles it is concluded that the surfactant-micelle hypothesis has not been tested extensively and at this point of time there is no concrete evidence in the literature to support this claim.

Gayet et al. performed studies on methane hydrate equilibrium conditions in presence of 0.02wt % SDS and found that SDS did not have any effect on the gas hydrate equilibrium but rather enhanced the hydrate formation rate. In addition to this, they visually observed that for a pure water system, nucleation and growth of hydrates usually occurred at the water–gas

interface whereas for a water-SDS system, hydrates grew as a porous structure on the reactor wall. It was observed that liquid migrates from the bulk phase to the gaseous phase through the porous hydrate structure (capillary driven water supply!) (Gayet et.al, 2005).

SDS has also been used in combination with thermodynamic promoters like THF (Ricaurte et.al, 2013; Kumar et.al, 2014) and CP (Zhong et.al, 2013; Sun et.al, 2003). It has been observed that presence of thermodynamic promoters like THF and CP reduces the influence of SDS and its effect as hydrate promoter compared to a pure water system. Zhong et al. studied the influence of cyclopentane (CP) and SDS on methane separation from low-concentration coal mine gas. They found that the gas uptake and rate of hydrate formation were dependent on SDS concentration, but the presence of SDS did not show any clear influence on methane recovery. The methane recovery obtained in the presence of SDS was 33.3%, while that obtained without SDS was 33.1% (Zhong et.al, 2013; Zhang et.al, 2010). They reported that SDS was not very effective in promoting methane enclathration in the presence of CP. However, methane enclathration is accelerated by adding salts like NaCl and NaClO₄. Li et al., found that the methane hydrate formation rate for a cyclopentane / water emulsion with tween-80 was better than that obtained in absence of tween-80, higher gas/liquid contact area in presence of surfactant was identified as one of the reasons for the obtained results (Li et.al, 2010).

Even though the data presented here overwhelmingly support the utility of surfactants as promoters for hydrate crystallization, the qualitative knowledge obtained so far is system specific. Dependencies on the surfactant concentration for hydrate-formation rate and the final water to hydrate conversion ratio has been established for many guest species. However, it is not clear whether such dependencies actually exist or it is more to do with different reactor configuration used in these studies. Neither is it yet well understood as to how, surfactants actually enhance the kinetics of hydrate formation and there is a constant need to further such enhancement. Additionally, although surfactants do improve hydrate formation kinetics significantly, they have their own shortcomings, prime among which is difficulty of handling, especially on an industrial scale due to excessive foam generation when using surfactants. As a result of all these concerns (the system specific nature of surfactants and problems of handling) there is an ever growing need to identify new additives that can help us further and further enhance the kinetics of gas hydrate formation while at the same time eliminating the common problems faced when using traditional additives (almost exclusively surfactants).

1.3.4. Amino Acids and their role in gas hydrate studies

Amino acids are biologically relevant compounds containing amine (-NH₂) and carboxylic acid (-COOH) functional groups, usually along with a side-chain (R group) specific to each amino acid. There are 20 distinct amino acids which are the building blocks of proteins. Amino acids can be categorized as charged, hydrophobic or polar (hydrophilic) based on the side chain. In gas hydrate based applications, amino acids have primarily been looked at as inhibitors for carbon dioxide or methane hydrate formation but recent studies have highlighted the role amino acids can play as kinetic hydrate promoters (Liu et. al, 2015; Veluswamy et. al, 2016).

The main attractiveness of using amino acids as either kinetic hydrate inhibitors or promoters stems from the rather benign nature of these molecules. For use as kinetic hydrate promoters, the non foaming property of amino acids as opposed to surfactants while having a similar physical structure (both hydrophilic and hydrophobic moieties) is one of the other major factors that have spurred recent research activities around the world involving these additives.

Liu et.al used the amino acid Leucine to promote the formation of methane hydrate with a view on storing methane in the form of hydrates. It was observed that in the presence of Leucine, methane could be stored in a hydrated form with a high hydrate formation rate and high storage capacity (Liu et.al, 2015). Veluswamy et.al in a recent study also used the amino acid L-leucine to promote methane hydrate formation kinetics. The study was performed with a view on understanding the morphology of methane hydrate formation in presence of L-leucine (Veluswamy et.al, 2016).

1.3.4.1. L-leucine as a kinetic promoter for methane hydrate formation

Liu et.al investigated the effects of about 15 different amino acids on methane hydrate formation kinetics. It was observed that out of all the different amino acids used, L-leucine was the most effective in promoting methane hydrate formation kinetics and the optimum concentration of L-leucine was found to be 0.5 wt%. The gravimetric capacity was reported to have reached a high of 144 mg/g which means around 95% of water was converted into hydrate according to the CH₄.5.89H₂O composition with a high gravimetric capacity of 151 mg/g. A number of other amino acids such as isoleucine, valine, proline, methionine, tryptophan and histidine were also found to promote methane hydrate formation kinetics

albeit with lower final gravimetric capacities. The major take away from this study was the observation of no foaming when degassing using the amino acids without compromising too much on the kinetics of formation as compared to SDS. SDS or other surfactants produce an excessive amount of foam on dissociation of gas hydrates and subsequent degassing which may pose immense technical difficulties especially when scaling up the gas hydrate based technologies which require the use of a kinetic promoter. The use of amino acids in place of surfactants thus sounds like a good idea (Liu et.al, 2015).

1.3.4.2. Morphology of methane hydrate formation in presence of L-leucine

Veluswamy et.al, 2016 based their study on L-leucine as a kinetic promoter on the results obtained by Liu et.al, 2015. The study by Liu et.al, 2015 was a kinetic study while the one by Veluswamy et.al focussed on the morphology of methane hydrate formation in the presence of L-leucine. The concentration of amino acid was varied between 0.1 and 0.5 wt%. It was observed that below 0.3 wt% there is no effect of the amino acid on methane hydrate formation kinetics. In presence of 0.3 wt% amino acid, a distinct methane bubble was observed to form after nucleation within the bulk solution that transfigured into methane hydrate during the hydrate growth phase. Hydrate crystals formed in presence of amino acid were observed to be very flexible and expandable which facilitated the methane bubble to channel more gas inside and enlarge in the liquid solution. At higher concentrations of amino acids greater than 0.3 wt %), mushy and indiscernible hydrate crystals were observed to drastically form in the bulk solution. Once again, dissociation in the presence of amino acid was found to be quick and easy and without the presence of an excessively foamy layer usually observed during dissociation of formed hydrates in the presence of surfactants. Figure 1.6 shows the morphology of hydrate formation in the presence of both 0.3 wt% and 0.5 wt% L-leucine. In the case of 0.3 wt% leucine, the formation of a characteristic methane bubble can be observed after about 4 minutes from nucleation whereas in the case of 0.5 wt% leucine, drastic methane hydrate formation can be observed (Liu et.al, 2015, Veluswamy et.al, 2016).

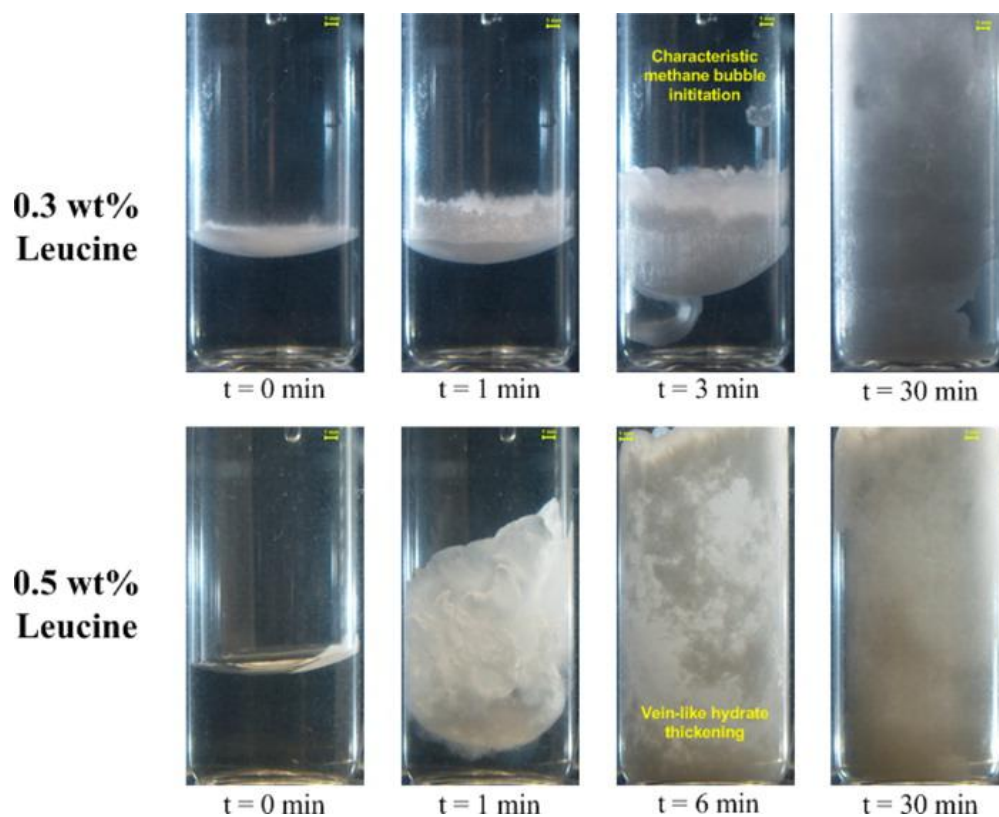


Figure 1.6: Morphology of methane hydrate formation in the presence of Leucine (adopted from Veluswamy et.al, 2016).

1.3.5. Fundamentals of hydrate dissociation and the various gas hydrate production methods:

In a methane hydrate (MH) reservoir, temperature and pressure conditions are in the hydrate stability region. To decompose the hydrate and produce gas from a hydrate bearing reservoir, the temperature and pressure conditions should be moved to the hydrate dissociation region. Three methods namely depressurization, thermal stimulation and inhibitor injection have been proposed as principle methods for the dissociation of methane hydrate which can be seen in Figure 1.7. In the depressurization method, the pressure of the methane hydrate reservoir is decreased below three phase (G-H-Water or G-H-Ice) equilibrium pressure, while in thermal stimulation method the temperature of the reservoir is increased above the three phase equilibrium temperature. In the inhibitor injection method, additives are injected into the hydrate reservoir to shift the three phase equilibrium curve to a more drastic pressure and

temperature side and thus the reservoir conditions are shifted to the unstable hydrate region. In order to increase gas production from a hydrate reservoir, a combination of these three basic methods and/or application of horizontal wells and hydraulic fracturing, which are widely used in the conventional oil/gas development, is proposed as the way forward.

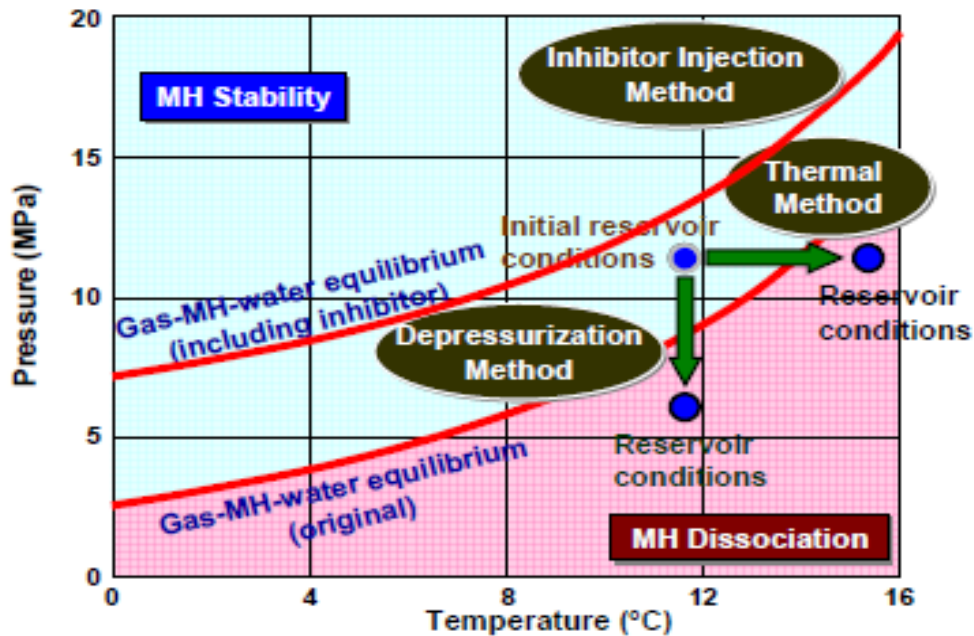


Figure 1.7: Principles of gas hydrate dissociation (adopted from Kurihara et al., 2011).

In addition to these three primary methods of hydrate dissociation, there is a fourth process which has attracted some interest from the gas hydrate community known as the CO_2 - CH_4 substitution/replacement process. The basic procedure for the proposed approach is as follows; first CO_2 gas mixture (fuel gas/ flue gas) would be captured from the point source such as thermal power station where generation of CO_2 is highest. Then, CO_2 from gas mixture would be separated and transported from to the point source to the naturally occurring gas hydrate sediments via pipe line or storage tanks. CO_2 would be then injected via injector well in natural gas hydrate formed zone. Thermodynamically CO_2 hydrate is more stable than methane hydrate. Thus CO_2 would be injected at such temperature and pressure conditions where methane hydrate would be unstable, whereas CO_2 hydrate would be stable. Thus CO_2 would replace methane in the hydrate structure (Lee et.al, 2003; Ota et.al, 2007). The mechanism of this swapping concept is shown in Figure 1.8 in which simultaneous recovery of methane and CO_2 sequestration can be achieved. This approach is very significant as it not only ensures recovery of methane but also sequestration of CO_2 . On the other hand as methane is recovered, the stability of the ocean floor is not compromised as CO_2 replaces

methane in the hydrate structure. Thus this approach can eliminate the major problems which would be caused during hydrate decomposition as discussed earlier. However, kinetics of methane recovery and CO₂ sequestration and the extent to which methane can be replaced should be evaluated.

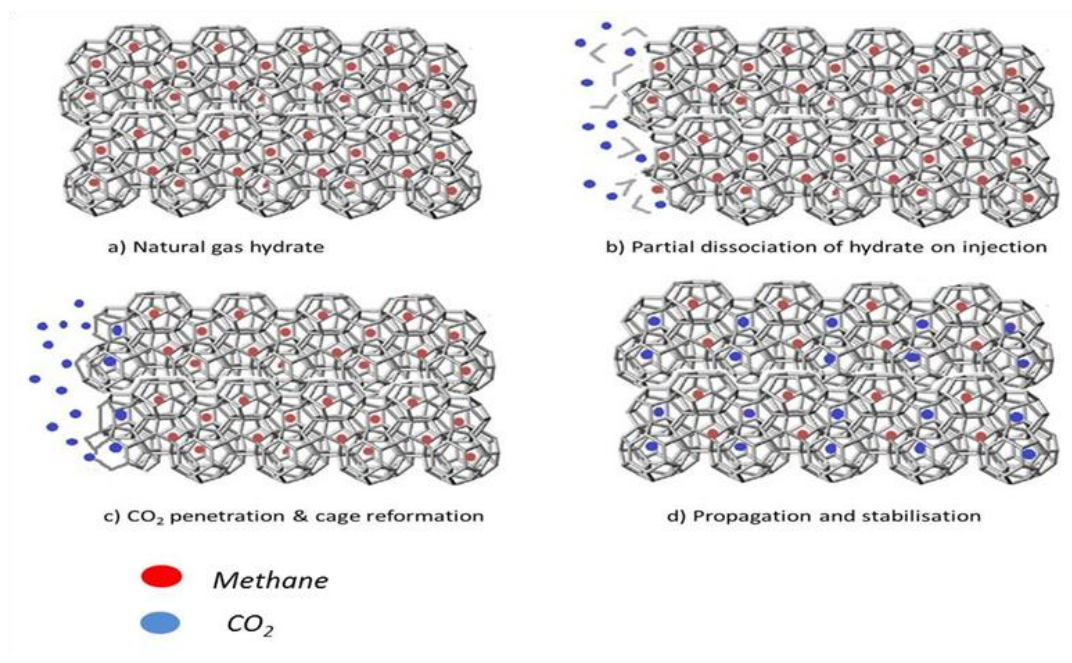


Figure 1.8: Mechanism of the simultaneous recovery of methane along with sequestration of CO₂.

1.4. Research Objectives

The current thesis focuses on the following major aspects:

- Study the kinetics of hydrate formation and dissociation process for application in technologies such as gas separation, storage and methane recovery.
- Identification of suitable additive to promote hydrate growth / dissociation kinetics.
- Understand the mechanism by which a particular additive affects the kinetics of hydrate growth and dissociation
- Enhancing the kinetics of CO₂ sequestration and storage through gas hydrate formation using a synthetic and natural porous media.

1.5. Organization of the Thesis

The current world energy scenario and a basic introduction to gas hydrates and their various applications have been given in Chapter 1. This chapter also clearly states the need for enhancing the kinetics of gas hydrate formation and dissociation while further discussing how such enhancement may be achieved.

Chapter 2 deals with the effects of surfactant micellization on methane hydrate formation. To understand the effect of surfactant micelles on hydrate formation kinetics, a novel surfactant system capable of producing micelles at hydrate forming temperature was developed and the presence of surfactant micelles in this new system (a combination of anionic surfactant SDS and zwitterionic surfactant CAPB) was determined through DLS measurements. Pure methane and a coal bed methane mixture were individually used to assess the efficacy of the surfactant mixture for hydrate formation.

Chapter 3 tackles the problem of foam generation that arises when using surfactants as kinetic hydrate promoters: a silicone based antifoam was used in conjunction with the surfactant SDS to prevent foam generation and at the same time enhance the kinetics of methane hydrate formation. Morphology studies reveal the actual prevention in form formation in presence of the silicone based antifoam.

Chapter 4 talks about using bio-derived additives instead of synthetic additives to enhance the kinetics of hydrate formation. Once again in this chapter, methane hydrate formation has been studied. Part 1) the biosurfactant Surfactin was used as a kinetic hydrate promoter and compared to the most commonly used synthetic promoter SDS. Part 2) an amino acid (L-histidine) which does not generate foam was used as a kinetic hydrate promoter and its efficacy compared to SDS. The chapter ends with a comparison of the different additives used to enhance methane hydrate formation kinetics, i.e. synthetic additives: synthetic surfactant and antifoam and bio-derived additives: biosurfactant and amino acid.

Chapter 5 entirely moves on from pure methane hydrates to hydrates of gas mixtures of methane. In this chapter, the problem of gas separation, more specifically, the problem of separating an industrially relevant CH₄-CO₂ natural gas mixture using the hydrate based gas separation process is investigated upon. Different additives were used which can improve the feasibility and economics of separating this gas mixture through hydrate formation.

Chapter 6 is the final chapter that deals with hydrate formation and investigates the influence of porous media on carbon dioxide hydrate formation kinetics. Two siliceous materials with

high porosities, pumice and fire hardened red clay (FHRC) were used as packing materials in a fixed bed setup to study hydrate formation kinetics. The effect of different factors such as bed height, volume of water used and particle size was investigated.

Chapter 7 deals exclusively with gas hydrate dissociation. The objective is to identify various benign additives which when used in exceedingly low concentrations, significantly enhance the kinetics of methane hydrate dissociation. The motivation is to develop an economical and efficient process for the recovery of methane from natural gas hydrates.

Finally, Chapter 8 is a brief conclusion of this thesis, summarizing overall accomplishments and potential future scopes of the research area. A list of publications made out during the research is also attached in the thesis.

1.6. References

1. B.P. Statistical Review of World Energy; British Petroleum: United Kingdom, 2005
2. Makogon, Y. F.; Holditch, S. A.; Makogon, T. Y. Natural gas-hydrates—A potential energy source for the 21st Century. *J. Petro. Sci. Eng.* **2007**, 56, 14-31.
3. BP Statistical Review of World Energy; British Petroleum: United Kingdom, 2016
4. International Energy Outlook; U.S. EIA: United States of America, 2016.
5. India Energy Outlook; IEA: India, 2015.
6. Boswell, R.; Collett, T. S. Current perspectives on gas hydrate resources. *Energy Environ Sci.* **2011**, 4, 1206-1215.
7. Sloan, E.D. Fundamental principles and applications of natural gas hydrates. *Nature* **2003**, 426, 353-363.
8. Sloan, E. D., Koh, C. A. Clathrate hydrates of natural gases; CRC press: New York, 2008.
9. Ripmeester, J. A.; John, S. T.; Ratcliffe, C. I.; Powell, B. M. A new clathrate hydrate structure. *Nature* 1987, 325, 135-136.
10. Ripmeester, J. A.; Ratcliffe, C. I.; Klug, D. D.; Tse, J. S. Molecular Perspectives on Structure and Dynamics in Clathrate Hydrates. In: Proceedings of the International Conference on Natural Gas Hydrates, 1994.
11. Arora, A.; Cameotra, S. S. Techniques for exploitation of gas hydrate (clathrates) an untapped resource of methane gas. *J. Microb. Biochem. Technol.* **2015**, 7:02.
12. Fire In The Ice, Vol. 13, Iss. 2; National Energy Technology Laboratory, U.S. Department of Energy: United States of America, 2013.

13. Kumar, A.; Bhattacharjee, G.; Kulkarni, B. D.; Kumar, R. Role of surfactants in promoting gas hydrate formation. *Ind. Eng. Chem. Res.* **2015a**, 54, 12217-12232.
14. Gayet, P.; Dicharry, C.; Marion, G.; Graciaa, A.; Lachaise, J.; Nesterov, A. Experimental determination of methane hydrate dissociation curve up to 55MPa by using a small amount of surfactant as hydrate promoter. *Chem. Eng. Sci.* **2005**, 60, 5751-5758.
15. Mori, Y. H. Recent advances in hydrate-based technologies for natural gas storage—a review. *J. Chem. Ind. Eng. (China)* **2003**, 54:1.
16. Linga, P.; Daraboina, N.; Ripmeester, J. A.; Englezos, P. Enhanced rate of gas hydrate formation in a fixed bed column filled with sand compared to a stirred vessel. *Chem. Eng. Sci.* **2012**, 68, 617-623.
17. Kumar, A.; Sakpal, T.; Bhattacharjee, G.; Kumar, A.; Kumar, R. Impact of H₂S impurity on carbon dioxide hydrate formation kinetics in fixed bed arrangements. *Ind. Eng. Chem. Res.* **2016b**, 55, 7964-7972.
18. Kalogerakis, N.; Jamaluddin, A. K. M.; Dholabhai, P. D.; Bishnoi, P. R. Effect of surfactants on hydrate formation kinetics. In: SPE international symposium on oilfield chemistry. Society of Petroleum Engineers, 1993.
19. Suradkar, Y. R.; Bhagwat, S. S. CMC Determination of an Odd Carbon Chain Surfactant (C₁₃E₂₀) Mixed with Other Surfactants Using a Spectrophotometric Technique. *J. Chem. Eng. Data* **2006**, 51, 2026-2031.
20. Shah, D. O. The World of Surface Science. In Chemical Engineering Education, Anderson, T. J., Ed.; American Society for Engineering Education: Washington, DC, 1977.
21. Vögtle, F. Supramolecular Chemistry; Wiley: Chichester, 1991.

22. Fuhrhop, J. H.; Koning, J. *Membranes and Molecular Assemblies: The Synkinetic Approach*; The Royal Society of Chemistry: Cambridge, UK, 1994.
23. Kutergin, O. B.; Mel'nikov, V. P.; Nesterov, A. N. Surfactant effect on the mechanism and kinetics of gas hydrate formation. *Doklady Acad. Sci.* **1992**, 323, 549-553.
24. Leporcher, E. M.; Peytavy, J. L.; Mollier, Y.; Sjoblom, J.; Labes-Carrier, C. Multiphase transportation: hydrate plugging prevention through crude oil natural surfactants. In: SPE Annual Technical Conference and Exhibition, New Orleans, LA, USA, 1998.
25. Lim, Y. A.; Babu, P.; Kumar, R.; Linga, P. Morphology of carbon dioxide–hydrogen–cyclopentane hydrates with or without sodium dodecyl sulfate. *Cryst. Growth Des.* **2013**, 13, 2047-2059.
26. Kumar, A.; Sakpal, T.; Linga, P.; Kumar, R. Enhanced carbon dioxide hydrate formation kinetics in a fixed bed reactor filled with metallic packing. *Chem. Eng. Sci.* **2015b**, 122, 78-85.
27. Karaaslan, U.; Parlaktuna, M. Surfactants as Hydrate Promoters? *Energy Fuels* **2000**, 14, 1103-1107.
28. Karaaslan, U.; Parlaktuna, M. PEO-A new hydrate inhibitor polymer. *Energy Fuels* **2002**, 16, 1387-1391.
29. Karaaslan, U.; Parlaktuna, M. Promotion Effect of Polymers and Surfactants on Hydrate Formation Rate. *Energy Fuels* **2002**, 16, 1413-1416.
30. Okutani, K.; Kuwabara, Y.; Mori, Y. H. Surfactant effects on hydrate formation in an unstirred gas/liquid system: An experimental study using methane and sodium alkyl sulfates. *Chem. Eng. Sci.* **2008**, 63, 183-194.
31. Yoslim, J.; Linga, P.; Englezos, P. Enhanced growth of methane propane clathrate hydrate crystals with sodium dodecylsulfate, sodium tetradecylsulfate, and sodium hexadecylsulfate surfactants. *J. Cryst. Growth* **2010**, 313, 68-80.

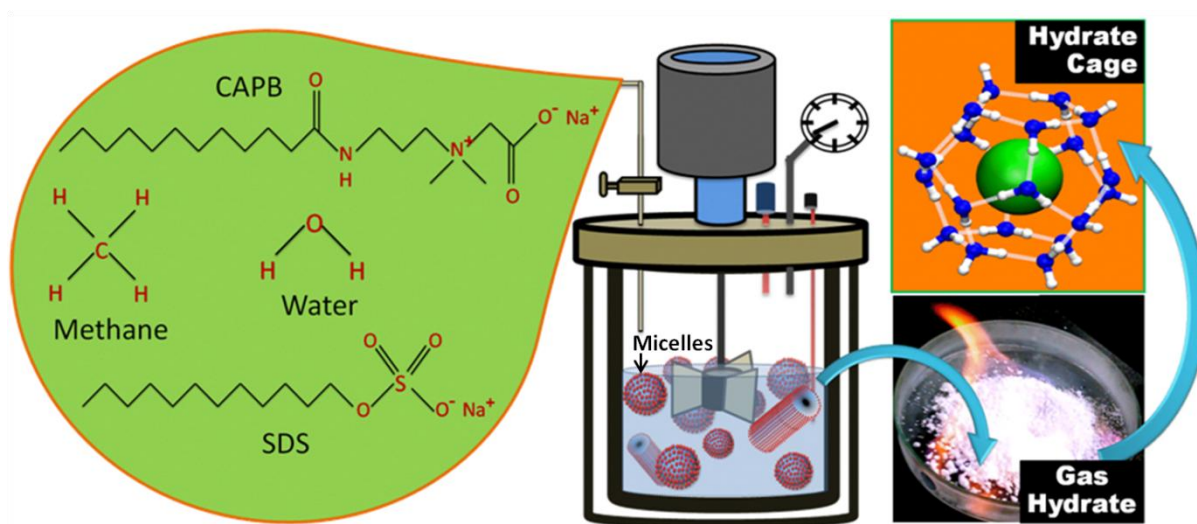
32. Kumar, A.; Sakpal, T.; Linga, P.; Kumar, R. Influence of contact medium and surfactants on carbon dioxide clathrate hydrate kinetics. *Fuel* **2013**, 105, 664-671.
33. Veluswamy, H. P.; Ang, W. J.; Zhao, D.; Linga, P. Influence of cationic and non-ionic surfactants on the kinetics of mixed hydrogen/tetrahydrofuran hydrates. *Chem. Eng. Sci.* **2015**, 132, 186-199.
34. Han, X.; Wang, S.; Chen, X.; Liu, F. Surfactant Accelerates Gas Hydrate Formation. In: 4th International Conference on Natural Gas Hydrates; Yokohama, Japan, 2002.
35. Link, D.; Ladner, E. P.; Elsen, H. A.; Taylor, C. E. Formation and Dissociation Studies for Optimizing the Uptake of Methane by Methane Hydrates. *Fluid Phase Equilib.* **2003**, 211, 1-10.
36. Zhang, J. S.; Lee, S.; Lee, J. W. Kinetics of Methane Hydrate Formation from SDS Solution. *Ind. Eng. Chem. Res.* **2007**, 46, 6353-6359.
37. Zhong, Y.; Rogers, R.E. Surfactant effects on gas hydrate formation. *Chem. Eng. Sci.* **2000**; 55, 4175-4187.
38. Kang, S. P.; Lee, J. W. Kinetic behaviors of CO₂ hydrates in porous media and effect of kinetic promoter on the formation kinetics. *Chem. Eng. Sci.* **2010**, 65, 1840-1845.
39. Mandal, A.; Laik, S. Effect of the Promoter on Gas Hydrate Formation and Dissociation. *Energy Fuels* **2008**, 22, 2527-2532.
40. Mori, Y. H. Comments on "Effect of Promoter on Gas Hydrate Formation and Dissociation" by Ajay Mandal and Sukumar Laik. *Energy Fuels* **2008**, 22, 4310-4311.
41. Ricaurte, M.; Dicharry, C.; Broseta, D.; Renaud, X.; Torr e, J. P. CO₂ removal from a CO₂-CH₄ gas mixture by clathrate hydrate formation using THF and SDS as water-soluble hydrate promoters. *Ind. Eng. Chem. Res.* **2012**, 52, 899-910.

-
42. Kumar, A.; Sakpal, T.; Linga, P.; Kumar, R. Impact of fly ash impurity on the hydrate based gas separation process for carbon dioxide capture from a flue gas mixture. *Ind. Eng. Chem. Res.* **2014**, *53*, 9849-9859.
 43. Zhong, D.L.; Ding, K.; Yan, J.; Yang, C.; Sun, D.J. Influence of cyclopentane and SDS on methane separation from coal mine gas by hydrate crystallization. *Energy Fuels* **2013**, *27*, 7252-7258.
 44. Sun, Z.; Wang, R.; Ma, R.; Guo, K.; Fan, S. S. Natural Gas Storage in Hydrate with the Presence of Promoters. *Energy Convers. Manage.* **2003**, *44*, 2733-2742.
 45. Zhang, J. S.; Lo, C.; Somasundaran, P.; Lee, J. W. Competitive adsorption between SDS and carbonate on tetrahydrofuran hydrates. *J. Colloid Interface Sci.* **2010**, *341*, 286-288.
 46. Li, S.; Fan, S.; Wang, J.; Lang, X.; Wang, Y. Clathrate Hydrate Capture of CO₂ from Simulated Flue Gas with Cyclopentane/Water Emulsion. *Chin. J. Chem. Eng.* **2010**, *20118*, 202-206.
 47. Liu, Y.; Chen, B.; Chen, Y.; Zhang, S.; Guo, W.; Cai, Y.; Tan, B.; Wang, W. Methane storage in a hydrated form as promoted by leucines for possible application to natural gas transportation and storage. *Energy Technol.* **2015**, *3*, 815-819.
 48. Veluswamy, H. P.; Hong, Q. W.; Linga, P. Morphology study of methane hydrate formation and dissociation in the presence of amino acid. *Cryst. Growth. Des.* **2016**, *16*, 5932-5945.
 49. Kurihara, M.; Ouchi, H.; Narita, H.; Masuda, Y. Gas production from methane hydrate reservoirs. In: Proceedings of the 7th International Conference on Gas Hydrates (ICGH), Edinburgh, UK, 2011.
 50. Lee, H.; Seo, Y.; Seo, Y. T.; Moudrakovski, I. L.; Ripmeester, J. A. Recovering methane from solid methane hydrate with carbon dioxide. *Angew. Chem. Int. Ed.* **2003**, *42*, 5048-5051.

51. Ota, M.; Saito, T.; Aida, T.; Watanabe, M.; Sato, Y.; Smith, R. L.; Inomata, H. Macro and microscopic CH₄-CO₂ replacement in CH₄ hydrate under pressurized CO₂. *AIChE J.* **2007**, *53*, 2715-2721.

Chapter 2

Effects of Micellization on Growth Kinetics of Methane Hydrate



2. Effects of Micellization on Growth Kinetics of Methane Hydrate²

²A version of this chapter has been published

Bhattacharjee, G.; Kushwaha, O. S.; Kumar, A.; Khan, M. Y.; Patel, J. N.; Kumar, R. Effects of Micellization on Growth Kinetics of Methane Hydrate. *Ind. Eng. Chem. Res.* 2017, 56, 3687-3698.

In the previous chapter, a comprehensive review of gas hydrates and the role of surfactants in gas hydrate studies were presented. This chapter deals with the use of surfactants as kinetic hydrate promoters with specific focus on enhancing the kinetics of methane hydrate formation. The study reported in this chapter uses a well-known additive SDS to enhance the kinetics of hydrate growth. A thorough work was carried out to understand the role of SDS in enhancing the gas hydrate kinetics. Carefully designed experiments try to understand the effects of micellization on the growth kinetics of methane hydrate. In the previous chapter, the different mechanisms through which surfactants may enhance hydrate formation kinetics were listed. One of the possible mechanisms mentioned was due to surfactant micelles acting as nucleation sites. It was also pointed out that the surfactant micelle hypothesis, although first proposed a long time ago, still requires concrete evidence to be accurately proven and as such is still subject to debate. It is quite clear that the surfactant micelle theory requires the formation of surfactant aggregates or micelles in the solution. The main roadblock for the surfactant micelle hypothesis was that the surfactant used in the studies that originally suggested and propagated the theory do not form micelles at hydrate forming conditions (the low hydrate formation temperatures being the bottleneck). Through our research, we have strived to develop a surfactant system capable of forming micelles at hydrate forming temperatures. The effects of the surfactant micelles on methane hydrate formation kinetics were then studied. Further, the efficacy of the newly developed surfactant mixture was tested on the kinetics and separation efficiency of hydrate formation from low concentration coal bed methane (CBM) gas mixture.

2.1. Introduction

Surfactants are specific functional materials that form various types of self assemblies and affect local water ordering alongside solution properties. Such surface active agents are used extensively in gas hydrate based applications as kinetic hydrate promoters. These include applications such as carbon dioxide capture and separation and methane storage (Kumar and Kumar, 2015; Wang et.al, 2014; Park et.al, 2011; Koh, 2002; Bhattacharjee et.al, 2016; Kumar et.al, 2016a; Komatsu et.al, 2015; Arora et.al, 2016; Kumar et.al, 2009; Veluswamy et.al,

2014; Kumar et.al, 2016b; Kumar et.al, 2016c). As has already been discussed in detail in the previous chapter, there are a number of different theories that have been put forward as to how surfactants may affect the kinetics of hydrate formation. One of these is commonly known as the surfactant micelle hypothesis and involves the formation of surfactant aggregates or micelles in the solution which act as preferred nucleation sites for gas hydrate formation thus promoting the kinetics of the process (Verret et.al, 2012; Kumar et.al, 2015a; Botimer et.al, 2016; Hayama et.al, 2016; Zhong and Rogers, 2000). However, it has also been suggested time and again that SDS molecules do not form micelles at gas hydrate formation conditions (Di Profio et.al, 2005; Zhang et.al, 2007a; Zhang et.al, 2007b). Micelles only form above a certain concentration (Critical Micelle Concentration (CMC)) and temperature (Krafft Point). The latter for SDS, at 282K is way above the temperatures at which gas hydrate formation studies are generally performed (Di Profio et.al, 2005; Vautier-Giongo and Bales, 2003; Israelachvili, 2011). Prajapati and Bhagwat, 2012, demonstrated that the Krafft point of SDS can be manipulated by adding a co-surfactant; one such surfactant is Cocoamidopropyl Betaine (CAPB) which is a zwitterionic surfactant obtained from coconut oil. 0.038 mole fraction of this surfactant reduces the Krafft point of SDS by one Kelvin (Prajapati and Bhagwat, 2012a). Moreover, addition of CAPB was found to reduce the CMC and the surface tension of SDS (Prajapati and Bhagwat, 2012b). It was assessed that if the Krafft point of SDS could be reduced up to the hydrate formation temperature by the addition of CAPB, the system would stand a very realistic chance of containing micelles which could then answer a number of questions regarding the kinetic promoting behaviour of surfactants on gas hydrate formation and whether the presence of micelles affects the same. Similar studies mapping the interaction between betaine type zwitterionic surfactants and anionic surfactants have also been performed highlighting the formation of mixed micelles in such systems (Iwasaki et.al, 1991). Additionally, literature suggests that the presence of surfactant micelles in solution would also enhance the solubility of gas in water (Bolden et.al, 1983; Roy et.al, 1997).

The hydrate based gas separation (HBGS) process is one of the unconventional processes that are currently being looked at to affect gas separation from different gas mixtures. The HBGS process is essentially a multistage hydrate formation and dissociation cycle which separates gases based on their feasibility to form hydrates, i.e. at a given temperature, one gas forms hydrates at moderate pressures than the other which results in the former gas getting trapped in the hydrate phase while the latter is now rich in the gaseous phase.

One of the gas mixtures that have been the recipient of extensive HBGS based research activity is the coal bed methane (CBM) mixture which is an unconventional source of natural gas associated with coal. The major components of CBM are usually nitrogen and methane with the nitrogen being the dominant gas in the mixture. CBM is primarily viewed as a hazard for underground coal workers as it poses a major risk of explosion and the possibility of an oxygen poor atmosphere (Flores, 1998; Moore, 2012). CBM gas that is released from coal mines is currently being used as a low energy fuel by power stations near coal mines while major efforts are being made to convert this low energy gas into a methane rich gas which is where the HBGS process comes into play. The equilibrium hydrate formation pressure for methane at a given temperature being much lower than that for nitrogen at the same temperature lends a sense of feasibility to the HBGS process for separating methane from CBM gas and the effectiveness of this process has been proven in previous studies available in the literature (Zhong and Englezos, 2012; Zhong et.al, 2013a; Sun et.al, 2012; Sun et.al, 2010; Zhang and Wu, 2010).

In the present study, a zwitterionic surfactant CAPB has been used in addition with SDS in a bid to reduce the Krafft temperature of SDS to as low as or lower than hydrate formation temperatures (275 K in the present case). This would allow the formation of surfactant micelles in the system, the effect of which on hydrate formation can then be analyzed. Dynamic Light Scattering (DLS) studies were performed to provide conclusive evidence of the formation of micelles at hydrate formation temperatures for the mixed (SDS-CAPB) surfactant system. The enhancement in solubility of methane, if any, in micellar solutions of surfactants as compared to that in pure water was also measured. Gas hydrate formation experiments were then carried out in the presence of the mixed surfactant system in order to study the effects of surfactant micelles on hydrate formation kinetics. Initially pure methane was used as the hydrate forming gas in a stirred tank reactor setup. The hydrate forming gas was then changed to a low concentration CBM mixture (30% CH₄+70% N₂). Methane hydrates were formed at 5.0 MPa and 275K pressure and temperature respectively whereas hydrates using the CBM mixture were formed at 3.5 MPa and 275K pressure and temperature respectively. As the CBM mixture forms hydrates at very high pressures (Zhong and Englezos, 2012; Zhong et.al, 2013a; Sun et.al, 2012; Sun et.al, 2010; Zhang and Wu, 2010), Tetrahydrofuran (THF) was used as a thermodynamic hydrate promoter for hydrate formation from the CBM mixture. The THF concentration was fixed at 5.56 mol% for all the

experiments conducted as this is the maximum possible concentration of THF that can be accommodated in a sII hydrate.

2.2. Experimental Section

2.2.1. Materials

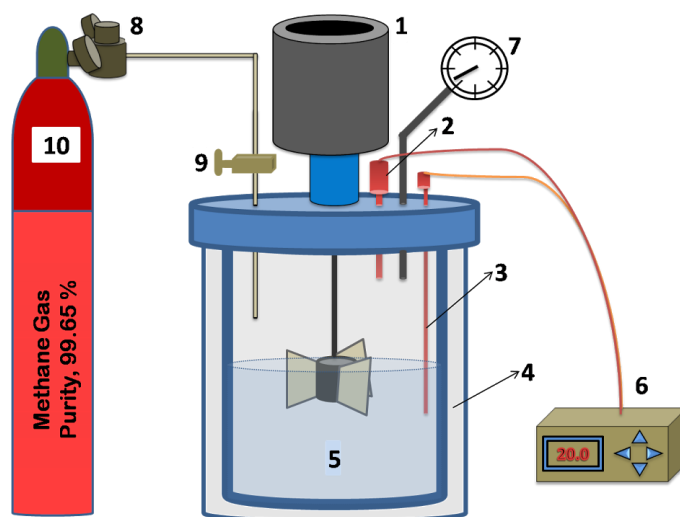
Structured stainless steel packing (SSP) was purchased from Lelesil, Mumbai, India. Sodium dodecyl sulfate (SDS) was purchased from Thermo Fischer Scientific Ltd., India. Cocoamidopropyl betaine (CAPB) was provided by Galaxy Surfactants Pvt. Ltd., India. Tetrahydrofuran (THF) was purchased from Tokyo Chemical Industries, Ltd., Japan. Methane gas with a purity of more than 99.5% and low concentration CBM gas mixture (30% CH₄+70% N₂) were purchased from Vadilal Gases Pvt. Ltd., India. Distilled and deionized water was used for all the experiments.

2.2.2. Procedure followed for carrying out Dynamic Light Scattering (DLS) studies

Individual stock solutions of concentration 10000 ppm were prepared for the two different surfactants, SDS and CAPB. NaCl (10 mM) was then added to each as a neutral electrolyte following which the stock solutions were filtered through a filter paper having pore size of 450 nm. The stock solutions were then sonicated for around twenty minutes and kept overnight to stabilize. The pure surfactant solutions were then mixed in volume fractions to make up 10 ml of mixed surfactant solutions. For example, 1ml of SDS was mixed with 9 ml of CAPB in order to obtain a mixed surfactant solution of SDS and CAPB with volume ratio of 1:9. 10 such surfactant mixtures were prepared with the range varying from (10 SDS: 0 CAPB) to (0 SDS: 10 CAPB). These mixed surfactant solutions were kept overnight at 275 K to stabilize. Around 2 ml of each solution was then loaded into disposable cuvettes to perform DLS studies. DLS studies were carried out in a Zetasizer NanoSeries Nano-Zs make dynamic light scattering instrument. The temperature of the sample holder in the DLS was set at 275K (hydrate forming temperature) for these experiments. The same procedure was followed for DLS measurements at 298K except that the mixed surfactant solutions were left to stabilize overnight at 298K and DLS studies were subsequently carried out at 298K. At least three readings were taken for each sample in order to calculate averages and standard deviations.

2.2.3. Apparatus used and procedure followed for carrying out solubility measurements

The solubility measurement experiments were performed in a 300 ml high pressure stirred tank reactor (Parr Instruments, USA). The reactor was fitted with a digital pressure transducer and data acquisition system to record the pressure drop due to solubility of gas in aqueous solution. In a typical solubility experiment, 200 ml of the liquid sample (aqueous solution) was loaded into the 300 ml high pressure reactor and kept undisturbed for 30 minutes in order for the system to reach thermal equilibrium (experiments were carried out at room temperature as even pure SDS can form micelles at room temperature). Methane gas from a reservoir was then passed to the reactor maintaining an approximate constant flow rate and time for the passage of gas (until the desired experimental pressure was reached). The dissolution of gas in aqueous solution was then facilitated by switching on a stirrer pre set to a value of ~1600 rpm. When the pressure inside the reactor reached a constant value, i.e. the pressure drop stopped, it was assumed that the liquid sample had been saturated with methane gas and the final pressure was noted down as the equilibrium pressure. The initial experimental pressure was systematically varied for each sample in order to find out the Henry's constants for methane in the different surfactant solutions being studied. A detailed schematic of the solubility setup has been given as Fig. 2.1.



- | | | |
|------------------------------|------------------------|--------------------|
| 1. Motor attached to stirrer | 2. Pressure Transducer | 3. Thermocouple |
| 4. Heating Mantle | 5. Liquid Sample | 6. Data Logger |
| 7. Analogue Pressure Gauge | 8. Gas Regulator | 9. Gas Inlet Valve |
| 10. Methane Gas Cylinder | | |

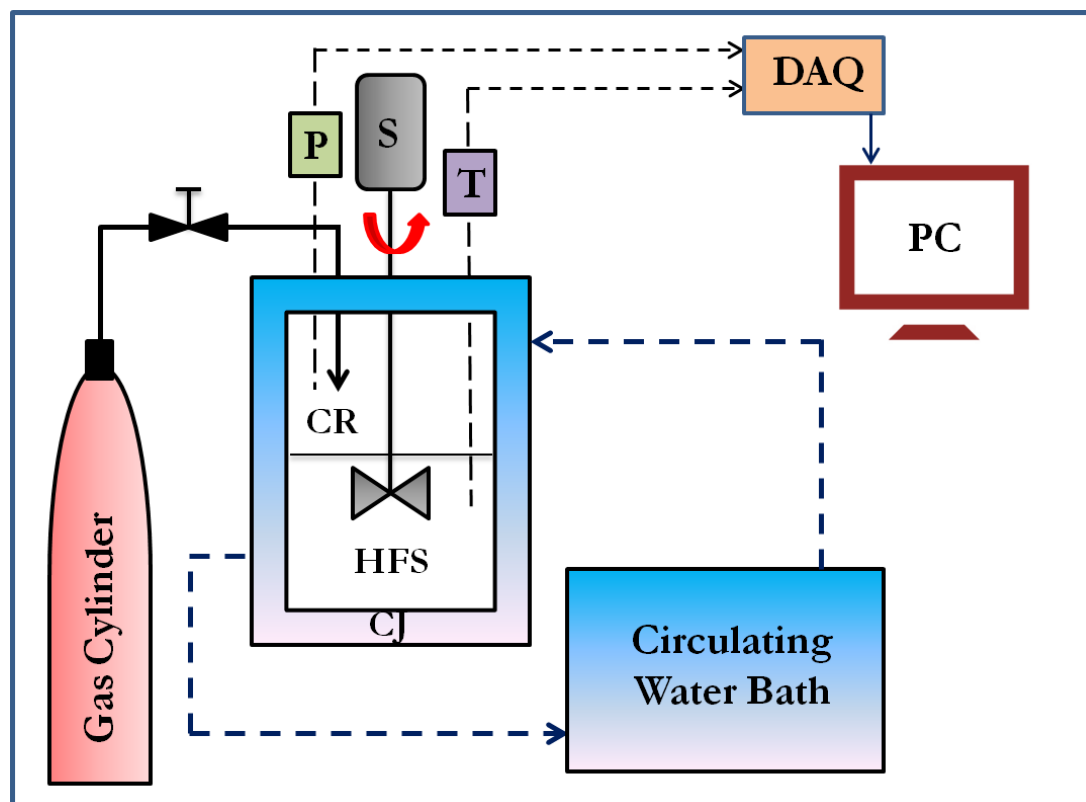
Fig. 2.1: Schematic of the solubility setup.

2.2.4. Apparatus used and procedure followed for hydrate formation experiments

Two different reactor configurations, a stirred tank reactor (STR) and a fixed bed reactor (FBR) were used in this study. Stainless steel packing (SSP) was used as the fixed bed medium. In line with part of the discussion in section 1.3.1 of the first chapter, the stainless steel packing with its high surface area for gas-liquid contact and high thermal conductivity is an ideal packing material for hydrate based technological applications. The procedure used for the hydrate formation experiments is briefly described below:

The STR and FBR used in the present study had total volumes of $\sim 250 \text{ cm}^3$ and $\sim 410 \text{ cm}^3$ respectively. First the aqueous hydrate forming solution with desired concentration of additives was loaded into the crystallizer ($\sim 100 \text{ cm}^3$ in case of STR and $\sim 62 \text{ cm}^3$ in case of FBR). The volume of water used was 80 cm^3 in case of STR and 50 cm^3 in case of FBR. Rest was THF. It is important to note here that in case of pure CH_4 , no THF was used and the total volume of the aqueous solution used in the STR was 80 cm^3 . Once the aqueous hydrate forming solution had been introduced into the crystallizer (CR) of choice, the CR was tightly sealed and placed inside a temperature controlled water bath so as to quickly attain the desired experimental temperature (275 K). The vessel was then flushed with the hydrate forming gas, pure CH_4 or low concentration CBM gas by repeating rapid pressurization ($\sim 0.5 \text{ MPa}$) and depressurization cycles. Next the CR was pressurized with the hydrate forming gas up to the desired hydrate formation pressure as would be required to provide sufficient driving force to initiate and sustain hydrate formation with the different gases being used (pure CH_4 and the low concentration CBM gas mixture). In case of the stirred tank reactor, as soon as the desired pressure was reached, the stirrer was turned on and set at 200 rpm while this step was not required in case of the fixed bed reactor. At this stage, gas uptake measurements were initiated. As the hydrate formation experiment proceeds, the pressure inside the reactor drops as a result of the hydrate forming gas moving from the gaseous phase to the solid hydrate phase. The pressure drop inside the CR was measured using a pressure transducer (WIKA make: 0-16 MPa in case of the STR and 0-25 MPa in case of the FBR) so as to calculate the number of moles of gas taking part in the hydrate formation process. Temperature and pressure inside the CR were recorded at regular intervals (every 5 seconds in case of the STR and every ten seconds in case of the FBR) using a data acquisition system (Micro Technics make) which was connected to a computer. Hydrate formation was assumed to be completed when no significant pressure drop (0.01 MPa) was observed for a long period of time, say thirty minutes. As the experiments were conducted entirely in batch mode, the effective

driving force for hydrate formation decreased as the reaction proceeded. This is a result of more and more gas migrating from the gaseous phase to the solid hydrate phase until there isn't sufficient pressure (driving force) left in the CR to sustain hydrate formation. Fig. 2.2 and 2.3 show schematics of the different setups used for the hydrate formation experiments.



P-Pressure Transducer	CR-Crystallizer	DAQ-Data Acquisition system
S-Stirrer	CJ-Crystallizer Jacket	PC-Personal Computer
T-Thermocouple	HFS-Hydrate Forming Solution	

Fig. 2.2: Detailed schematic of the stirred tank reactor setup for hydrate formation (Bhattacharjee et.al, 2016).

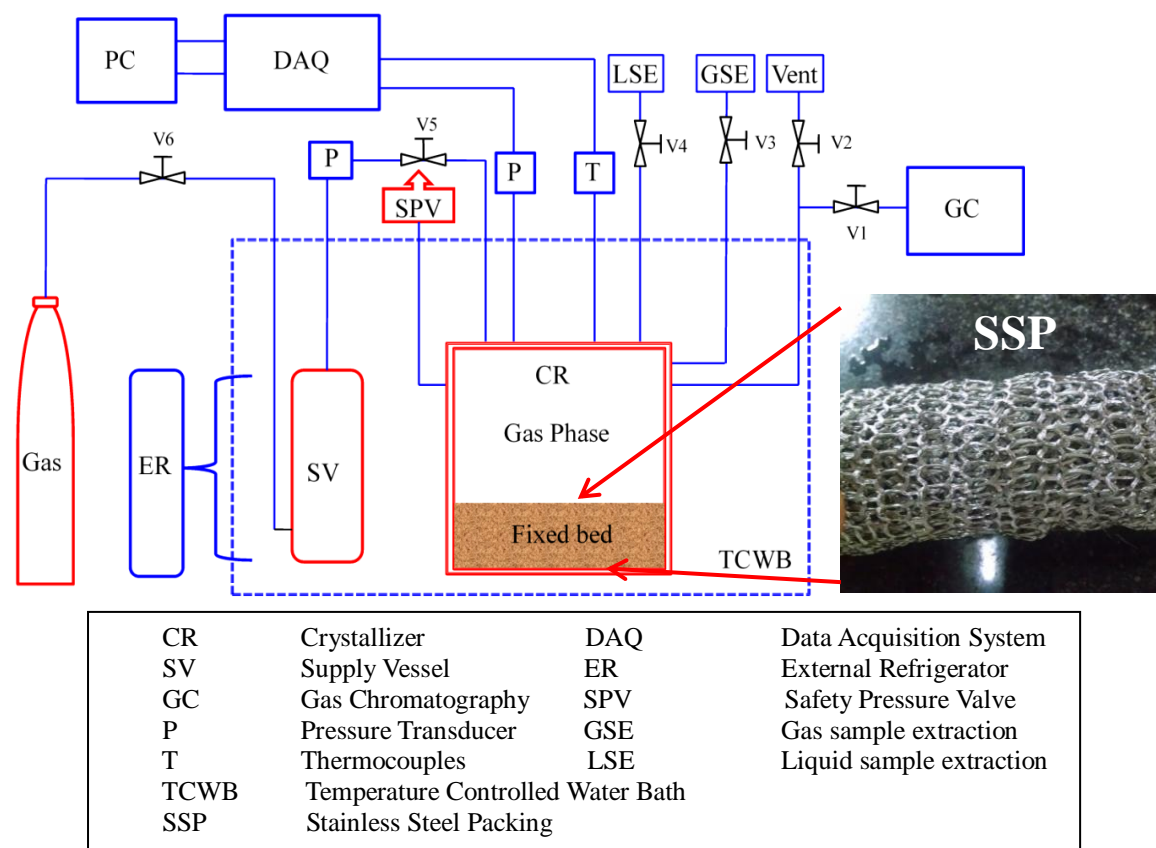


Fig. 2.3: Detailed schematic of the fixed bed reactor setup for hydrate formation (Kumar et.al, 2015b).

2.2.5. Procedure used for analysing the composition of the gas phase

Since the composition of the initial feed gas was already known, for the analysis of the gas phase, the unknown entities that were analysed were the gas phase at the end of every hydrate forming run and the gas phase inside the hydrate which was obtained after completely dissociating the formed hydrates. Once the gas phase samples had been collected (using a Tedler bag), a gas chromatograph instrument (Shimadzu make) was used to determine the compositions of the different gas phase samples.

2.2.6. Calculation of the solubility of gas in aqueous solution

The number of moles of methane dissolved in aqueous solution was calculated using the Redlich-Kwong equation of state (Smith et.al, 2004),

$$P = \frac{RT}{(V/n)-b} - \frac{a}{\sqrt{T}(V/n)(V/n+b)} \quad (2.1)$$

$$a = 0.42748 \frac{R^2 T_c^{2.5}}{P_c} \quad (2.2)$$

$$b = 0.08664 \frac{RT_c}{P_c} \quad (2.3)$$

where a is a constant (correction for attractive potential of molecules), b is a constant (correction for volume), T_c and P_c are the critical temperature and pressure of methane respectively, n is the number of moles gas, P is pressure, V is the volume of overhead gas, R is the Gas Constant and T is temperature.

Using this equation of state, the number of moles (n_1, n_2) at initial set pressure (P_1) and equilibrium pressure (P_2) were calculated.

The number of moles of gas dissolved in aqueous solution could be then calculated as [$\Delta n = n_1 - n_2$].

Once the number of moles of gas dissolved in aqueous solution is obtained, the solubility at the different equilibrium pressures can be calculated as,

$$\text{Solubility} = \frac{\Delta n}{\text{Volume of liquid}} \text{ moles/dm}^3 \quad (2.4)$$

Finally the solubility data at different pressures is fitted to obtain Henry's constants for methane in the different micellar solutions of surfactants expressed in (mol/ dm³.MPa).

2.2.7. Calculation of the amount of gas consumed during hydrate formation

The total number of moles of gas that was consumed in the hydrate formation process at any given time is the difference between the number of moles of gas present in the gas phase of the CR at time $t = 0$ and the number of moles of gas present in the gas phase of the CR at time $t = t$. The same is given by the following equation (Bhattacharjee et.al, 2015):

$$(\Delta n_{H,\downarrow})_t = V_{CR} \left[\frac{P}{zRT} \right]_0 - V_{CR} \left[\frac{P}{zRT} \right]_t \quad (2.5)$$

where z is the compressibility factor calculated by using Pitzer's correlation (Smith et.al, 2004), V_{CR} is the volume of the gas phase inside the crystallizer and P and T are the pressure and temperature of the crystallizer respectively.

2.2.8. Calculation of the Split Fraction and Separation Factor from gas phase analysis

The split fraction (S.Fr.) of CH₄ in the hydrate phase and the separation factor (S.F.) for hydrate formation from the CMM gas mixture were calculated as shown below (Sun et.al, 2012):

$$\text{Split Fraction (S. Fr. (\%))} = \frac{n_{CH_4}^H}{n_{CH_4}^F} \times 100 \quad (2.6)$$

$$\text{Separation Factor (S.F.)} = \frac{y_{CH_4}^H y_{N_2}^G}{y_{CH_4}^G y_{N_2}^H} \quad (2.7)$$

, where $n_{CH_4}^H$ and $n_{CH_4}^F$ are the total number of moles of methane present in the hydrate gas and feed gas streams respectively, $y_{CH_4}^H$ and $y_{CH_4}^G$ are the mole fractions of methane in the hydrate gas and residual gas streams respectively and $y_{N_2}^H$ and $y_{N_2}^G$ are the mole fractions of nitrogen in the hydrate gas and residual gas streams respectively. $n_{CH_4}^H$ and $n_{CH_4}^F$ were calculated as follows:

$$n_{CH_4}^H = y_{CH_4}^H n^H \quad (2.8)$$

$$n_{CH_4}^F = y_{CH_4}^F n^F \quad (2.9)$$

, where n^H and n^F are the total number of moles of the hydrate and feed gases respectively which was calculated from the pressure drop data. The total number of moles of feed gas was the initial number of moles present in the system before the start of hydrate formation, i.e. induction and the total number of moles of hydrate gas was the total number of moles of gas that had participated in the formation of hydrate as calculated using equation 2.5 (total number of moles of feed gas minus the total number of moles of residual gas).

2.3. Results and Discussions

2.3.1. Determination of the presence of surfactant micelles at hydrate forming temperature using dynamic light scattering experiments (DLS)

Figures 2.4(a) and (b) and 2.5(a) and (b) show Dynamic Light Scattering (DLS) data for different surfactant solutions; pure SDS, pure CAPB and SDS-CAPB mixed in different volume fractions. DLS data is shown at two different temperatures, 298K (where pure SDS forms micelles; Fig 2.4(a) and (b)) and 275K (hydrate formation temperature; Fig 2.5(a) and (b)) where pure SDS does not form micelles. As can be clearly seen, at 275K, initially SDS does not form micelles but on the addition of an adequate amount of CAPB to the system

(SDS: CAPB volumetric ratio 7:3), the resultant surfactant solution begins to form micelles which is sustained as more and more CAPB is added to the solution). Thus it can be concluded that the addition of the zwitterionic surfactant CAPB to the system allows SDS to form micelles at hydrate formation conditions. It now remains to be seen whether the presence of these micelles in the system has any effect on the kinetics of hydrate formation as has been suggested multiple times in the literature (Kumar et.al, 2015a; Zhong and Rogers, 2000).

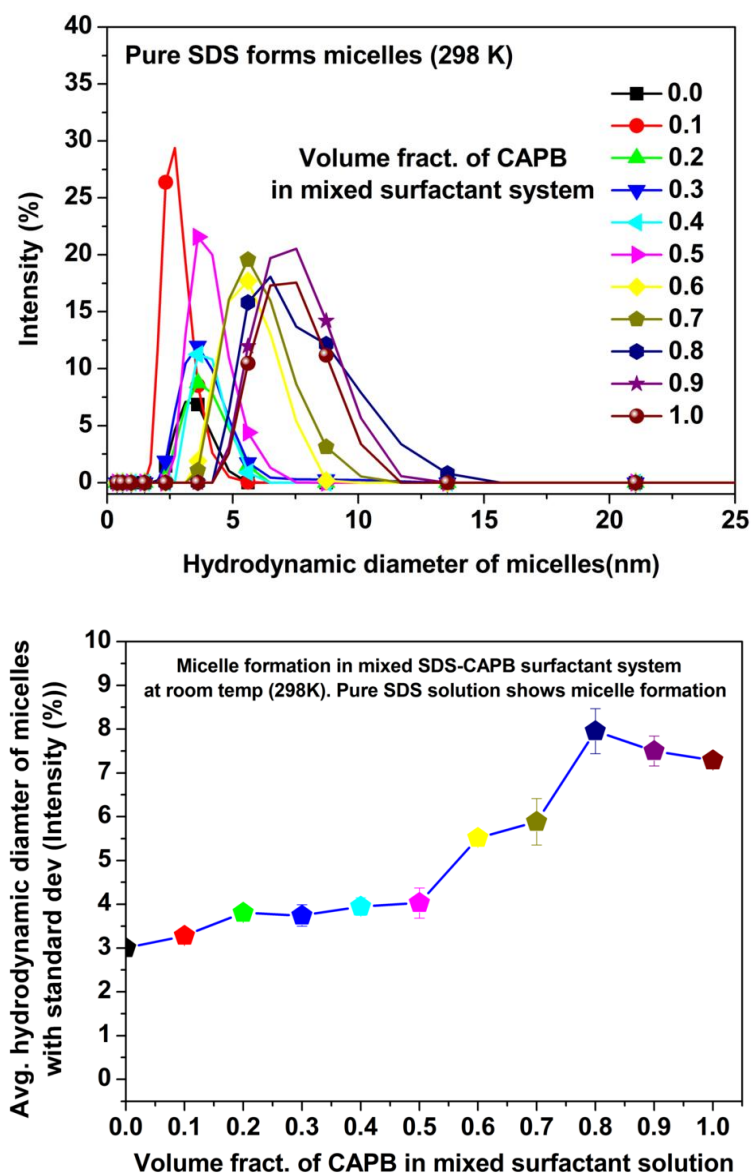


Fig. 2.4(a) and (b): Micelle formation in mixed SDS-CAPB surfactant system at 298 K. Micelle formation occurs even for pure SDS solution at 298 K. The size of the micelles increases with increase in concentration of CAPB.

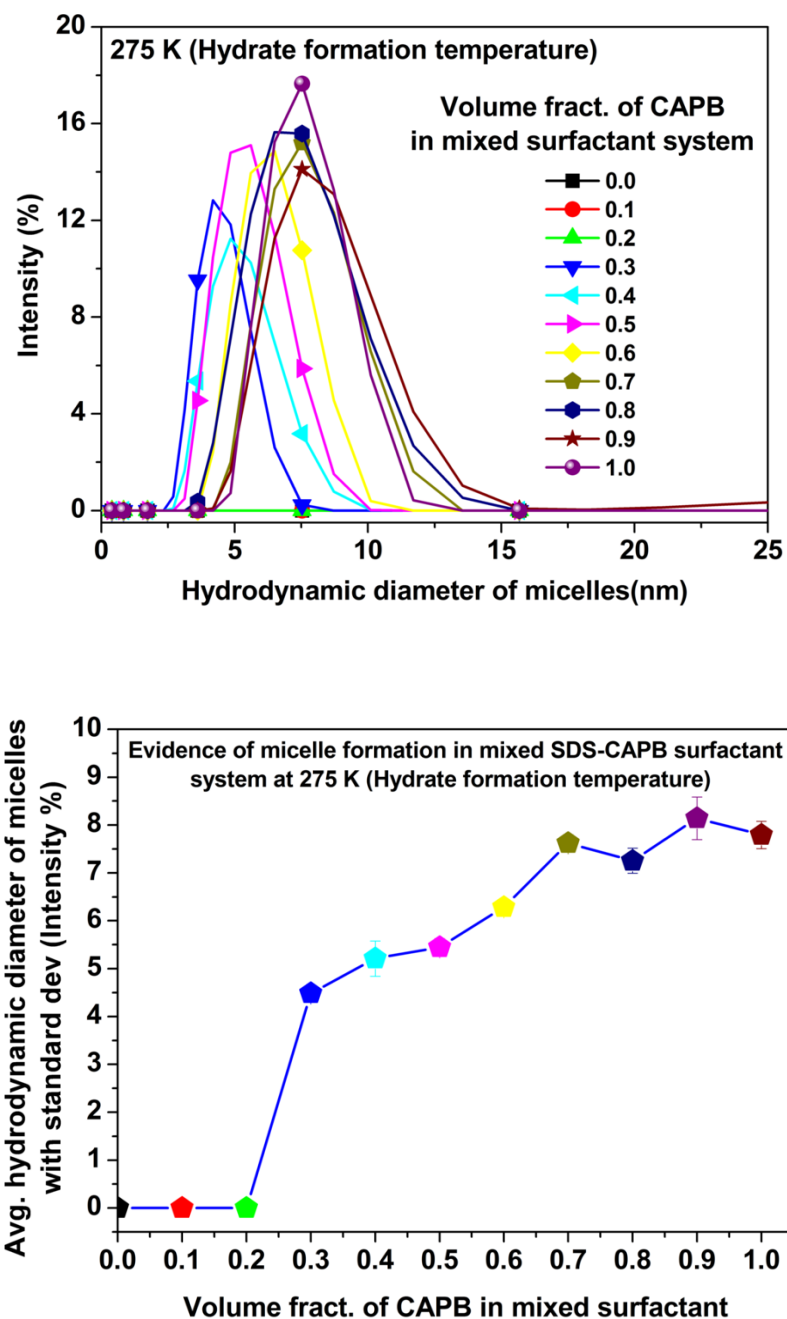


Fig. 2.5(a) and (b): Micelle formation in mixed SDS-CAPB surfactant system at 275 K. No micelle formation for pure SDS solution. Micelles begin to form when SDS and CAPB are mixed in volumetric ratio 7:3. The size of the micelles increases with increase in concentration of CAPB.

2.3.2. Enhancement in solubility of methane in micellar solutions of surfactants

The solubility of methane in distilled water and different solutions of SDS and CAPB in water was determined experimentally using the pressure drop method. The pressure drop method estimates the number of moles dissolved in solution from the pressure difference between the initial and equilibrium pressures (pressure when the liquid is completely saturated with gas). All the experiments were conducted at room temperature (33 °C). Validation of the present method used for determining solubility was done by comparison with already published experimental data for solubility of methane in water at 33 °C. The same can be seen in Fig. 2.6. As is clear from the figure, the experimental data obtained in the present study is a good fit with the data published in the study by Duan and Mao, 2006 (Duan and Mao, 2006) Fig. 2.7 compares the solubility of methane in water with that in the different aqueous surfactant solutions with respect to increasing initial pressure. As is expected, the solubility of methane in aqueous solution increases with increasing initial pressure of methane. It can also be seen from Fig. 2.7 that the solubility of methane in all three surfactant solutions studied, while more than that in water remains largely constant. In fact there is no way of separating the three surfactant systems in terms of increased solubility of methane as compared to that in pure water. Table 2.1 lists the calculated Henry's constants for methane in pure water and the different aqueous solutions used in this study. As can be seen in Table 2.1, the Henry's constant for methane increases in the different solutions of SDS and CAPB as compared to pure water thus indicating an enhanced solubility of methane in micellar solutions of surfactants. The results obtained in the present study are in good agreement with those reported in previous studies carried out by Bolden et.al., 1982 and Roy et.al, 1997 (Bolden et.al, 1982; Roy et.al, 1997). This enhanced solubility of methane in micellar solutions of surfactants may also play a hand in enhancing the kinetics of hydrate formation using surfactants or surfactant mixtures which are capable of forming micelles at hydrate formation temperatures and has been discussed later in the manuscript.

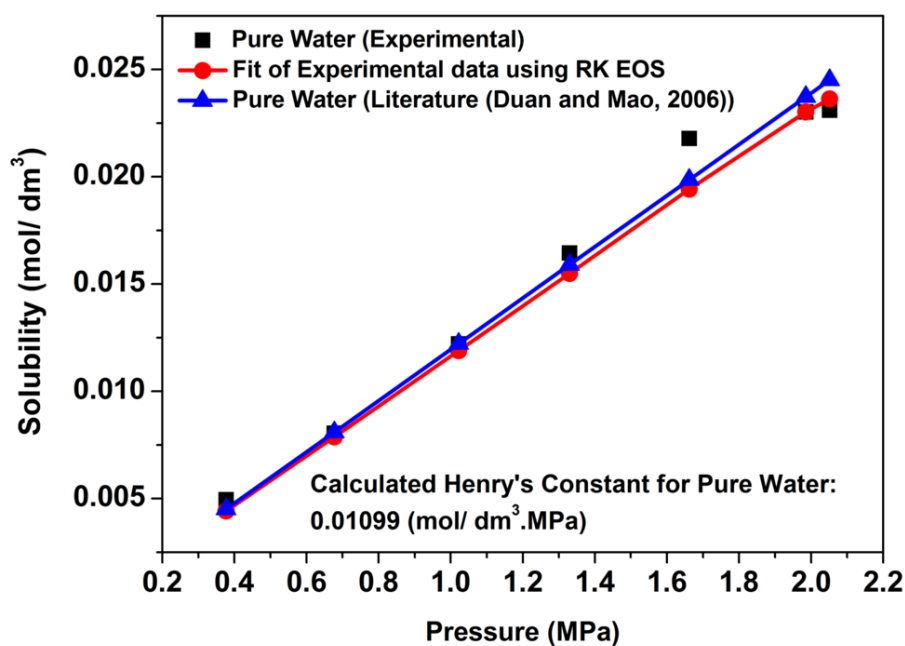


Fig. 2.6: Solubility of methane in distilled water at 33 °C using the current method and comparison with literature data (Duan and Mao, 2006).

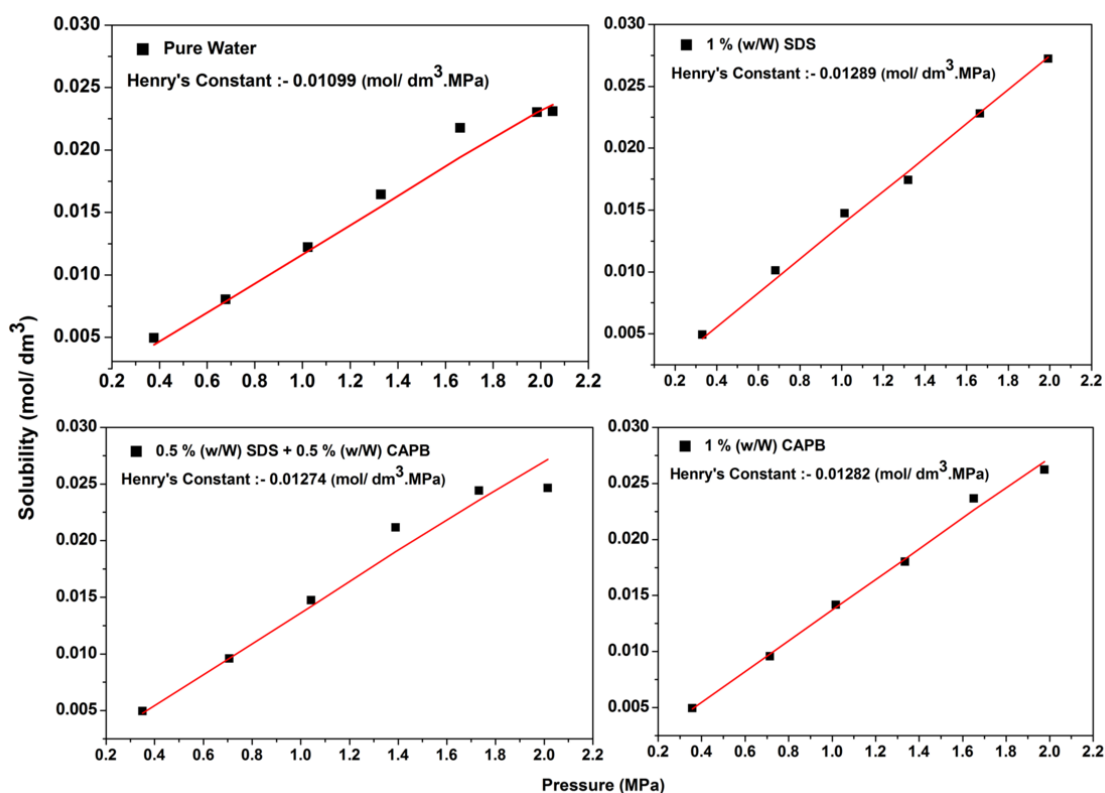


Fig. 2.7: Comparison of solubility of methane in different micellar solutions of surfactants and in pure water at 33 °C.

Table 2.1: Solubility (Henry's Constant) of methane in pure water and in the different surfactant solutions used in the present study.

System	Henry's Constant (mol/ dm ³ .MPa)
Pure Water	0.01099
1 wt% SDS	0.01289
1 wt% CAPB	0.01282
0.5 wt% SDS + 0.5 wt% CAPB	0.01274

2.3.3. Hydrate formation kinetics in presence of surfactants

Having successfully managed to synthesize surfactant micelles at hydrate formation conditions and established that the solubility of methane is enhanced in micellar solutions of surfactants, it remains to be seen whether the surfactant micelles indeed have any effect on hydrate formation kinetics. Tables 2.2 and 2.3 give a summary of all the experiments performed in the course of this study. Relevant data such as the sample state, initial hydrate formation pressure, run time of each experiment, amount of gas consumed at the end of each experiment (mol of gas consumed/ mol of water) and the induction time for hydrate formation in each experiment have been reported. Table 2.2 lists the data for all experiments performed using pure methane while Table 2.3 does the same for experiments performed using the CBM gas mixture.

Table 2.2: Summary of all the experiments conducted with pure methane gas. Relevant data such as the sample state, initial hydrate formation pressure, run time of each experiment, amount of gas consumed at the end of each experiment (mol of gas consumed/ mol of water) and the induction time for hydrate formation in each experiment have been reported. The hydrate formation temperature was kept constant (275.15K) for all the systems.

System	Reactor Configuration	Exp No.	Sample State	Initial Pressure (MPa)	Run Time (h)	Gas Uptake (mol of gas cons/ mol of water)	Induction Time (min)
Pure Water/CH ₄	STR	1	Fresh	5.0	1	0.013	0.240
		2				0.005	0.240
		3				0.015	0.333
1 wt % SDS/CH ₄	STR	4	Fresh	5.0	1	0.023	1194.000
		5				0.029	12.000
		6				0.019	10.200
		7				0.022	15.240
1 wt % CAPB/CH ₄	STR	8	Fresh	5.0	1	0.020	7.500
		9				0.030	0.166
		10				0.023	14.446
		11				0.017	145.500
0.5 wt % SDS + 0.5 wt% CAPB/CH ₄ (micelles)	STR	12	Fresh	5.0	1	0.031	1.800
		13				0.031	1.500
		14				0.034	9.360
0.8 wt % SDS + 0.2 wt% CAPB/CH ₄ (no micelles)	STR	15	Fresh	5.0	1	0.026	252.24
		16				0.020	9.078
		17				0.020	25.680

Table 2.3: Summary of all the experiments conducted with the CBM gas mixture. Relevant data such as the sample state, initial hydrate formation pressure, run time of each experiment, amount of gas consumed at the end of each experiment (mol of gas consumed/ mol of water) and the induction time for hydrate formation in each experiment have been reported. The hydrate formation temperature was kept constant (275.15K) for all the systems if not otherwise denoted by *.

System	Reactor Configuration	Exp No.	Sample State	Initial Pressure (MPa)	Run Time (h)	Gas Uptake (mol of gas cons/ mol of water)	Induction Time (min)
Pure Water/ CBM*	STR	18	Fresh	9.2	0.5	0.001	12.246
		19				0.002	1.080
1 wt % SDS/ 5.56 mol% THF/ CBM	STR	20	Fresh	3.5	0.5	0.020	0.416
		21				0.016	1.000
		22				0.017	0.250
		23				0.018	1.166
1 wt% CAPB/ 5.56 mol% THF/ CBM	STR	24	Fresh	3.5	0.5	0.022	0.250
		25				0.018	0.917
		26				0.018	3.833
0.5 wt% SDS/ 0.5 wt% CAPB/ 5.56 mol% THF/ CBM	STR	27	Fresh	3.5	0.5	0.020	0.083
		28				0.017	3.750
		29				0.018	0.083
Pure Water/ CBM*	FBR	30	Fresh	9.0	35	**NN	-
		31		9.5	25	**NN	-
1 wt% SDS/ 5.56 mol% THF/ CBM	FBR	32	Fresh	3.5	1	0.039	1.830
		33	Fresh			0.033	1.830
		34	Repeat			0.033	1.332
1 wt% CAPB/ 5.6 mol% THF/ CBM	FBR	35	Fresh	3.5	1	0.036	1.500
		36	Fresh			0.033	0.500
		37	Repeat			0.034	2.664
		38	Repeat			0.033	1.666

0.5 wt% SDS/ 0.5 wt% CAPB/ 5.56 mol% THF/ CBM	FBR	39	Fresh	3.5	1	0.032	1.332
		40	Fresh			0.035	22.500
		41	Repeat			0.032	0.166
		42	Repeat			0.032	25.980
5.56 mol% THF/ CBM	FBR	43	Fresh	3.5	1	0.026	23.250
		44	Fresh			0.036	50.333

*For these systems, hydrate formation temperature was 273.15K

**NN: Not Nucleated

2.3.3.1. Hydrate formation in stirred tank reactor

A stirred tank reactor was used initially to gauge the effect of introducing CAPB into the system. It was decided to first use pure methane gas to test the hypothesis. It has already been shown that the presence of surfactant micelles in the system increases the solubility of gas in water which, as such, should contribute to enhancing the kinetics of hydrate formation. The hydrate formation temperature for these experiments was set at 275.15 K and the initial pressure was 5.0 MPa which provides sufficient driving force for hydrate formation. The concentration of CAPB in the aqueous hydrate forming solution was adjusted such that in one case, no micelles would be present in the system (0.8 wt% SDS + 0.2 wt% CAPB) whereas in another case, micelle formation would have taken place (0.5 wt% SDS + 0.5 wt% CAPB). Apart from these, hydrates were also formed from pure water, 1 wt% SDS and 1 wt% CAPB solutions and hydrate formation kinetics for all the different systems were compared. Fig. 2.8 compares the average gas uptake and standard deviation (mol of gas consumed/ mol of water) obtained for methane hydrate formation with the different surfactant solutions used. Gas uptake has been shown for one hour from hydrate nucleation. Time zero corresponds to induction time for all the experiments conducted. As can be seen in Fig. 2.8, the introduction of CAPB into the system enhances methane hydrate formation kinetics with the micelle forming (0.5 wt % SDS + 0.5 wt % CAPB) system in particular showing a very interesting synergistic effect. Out of all the systems studied, the enhancement in hydrate formation kinetics was maximum with the 0.5 wt% SDS + 0.5 wt% CAPB system telling us the presence of micelles and enhanced solubility of methane in micellar solutions of surfactants may in fact have some effect on hydrate formation kinetics. The system which contained CAPB in association with SDS but not in enough concentration that it would allow formation of micelles too enhanced hydrate formation kinetics as compared to pure water but the kinetics was largely same when compared to the 1 wt% SDS system. There was a slight

increase in the initial kinetics which may be down to the fact that the addition of CAPB lowers the surface tension of the system allowing greater diffusivity of the gas initially (Prajapati and Bhagwat, 2012b). The 1 wt% CAPB system too showed kinetics akin to that for the 1 wt% SDS system with a considerable enhancement in the same when compared to pure water. Thus, to sum up, when using pure methane as the hydrate forming gas, maximum enhancement in growth kinetics was observed with the (0.5 wt% SDS + 0.5 wt% CAPB) system with the other three systems following close behind (the kinetics obtained for the latter three systems being too close to each other to confidently place them in an order).

Figure A1 in Appendix A shows a linear fit of the first twenty minutes of hydrate growth in the STR setup with pure methane for the different systems studied. The average initial apparent rates of hydrate formation for the first twenty minutes of hydrate growth (mol of gas consumed/h) obtained for the different systems as a result of the linear fitting have been reported in Table A1, Appendix A.

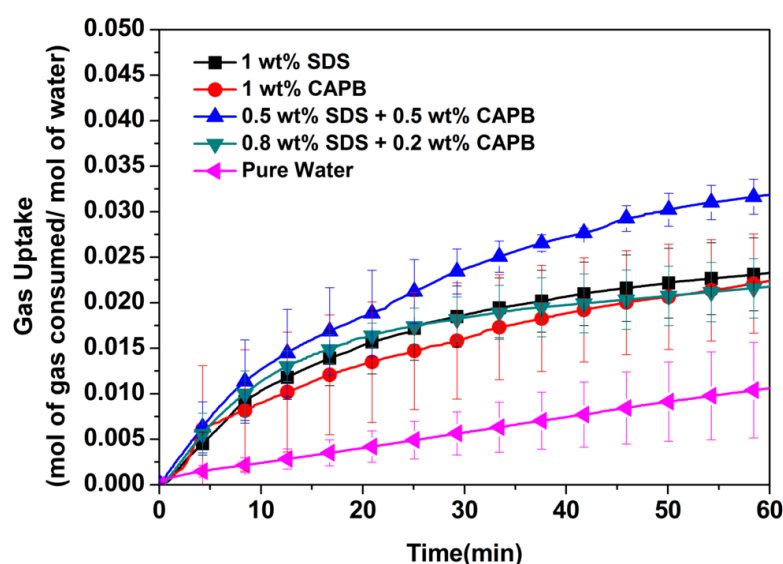


Fig. 2.8: Comparison of the gas uptake obtained for pure methane gas with different surfactant solutions and pure water. Gas uptake has been shown for one hour from the start of hydrate formation. STR configuration was used.

After the results using pure CH_4 were validated multiple times, it was decided to test the efficacy of the new surfactant mixture on hydrate formation from a gas mixture. A low concentration coal bed gas mixture (30% CH_4 and 70% N_2) was used with the objective of separating CH_4 from the gas mixture through hydrate crystallization, the hydrate based gas separation (HBGS) process. Since this gas mixture forms hydrates at a considerably high pressure, equilibrium pressure of 7.912 MPa at 275.15 K as predicted by CSMHYD, it was

decided to use a thermodynamic promoter, Tetrahydrofuran (THF) to lower the hydrate equilibrium pressure. Accordingly the temperature and pressure for hydrate formation were set at 275.15 K and 3.5 MPa respectively. A fixed concentration of THF (5.56 mol%) was used for all the experiments as this is the maximum amount of THF that would be required to fully occupy the large cages of sII hydrate. For the case of pure water, no THF was used and hence the temperature and pressure for hydrate formation were set at 273.15 K and 9.2 MPa respectively (experiments 18 and 19) (refer Table 3). Fig. 2.9 given below plots the average gas uptake and standard deviation (mol of gas/ mol of water) versus time during hydrate formation for the different systems studied using the low conc. CBM gas mixture. Gas uptake data has been reported for a fixed time of 30 minutes from the onset of hydrate formation. Time zero corresponds to induction time for all the experiments considered. Just as was observed with pure methane gas, the 0.5 wt% SDS + 0.5 wt% CAPB mixture shows the fastest hydrate formation kinetics with the CBM gas closely followed by the 1 wt% CAPB and 1 wt% SDS systems respectively. According to the knowledge that has been gathered up till now, this synergistic effect (enhancement in hydrate formation kinetics) observed when mixing SDS and CAPB together stems from at least a couple of factors: a) micelle formation at appropriate concentration of CAPB and at hydrate formation temperature which enhances the solubility of gas in water and b) reduced surface tension in presence of CAPB which enhances diffusion of gas in the hydrate forming solution.

Figure A2 in Appendix A shows a linear fit of the first twenty minutes of hydrate growth in the STR setup with the CBM gas mixture for the different systems studied. The average initial apparent rates of hydrate formation for the first twenty minutes of hydrate growth (mol of gas consumed/h) obtained for the different systems as a result of the linear fitting have been reported in Table A1, Appendix A.

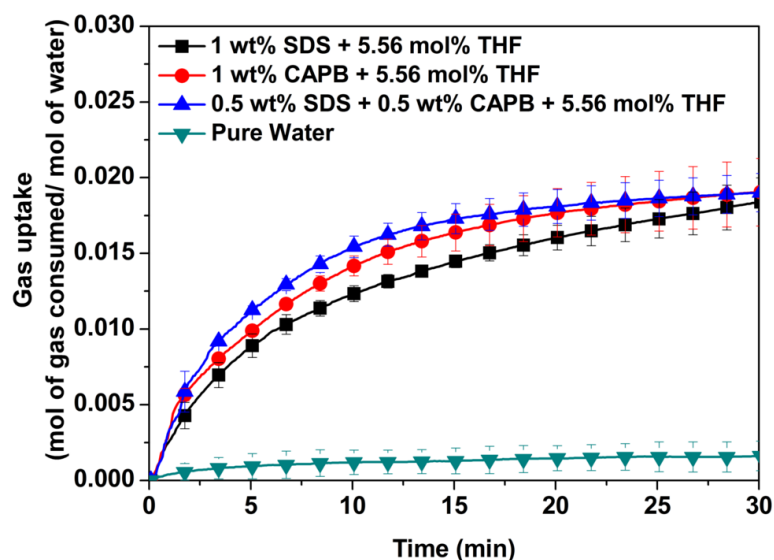


Fig. 2.9: Comparison of the gas uptake obtained for CBM gas mixture with different surfactant solutions in conjunction with THF and with pure water (without the presence of any additives in the system). Gas uptake has been shown for thirty minutes from the start of hydrate formation. STR configuration was used.

2.3.3.2. Hydrate formation in fixed bed reactor using Stainless Steel Packing and low concentration CBM gas in presence of surfactants

Following the results obtained from experiments conducted in the stirred tank reactor setup, it was decided to further test the effectiveness of the new surfactant solution by using it in a fixed bed setup. Stainless steel packing which was first reported by our group in a previous work was used as the fixed bed medium (Kumar et.al, 2015b). Low concentration CBM gas was used as the hydrate forming gas for the experiments carried out in the FBR. THF was used as a thermodynamic promoter (fixed quantity of 5.56 mol% as discussed above) which allowed for a somewhat mild initial operating pressure (3.5 MPa) for all the experiments conducted. 70 gm of SSP, 50 cm³ of water and ~11 cm³ of THF were used for these experiments thus leaving a gaseous volume of 350 cm³ in our reactor which had a total volume of ~410 cm³. For the systems containing THF, the temperature and pressure for hydrate formation were set at 275.15 K and 3.5 MPa respectively. For the pure water system which did not contain any additives, the temperature for hydrate formation was 273.15 K and the initial pressure was varied, 9.0 MPa for experiment no. 30 (refer Table 2.3) and 9.5 MPa for experiment no. 31 (refer Table 2.3) respectively. Average gas uptake and standard deviation (mol of gas consumed/ mol of water) has been plotted with respect to time in Fig. 2.10. Gas uptake has been shown for a fixed time of thirty minutes from the onset of hydrate

formation. Time zero in the figure corresponds to induction time for all the different systems studied. As can be seen in Fig. 2.10, hydrate formation kinetics is drastically enhanced in the presence of different additives in the system as compared to pure water which doesn't show any hydrate formation even after the systems were left undisturbed for more than 25 hours (as a result, gas uptake for the runs with pure water hasn't been plotted in Fig. 2.10). There is also a pronounced enhancement in kinetics with these systems as compared to the system which contains only THF and no kinetic promoters. However, there is nothing but a negligible difference in hydrate formation kinetics between the 1 wt% SDS, 1 wt% CAPB and 0.5 wt% SDS + 0.5 wt% CAPB systems. This leads us to the conclusion that the enhanced solubility of methane in the hydrate forming solution in presence of CAPB and the enhanced diffusion of methane in the system that had been discussed before do not hold much ground in case of the fixed bed system. What is more interesting to note here though is that a final gas uptake of around 0.035 mol of gas/ mol of water was obtained within 1 hour using the 1 wt% SDS and 0.5 wt% SDS + 0.5 wt% CAPB systems. This is comparably one of the highest values of gas uptake that has been achieved for hydrate formation using a low concentration CBM gas which is all the more significant because it was achieved within 30 minutes of hydrate growth. An illustration of the same is given as Fig. 2.11.

Figure A3 in Appendix A shows a linear fit of the first twenty minutes of hydrate growth in the FBR setup with pure methane for the different systems studied. The average initial apparent rates of hydrate formation for the first twenty minutes of hydrate growth (mol of gas consumed/h) obtained for the different systems as a result of the linear fitting have been reported in Table A1, Appendix A.

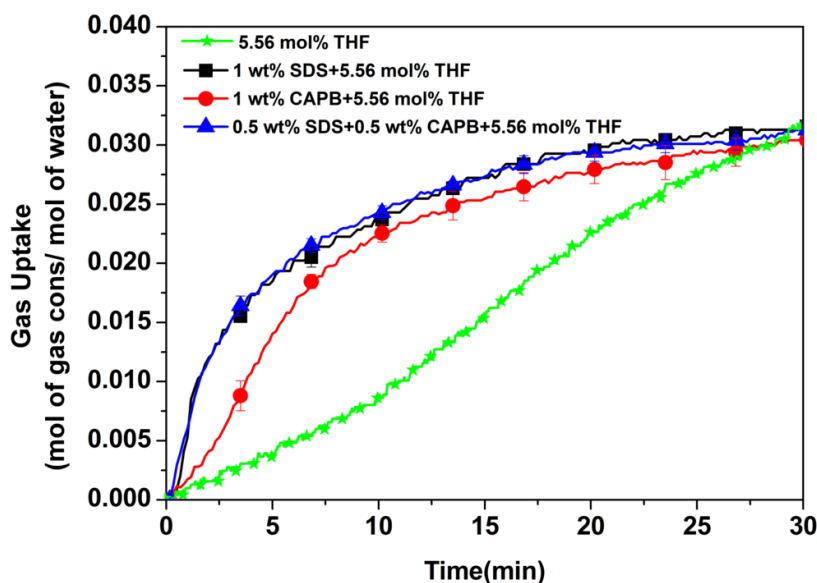


Fig. 2.10: Comparison of the gas uptake obtained for CBM gas mixture with different surfactant solutions in conjunction with THF and with only THF. Gas uptake has been shown for a fixed time of thirty minutes from the start of hydrate formation. FBR configuration was used. No nucleation of hydrates could be observed with pure water and CBM gas, i.e. without the presence of any additives.

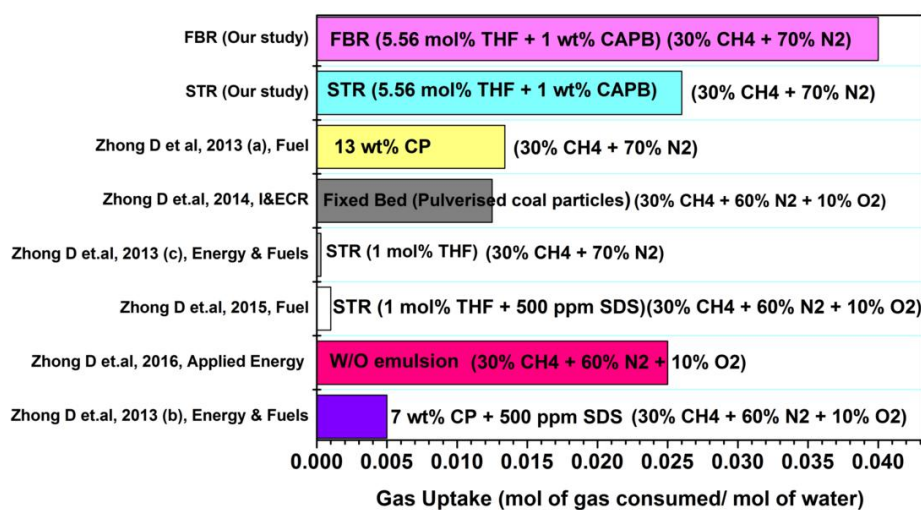


Fig. 2.11: Comparison of final gas uptake (mol of gas consumed/ mol of water) obtained in present study with data already reported in literature for different CBM gas mixtures. Only the maximum values obtained in each of these studies have been compared (Zhong et.al, 2013a; Zhong et.al, 2013b; Zhong et.al, 2013c; Zhong et.al, 2015; Zhong et.al, 2016; Zhong et.al, 2014).

2.3.6. Gas phase analysis: split fraction of CH₄ in hydrate gas and separation factor

It is known that the 30% CH₄-70% N₂ gas mixture used in the present study forms structure II hydrates with pure water (Sloan and Koh, 2008). In such a case, it would be CH₄ which would be occupying the 5¹²6⁴ large cages. When THF is introduced into the system, THF readily occupies the large cages leaving the methane and nitrogen molecules to compete for the small cages. Methane as a result of being able to form hydrates more easily than nitrogen (at lower pressures) enters the small cages faster than its competitor leading to its separation from the CMM gas mixture.

Results obtained from the gas phase analysis have been tabulated in Table 2.4. From the experimental data in Table 2.4, it can be seen that the low concentration CMM gas mixture used in this study can be separated to a certain extent using our different combinations of thermodynamic and kinetic hydrate promoters. For the three such combinations used in the present study, the combination of 5.56 mol% THF and 1 wt% CAPB proved to be the most effective in separating CH₄ from the feed gas mixture returning a maximum split fraction (%) of ~70% followed by the 5.56 mol% THF and 0.5 wt% SDS + 0.5 wt% CAPB and 5.56 mol% THF and 1 wt% SDS combinations which returned maximum split fractions of ~60% and ~53% respectively. The same trend was observed for both the types of reactor configurations used in this study. The split fraction and separation factor were both higher in case of the STR as compared to the FBR even though the final gas uptake obtained (mol of gas consumed/ mol of water) was higher for the FBR (just shy of double that for the STR). This is because in the case of the FBR, the gas phase had a much larger volume available as compared to the STR (350 cm³ for the FBR and 150 cm³ for the STR) and the volume of water used was also less as compared to the STR (50 cm³ and 80 cm³ for the FBR and STR respectively). The former resulted in higher final gas uptake in case of the FBR while the latter affected the amount of THF used for the two systems.

Table 2.4: Split Fraction (%) of CH₄ in hydrate phase and Separation Factor obtained via gas phase analysis.

System		Split Fraction	Separation Factor
STR: CMM Gas	1 wt% SDS	52.342	2.762
	1 wt% CAPB	69.154	3.034
	0.5 wt% SDS+0.5 wt% CAPB	59.780	2.882
FBR (SSP): CMM Gas	1 wt% SDS	26.387	2.130
	1 wt% CAPB	32.550	2.612
	0.5 wt% SDS+0.5 wt% CAPB	28.0237	2.270

2.4. Conclusions

Surfactant micelles were synthesized at hydrate forming temperature (275 K) by the addition of a small amount of zwitterionic surfactant CAPB to the anionic surfactant SDS and their presence was confirmed using DLS measurements. A 7:3 volumetric ratio of SDS:CAPB was sufficient to trigger the formation of micelles at hydrate forming temperature of 275K. Solubility determination experiments established the enhancement in solubility of methane in micellar solutions of surfactants which is in good agreement to literature data. In accordance with the objectives of the present work, hydrate formation experiments were carried out in presence of the mixed surfactant system. Pure methane hydrate was synthesized for the comparison study and a low concentration coal mine gas (30% CH₄ and 70% N₂) was used for separation studies. For both gas systems studied, efficient promotion of hydrate formation kinetics was observed in the presence of surfactant micelles as compared to pure water and micelle-less surfactant systems.

2.5. References

1. Sloan, E.D. Fundamental principles and applications of natural gas hydrates. *Nature* **2003**, 426, 353-363.
2. Koh C.A.; Sloan E.D. Natural gas hydrates: Recent advances and challenges in energy and environmental applications. *AIChE J.* **2007**, 53, 1636-1643.
3. Kumar, A.; Kumar, R. Role of metallic packing and kinetic promoter in designing a hydrate-based gas separation process. *Energy Fuels* **2015**, 29, 4463-4471.
4. Wang, W.; Zeng, P.; Long, X.; Huang, J.; Liu, Y.; Tan, B.; Sun, L. Methane storage in tea clathrates. *Chem. Commun.* **2014**, 50, 1244-1246.
5. Park, K.N.; Hong, S.Y.; Lee, J.W.; Kang, K.C.; Lee, Y.C.; Ha, M.G.; Lee, J.D. A new apparatus for seawater desalination by gas hydrate process and removal characteristics of dissolved minerals (Na⁺, Mg²⁺, Ca²⁺, K⁺, B³⁺). *Desalination* **2011**, 274, 91-96.
6. Koh, C.A. Towards a fundamental understanding of natural gas hydrates. *Chem. Soc. Rev.* **2002**, 31, 157-167.
7. Bhattacharjee, G.; Choudhary, N.; Kumar, A.; Chakrabarty, S.; Kumar, R. Effect of the amino acid l-histidine on methane hydrate growth kinetics. *J. Nat. Gas. Sci. Eng.* **2016**, 35, 1453-1462.
8. Kumar, A.; Kushwaha, O. S.; Rangsunvigit, P.; Linga, P.; Kumar, R. Effect of additives on formation and decomposition kinetics of methane clathrate hydrates: Application in energy storage and transportation. *Can. J. Chem. Eng.* **2016a**, 94, 2160-2167.
9. Komatsu H.; Ota M.; Sato Y.; Watanabe M.; Smith R.L. Hydrogen and carbon dioxide adsorption with tetra-n-butyl ammonium semi-clathrate hydrates for gas separations. *AIChE J.* **2015**, 61, 992-1003.

10. Arora, A.; Kumar, A.; Bhattacharjee, G.; Kumar, P.; Balomajumder, C. Effect of different fixed bed media on the performance of sodium dodecyl sulfate for hydrate based CO₂ capture. *Mater. Des.* **2016**, 90, 1186-1191.
11. Kumar, R.; Englezos, P.; Moudrakovski, I.; Ripmeester, J.A. Structure and composition of CO₂/H₂ and CO₂/H₂/C₃H₈ hydrate in relation to simultaneous CO₂ capture and H₂ production. *AIChE J.* **2009**, 55, 1584-94.
12. Veluswamy, H. P.; Kumar, R.; Linga, P. Hydrogen storage in clathrate hydrates: current state of the art and future directions. *Appl. Energy* **2014**, 122, 112-132.
13. Kumar, A.; Sakpal, T.; Bhattacharjee, G.; Kumar, A.; Kumar, R. Impact of H₂S impurity on carbon dioxide hydrate formation kinetics in fixed bed arrangements. *Ind. Eng. Chem. Res.* **2016b**, 55, 7964-7972.
14. Kumar, A.; Bhattacharjee, G.; Barmecha, V.; Diwan, S.; Kushwaha, O. S. Influence of kinetic and thermodynamic promoters on post-combustion carbon dioxide capture through gas hydrate crystallization. *J. Envir. Chem. Eng.* **2016c**, 4, 1955-1961.
15. Okutani, K.; Kuwabara, Y.; Mori, Y. H. Surfactant effects on hydrate formation in an unstirred gas/liquid system: An experimental study using methane and sodium alkyl sulphates. *Chem. Eng. Sci.* **2008**, 63, 183-194.
16. Rogers, R.; Zhang, G.; Dearman, J.; Woods, C. Investigations into surfactant/gas hydrate relationship. *J. Petro. Sci. Eng.* **2007**, 56, 82-88.
17. Verrett, J., Servio, P. Evaluating surfactants and their effect on methane mole fraction during hydrate growth. *Ind. Eng. Chem. Res.* **2012**, 51, 13144-13149.
18. Kumar, A.; Bhattacharjee, G.; Kulkarni, B. D.; Kumar, R. Role of surfactants in promoting gas hydrate formation. *Ind. Eng. Chem. Res.* **2015a**, 54, 12217-12232.
19. Botimer, J.D.; Dunn-Rankin, D.; Taborek, P. Evidence for immobile transitional state of water in methane clathrate hydrates grown from surfactant solutions. *Chem. Eng. Sci.* **2016**; 142, 89-96.

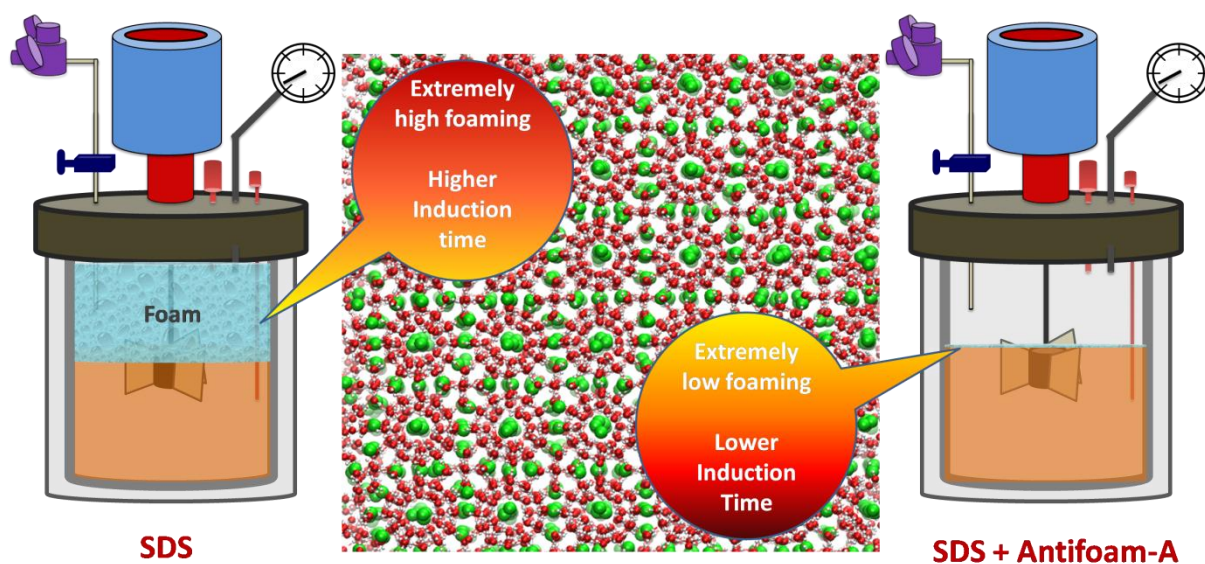
20. Hayama, H.; Mitarai, M.; Mori, H.; Verrett, J.; Servio, P.; Ohmura, R. Surfactant Effects on Crystal Growth Dynamics and Crystal Morphology of Methane Hydrate Formed at Gas/Liquid Interface. *Cryst. Growth. Des.* **2016**; DOI: abs/10.1021/acs.cgd.6b01124.
21. Zhong, Y.; Rogers, R.E. Surfactant effects on gas hydrate formation. *Chem. Eng. Sci.* **2000**; *55*, 4175-4187.
22. Di Profio, P.; Arca, S.; Germani, R.; Savelli, G. Surfactant promoting effects on clathrate hydrate formation: Are micelles really involved? *Chem. Eng. Sci.* **2005**; *60*, 4141-4145.
23. Zhang, J.S.; Lee, S.; Lee, J.W. Kinetics of methane hydrate formation from SDS solution. *Ind. Eng. Chem. Res.* **2007a**, *46*, 6353-6359.
24. Zhang, J.S.; Lee, S.; Lee, J.W. Solubility of sodium dodecyl sulfate near propane and carbon dioxide hydrate-forming conditions. *J. Chem. Eng. Data* **2007b**, *52*, 2480-2483.
25. Vautier-Giongo, C.; Bales B.L. Estimate of the ionization degree of ionic micelles based on Krafft temperature measurements. *J. Phys. Chem. B* **2003**, *107*, 5398-5403.
26. Israelachvili, J. *Intermolecular and Surface Forces*; Academic Press: London, 2011.
27. Prajapati, R.R.; Bhagwat, S.S. Effect of foam boosters on Krafft temperature. *J. Chem. Eng. Data* **2012a**, *57*, 869-874.
28. Prajapati, R.R.; Bhagwat, S.S. Effect of Foam Boosters on the Micellization and Adsorption of Sodium Dodecyl Sulfate. *J. Chem. Eng. Data* **2012b**, *57*, 3644-3650.
29. Iwasaki, T.; Ogawa, M.; Esumi, K.; Meguro, K. Interactions between betaine-type zwitterionic and anionic surfactants in mixed micelles. *Langmuir* **1991**, *7*, 30-35.

30. Bolden, P.L.; Hoskins, J.C.; King, A.D. The solubility of gases in solutions containing sodium alkylsulfates of various chain lengths. *J. Colloid. Interface. Sci.* **1983** 91, 454-463.
31. Roy, S.; Mehra, A.; Bhowmick, D. Prediction of solubility of nonpolar gases in micellar solutions of ionic surfactants. *J. Colloid. Interface. Sci.* **1997**, 196, 53-61.
32. Flores, R.M. Coalbed methane: from hazard to resource. *Int. J. Coal. Geol.* **1998**, 35, 3-26.
33. Moore, T.A. Coalbed methane: A review. *Int. J. Coal. Geol.* **2012**, 101, 36-81.
34. Zhong, D.; Englezos, P. Methane separation from coal mine methane gas by tetrabutyl ammonium bromide semiclathrate hydrate formation. *Energy Fuels* **2012**, 26, 2098-2106.
35. Zhong, D.L.; Daraboina, N.; Englezos, P. Recovery of CH₄ from coal mine model gas mixture (CH₄/N₂) by hydrate crystallization in the presence of cyclopentane. *Fuel* **2013a**, 106, 425-430.
36. Sun, Q.; Guo, X.; Liu, A.; Dong, J.; Liu, B.; Zhang, J.; Chen, G. Experiment on the separation of air-mixed coal bed methane in THF solution by hydrate formation. *Energy Fuels* **2012**, 26, 4507-4513.
37. Sun, Q.; Guo, X.; Liu, A.; Liu, B.; Huo, Y.; Chen, G. Experimental study on the separation of CH₄ and N₂ via hydrate formation in TBAB solution. *Ind. Eng. Chem. Res.* **2010**, 50, 2284-2288.
38. Smith, J.M.; Van Ness, H.C.; Abbott, M.M. Introduction to chemical engineering thermodynamics; McGraw-Hill: New York, 2004.
39. Zhang, B.; Wu, Q. Thermodynamic promotion of tetrahydrofuran on methane separation from low-concentration coal mine methane based on hydrate. *Energy Fuels* **2010**, 24, 2530-2535.

40. Bhattacharjee, G.; Kumar, A.; Sakpal, T.; Kumar, R. Carbon dioxide sequestration: influence of porous media on hydrate formation kinetics. *ACS Sustain. Chem. Eng.* **2015**, *3*, 1205-1214.
41. Duan, Z.; Mao, S. A thermodynamic model for calculating methane solubility, density and gas phase composition of methane-bearing aqueous fluids from 273 to 523K and from 1 to 2000 bar. *Geochim. Cosmochim. Acta.* **2006**, *70*, 3369-3386.
42. Kumar, A.; Sakpal, T.; Linga, P.; Kumar, R. Enhanced carbon dioxide hydrate formation kinetics in a fixed bed reactor filled with metallic packing. *Chem. Eng. Sci.* **2015b**, *122*, 78-85.
43. Zhong, D.L.; Daraboina, N.; Englezos, P. Coal mine methane gas recovery by hydrate formation in a fixed bed of silica sand particles. *Energy Fuels* **2013b**, *27*, 4581-4588.
44. Zhong, D.L.; Ding, K.; Yan, J.; Yang, C.; Sun, D.J. Influence of cyclopentane and SDS on methane separation from coal mine gas by hydrate crystallization. *Energy Fuels* **2013c**, *27*, 7252-7258.
45. Zhong, D.L.; Lu, Y.Y.; Sun, D.J.; Zhao, W.L.; Li, Z. Performance evaluation of methane separation from coal mine gas by gas hydrate formation in a stirred reactor and in a fixed bed of silica sand. *Fuel* **2015**, *143*, 586-594.
46. Zhong, D.L.; Ding, K.; Lu, Y.Y.; Yan, J.; Zhao, W.L. Methane recovery from coal mine gas using hydrate formation in water-in-oil emulsions. *Appl. Energy* **2016**, *162*, 1619- 1626.
47. Zhong, D.L.; Sun, D.J.; Lu, Y.Y.; Yan, J.; Wang, J. L. Adsorption-hydrate hybrid process for methane separation from a CH₄/N₂/O₂ gas mixture using pulverized coal particles. *Ind. Eng. Chem. Res.* **2014**, *53*, 15738-15746.

Chapter 3

Kinetic promotion of methane hydrate formation by combining anionic and silicone surfactants: scalability promise of methane storage due to prevention of foam formation



3. Kinetic promotion of methane hydrate formation by combining anionic and silicone surfactants: scalability promise of methane storage due to prevention of foam formation³

³A version of this chapter has been submitted for publication

Bhattacharjee, G.; Barmecha, V.; Kushwaha, O. S.; Kumar, R. Kinetic promotion of methane hydrate formation by combining anionic and silicone surfactants: scalability promise of methane storage due to prevention of foam formation. Submitted for publication in *J. Chem. Thermodyn.*, 2017.

3.1. Introduction

The use of surfactants to enhance the kinetics of hydrate formation is one of the central themes of this thesis and one that has been explored in great detail in the preceding chapters. Surfactants such as Sodium dodecyl sulfate (SDS), individually or even in combination with other surfactants have been known to significantly enhance methane hydrate formation kinetics and as such, there can be no denying the efficacy and usefulness of these additives as far as enhancing the kinetics of hydrate formation is concerned (Kumar et.al, 2015; Link et.al, 2003; Lin et.al, 2004; Zhang et.al, 2007; Okutani et.al, 2008; Bhattacharjee et.al, 2017a; Bhattacharjee et.al, 2017b). However, there is a real concern regarding the ease of handling of these additives. Surfactants generally produce a huge amount of foam during hydrate formation which further escalates during the dissociation process as gas diffuses out of the system. The excessive foam generation becomes too much to handle even on a lab scale setup and is expected to be a major deterrent in the ultimate goal of commercialization of the hydrate based methane gas storage technology. To avoid the problem of foam formation, one of the options is to look for a different class of additives which offer similar promotion in hydrate formation kinetics but in a much cleaner manner (no foam formation). Amino acids are one class of compounds that have been suggested as kinetic hydrate promoters (Bhattacharjee et.al, 2016; Liu et.al, 2015; Veluswamy et.al, 2016; Cat et.al, 2017). Using these additives does do away with any sort of foam generation³ but there is a definite compromise in the extent of enhancement in the kinetics of hydrate formation that can be achieved as compared to surfactants. It is thus very important to identify additives, which when used either individually or in conjunction with conventional surfactants effectively prevent the foam formation while also not lowering the extent of enhancement in hydrate formation kinetics.

As has been mentioned in the previous chapters, one of the possible mechanisms through which surfactants enhance the kinetics of hydrate formation is reducing the surface tension of the aqueous hydrate forming solution which results in the formation of a thin film of liquid on the reactor wall which in turn becomes the preferred spot for hydrate nucleation and ends up altering the morphology of hydrate formation with the hydrates climbing up the reactor wall from the nucleation spot.

Silicones are another class of compounds that may be utilized based on the fact that they are also highly surface active. This property of silicones is a result of the large number of methane molecules present in their structure and small intermolecular interactions between the hydrophobic siloxane groups. The highly flexible nature of the siloxane backbone also allows for maximum orientation of the attached functional groups at interfaces. Silicone based surfactants which are composed out of silicone copolymers (the most common being silicone polyethers) are mainly used to modify the surface properties (such as surface tension) of waterborne systems. However they may also be used as de-foaming or antifoaming agents depending on their solubility in water. Lesser is the solubility of the silicone surfactant in water, better is the antifoaming property (Perry, 2005; O'Lenick Jr, 2000). We propose to utilize this antifoaming property of certain silicone based surfactants to counter the excessive foam generation observed during hydrate formation and dissociation in presence of conventional surfactants. In addition to being effective antifoaming agents, the high hydrophobicity of these compounds is also expected to have a significant say on the promotion of hydrate formation kinetics. It is a well known fact that non-polar hydrophobic additives and hydrophobic solid surfaces significantly enhance the kinetics of gas hydrate formation [(Bhattacharjee et.al, 2016; Wang et.al, 2008; Liu et.al, 2015; Veluswamy et.al, 2016; Cat et.al, 2017). According to a recent study, this promotion is due to the development of an interfacial gas enrichment (IGE) coupled with greater local water ordering; both of these immediately near the hydrophobic surface as compared to the surrounding environment i.e. the creation of an environment super conducive to the formation of gas hydrate crystals in the vicinity of the source of the hydrophobicity (Nguyen et.al, 2017).

In the current study, a silicone based antifoam formed of silicone copolymers has been used in conjunction with the anionic surfactant SDS in order to create a hybrid SDS-Silicone complex (in the physical sense) which would have a) much lower surface tension, b) much greater hydrophobicity and c) much lesser tendency to form and stabilize foams than pure SDS. The SDS and silicone surfactants have been mixed in various concentrations in order to find out

the optimal mixing ratio for the two additives and the gas uptake (due to hydrate formation) results obtained for the various mixtures have been compared with those for the pure additives. Hydrate formation has been carried out in a stirred tank reactor system using pure methane gas with the application in focus being methane storage. Pressure and temperature conditions for hydrate formation are 6.0 MPa and 274 K respectively.

3.2. Experimental Section

3.2.1. Materials

Methane gas with a purity of more than 99.5% was supplied by Vadilal Gases Pvt. Ltd., India. The silicone based antifoam containing 100 % active silicone polymer was purchased from Sigma-Aldrich. This compound called as *Antifoam-A Concentrate* by the manufacturing company (henceforth referred to in this study as Antifoam A) is a proprietary of the Sigma brand and hence the exact composition of the compound is unknown. Sodium dodecyl sulfate (SDS) was purchased from Thermo Fischer Scientific India. Distilled and deionized water was used for all the experiments.

3.2.2. Procedure followed for making the SDS-Silicone complex

It was very difficult to measure out and transfer to the reactor the exact amount of antifoam due to its hydrophobic nature hence this led to the formation of the SDS-Silicone complex even before the additives are transferred to the reactor. A very specific procedure was followed to ensure that the additives were used in the correct concentrations even in the presence of physical limitations. First, the requisite weight of silicone surfactant or antifoam (Antifoam-A) was weighed out onto a Petri dish first and then the requisite weight of SDS was added to it. The SDS totally absorbs the antifoam leading to the formation of a SDS-Silicone complex which may be an antifoam coated SDS powder. The resultant powder (which is a combination of SDS and Antifoam-A) can be easily transferred into the reactor. The Petri dish containing the SDS-Silicone complex/mixture was washed multiple times with small amounts of DI water after transferring the mixture to the reactor so as to minimize additive loss to the maximum extent. It is to be noted that the water used for washing the Petri dish came out from the total amount of water that was to be used for hydrate formation. Once all the additive mixture had been transferred to the reactor, the rest of the measured DI water was added to it and the final hydrate forming solution was agitated to ensure complete mixing of the additive with the water.

3.2.3. Apparatus and procedure for hydrate formation experiment

A stirred tank reactor (STR) setup as shown in Figure 3.1 was used to carry out the experiments in this study. Given below is the procedure used for the hydrate formation experiments which in the process also gives a detailed description of the stirred tank apparatus used:

The SDS-Silicone complex was prepared and transferred along with the requisite amount of distilled and deionized water (80 cm^3 into a (250 cm^3) stainless steel crystallizer (CR; Alpro Make, India). The CR was then sealed tightly and placed inside a temperature controlled water bath in order to attain the desired experimental temperature (274 K). The vessel was flushed with pure methane gas by repeating rapid pressurization ($\sim 0.5 \text{ MPa}$) and depressurization cycles. Next, the CR was pressurized with the pure methane gas up to the pre determined experimental pressure of 6.0 MPa (equilibrium hydrate formation pressure for pure methane at 274 K is 2.8 MPa) thus providing sufficient driving force for hydrate formation. As soon as the desired experimental pressure was reached, the stirrer was turned on at 400 rpm to provide enough external agitation to the system to facilitate rapid formation of hydrates. At this stage, gas uptake measurements were initiated. With the progress of hydrate formation, the pressure inside the CR dropped as a result of the gas moving from the gaseous phase to the solid hydrate phase. This pressure drop inside the CR was measured using a pressure transducer (WIKA make; 0-25 MPa) to calculate the moles of gas taking part in the hydrate formation process. Temperature and pressure inside the CR were recorded every ten seconds using a data acquisition system (PPI make) which was connected to a computer. Since the experiments were effectively an isochoric (batch) process, the effective driving force for hydrate formation decreased as the reaction proceeded. This is a direct consequence of gas continuously migrating from the gaseous phase to the solid hydrate phase leading to a point in the process where there isn't enough pressure (driving force) left in the CR to sustain hydrate formation.

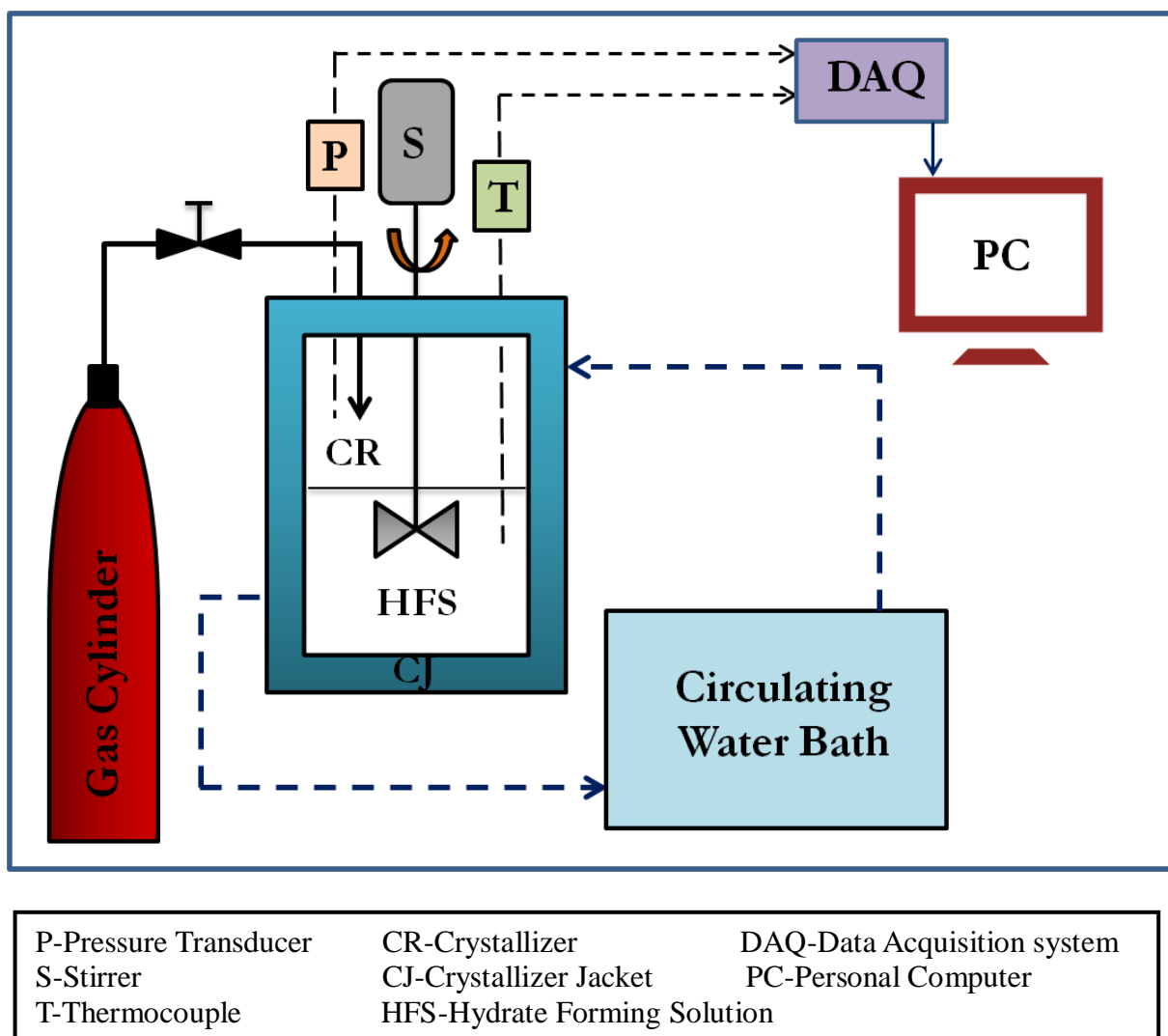


Fig. 3.1: Detailed schematic of the stirred tank reactor setup for hydrate formation (Bhattacharjee et.al, 2017b).

3.2.4. Apparatus and procedure for morphology study

A hollow, cylindrical and transparent polymethylmethacrylate (PMMA) reactor was used for these experiments so as to allow for visualization of the formation and dissociation of methane hydrates. The PMMA column was vertically supported by two stainless steel lids and had a maximum pressure rating of 10.0 MPa. Figure 3.2 shows a schematic of this experimental setup. Similar to the gas uptake experiments, the morphology experiments were also carried out in batch mode. 5 ml of the experimental solution was first pipetted out into the acrylic column reactor. The reactor was then tightly sealed and connected to a circulating water bath in order to attain the desired hydrate formation temperature. The circulating coolant (water-methanol mixture) was provided using a Julabo F54 external refrigerator. On reaching the desired temperature, the vessel was flushed with pure methane gas by repeating

rapid pressurization (~ 0.5 MPa) and depressurization cycles. Next, the reactor was pressurized with the pure methane gas up to the pre determined experimental pressure of 6.0 MPa thus keeping the pressure and temperature conditions for the morphology experiments same as those for the gas uptake experiments. The morphology experiments were all carried out in an unstirred reactor configuration; hence as soon as the desired experimental pressure was reached, data acquisition was turned on. The reactor pressure was measured using a Rosemount 3051 Pressure Transmitter (PT) having an uncertainty of 0.1% and a pressure range of 0–20 MPa while the reactor temperature was measured using a copper constantan T type thermocouple with an uncertainty of 0.1 K. Data Acquisition (DAQ) system supplied by National Instruments was used to record the temperature and pressure data every 20 seconds throughout each experiment. Morphological images of hydrate formation and dissociation which were the main point of conducting these experiments were captured every 10 seconds through out each experiment with the help of a microscope (SMZ1000 from Nikon with 0.5X objective lens) and a camera (Nikon Digital Sight-DSFi1) (Veluswamy et.al, 2014).

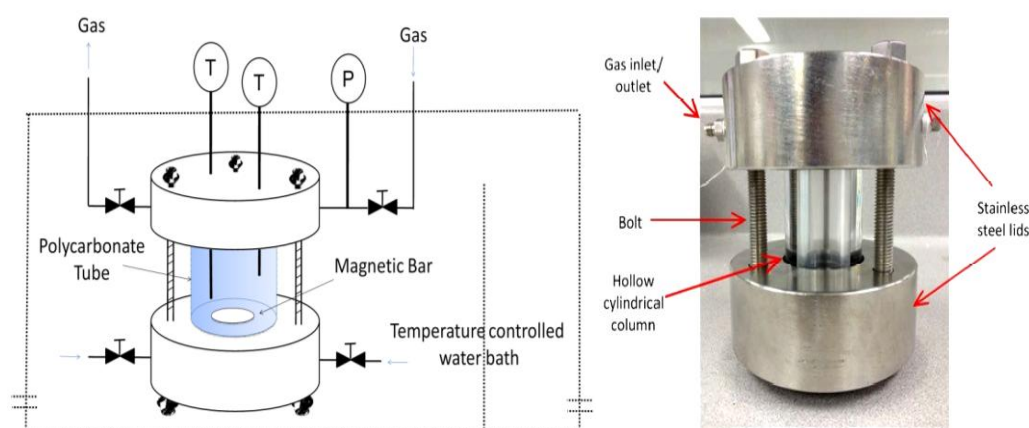


Fig. 3.2: Detailed schematic of the reactor setup for morphology study of hydrate formation and dissociation.

3.2.5. Calculation of the amount of gas consumed during the hydrate formation experiments

The total number of moles of gas that was consumed in the hydrate formation process at any given time is the difference between the number of moles of gas present in the gas phase of the CR at time $t = 0$ and the number of moles of gas present in the gas phase of the CR at time $t = t$. The same is given by the following equation (Bhattacharjee et.al, 2015):

$$(\Delta n_{H,\downarrow})_t = V_{CR} \left[\frac{P}{zRT} \right]_0 - V_{CR} \left[\frac{P}{zRT} \right]_t \quad (3.1)$$

where z is the compressibility factor calculated by using Pitzer's correlation (Smith et.al, 2004), V_{CR} is the volume of the gas phase inside the crystallizer and P and T are the pressure and temperature of the crystallizer respectively.

3.2.6. Calculation of the rate of hydrate formation

The rate of hydrate formation was calculated by the forward difference method as given below (Bhattacharjee et.al, 2015):

$$\left(\frac{d\Delta n_{H,\downarrow}}{dt} \right)_t = \frac{\Delta n_{H,\downarrow}(t+\Delta t) - \Delta n_{H,\downarrow}(t)}{\Delta t}; \Delta t=5 \text{ sec} \quad (3.2)$$

The average of these rates was calculated for every 20 minutes and reported.

3.3. Results and Discussions

Table 3.1 given below summarizes all the experiments performed in the course of this study. Relevant information such as the sample state, initial hydrate formation pressure, run time of each experiment, amount of gas consumed at the end of each experiment (mol of gas consumed/ mol of water) and the induction time for hydrate formation in each experiment have been reported.

Table 3.1: Summary of all the experiments conducted in the course of this study. Relevant data such as the sample state, initial hydrate formation pressure, run time of each experiment, amount of gas consumed at the end of each experiment (mol of gas consumed/ mol of water) and the induction time for hydrate formation in each experiment have been reported.

System	Reactor Configuration	Exp No.	Sample State	Initial Pressure (MPa)	Run Time (h)	Gas Uptake (mol of gas cons/ mol of water)	Induction Time (h)
Pure Water	STR	1	Fresh	6.0	1.0	0.028	1.958
		2	Fresh	6.0	1.0	0.032	0.025
		3	Fresh	6.0	1.0	0.020	0.032
		4	Memory	6.0	1.0	0.025	1.277
		5	Memory	6.0	1.0	0.030	2.950
		6	Memory	6.0	1.0	0.025	0.030
1 wt % SDS	STR	7	Fresh	6.0	1.0	0.050	0.015
		8	Fresh	6.0	1.0	0.052	0.020
		9	Fresh	6.0	1.0	0.054	0.385
		10	Fresh	6.0	1.0	0.036	0.450
1 wt % Antifoam -A	STR	11	Fresh	6.0	1.0	0.026	0.414
		12	Fresh	6.0	1.0	0.018	0.147
		13	Fresh	6.0	1.0	0.031	0.007
		14	Memory	6.0	1.0	0.024	0.271
		15	Memory	6.0	1.0	0.027	0.213
		16	Memory	6.0	1.0	0.032	0.057
1 wt % SDS + 0.1 wt % Antifoam -A	STR	17	Fresh	6.0	1.0	0.050	0.101
		18	Fresh	6.0	1.0	0.041	1.113
		19	Fresh	6.0	1.0	0.034	0.133
		20	Fresh	6.0	1.0	0.035	0.480
		21	Memory	6.0	1.0	0.056	0.044
		22	Memory	6.0	1.0	0.048	0.540
		23	Memory	6.0	1.0	0.052	0.136
		24	Memory	6.0	1.0	0.051	0.268

1 wt % SDS + 0.5 wt % Antifoam -A	STR	25	Fresh	6.0	1.0	0.053	0.063
		26	Fresh	6.0	1.0	0.051	0.174
		27	Fresh	6.0	1.0	0.048	0.139
		28	Memory	6.0	1.0	0.053	0.161
		29	Memory	6.0	1.0	0.048	0.313
		30	Memory	6.0	1.0	0.050	0.092
1 wt % SDS + 1 wt % Antifoam -A	STR	31	Fresh	6.0	1.0	0.032	0.867
		32	Fresh	6.0	1.0	0.036	0.917
		33	Fresh	6.0	1.0	0.039	0.636
		34	Fresh	6.0	1.0	0.038	0.217
		35	Memory	6.0	1.0	0.040	1.722
		36	Memory	6.0	1.0	0.040	0.111
		37	Memory	6.0	1.0	0.048	0.033

3.3.1. Methane hydrate formation in the presence of Antifoam-A: promotion in hydrate formation kinetics and reduction in induction time

Figure 3.3 given below compares the gas uptake for the fresh runs of hydrate formation (first hour only) in presence of the additive mixtures in different concentrations. Averages and standard deviations of the gas uptakes have been plotted. Time zero in Figure 3.3 corresponds to the nucleation point and hence whatever gas uptake has been portrayed in the figure corresponds to that for hydrate formation. The gas uptake profiles obtained in presence of the various additive mixtures have been compared with those obtained in presence of the pure additives, i.e. SDS and Antifoam A and also with that for pure water. As can be clearly seen in Figure 3.3, the kinetics of methane hydrate formation is significantly enhanced in the presence of pure SDS as expected. However, what is very interesting to note here is that even though methane hydrate formation kinetics are somewhat depressed in the presence of pure Antifoam-A, the kinetics recorded for the mixtures of SDS and Antifoam were as good as those for the pure SDS runs. Three different SDS-Antifoam mixtures were prepared for use with the concentration of SDS being kept constant and the concentration of Antifoam-A being varied from 0.1 to 1 wt % in order to properly understand the effect that maxing this additive with SDS might have on methane hydrate formation kinetics. It can be seen in Figure 3.3 that out of the three additive mixtures studied, the 1 wt % SDS + 0.5 wt % Antifoam A mixture

showed the highest promotion in methane hydrate formation kinetics and this promotion was in fact toe to toe in comparison with that observed with pure SDS (1 wt %). The 1 wt % SDS + 0.5 wt % Antifoam A mixture was followed by the 1 wt % SDS + 0.1 wt % Antifoam A and the 1 wt % SDS + 1 wt % Antifoam A mixtures as far as the promotion of methane hydrate formation is concerned. These results hold great importance as it indicates that in order to obtain the maximum enhancement in hydrate formation kinetics using this additive mixture, there is an optimum ratio in which the additive mixtures are supposed to be mixed together which here is 1:0.5 for SDS : Antifoam-A. Figure 3.4 plots the rate of hydrate formation/ gas uptake (mol of gas consumed/ mol of water/ h) for the fresh runs of the different systems studied. The rate of hydrate formation has been plotted for the first three hours of hydrate formation. It can be seen in the figure that after the first hour, the rate hydrate formation nears zero for all but one of the systems thus indicating that hydrate formation is all but over after the first hour for the various systems being studied. The plot follows the same trend as the gas uptake one in that the 1 wt % SDS and 1 wt % SDS + 0.5 wt % Antifoam-A systems exhibit the highest rate of gas uptake, closely followed by the other additive mixture systems and then the pure water and 1 wt % Antifoam--A systems.

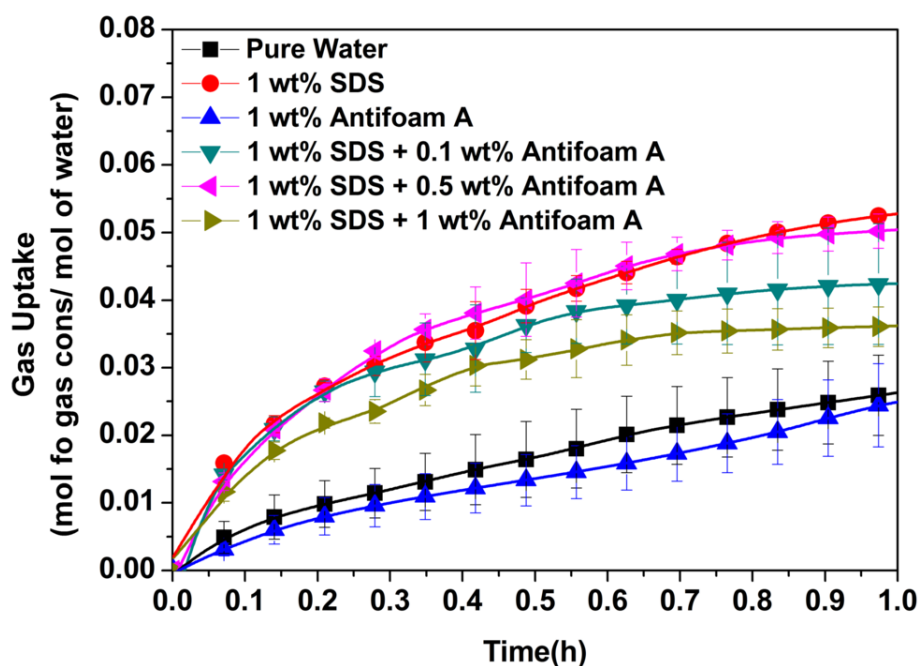


Fig. 3.3: Comparison of the gas uptake for the different systems studied (fresh runs) with average and standard deviation.

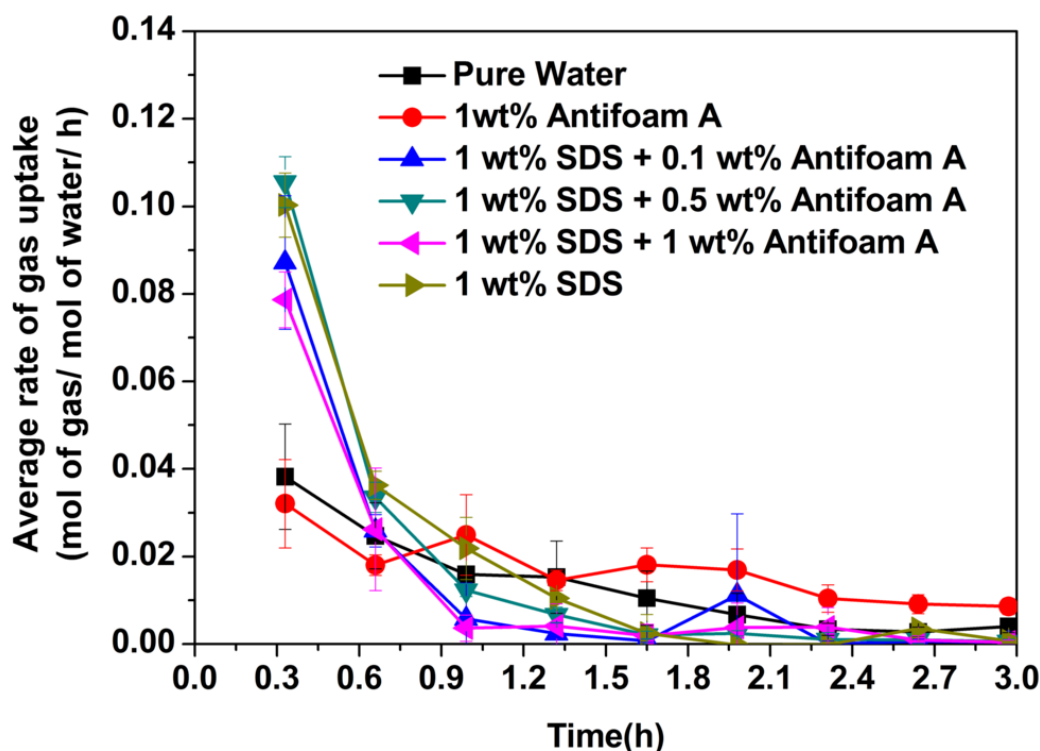


Fig. 3.4: Average rate of gas uptake for the different systems studied (fresh runs) with standard deviation.

Figure 3.5 compares the gas uptake for the memory runs of hydrate formation (only first hour) in presence of the additive mixtures in different concentrations. Averages and standard deviations of the gas uptakes have been plotted. Time zero in Figure 3.5 corresponds to the nucleation point and hence whatever gas uptake has been portrayed in the figure corresponds to that for hydrate formation. This figure can actually give an indication of the antifoaming property of the silicone surfactant. It can be seen in Figure 3.5, that all the systems that were compared in Figure 3.3 have also been compared here with the sole exception of the pure SDS system. The reason for this is that there is so much foam formation during hydrate formation and dissociation with pure SDS that it becomes very difficult to perform memory experiments. However, with the addition of even a very small amount of Antifoam-A to the system (say ~ 0.1 wt %), the foam generation is cut down to such an extent that memory experiments become possible. Additionally, when one factors in the fact that all the experiments in the present study have been conducted in a stirred tank reactor at a high stirring speed of 400 rpm, the antifoaming effect of the silicone surfactant becomes all the more impressive. As can be seen in Figure 3.5, the kinetics of methane hydrate formation is greatly enhanced with the various additive mixtures as compared to pure water. The

promotion observed is significant and almost similar for the 1 wt % SDS + 0.5 wt % Antifoam A and 1 wt % SDS + 0.1 wt % Antifoam A systems which are followed by the 1 wt % SDS + 1 wt % Antifoam A mixture. Figure 3.6 plots the rates of gas uptake (mol of gas consumed/mol of water/h) corresponding to Figure 3.5 for the first three hours of hydrate formation. As expected, the trend observed is similar to that seen in Figure 3.5 with two of the additive mixture systems (1 wt % SDS + 0.5 wt % Antifoam A and 1 wt % SDS + 0.1 wt % Antifoam A) being virtually undistinguishable at the top of the pack. Similar to the fresh runs, the promotion observed with the additive mixtures here is relative to the fact that there is literally no promotion in the case of the pure antifoam system.

Figure A4 in Appendix A shows a linear fit of the first twenty minutes of hydrate growth for both fresh and memory runs for the different systems studied. The average initial apparent rates of hydrate formation for the first twenty minutes of hydrate growth (mol of gas consumed/h) obtained for the different systems as a result of the linear fitting have been reported in Table A2, Appendix A.

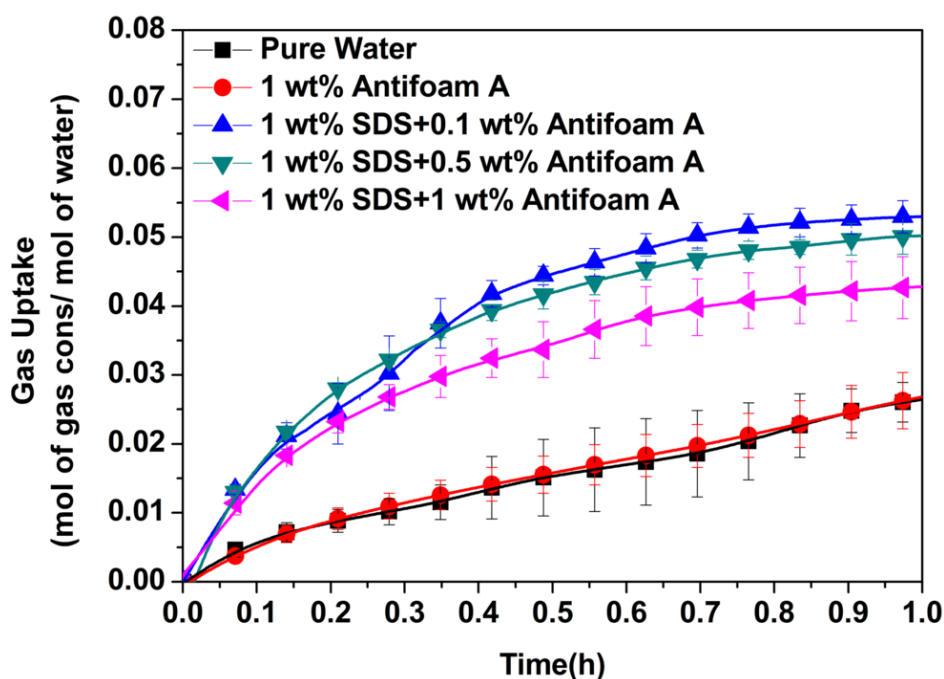


Fig. 3.5: Comparison of the gas uptake for the different systems studied (memory runs) with average and standard deviation. Memory runs could not be performed with the pure SDS system due to excessive foam generation.

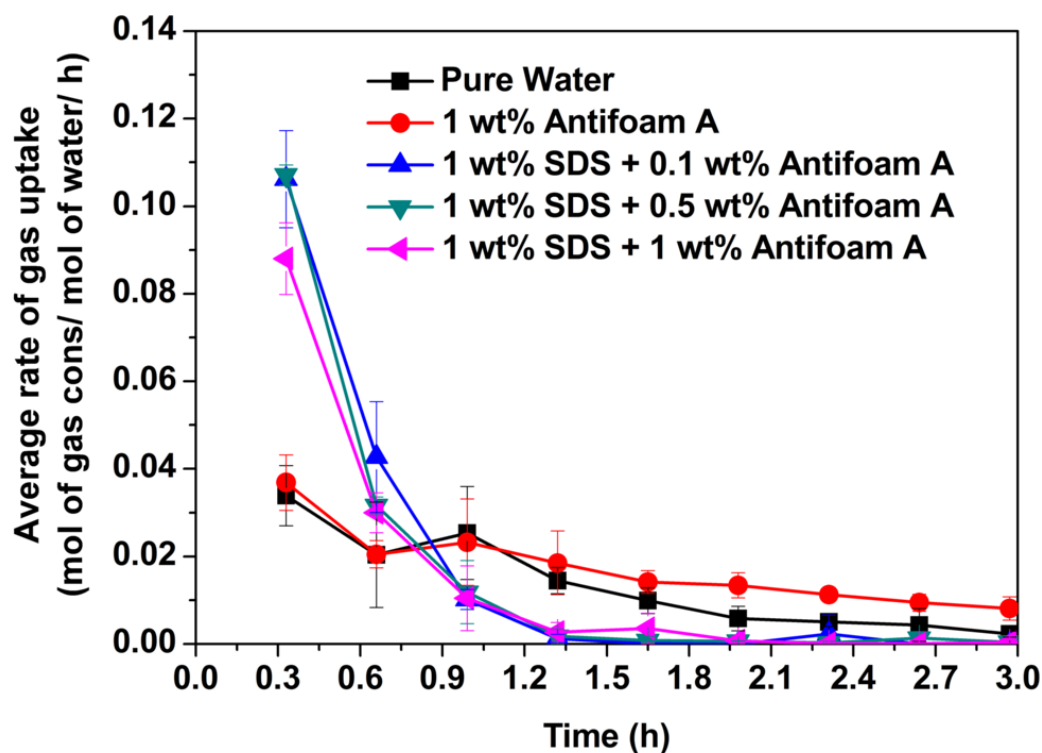


Fig. 3.6: Average rate of gas uptake for the different systems studied (memory runs) with standard deviation.

In the case of the pure antifoam system, in spite of the highly hydrophobic nature of the additive, no promotion in methane hydrate formation is observed owing to its high viscosity which may create mass transfer limitations in the system; not allowing the gas to rapidly penetrate the gas-water interface. On the other hand, in the case of the additive mixtures, it is the formation of the SDS-Silicone complexes which results in the promotion of methane hydrate formation kinetics. The high viscosity of the antifoam stops being a rate limiting factor when mixed with SDS in particular ratios; SDS with its various promoting properties and Antifoam-A with its high hydrophobicity come together to form a hybrid mixture which greatly enhances the kinetics of hydrate formation as compared to pure water. All the various factors such as lowering of surface tension, better localized water arrangement, development of interfacial gas enrichment come together to effect this enhancement. It is important to note that even for the additive mixtures, the mass transfer limitations persist when the additives are mixed in equal concentrations. It is only when the SDS: Antifoam-A ratio is dropped to 1:0.5 % by weight that the promotion in methane hydrate formation is observed.

The development of interfacial gas enrichment at the hydrophobic surface and the greater local water ordering in the vicinity of the same, in particular, lend their weight to reducing the

nucleation/ induction time for hydrate formation. As can be seen in Figure 3.7 and Figure 3.8 (fresh and memory runs respectively), as compared to pure water, the average induction times are significantly reduced for all of the systems containing Antifoam-A. What is interesting is that despite not turning in any enhancement in the kinetics of methane hydrate formation, the pure (1 wt %) Antifoam-A system shows a significant reduction in the induction time as compared to pure water and even the 1 wt % SDS system. Based on this result and our knowledge of interfacial gas enrichment and greater localized water ordering in the vicinity of hydrophobic surfaces, one can speculate that in the presence of the antifoam, hydrate formation begins at the walls of the reactor where the antifoam, owing to its hydrophobic nature and low surface tension, forms a hydrophobic solid-liquid interface which quickly transforms into a hydrophobic three phase (solid-liquid-gas) interface when gas (methane in this case) is introduced into the system. A through study on this aspect is currently being carried out.

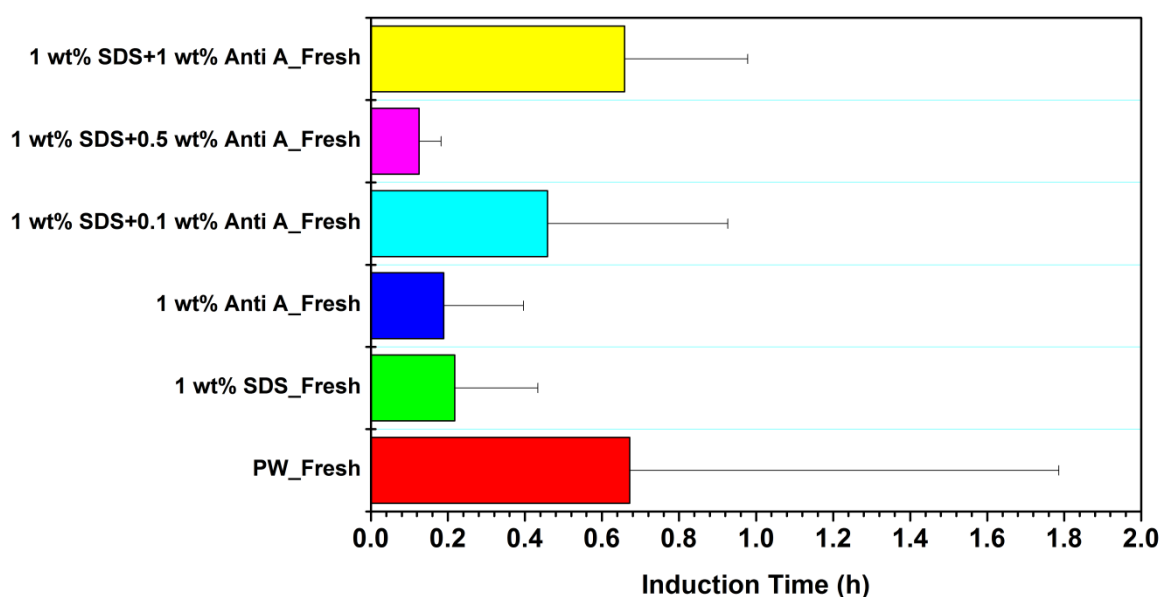


Fig. 3.7: Comparison of the average induction times for the different systems studied (fresh runs) with standard deviation.

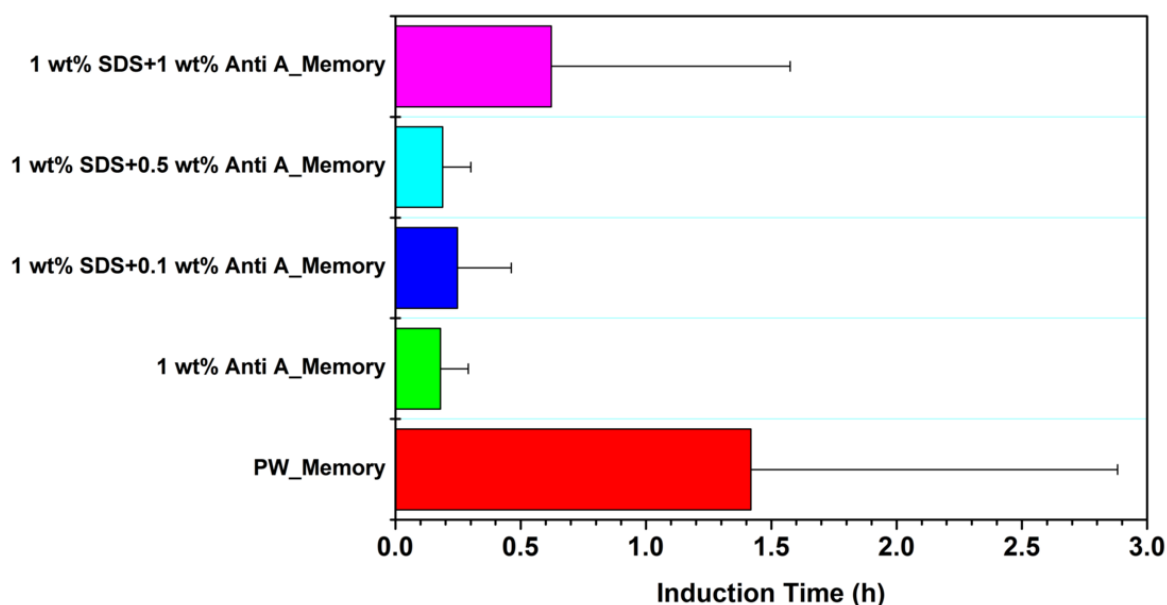


Fig. 3.8: Comparison of the average induction times for the different systems studied (memory runs) with standard deviation.

The 1 wt % SDS + 0.5 wt % Antifoam-A and 1 wt % SDS + 0.1 wt % Antifoam-A systems don't fare pretty badly themselves in terms of induction time; in fact the average induction time recorded for the 1 wt % SDS + 0.5 wt % Antifoam-A system is much lesser than that recorded for the pure (1 wt %) SDS system which is an excellent result from our point of view of introducing the silicone based surfactant/ antifoam as an additive that may be employed (as part of an additive mixture) to promote methane hydrate formation kinetics.

3.3.2. Suppression in foam formation in the presence of Antifoam-A

Figure 3.9 shows the suppression in foam formation that is achieved when Antifoam-A and SDS are mixed together with water and agitated. In Figure 3.8, four vials can be seen, each containing an additive solution. The one at the extreme left is the pure SDS solution and the concentration of antifoam increases as we go to the right in the figure. Once prepared, the additive solution were first agitated vigorously by hand and then shaken for about thirty minutes using a shaker. The pictures were taken immediately after the completion of the shaking process. As can be seen from the figure, the suppression in foam formation from the 1 wt % pure SDS solution to the 1 wt % SDS + 0.1 wt % Antifoam-A solution is remarkable. However, it can also be seen that the foam formation is further suppressed as we move from the 1 wt % SDS + 0.1 wt % Antifoam-A solution to the 1 wt % SDS + 0.5 wt % Antifoam-A. There is no further noticeable suppression in the foam formation as the concentration of the

Antifoam is increased further, i.e. between the 1 wt % SDS + 0.5 wt % Antifoam-A and the 1 wt % SDS + 1 wt % Antifoam-A solutions.

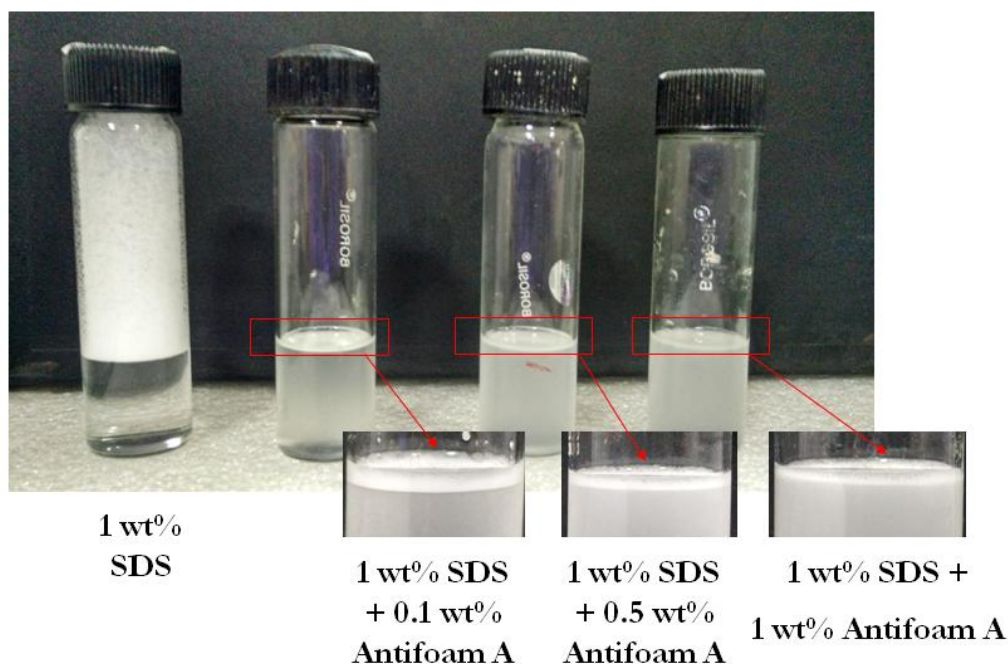


Fig. 3.9: Foam Suppression in presence of Silicone based surfactant.

3.3.3. Morphology of methane hydrate formation and dissociation in presence of Antifoam-A

Figures 3.10 and 3.11 show the morphology of methane hydrate formation and dissociation in the presence of Antifoam-A respectively. The four systems studied in the morphology experiments were a pure SDS system (0.25 wt %), a 1:0.1 SDS:Antifoam weight ratio system (0.25 wt % SDS + 0.025 wt % Antifoam-A), a 1:0.5 SDS:Antifoam weight ratio system (0.25 wt % SDS + 0.125 wt % Antifoam-A) and a 1:1 SDS:Antifoam weight ratio system (0.25 wt % SDS + 0.25 wt % Antifoam-A). The reason that the concentrations of additives in the system for the morphology study were lowered as compared to the gas uptake study discussed earlier was that the morphology experiments were all carried out in a quiescent (unstirred) condition and in such a case, a very high concentration of SDS in the system (say 1 wt % as used in the kinetic study) may actually inhibit methane hydrate formation (Kang et.al, 2010).

Figure 3.10 shows that the morphology of hydrate formation is more or less similar for all the systems studied with hydrate formation starting at the gas liquid interface and then expanding

along the length of the reactor vial in both (upward and downward) directions. Catastrophic hydrate growth can be observed even for the 1:1 SDS:Antifoam weight ratio system; almost the entire reactor vial is filled with hydrates after ten minutes of hydrate formation for all the systems studied. This goes perfectly with the results obtained from the gas uptake study and indicates that any effect that the addition of antifoam to the system may have had on the kinetics of hydrate formation is too insignificant to consider.

During hydrate dissociation, foam generation escalates as a result of diffusion of hydrate gas into the liquid. Handling the foam becomes a pertinent issue due to the sheer quantities generated. Figure 3.11 shows the morphology of hydrate dissociation for the four different systems studied. An excessive amount of foam can be seen generated for the pure SDS system, which persists when the weight ratio of SDS:Antifoam in the system is 1:0.1 but completely disappears when the weight ratio of SDS:Antifoam in the system becomes 1:0.5. This observation is extremely interesting and particularly important to us as it becomes abundantly clear that a minimum 1:0.5 weight ratio of SDS:Antifoam is required to efficiently do away with the problem of foam generation encountered when using surfactants alone. However, it is also observed that although the foam generation is reduced as compared to pure SDS, it is not fully eliminated for the 1:1 SDS:Antifoam weight ratio system. This is unexpected as the 1:0.5 SDS:Antifoam weight ratio system was already observed to completely do away with the foam formation and it is only expected that this effect of the antifoam will be further enhanced as its concentration in the system is increased. Understanding this unexpected phenomenon will require a study in greater detail with investigations on a molecular scale. Although advances have been made in this regard, currently such a study is out of the scope of this thesis.

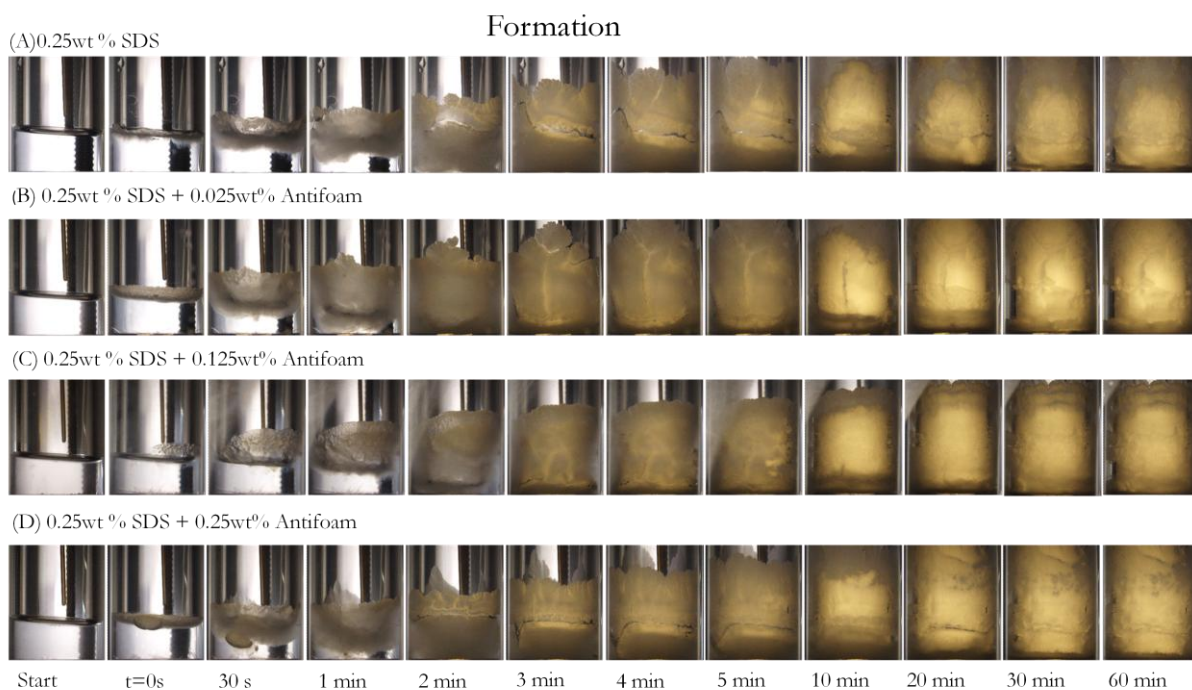


Fig. 3.10: Morphology of formation of methane hydrate for the different systems studied.

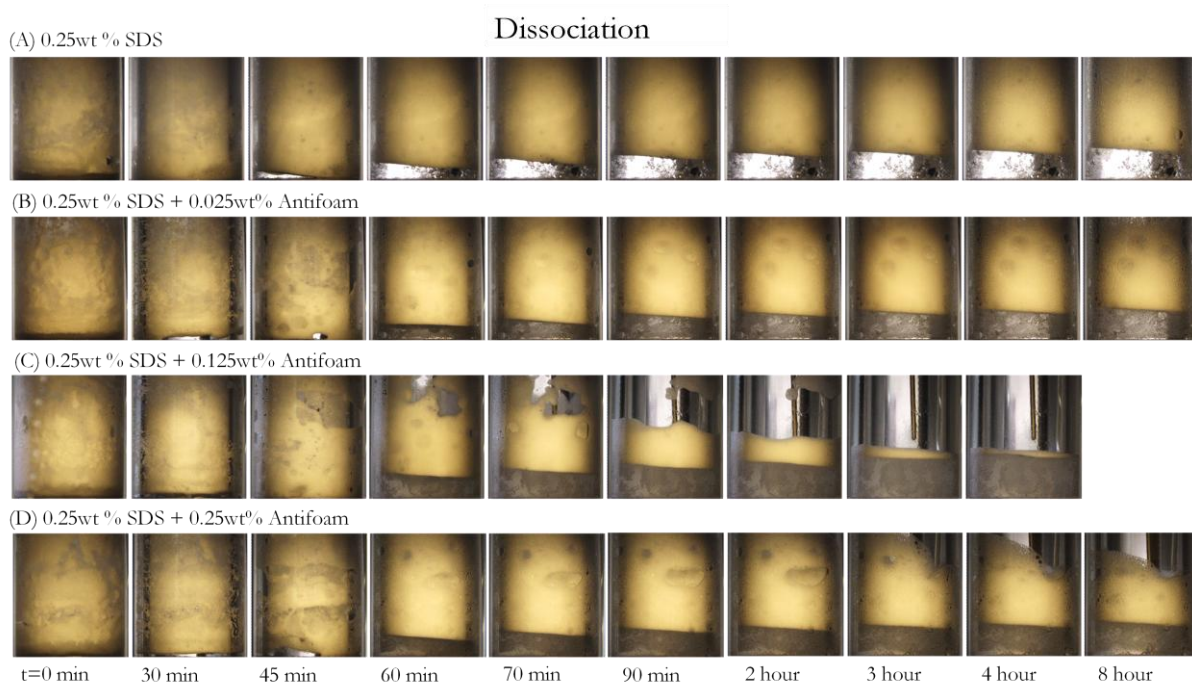


Fig. 3.11: Morphology of dissociation of methane hydrate for the different systems studied.

From the gas uptake study, it was concluded that the 1 wt % SDS + 0.5 wt % Antifoam-A system performs just as well as pure SDS as far as enhancing the kinetics of methane hydrate formation is concerned. The study of foam suppression in presence of Antifoam-A revealed that foam formation is effectively suppressed for the 1 wt % SDS + 0.5 wt % Antifoam-A

system and that there is no further noticeable suppression in the foam formation as the concentration of Antifoam in the system is increased. These results match up well with the one obtained in the morphology study which says that the 1:0.5 SDS:Antifoam weight ratio mixture is the best suited to prevent foam generation during the hydrate formation and dissociation cycle. All three results combined therefore lead to the conclusion that the 1:0.5 SDS:Antifoam weight ratio systems are the best performing case from all aspects of the current study and 1:0.5 is the optimum weight ratio for mixing the two additives (SDS and Antifoam-A) being studied here.

3.4. Conclusions

In the present study, a hydrophobic silicone based surfactant was identified to act as an antifoaming agent; the objective being to suppress the excessive foaming observed when using surfactants such as SDS as kinetic hydrate promoters without losing out on the kinetic promotion in hydrate formation. SDS-Silicone complexes were formed by combining two additives (anionic surfactant SDS and silicone based surfactant Antifoam-A). These complexes are supposed to retain the various properties of SDS while also having reduced surface tension and increased hydrophobicity as compared to pure SDS. A number of different additive complexes or mixtures were prepared depending on the ratios in which the two additives were mixed. This was done to zero in on the optimal ratio in which the two additives are to be mixed in order to obtain the desired results. The antifoam based systems clearly reduce the induction time for methane hydrate formation as compared to pure water and pure SDS (1 wt %), which is most likely a direct consequence of the antifoam's highly hydrophobic nature. Of all the systems studied, the 1 wt % SDS + 0.5 wt % Antifoam-A system was found to be the most effective in lowering the induction time for hydrate formation. Based on the gas uptake data obtained during hydrate formation, it can be concluded that the 1 wt % SDS + 0.5 wt % Antifoam-A system performs the best in terms of enhancing the kinetics of methane hydrate formation and the hydrate formation kinetics observed with this system were on par with those observed with pure SDS. The fact that memory experiments became possible even with the introduction of a very small amount (0.1 wt %) of the antifoam to the system, indicates very efficient foam suppression using the silicone based antifoam. The foam formation study in presence of the additive mixtures makes the effect of the antifoam on foam suppression extremely clear. The foam suppression from the 1 wt % SDS to the 1 wt % SDS + 0.1 wt % Antifoam-A system is the most pronounced while this suppression is further prominent as the concentration of Antifoam-A in the system

is increased. However no significant difference in foaming characteristics were observed between the 1 wt % SDS + 0.5 wt % Antifoam-A and the 1 wt % SDS + 1 wt % Antifoam-A systems. From the morphology study, it becomes clear that there is a certain optimal ratio in which SDS and Antifoam-A should be mixed in order to completely eliminate the problem of foam generation. As it turns out, this ratio of SDS:Antifoam was found to be 1:0.5 by weight. Clubbing all the results obtained together, it seems a pretty straightforward conclusion that 1:0.5 is the optimum weight ratio in which SDS and Antifoam-A should be mixed in order to obtain maximum foam suppression while at the same time not compromising on enhancing the kinetics of methane hydrate formation. The discovery of this silicone based antifoam now lends much more feasibility to the gas hydrate based methane storage technology on a commercial scale which employs surfactants like SDS as kinetic hydrate promoters to achieve rapid methane hydrate formation kinetics.

3.5. References

1. Kumar, A.; Bhattacharjee, G.; Kulkarni, B. D.; Kumar, R. Role of surfactants in promoting gas hydrate formation. *Ind. Eng. Chem. Res.* **2015**, 54, 12217-12232.
2. Link, D.D.; Ladner, E. P.; Elsen, H. A.; Taylor, C. E. Formation and Dissociation Studies for Optimizing the Uptake of Methane by Methane Hydrates. *Fluid Phase Equilib.* **2003**, 211, 1-10.
3. Lin, W.; Chen, G.J.; Sun, C.Y.; Guo, X.Q.; Wu, Z.K.; Liang, M.Y.; Chen, L.T.; Yang, L.Y. Effect of surfactant on the formation and dissociation kinetic behavior of methane hydrate. *Chem. Eng. Sci.* **2004**, 59, 4449-4455.
4. Zhang, J. S.; Lee, S.; Lee, J. W. Kinetics of Methane Hydrate Formation from SDS Solution. *Ind. Eng. Chem. Res.* **2007**, 46, 6353-6359.
5. Okutani, K.; Kuwabara, Y.; Mori, Y. H. Surfactant effects on hydrate formation in an unstirred gas/liquid system: An experimental study using methane and sodium alkyl sulfates. *Chem. Eng. Sci.* **2008**, 63, 183-194.
6. Bhattacharjee, G.; Barmecha, V.; Pradhan, D.; Naik, R.; Zare, K.; Mawlankar, R.B.; Dastager, S.G.; Kushwaha, O.S.; Kumar, R. The Biosurfactant Surfactin as a Kinetic Promoter for Methane Hydrate Formation. *Energy Procedia*, **2017**, 105, 5011-5017.
7. Bhattacharjee, G.; Kushwaha, O. S.; Kumar, A.; Khan, M. Y.; Patel, J. N.; Kumar, R. Effects of Micellization on Growth Kinetics of Methane Hydrate. *Ind. Eng. Chem. Res.* **2017**, 56, 3687-3698.
8. Bhattacharjee, G.; Choudhary, N.; Kumar, A.; Chakrabarty, S.; Kumar, R. Effect of the amino acid l-histidine on methane hydrate growth kinetics. *J. Nat. Gas. Sci. Eng.* **2016**, 35, 1453-1462.

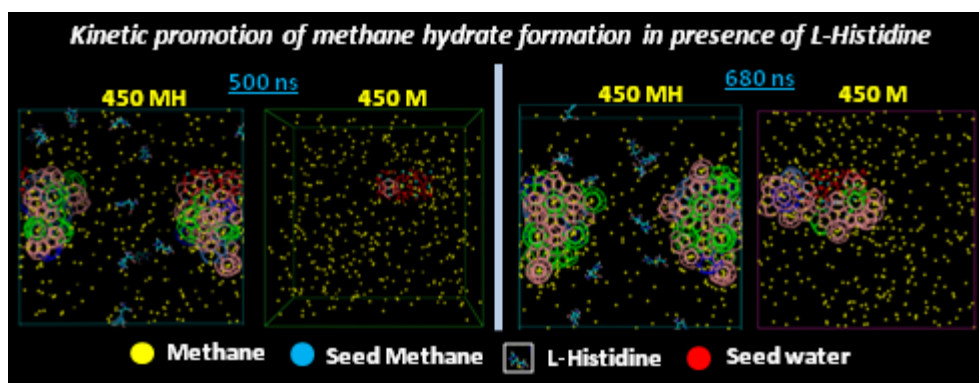
9. Liu, Y.; Chen, B.; Chen, Y.; Zhang, S.; Guo, W.; Cai, Y.; Tan, B.; Wang, W. Methane storage in a hydrated form as promoted by leucines for possible application to natural gas transportation and storage. *Energy Technol.* **2015**, 3, 815-819.
10. Veluswamy, H. P.; Hong, Q. W.; Linga, P. Morphology study of methane hydrate formation and dissociation in the presence of amino acid. *Cryst. Growth. Des.* **2016**, 16, 5932-5945.
11. Cai, Y.; Chen, Y.; Li, Q.; Li, L.; Huang, H.; Wang, S.; Wang, W. CO₂ Hydrate Formation Promoted by a Natural Amino Acid L-Methionine for Possible Application to CO₂ Capture and Storage. *Energy Technol.* 2017, DOI: 10.1002/ente.201600731
12. Perry, D. Silicone Surface-Active Agents; Dow Corning Corporation: United States, 2005
13. O'Lenick Jr, A.J. Silicone Emulsions and Surfactants-A Review; Silicone Spectator: United States, 2000
14. Wang, W.; Bray, C. L.; Adams, D. J.; Cooper, A. I. Methane storage in dry water gas hydrates. *J. Am. Chem. Soc.* **2008**, 130, 11608-11609.
15. Nguyen, N. N.; Nguyen, A. V.; Steel, K. M.; Dang, L. X.; Galib, M. Interfacial gas enrichment at hydrophobic surfaces and the origin of promotion of gas hydrate formation by hydrophobic solid particles. *J. Phys. Chem. C.* **2017**, 121, 3830-3840.
16. Veluswamy, H. P.; Yang, T.; Linga, P. Crystal growth of hydrogen/tetra-n-butylammonium bromide semiclathrates based on morphology study. *Cryst. Growth Des.* **2014**, 14, 1950-1960.
17. Bhattacharjee, G.; Kumar, A.; Sakpal, T.; Kumar, R. Carbon dioxide sequestration: influence of porous media on hydrate formation kinetics. *ACS Sustain. Chem. Eng.* **2015**, 3, 1205-1214.

18. Smith, J.M.; Van Ness, H.C.; Abbott, M.M. Introduction to chemical engineering thermodynamics; McGraw-Hill: New York, 2004.

19. Kang, S. P.; Lee, J.W. Kinetic behaviors of CO₂ hydrates in porous media and effect of kinetic promoter on the formation kinetics. *Chem. Eng. Sci.* **2010**, 65, 1840-1845.

Chapter 4

Bio based additives as kinetic promoters for methane hydrate formation



4. Bio based additives as kinetic promoters for methane hydrate formation⁴

⁴Versions of this chapter have been published

1. Bhattacharjee, G.; Barmecha, V.; Pradhan, D.; Naik, R.; Zare, K.; Mawlankar, R.B.; Dastager, S.G.; Kushwaha, O.S.; Kumar, R. The Biosurfactant Surfactin as a Kinetic Promoter for Methane Hydrate Formation. *Energy Procedia*, **2017**, 105, 5011-5017.
 2. Bhattacharjee, G.; Choudhary, N.; Kumar, A.; Chakrabarty, S.; Kumar, R. Effect of the amino acid l-histidine on methane hydrate growth kinetics. *J. Nat. Gas. Sci. Eng.* **2016**, 35, 1453-1462.
-

4.1. Introduction

The previous two chapters have dealt with kinetic hydrate promoters which are largely of a synthetic nature. While in Chapter 2, the anionic surfactant SDS and the zwitterionic surfactant CAPB were used to understand the effects of micellization on hydrate formation kinetics; to counter the excessive foam generation that is usually observed when conventional surfactants are used as kinetic hydrate promoters, Chapter 3 saw the introduction of a silicone based surfactant which was used as an antifoam and known simply as Antifoam-A.

The current chapter once again deals with kinetics hydrate promoters and enhancing the kinetics of hydrate formation. However, the additives used here are bio-derived unlike the synthetic ones used in the previous two chapters.

The first part of the chapter employs a bio based surfactant or biosurfactant called Surfactin to enhance the kinetics of methane hydrate formation. The biosurfactant would not only mimic the behaviour exhibited by a classic chemically derived surfactant such as SDS but would also provide the user with a much cleaner option. The main objective of this study is to get a fair comparison between the potentials of a typical biosurfactant and a synthetically derived surfactant for use as kinetic hydrate promoters

The second part of the chapter circles back to the problem of foam generation observed when using surfactants as kinetic hydrate promoters. In this case, a bio based additive, L-histidine which is an amino acid has been used as a kinetic hydrate promoter for methane hydrate formation. The foam generation that is observed with surfactants like SDS completely vanishes in the case of L-histidine. However, it also needs to be seen if the kinetics of methane hydrate formation is enhanced in the presence of L-histidine and if so, whether the kinetic promotion observed is comparable to that observed with conventional hydrate promoters such as SDS. The same has been investigated upon in this study.

4.2. The biosurfactant Surfactin as a kinetic promoter for methane hydrate formation

4.2.1. Introduction

Surfactants can be divided into two classes based on their origin. These are chemically derived and bio derived surfactants. Chemically derived surfactants (synthetic surfactants) are the classical surfactants such as SDS and CTAB that are used in most surfactant based applications whereas bio derived or bio based surfactants, known commonly as biosurfactants (ex-Surfactin) are usually produced on living surfaces, usually microbial cell surfaces or excreted extracellularly by microorganisms such as bacteria (Arora et al, 2016). In some cases, surfactants whose major components are derived from biological sources as with CAPB (discussed in the first part of this chapter) whose major component is derived from coconut oil may also be classified as biosurfactants.

The surfactants that are used as kinetic promoters for hydrate formation such as SDS are generally synthetic in nature (Kumar et.al, 2013). Although the use of such additives has proven to be very beneficial for gas hydrate formation, there's a big concern with regards to the toxicity of these compounds and their mode of disposal thereof. This ushers in the need to look for more benign additives which are low on the toxicity front and do not pose any threat to the environment, serious or otherwise. Biosurfactants, quite simply surfactants of biological origin are one such class of compounds fit the above mentioned criteria perfectly in that being of biological origin, they are essentially green additives. The extreme robustness of biosurfactants (stability at extreme conditions of temperature, salinity and pH) makes the investigation into these compounds as kinetic hydrate promoters all the more worthwhile (Arora et.al, 2016, Banat et.al, 2014, Rogers et.al, 2003).

Lipopeptides are compounds with cyclic structures generally produced from *Bacillus* and *Pseudomonas* species and exhibit diverse properties such as anti-microbial, cytotoxicity and surfactant like behavior. As a result of these various different characteristics, lipopeptides find application in a variety of areas such as food production (as emulsifiers), oil recovery from reservoirs, bioremediation etc.

Surfactin, the most popular and widely studied lipopeptide is an excellent biosurfactant and can reduce the surface tension of water from 72 to 27 mN/m. In fact it shows better surface activity than SDS, the surfactant of choice for gas hydrate studies (Ohno et.al, 1995). Surfactin was discovered by Arima et al., 1968 from the culture broth of *Bacillus subtilis* in an attempt to discover fibrin clot inhibitor (Arima et.al, 1968).

In the present study, a few different marine derived bacterial species were screened to test for the presence of Surfactin. The Polymerase Chain Reaction (PCR) technique was used for the preliminary screening based on which one of the bacterial isolates D-9 showed the presence of surfactin. The PCR results were followed upon with a few different assays such as oil spread assay and emulsification assay on the isolate D-9 to definitively prove the presence of surfactin. The effect of Surfactin on methane hydrate formation kinetics was then looked into by carrying out hydrate formation experiments in a stirred tank reactor.

4.2.2. Experimental Section

4.2.2.1. Materials

The marine derived bacterial strains to be screened for the production of Surfactin were field collected. Pure methane gas (purity > 99.5 %) was purchased from Vadilal Gases Pvt. Ltd., India. Peptone, Beef Extract and NaCl were purchased from HiMedia Laboratories, Pvt. Ltd., India. Distilled and deionized water was used for all the experiments performed.

4.2.2.2. Procedure followed for the production of Surfactin

The first step for the production of Surfactin is the preparation of the nutrient broth. The nutrient broth used in the present study consisted of 10 gm Peptone, 10 gm Beef Extract and 5 gm NaCl in 1 litre of water. Once the nutrient broth had been prepared, the previously isolated marine bacteria was grown in the nutrient broth for 48-72 hours at 30 °C and the cell free supernatant was obtained through centrifugation at 10,000 rpm for 20 minutes. The supernatant was then subjected to acid precipitation by adjusting the pH to 2.0 with 6M HCl and keeping it overnight at 4°C. The precipitate formed was recovered by centrifugation at 10,000 rpm for 20 minutes at 4°C and then extracted with methanol and concentrated with help of rotary evaporator (Vater et.al, 2002).

4.2.2.3. Procedure followed for hydrate formation experiments

A stirred tank reactor was used for the hydrate formation experiments. The components used in the setup were the same as shown in Fig. 2.2. The procedure used for the hydrate formation experiments is as follows. The aqueous hydrate forming solution with desired concentration of additive (140 cm³) was introduced into a 320 cm³ stainless steel crystallizer (CR; Parr Instrument Company, USA). In case of the biosurfactant Surfactin, 140 cm³ of the cell free supernatant liquid itself was taken as the hydrate forming solution. The CR was then sealed tightly and placed inside a temperature controlled water bath in order to attain the desired

experimental temperature (274.15.15 K). The vessel was flushed with pure methane gas by repeating rapid pressurization (~0.5 MPa) and depressurization cycles. Next, the CR was pressurized with the pure methane gas up to the pre determined experimental pressure of 5.0 MPa (equilibrium hydrate formation pressure for pure methane at 274.15 K is 2.8 MPa) thus providing sufficient driving force for hydrate formation. As soon as the desired experimental pressure is reached, the stirrer is turned on. The stirrer was set at a speed of 400 rpm to properly agitate the system and facilitate gas-water contact and mixing. At this stage, gas uptake measurements were initiated. As the hydrate formation experiment proceeded, the pressure inside the CR dropped as a result of the gas moving from the gaseous phase to the solid hydrate phase. This pressure drop inside the CR was measured using a pressure transducer (WIKA make; 0-25 MPa) to calculate the moles of gas taking part in the hydrate formation process. Temperature and pressure inside the CR were recorded every ten seconds using a data acquisition system (Micro Technics make) which was connected to a computer. As the experiments were conducted entirely in batch mode, the effective driving force for hydrate formation decreased as the reaction proceeded. This is a result of more and more gas migrating from the gaseous phase to the solid hydrate phase until there isn't sufficient pressure (driving force) left in the CR to sustain hydrate formation. The calculation for the amount of gas consumed during hydrate formation was exactly the same as given in section 2.2.7.

The important thing to note here is that for the hydrate formation experiments, the cell free supernatant containing Surfactin itself was used as the hydrate forming solution. Since this was a basic study performed mainly to gauge whether the presence of Surfactin in the system has any effect on methane hydrate formation kinetics or not, using the crude supernatant sufficed and further processing of the supernatant to exclusively isolate Surfactin was not carried out.

4.2.3. Results and Discussions

4.2.3.1. Screening for the presence of Surfactin

A preliminary screening for the presence of Surfactin was done using the polymerase chain reaction (PCR) technique which was followed by secondary tests such as oil spreading and emulsification assays to conclusively prove the presence of Surfactin. These procedures were carried out at the National Collection of Industrial Microorganisms, CSIR-National Chemical

Laboratory, Pune, India and as such are beyond the scope of the current thesis. Details of the same can be found in the thesis by Lakdawala, 2014.

4.2.3.2. Effect of Surfactin on Methane Hydrate formation kinetics

The effect of Surfactin on methane hydrate formation kinetics was investigated by using the Surfactin containing cell free supernatant as the hydrate forming solution in a stirred tank reactor. Fig. 4.1 given below compares the average gas uptake (mol of gas consumed/ mol of water) obtained using the Surfactin containing supernatant with that for pure water. Hydrate formation kinetics was also recorded using just the nutrient broth as the hydrate forming solution and has been included in Fig. 4.1. Time zero in Fig. 4.1 corresponds to the induction time for all the experiments carried out. As can be seen in the figure, hydrate formation kinetics is significantly enhanced in the presence of Surfactin as compared to pure water. The considerable enhancement observed when compared with the kinetics in presence of just the nutrient broth also proves the presence of Surfactin in the supernatant solution used. It also tells us that the biosurfactant Surfactin as an individual has a definite significant promoting effect on methane hydrate formation.

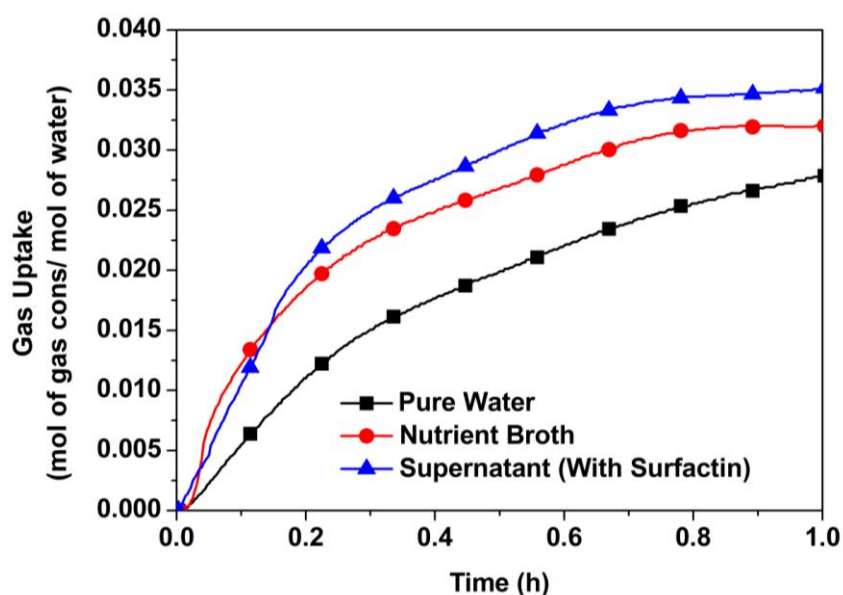


Fig. 4.1: Comparison of average gas uptake during methane hydrate formation from different hydrate forming solutions: pure water, nutrient broth and cell free Surfactin containing supernatant.

Since the nutrient broth consists of three different components, NaCl, Beef extract and Peptone, it was decided to individually check the effect of these three compounds on methane hydrate formation kinetics. Fig. 4.2 given below plots the average rate of gas uptake in

presence of these three additives in the system and compares the methane hydrate formation kinetics obtained with that for pure water. The concentrations of the three individual components were kept the same as in the nutrient broth. It can be observed from Fig. 4.2 that while Peptone and Beef extract both significantly enhance hydrate formation kinetics, the introduction of NaCl into the system hardly has any effect on the same.

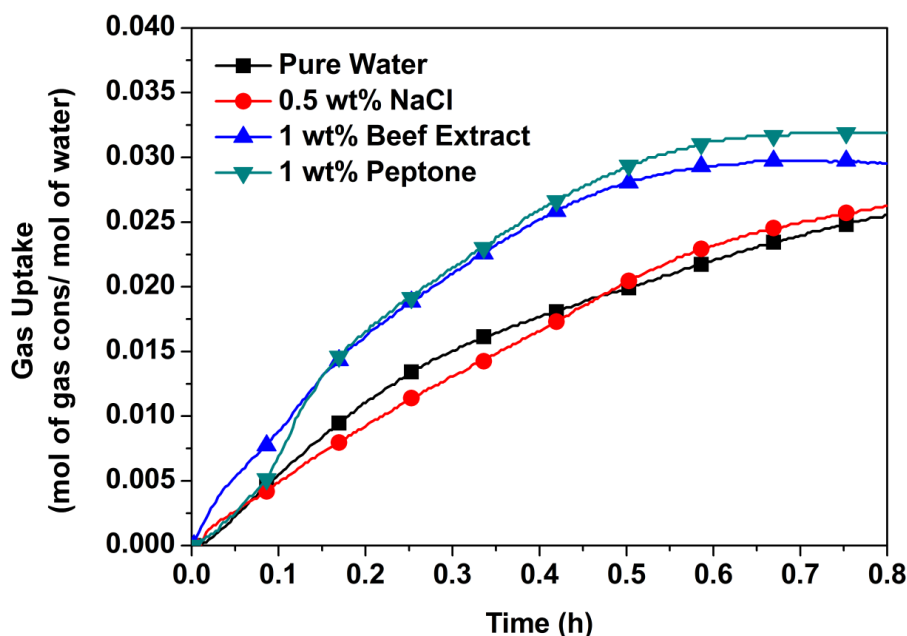


Fig. 4.2: Comparison of average gas uptake during methane hydrate formation individually with pure water, NaCl, Beef Extract and Peptone (the different components present in the Nutrient Broth).

Fig. 4.3 compares the gas uptake obtained in presence of biosurfactant Surfactin with that obtained in presence of SDS, the most commonly used synthetic kinetic hydrate promoter. The concentration of SDS used was 1 wt % while for Surfactin, the cell free supernatant solution was used. As can be clearly seen in Fig. 4.3, although the initial kinetics is higher with SDS, the overall hydrate formation kinetics is significantly higher for the Surfactin containing supernatant system. There is a considerable jump in the final gas uptake after one hour of hydrate formation for the system containing Surfactin as compared to the 1 wt % SDS system and as hydrate formation has nearly reached saturation at the end of one hour for both systems, the gas uptake at the end of one hour can well be taken as the final gas uptake for hydrate formation for both the systems in consideration here. This result is extremely vital as it shows that the non-toxic and environment friendly biosurfactant Surfactin actually shows better methane hydrate formation kinetics as compared to the commonly used synthetic kinetic hydrate promoter SDS. However, there is ground for debate as to which kind of

surfactant may actually be used when it comes to running these operations on an industrial scale as biosurfactants are incredibly expensive and in case the promotion in hydrate formation kinetics with biosurfactants is not considerable as compared to common chemically derived synthetic surfactants such as SDS, the whole feasibility aspect of the operation goes for a toss.

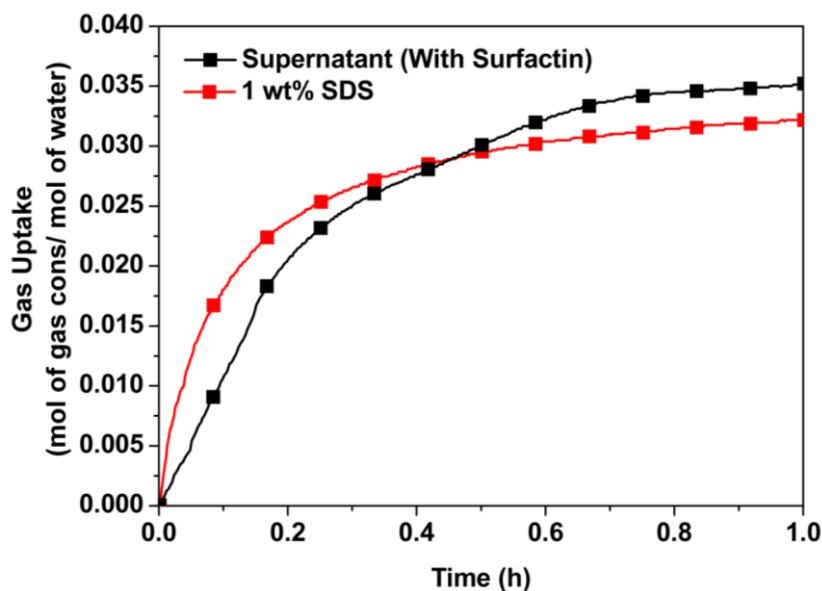


Fig. 4.3: Comparison of average gas uptake during methane hydrate formation with cell free supernatant containing the biosurfactant Surfactin and with 1 wt% SDS.

Figure A5 in Appendix A shows a linear fit of the first twenty minutes of hydrate growth in the STR setup with pure methane for the different surfactant systems studied. The average initial apparent rates of hydrate formation for the first twenty minutes (mol of gas consumed/h) obtained for the different systems as a result of the linear fitting have been reported in Table A3, Appendix A.

4.2.4. Conclusions

The present study deals with testing the effect of the biosurfactant Surfactin on methane hydrate formation kinetics. Based on preliminary screening using the polymerase chain reaction technique and a couple of other assays, namely the oil spread assay and emulsification assay, the D-9 bacterial strain was concluded to be a producer of Surfactin. Methane hydrate formation experiments were carried out in the presence of Surfactin using a stirred tank reactor. It was found out that the presence of Surfactin favorably affects methane hydrate formation kinetics showing a significant enhancement as compared to pure water. The enhancement in kinetics observed with Surfactin was found to be much greater than that

obtained with 1 wt % SDS. The results obtained in this study hold great importance as we look to move away from synthetic additives to benign, environment friendly ones for use as kinetic promoters in gas hydrate based applications such as methane separation, storage and transport.

4.3. Effect of the amino acid L-histidine on methane hydrate growth kinetics

4.3.1. Introduction

Over the past decade or so of hydrate research, a large number of additives have been identified that when mixed with water, alter the kinetics of hydrate formation and given the application in hand, these additives can be classified into two broad categories, promoters and inhibitors (Bagherzadeh et al., 2015; Kelland, 2006; Perrin et al., 2013).

It has already been discussed in the previous chapters that hydrate promoters can be divided into two categories: thermodynamic and kinetic promoters. A basic discussion on these two kinds of hydrate promoters and their mode of action to promote hydrate formation can be found in Section 1.3.1.

Similar to hydrate promoters, hydrate inhibitors can also be divided into two groups; thermodynamic and low dosage hydrate inhibitors (LDHIs). As expected, thermodynamic inhibitors shift the hydrate equilibrium conditions to much more drastic conditions; i.e. higher pressures and lower temperatures. LDHIs on the other hand, can be further broken down into anti-agglomerants and kinetic inhibitors. While anti-agglomerants prevent the agglomeration of formed hydrate nuclei, kinetic inhibitors may either delay hydrate nucleation or retard hydrate growth or both (Kelland, 2006; Kumar et al., 2015b). Both thermodynamic inhibitors and LDHIs primarily find importance in flow assurance where the formation of gas hydrates inside oil and gas pipelines results in plugging of the same. The use of hydrate inhibitors in appropriate concentrations is able to prevent/delay the formation of gas hydrates in these pipelines thus significantly reducing the uncertainty in operation and maintenance of the same. At the moment, thermodynamic inhibitors such as ethylene glycol are being used to prevent hydrate plug formation but due to the limitation of these additives being required in large quantities to effect hydrate inhibition, there is a need to shift towards LDHIs which can be used in exceedingly small doses to achieve the same (Anderson et al., 2005; Daraboina et al., 2011; Frostman et al., 2003; Lederhos et al., 1996; Perrin et al., 2013; Yagasaki et al., 2015).

The use of hydrophobic amino acids as KHIs has been studied in the past. Sa et.al. (2013) and (2015) conducted two different studies using a number of hydrophobic amino acids. CO₂ hydrate formation kinetics was reported in both the studies. It was observed that the kinetic inhibiting effect of the amino acids decreased with increase in their hydrophobicity. A perturbation mechanism was used to explain the kinetic inhibiting behavior of the amino acids. The less hydrophobic amino acids would disrupt the hydrogen bonding between water molecules thus preventing the formation of water cages and subsequently inhibiting hydrate formation whereas the more hydrophobic amino acids would strengthen the local organization of the water structure due to the presence of long alkyl chains in their structures (Sa et al., 2015, 2013). Roosta et.al. (2016) reported similar results (kinetic inhibiting behavior of some new structures of amino acids on CO₂ hydrate formation) in a recently conducted study (Roosta et al., 2016). Hydrophobic amino acids have also been known to act as THIs for CO₂ hydrate formation. Sa et.al. (2011) tested the potential of three different amino acids; glycine, L-alanine and L-valine as THIs on CO₂ hydrate inhibition. L-valine was found to be the most effective THI (on a mole concentration basis) followed by L-alanine and then glycine (Sa et al., 2011). Oluwunmi et.al. (2015) used molecular dynamics simulation to screen for new kinetic inhibitors of methane hydrate. One of the compounds investigated was a natural amino acid, Asparagine which was found to be a more active inhibitor than a number of synthetic inhibitors such as PVCap (Oluwunmi et al., 2015). Amino acids have also been used to inhibit the formation of tetrahydrofuran (THF) hydrate. Naeiji et.al. (2014) studied the individual effects of the amino acids Glycine and Leucine on THF hydrate formation. While both amino acids showed considerable inhibition performance, it was observed that the amino acid with lower hydrophobicity, Glycine was more effective in delaying the nucleation and reducing growth of THF hydrate (Naeiji et al., 2014).

Antifreeze proteins (AFPs) which are essentially made up of amino acids have been long known to cause depression in freezing point of water. The AFPs bind on the surface of ice crystals (to a specific ice plane) and inhibit their growth (Bagherzadeh et al., 2015; Ewart et al., 2014; Yeh and Feeney, 1996). Consequently, it was observed that AFPs can also act as effective kinetic hydrate inhibitors (Daraboina et al., 2011; Gordienko et al., 2010; Ohno et al., 2010; Perfeldt et al., 2014). It can thus be hypothesized that amino acids by themselves should always show hydrate inhibiting behavior. However this is not always the case and contradicting results have also been reported in literature. In one such study, Perfeldt et.al. (2014) report the efficacy of an AFP (Rhagium mordax (RmAFP1)) for inhibiting methane

hydrate growth and compare the results obtained with those for two different amino acids, L-valine and L-threonine. It was found that the amino acids did not show any inhibiting effect as they could not delay the induction times as compared to the non-inhibited system whereas the AFP showed kinetic inhibiting activity comparable to polyvinyl pyrrolidone (PVP), a well-known KHI under similar experimental conditions. No kinetic inhibiting activity was observed for the hydrate growth phase either using the two amino acids. While the L-valine system showed more or less similar growth kinetics as compared to the non-inhibited system, the threonine system showed a slight promoting effect (Perfeldt et al., 2014). Liu et.al. (2015) used the amino acid Leucine to promote the formation of methane hydrate with a view on storing methane in the form of hydrates. It was observed that in the presence of Leucine, methane could be stored in a hydrated form with a high hydrate formation rate and high storage capacity (Liu et al., 2015). Bagderzah et.al. (2015) studied the mechanism through which the Winter Flounder AFP (*wf*-AFP) inhibits the growth of methane hydrate. The *wf*-AFP is mainly made up of the amino acids threonine and alanine. It was observed using MD simulations that a set of hydrophobic pendant methyl groups present on the *wf*-AFP binds to the empty half cages at the hydrate-water interface. The pendant methyl side chains in the *wf*-AFP are actually the side chains of the two amino acids (threonine and alanine) present in the AFP. The discussion presented by the authors therefore presents a different take on the inhibition mechanism of the *wf*-AFP, which is separate from the mechanism predicted in an earlier study that inhibition is due to the hydrogen bonding between the OH group of threonine residues and water oxygen at the ice surface (Bagherzadeh et al., 2015; Cheng and Merz, 1997; McDonald et al., 1993).

Clearly, there is some ambiguity regarding the effect of different amino acids on gas hydrate formation, there is a possibility that inhibiting effect also depends on the hydrate forming gas, additive concentration etc. Being zwitterionic molecules, the presence of electric charges on amino acid molecules are expected to aid the interaction between amino acids and water. In addition, the presence of hydrophilic (carboxylic and amine) groups aids in hydrogen bonds interaction; while from the work carried out by Bagderzah et.al. (2015) the possibility of hydrophobic-hydrophobic interactions between the non-polar side chains and empty half hydrate cages cannot be ignored (Bagherzadeh et al., 2015).

In the present work, the effect of L-histidine, a relatively less hydrophobic amino acid on methane hydrate formation was investigated. In terms of descending order of hydrophobicity (hydropathy scores), the commonly used amino acids for hydrate based studies rank in the

order isoleucine (4.5) > valine (4.2) > leucine (3.8) > alanine (1.8) > glycine (-0.4) > threonine (-0.7) > histidine (-3.2) (Kyte and Doolittle, 1982). Unlike other amino acids such as valine, leucine, alanine etc, histidine molecules have no hydrophobic side chains which rules out the likelihood of hydrophobic-hydrophobic interactions thus making the system much simpler. A schematic of the structure of L-histidine is given as Figure 4.4. Experimental studies were carried out to gauge the effect of L-histidine on methane hydrate formation kinetics. Pure methane was chosen as the hydrate forming gas with hydrate based methane storage being the application in focus. The experimental results were complemented by results obtained from a simulation study. However reporting the results of the simulation study are beyond the scope of this thesis and have been presented elsewhere (Bhattacharjee et.al, 2016).

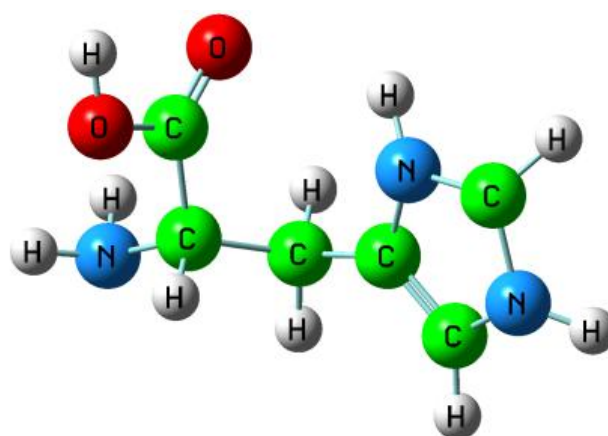


Fig. 4.4: Schematic of the structure of L-histidine.

4.3.2. Experimental Section

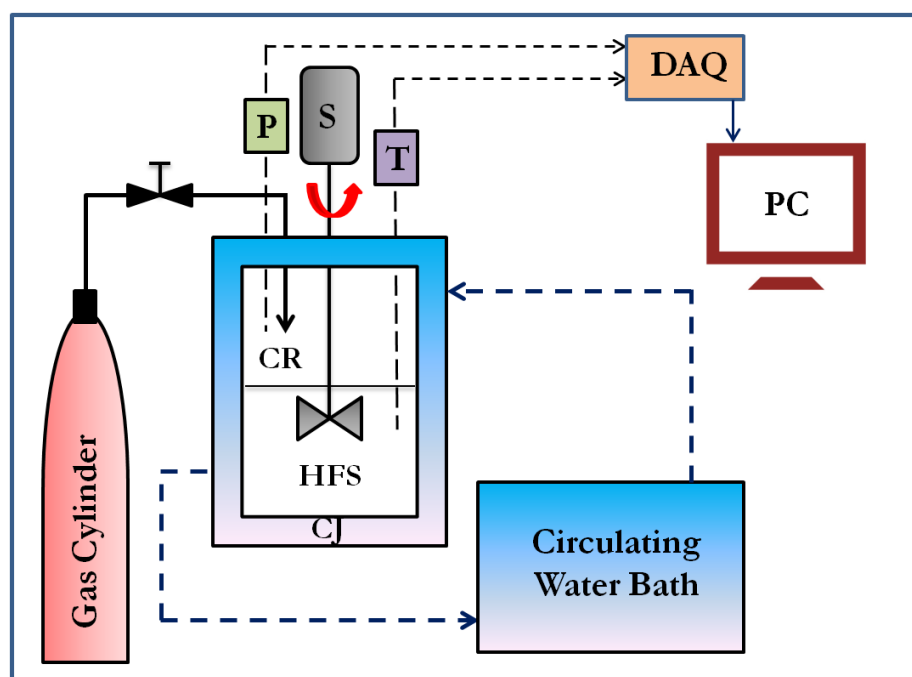
4.3.2.1. Materials

Methane gas with a purity of more than 99.5% was supplied by Vadilal Gases Pvt. Ltd., India. L-histidine with a minimum purity of 99% was purchased from HiMedia Laboratories Pvt. Ltd. Sodium dodecyl sulfate (SDS) was purchased from Thermo Fischer Scientific India Pvt. Ltd. Distilled and deionized water was used for all the experiments.

4.3.2.2. Apparatus and procedure for hydrate formation experiments

A stirred tank reactor setup as shown in Figure 4.5 was used to carry out the experiments in this study. Given below is the procedure used for the hydrate formation experiments which in the process also gives a detailed description of the stirred tank apparatus used:

The aqueous hydrate forming solution with desired concentration of additive (140 cm^3) was introduced into a (320 cm^3) stainless steel crystallizer (CR; Parr Instrument Company, USA). The CR was then sealed tightly and placed inside a temperature controlled water bath in order to attain the desired experimental temperature (274.15 K). The vessel was flushed with pure methane gas by repeating rapid pressurization ($\sim 0.5\text{ MPa}$) and depressurization cycles. Next, the CR was pressurized with the pure methane gas up to the pre determined experimental pressure of 5.0 MPa (equilibrium hydrate formation pressure for pure methane at 274.15 K is 2.8 MPa) thus providing sufficient driving force for hydrate formation. As soon as the desired experimental pressure is reached, the stirrer was turned on. The stirrer is set at a low speed (150 rpm) to appropriately study the effect of L-histidine on the kinetics of hydrate growth. At this stage, gas uptake measurements were initiated. As the hydrate formation experiment proceeded, the pressure inside the CR dropped as a result of the gas moving from the gaseous phase to the solid hydrate phase. This pressure drop inside the CR was measured using a pressure transducer (WIKA make; $0\text{-}25\text{ MPa}$) to calculate the moles of gas taking part in the hydrate formation process. Temperature and pressure inside the CR were recorded every ten seconds using a data acquisition system (Micro Technics make) which was connected to a computer. As the experiments were conducted entirely in batch mode, the effective driving force for hydrate formation decreased as the reaction proceeded. This is a result of more and more gas migrating from the gaseous phase to the solid hydrate phase until there isn't sufficient pressure (driving force) left in the CR to sustain hydrate formation.



P-Pressure Transducer	CR-Crystallizer	DAQ-Data Acquisition system
S-Stirrer	CJ-Crystallizer Jacket	PC-Personal Computer
T-Thermocouple	HFS-Hydrate Forming Solution	

Fig. 4.5: Detailed schematic of the experimental setup.

4.3.2.3. Calculation of the amount of gas consumed during the hydrate formation experiments

The calculation of the amount of gas consumed during hydrate formation was exactly the same as described in Chapter 2, Section 2.2.7.

4.3.2.4. Calculation of the rate of hydrate formation

The rate of hydrate formation was calculated by the forward difference method as given by the following equation: (Bhattacharjee et al., 2015)

$$\left(\frac{d\Delta n_{H,\downarrow}}{dt} \right)_t = \frac{\Delta n_{H,\downarrow}(t+\Delta t) - \Delta n_{H,\downarrow}(t)}{\Delta t}; \Delta t=10 \text{ sec} \quad (4.1)$$

The average of these rates was calculated for every 20 minutes and reported.

The rate of hydrate formation for the first 20 minutes (mol/h) was calculated by fitting the hydrate growth (gas uptake) data versus time (h) for the first 20 minutes of hydrate formation/growth to a straight line using the least squares method.

4.3.3. Results and Discussions

Table 4.1 summarizes all the experiments performed in the course of this study. Relevant information such as the amount of gas consumed (milimoles) after three hours of hydrate growth, the induction time and the average rate of gas uptake (mol/ h) for the first 20 minutes of hydrate formation have been reported.

4.3.3.1. Methane Hydrate formation kinetics in presence of L-Histidine

Figure 4.6 compares methane hydrate formation kinetics in presence of different concentrations of L-histidine with that for pure water and that for a 1 wt% SDS system. Milimoles of gas consumed for hydrate formation per mole of water has been plotted with respect to time. Time zero corresponds to the nucleation points for the different systems studied. As can be observed from Figure 4.6, methane hydrate formation kinetics is significantly enhanced in the presence of L-histidine. L-histidine is a polar amino acid with a very low hydrophathy index (-3.2) i.e. it has a high propensity to be in contact with water. As such, L-histidine is expected to form hydrogen bonds with its surrounding water molecules, i.e. classically L-histidine should delay the formation of water cages for hydrate formation. But it is clear from our experiments which were repeated at least three times that L-histidine actually acts as a kinetic hydrate promoter significantly speeding up the hydrate formation process. However, it can also be seen in Figure 4.6 that L-histidine however falls short when it comes to the kinetics of hydrate formation as compared to a system having similar concentration (1 wt %) of Sodium dodecyl sulfate (SDS), a conventional kinetic hydrate promoter. The effect of L-histidine on the induction time for hydrate formation has been discussed later. Inset, Figure 4.6 shows the pressure profile during hydrate formation for fresh runs of the different systems used. Rapid pressure drop can be observed for the SDS (1 wt %) system followed by the L-histidine (1 wt %) system, L-histidine (0.1 wt %) and pure water systems respectively. It can also be seen from inset, Figure 4.6 that induction time is greatly reduced in presence of L-histidine as compared to pure water. Figure 4.7 plots the average induction times along with the standard deviations for the different systems studied. Induction times for the fresh and memory runs have been plotted individually. It is clear from

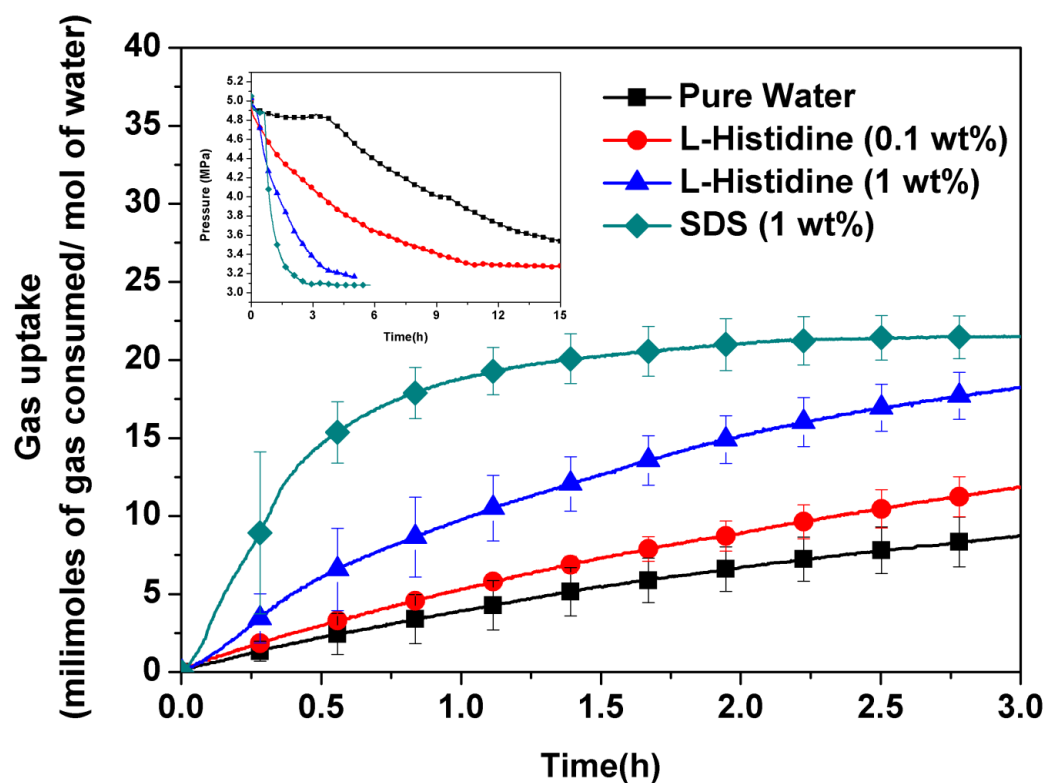
Figure 4.7 that the introduction of L-histidine into the system reduces the induction time for methane hydrate formation which further strengthens the argument for using L-histidine as a kinetic hydrate promoter. Figures 4.8 and 4.9 show the gas uptake (milimoles of gas

consumed per mole of water) for all the experiments conducted in this study. Fresh and memory experiments have been plotted individually.

Table 4.1: Summary of all the experiments conducted. Gas consumption is reported for a set time of 3 hours after nucleation. A fixed volume of water (140 ml) was used for all the experiments.

System	Exp No.	Sample State	Gas Consumed (milimoles)	Induction Time (min)	$\zeta \pm SD$
Pure Water	1	Fresh	54.23	222.50	0.0345±0.000031
	2	Memory	58.76	113.46	
	3	Memory	73.28	10.83	
	4	Fresh	69.93	70.00	
	5	Memory	64.24	31.33	
	6	Fresh	79.60	484.62	
L-Histidine (0.1 wt %)	7	Fresh	79.58	2.83	0.0463±0.000350
	8	Memory	95.58	1.50	
	9	Memory	105.14	0.00	
	10	Fresh	101.31	2.17	
	11	Memory	104.44	5.00	
	12	Fresh	94.48	94.50	
L-Histidine (1 wt %)	13	Fresh	154.35	13.32	0.1012±0.000686
	14	Memory	100.58	24.48	
	15	Memory	83.46	34.00	
	16	Fresh	131.05	469.98	
	17	Memory	131.61	44.82	
	18	Fresh	139.34	36.00	
SDS (1 wt%)	19	Fresh	171.514	37.5	0.2474±0.000994
	20	Fresh	154.701	1128	
	21	Fresh	174.790	1.332	

ζ : Average rate of hydrate formation for first 20 minutes (gas uptake) (mol of gas / h)



- Volume of aqueous hydrate forming solution used: 140 cm^3 .
- Volume of gaseous phase available: 180 cm^3 .

Fig. 4.6: Comparison of the gas uptake for the different systems studied (fresh runs) with average and standard deviation.

Inset: Pressure profile during hydrate formation; Pure Water: Exp. No.1, L-histidine (0.1 wt %): Exp. No.7, L-histidine (1 wt %): Exp No.13, SDS (1 wt %): Exp No. 19. Rapid pressure drop for the L-histidine (1 wt %) and SDS (1 wt %) systems can be observed signifying enhanced methane hydrate formation kinetics compared to the pure water system.

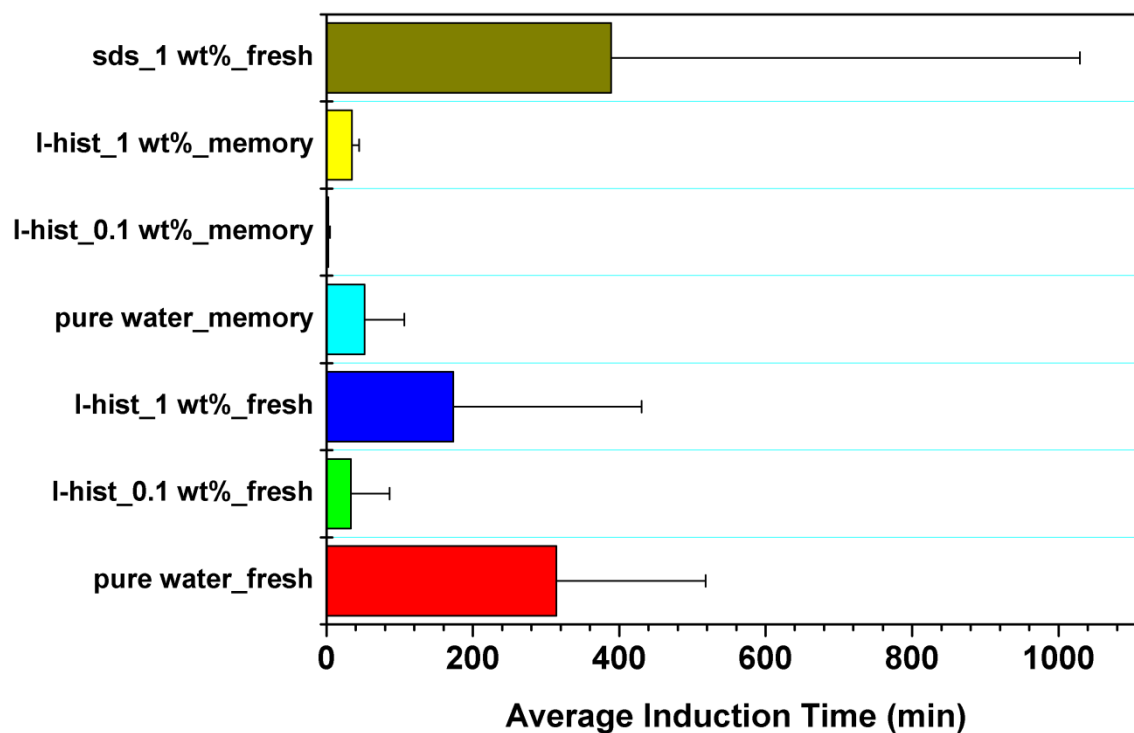


Fig. 4.7: Average induction times for the different systems studied (fresh and memory runs) with standard deviation.

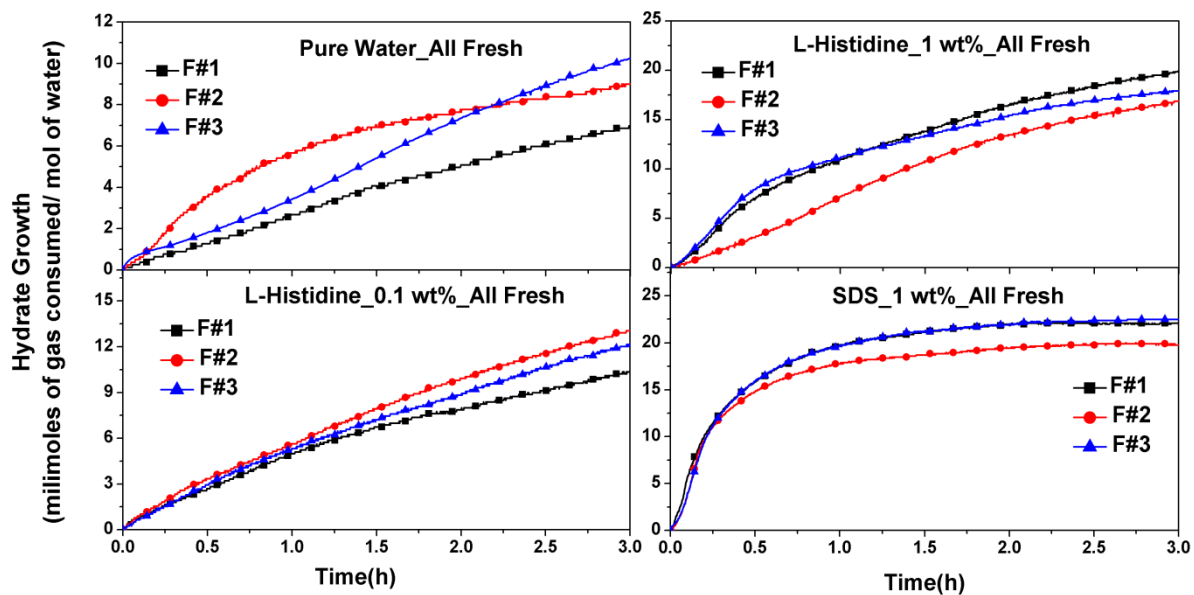


Fig. 4.8: Hydrate growth (millimoles of gas consumed per mole of water) for the individual fresh runs of all three systems studied

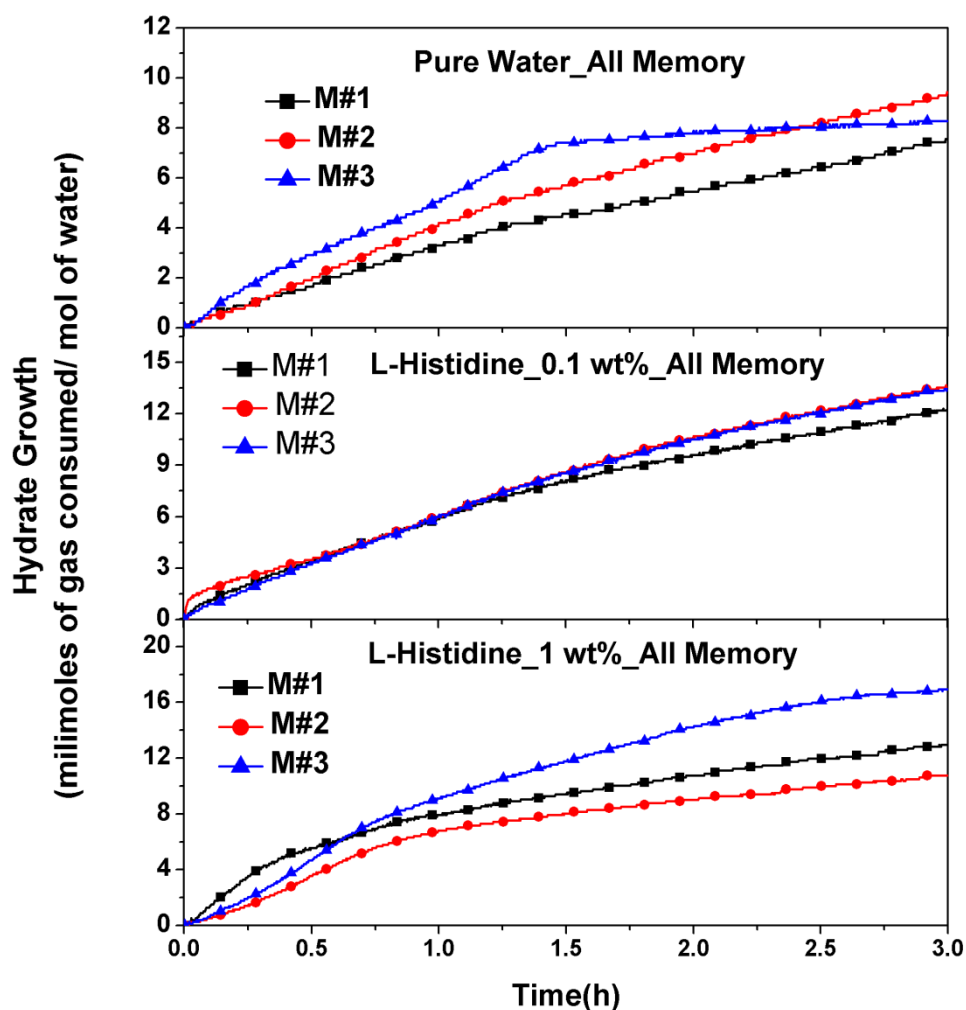


Fig. 4.9: Hydrate growth (millimoles of gas consumed per mole of water) for the individual memory runs of all three systems studied.

4.3.3.2. Rate of hydrate formation

Figure 4.10 plots the average rate of gas uptake (mol of gas/ mol of water/ h) against time (h) for the different systems studied. As can be seen from Figure 4.10, initial rates of hydrate formation in presence of L-histidine are significantly enhanced as compared to pure water for both the concentrations of L-histidine studied but the rate of hydrate formation in presence of 1 wt % SDS surpasses that in presence of 1 wt % L-histidine which is in agreement to the hydrate growth kinetics observed in Figure 4.6. Inset, Figure 4.10 plots the rate of hydrate formation (gas uptake) (mol of gas consumed/ h) for the first 20 minutes of hydrate growth for each of the systems studied. It follows from Figure 4.10 that the SDS (1 wt %) system shows the fastest average rate of gas uptake for the first twenty minutes of hydrate growth (0.2474) followed by the L-histidine (1 wt %) system (0.1012) and then the L-histidine (0.1

wt %) and pure water systems (0.0463 and 0.0345) respectively. An increase of almost 66 % was thus observed in the average rate of hydrate formation for the first twenty minutes from the pure water system to the L-histidine (1 wt %) system. Linear fits of the gas uptake data for the first 20 minutes of hydrate growth for the fresh runs of the different systems studied are shown in Figure 4.11. The same has been done for the memory runs of the different systems studied and shown in Figure A6, Appendix A. The average initial apparent rates of hydrate formation for the first twenty minutes of hydrate growth for both fresh and memory runs for the different systems studied obtained as a result of the linear fitting have been reported in Table A4, Appendix A.

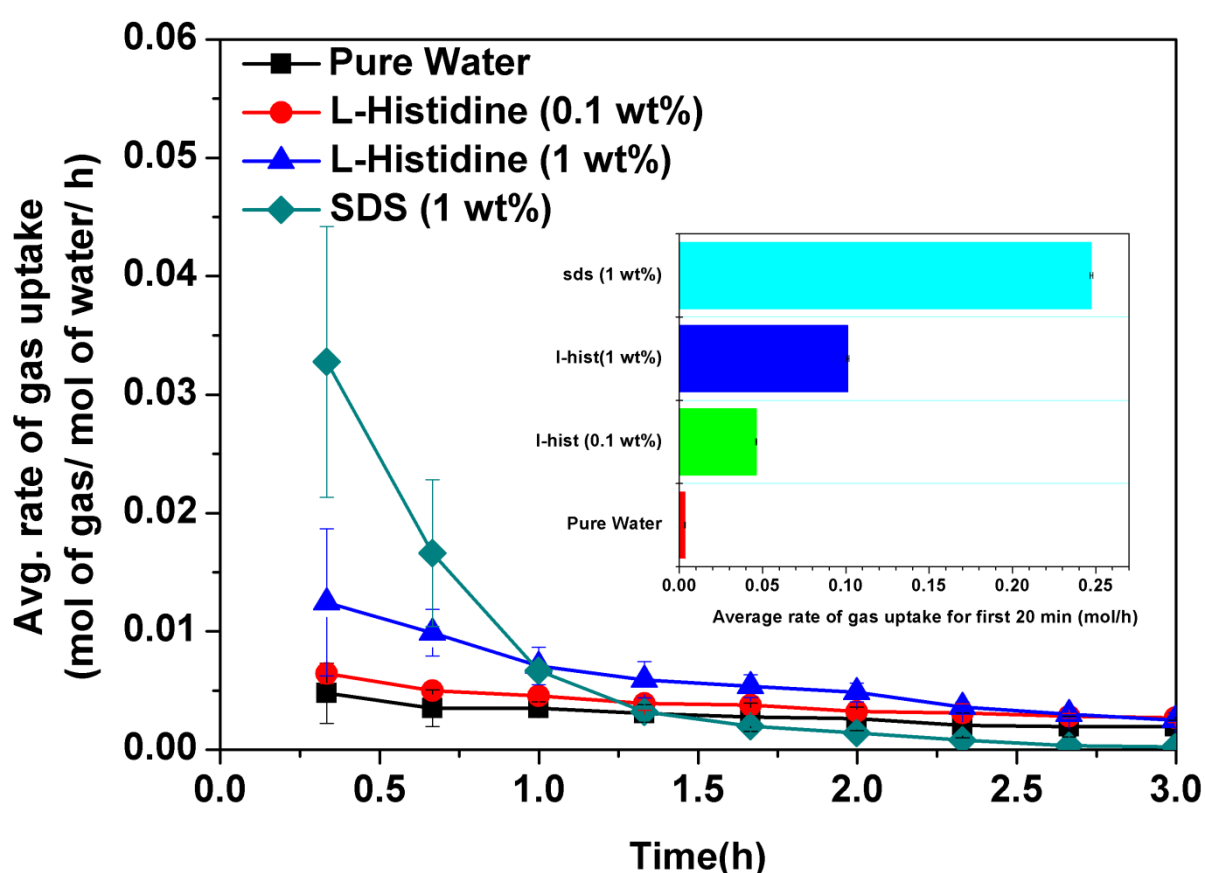


Fig. 4.10: Average rate of gas uptake for the different systems studied (fresh runs) with standard deviation.

Inset: Average rate of gas uptake in mol/ h for the first 20 minutes of hydrate growth with standard deviation. The rate of hydrate formation for the first 20 minutes shows an increase of approximately 190% from the pure water system to the L-histidine (1 wt %) system while there's an even bigger increase for the SDS (1 wt %) system.

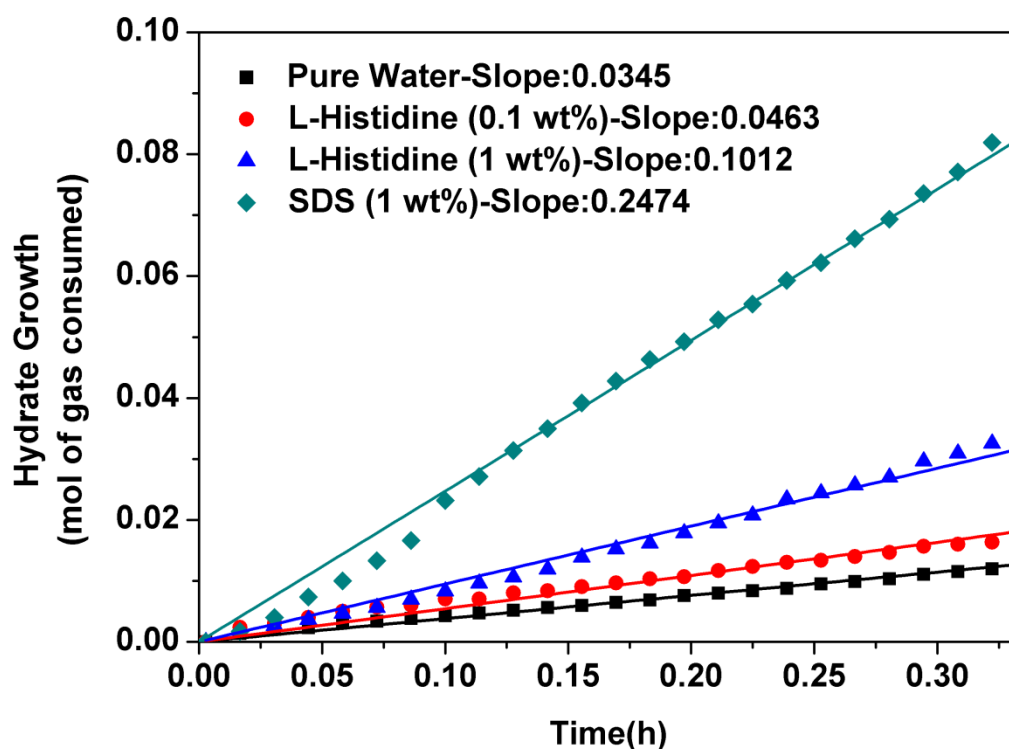


Fig. 4.11: Linear fit of the first 20 minutes (0.334h) of hydrate growth for the different systems studied: Average of fresh runs.

4.3.3.3. Final gas consumption in presence of L-histidine and comparison with SDS

Figure 4.12 shows the average final gas consumption for hydrate formation (milimoles of gas consumed per mole of water) after 5 hours of hydrate growth for the different systems studied. The final gas consumption in presence of L-histidine is compared with that obtained using SDS (1 wt %) which is the additive of choice in most hydrate studies where rapid hydrate formation (hydrate promotion) is required. SDS experiments were performed using the same setup and at the same operating conditions as used for the other experiments performed in this study. It can be observed from Figure 4.12 that there was a very minute or no difference in the average final gas uptake for hydrate formation after 5 h between L-histidine and SDS. This bodes extremely well for L-histidine as it is significantly easier to handle as compared to SDS.

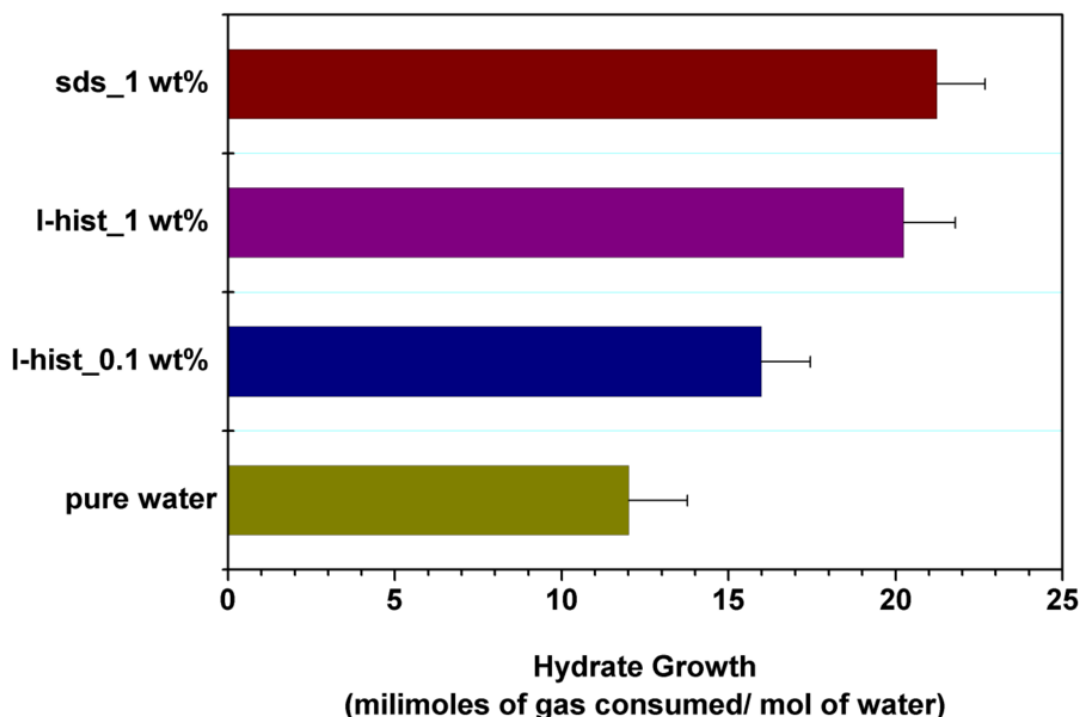


Fig. 4.12: Average final gas consumption (milimoles of gas consumed/ mol of water) after 5 hours for the different systems studied (fresh runs) with standard deviation. Similar final gas consumption can be observed for both L-histidine (1 wt %) and SDS (1 wt %) systems.

4.3.3.4. Ease of handling L-histidine as compared to SDS with regards to foam generation

One of the main or perhaps the only disadvantage when it comes to working with SDS is the large amount of foam that SDS, being a surfactant generates during the dissociation of gas hydrates. The excessive foam generation with SDS is sure to pose severe operational challenges when using hydrate based technologies on a commercial scale such as limiting the continuity of the process and severely affecting the economics of the process as a result of the additional steps involved in disposing of the additive and cleaning of the system. Moreover, it also slows down the kinetics of the hydrate dissociation process. The issue of foam generation can be completely done off with by using the amino acid L-histidine instead of SDS as the kinetic hydrate inhibitor as illustrated in Figure 4.13. The figure shows two different vials each containing a different water-additive solution. Vial A contains a 1 wt % solution of SDS whereas Vial B contains a 1 wt% solution of L-histidine. The vials were shaken thoroughly and then rested in normal room conditions for 15 minutes. A large amount of foam can be seen to have generated above the liquid interface for the 1 wt % SDS solution whereas the

same is clearly missing for the 1 wt % L-histidine solution in Vial B thus confirming that there is no foam formation when using L-histidine and laying down a marker on the greater ease of handling of the L-histidine system.

This is a very significant finding as far as the hydrate based methane storage technology is concerned as ideally, now, by using L-histidine as a kinetic hydrate promoter, similar final gas uptake as compared to SDS can be obtained (Figure 4.12) while also avoiding the added hassle of dealing with the large amount of foam that is generated in presence of SDS (Figure 4.13) thus greatly increasing the scalability potential of the hydrate based methane storage technology.

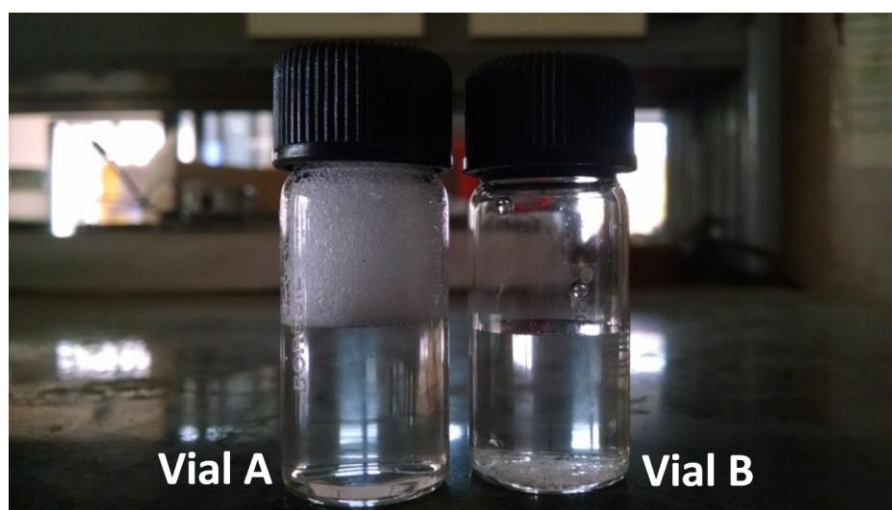


Fig. 4.13: Ease of handling of l-histidine as compared to SDS: Vial A (1 wt % SDS) shows the generation of a large amount of foam whereas no foam generation can be seen in Vial B (1 wt % L-histidine).

4.3.4. Conclusions

Methane hydrate formation experiments were carried out in a stirred tank reactor setup to study the effect of L-histidine on methane hydrate formation kinetics. MD simulations were carried out to further validate the results obtained from the experiments. Although the MD simulation study is beyond the scope of this thesis, the results obtained/ conclusions drawn from the two studies have been compared here to better understand the subject matter at hand. Two different concentrations of L-histidine were used in the experiments (0.1 wt % and 1 wt %) whereas for the simulation runs, the concentration of L-histidine was kept fixed at approximately 1 wt % (0.94 wt %). From the experiments it was observed that hydrate growth

kinetics shows an improvement in presence of L-histidine. For both the concentrations of L-histidine used, methane hydrate formation kinetics was observed to be enhanced in comparison to pure water. The final gas consumption for hydrate formation with 1 wt % L-histidine was found to be comparable with that for 1 wt % SDS although the kinetics of hydrate formation with 1 wt % L-histidine was surpassed by that with 1 wt % SDS. Results obtained from MD simulation supported the observations made from experiments as hydrate formation in the presence of L-histidine showed lower induction time and faster hydrate growth as compared to a pure water system. For the experiments conducted, approximately 66 % increase in the hydrate growth rate for the first 20 minutes of hydrate formation was observed from the pure water system to the L-histidine (1 wt %) system whereas for the simulations, an approximate increase of 34 % was observed. The importance of this study stems from the fact that comparable gas uptake for methane hydrate formation can be observed between L-histidine (a benign kinetic hydrate promoter) and SDS (the most commonly kinetic hydrate promoter). Moreover, the use of L-histidine lends a greater edge to the application of hydrate based technology for methane storage as there is absolutely no foam formation with L-histidine which is a major bottleneck encountered when using surfactants like SDS and therefore in scale up.

4.4. Comparison between the different synthetic and bio based additives used as kinetic hydrate promoters for methane hydrate formation

Synthetic Additives		Bio Based Additives	
Synthetic Surfactants	Silicone Based Surfactant/Antifoam	Biosurfactants	Amino Acids
Produced by chemical reactions. Chemicals such as sulphuric acid and ethylene oxide react with hydrocarbons derived from petroleum or fat to produce intermediates similar to fatty acids. Addition of alkali such as sodium hydroxide causes a second chemical reaction and leads to formation of surfactants (anionic).	Made out of silicone copolymers (the most common being silicone polyethers). Can modify surface properties such as surface tension of waterborne systems, i.e. act as surfactants and can also be used as antifoaming or defoaming agents depending on their solubility in water.	Surface active molecules synthesised by living cells capable of use in a diverse range of applications. May have one of the following structures: mycolic acid, glycolipids, polysaccharide–lipid complex, lipoprotein or lipopeptide, phospholipid, or the microbial cell surface itself.	Amino acids are the building blocks of proteins and are essential for life as they are at the basis of all life processes. Hence amino acids are extremely benign substances and do not have a detrimental effect on any sort of life whatsoever.
Contain a hydrophilic head and a hydrophobic tail).	The structure consists of a siloxane backbone and a large number of methyl groups as moieties.	Contain a hydrophilic head and a hydrophobic tail).	Consist of an amine and a carboxyl functional group along with a side chain, the latter specific to each amino acid. Based on the side chain, these can be classified into hydrophobic, hydrophilic and charged.

Mostly inexpensive and can be obtained in as much quantity as required.	Inexpensive and readily available.	Biosurfactant yield depends on the nutritional environment of the growing microorganism. Since these are produced by living organisms, most biosurfactants are very expensive. Biosurfactants are extremely robust molecules (stable at severe conditions of temperature, salinity and pH).	Mostly inexpensive and readily available.
Disposal may be a problem due to their synthetic nature and origin.	Disposal may be a problem due to their synthetic nature and origin.	Essentially green compounds and hence disposal is safe and easy.	Amino acids are essential compounds for life hence disposal is very safe and straightforward.
The addition of a small amount of synthetic surfactant to the system causes considerable enhancement in the kinetics of methane hydrate formation although not all classes of surfactants show equal enhancement. Anionic surfactants have been widely shown to be the best to	The addition of a small amount of silicone based antifoam to the system may not necessarily enhance the kinetics of methane hydrate formation. However, if used in the form of a mixture with SDS, the kinetics of methane hydrate formation is enhanced and the extent of enhancement observed is similar to that with pure SDS.	Presence of a small amount of biosurfactant in the system leads to considerable enhancement in the kinetics of methane hydrate formation.	A small amount of amino acid in the system significantly enhances the kinetics of methane hydrate formation. Both hydrophobic and hydrophilic amino acids have been known to enhance methane hydrate formation kinetics.

enhance hydrate formation kinetics.			
A 1 wt % SDS in water system was observed to show marginally less enhancement in methane hydrate formation kinetics as compared to a system in which the cell supernatant liquid containing the biosurfactant Surfactin was used by itself as the hydrate forming solution. Hydrate formation was carried out in a stirred tank reactor setup at 400 rpm.	A system having a 1 wt % SDS + 0.5 wt % Antifoam-A mixture was observed to be just as good as a system having pure SDS (1 wt %) with regards to enhancing the kinetics of methane hydrate formation. Hydrate formation was carried out in a stirred tank reactor setup at 400 rpm.	Cell free supernatant liquid containing the biosurfactant Surfactin when used by itself as the hydrate forming solution was observed to show slightly more enhancement in methane hydrate formation kinetics as compared to a 1 wt% SDS system. Hydrate formation was carried out in a stirred tank reactor setup at 400 rpm.	A 1 wt % L-histidine in water system (L-histidine is a hydrophilic amino acid) was found to significantly enhance the kinetics of methane hydrate formation as compared to pure water. However, this enhancement fell short as compared to that obtained with a 1 wt % SDS in water system. However, the final gas uptake obtained for a given period of time was approximately the same for both the systems (1 wt % L-histidine in water and 1 wt % SDS in water).
The small margin in enhancement between Surfactin and SDS bodes well for synthetic surfactants at	The fact that the SDS-Antifoam-A mixture performs as well as pure SDS in terms of enhancing the kinetics of methane hydrate formation is very encouraging as the real	The small margin in enhancement observed with the biosurfactant may not be enough to tip the scales in its favour as biosurfactants are	Although amino acids may not enhance the kinetics of methane hydrate formation as much as SDS, the enhancement obtained is still pretty significant compared to pure water. Moreover, the final gas

<p>least or now, as the low cost of these surfactants makes their use much more feasible as compared to their bio based counterparts.</p>	<p>objective of using the antifoam is to counter the problem of excessive foam generation usually faced with surfactants. If by using a SDS-Antifoam mixture, the problem of foam generation can be dealt with while at the same time ensuring that the enhancement in hydrate formation kinetics is not compromised, it would be a major breakthrough in gas hydrate studies for applications such as methane storage and separation.</p>	<p>expensive and will be required in large quantities for operations on an industrial scale. With such a small enhancement over synthetic surfactants, it may not be feasible to go for this option as yet.</p>	<p>uptake for a given period of time is the same for amino acids and SDS. If the problem of foam generation encountered when using surfactants can also be solved by using amino acids, being green, benign substances, these can be a viable class of compounds for use as kinetic hydrate promoters.</p>
<p>Problem of huge amount of foam generation which will prove to be a major bottleneck during scale up of hydrate based gas storage and separation technologies.</p>	<p>The problem of foam generation is completely averted when SDS and Antifom-A are mixed in a ratio of 1:0.5 by weight. At the same time, with this mixture ratio, there is no compromise on the enhancement in kinetics of methane hydrate formation as compared to pure SDS thus significantly boosting the possibility of scale-up of hydrate based gas storage and separation technologies.</p>	<p>Problem of foam generation is the present in the case of biosurfactants too and this needs to be tackled before hydrate based gas storage and separation technologies employing surfactants can be executed on an industrial scale.</p>	<p>No foam generation whatsoever when using amino acids as kinetic hydrate promoters thus enhancing multi-fold, the feasibility of scale-up of hydrate based gas storage and separation technologies.</p>

4.5. References

1. Abascal, J.L.F., Sanz, E., Fernández, R.G., Vega, C. A potential model for the study of ices and amorphous water: TIP4P/Ice. *J. Chem. Phys.* **2005**, 122, 234511.
2. Anderson, B.J., Tester, J.W., Borghi, G.P., Trout, B.L. Properties of inhibitors of methane hydrate formation via molecular dynamics simulations. *J. Am. Chem. Soc.* **2005**, 127, 17852–17862.
3. Arima, K., Kakinuma, A., Tamura, G. Surfactin, a crystalline peptidolipid surfactant produced by *Bacillus subtilis*: Isolation, characterization and its inhibition of fibrin clot formation. *Biochem. Biophys. Res. Commun.* **1968**, 31, 488-494.
4. Arora, A., Cameotra, S.S., Kumar, R., Balomajumder, C., Singh, A.K., Santhakumari, B., Laik, S. Biosurfactant as a Promoter of Methane Hydrate Formation: Thermodynamic and Kinetic Studies. *Sci. Rep.* **2016**, 6:20893.
5. Baghel, V.S., Kumar, R., Roy, S. Heat Transfer Calculations for Decomposition of Structure I Methane Hydrates by Molecular Dynamics Simulation. *J. Phys. Chem. C* **2013**, 117, 12172–12182.
6. Bagherzadeh, S.A., Alavi, S., Ripmeester, J.A., Englezos, P. Why ice-binding type I antifreeze protein acts as a gas hydrate crystal inhibitor. *Phys. Chem. Chem. Phys.* **2015**, 17, 9984–9990.
7. Banat, I.M., Satpute, S.K., Cameotra, S.S., Patil, R., Nyayanit, N.V. Cost effective technologies and renewable substrates for biosurfactants production. *Front Microbiol.* **2014**, 5:697.
8. Barnes, B.C., Knott, B.C., Beckham, G.T., Wu, D.T., Sum, A.K. Reaction coordinate of incipient methane clathrate hydrate nucleation. *J. Phys. Chem. B* **2014**, 118, 13236–43.

9. Bhattacharjee, G., Kumar, A., Sakpal, T., Kumar, R. Carbon Dioxide Sequestration: Influence of Porous Media on Hydrate Formation Kinetics. *ACS Sustain. Chem. Eng.* **2015**, 3, 1205–1214.
10. Cheng, A., Merz, K.M. Ice-binding mechanism of winter flounder antifreeze proteins. *Biophys. J.* **1997**, 73, 2851–73.
11. Daraboina, N., Linga, P., Ripmeester, J., Walker, V.K., Englezos, P. Natural gas hydrate formation and decomposition in the presence of kinetic inhibitors. 2. Stirred reactor experiments. *Energy Fuels* **2011**, 25, 4384–4391.
12. der Spoel, D., Lindahl, E., Hess, B., n.d. the GROMACS development team, GROMACS User Manual version 4.6.3, 2013.
13. Ewart, K. V., Lin, Q., Hew, C.L. Structure, function and evolution of antifreeze proteins. *Cell. Mol. Life Sci. C.* **2014**, 55, 271–283.
14. Frostman, L.M., Thieu, V., Crosby, D.L., Downs, H.H. Low-Dosage Hydrate Inhibitors (LDHIs): Reducing Costs in Existing Systems and Designing for the Future, In: International Symposium on Oilfield Chemistry, **2003**
15. Gordienko, R., Ohno, H., Singh, V.K., Jia, Z., Ripmeester, J.A., Walker, V.K. Towards a green hydrate inhibitor: imaging antifreeze proteins on clathrates. *PLoS One* **2010**, 5, e8953.
16. Jacobson, L.C., Molinero, V. A methane-water model for coarse-grained simulations of solutions and clathrate hydrates. *J. Phys. Chem. B* **2010**, 114, 7302–7311.

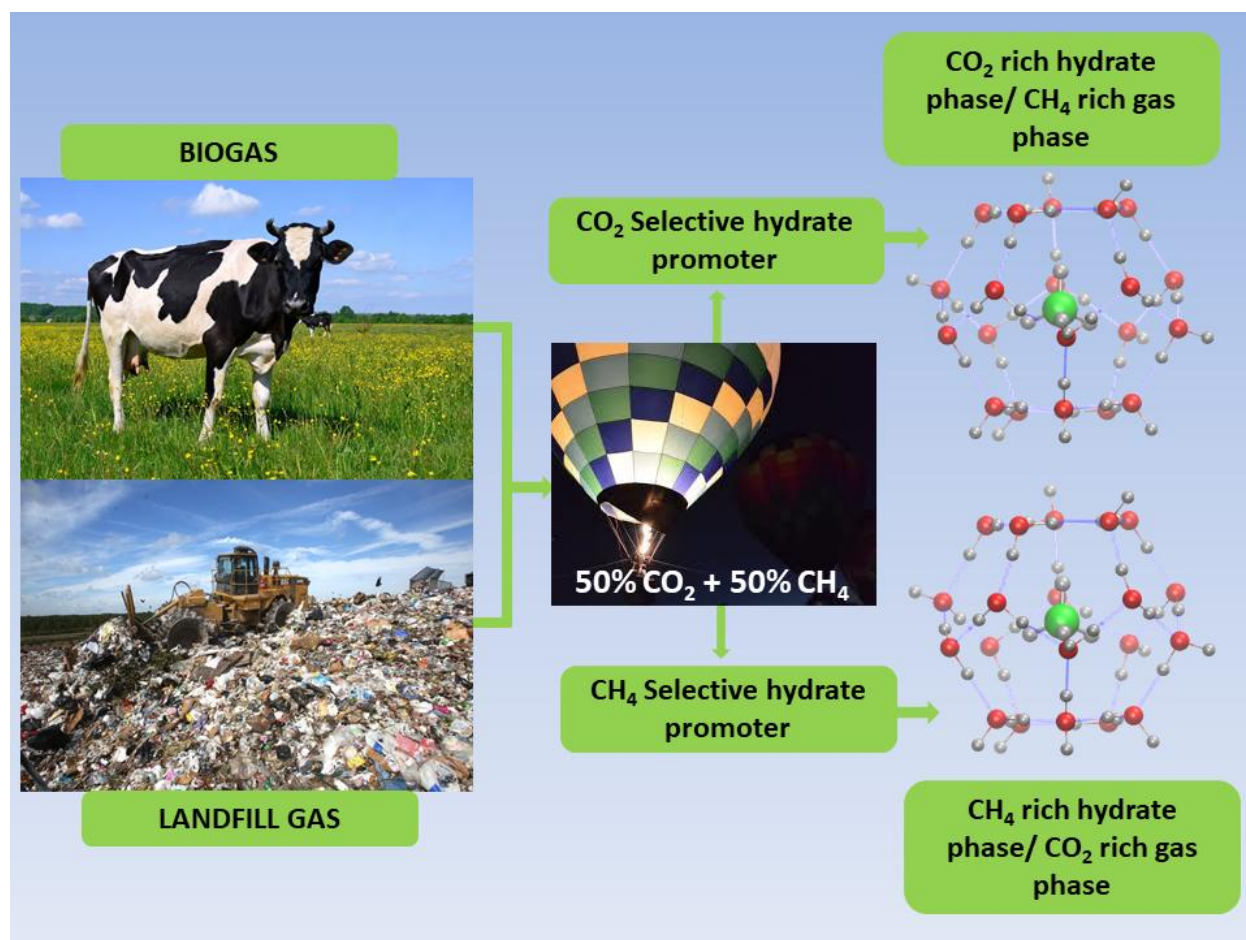
17. Jiménez-Ángeles, F., Firoozabadi, A. Nucleation of Methane Hydrates at Moderate Subcooling by Molecular Dynamics Simulations. *J. Phys. Chem. C* **2014**, 118, 11310-11318.
18. Kelland, M.A. History of the development of low dosage hydrate inhibitors. *Energy Fuels* **2006**, 20, 825–847.
19. Kumar, A., Sakpal, T., Linga, P., & Kumar, R. Influence of contact medium and surfactants on carbon dioxide clathrate hydrate kinetics. *Fuel* **2013**, 105, 664-671.
20. Kumar, A., Sakpal, T., Kumar, R. Influence of Low-Dosage Hydrate Inhibitors on Methane Clathrate Hydrate Formation and Dissociation Kinetics. *Energy Technol.* **2015**, 3, 717–725.
21. Kyte, J., Doolittle, R.F. A simple method for displaying the hydropathic character of a protein. *J. Mol. Biol.* **1982**, 157, 105–132.
22. Lakdawala, M.F.A. Lipopeptides produced by marine-derived bacterial species; M.Tech thesis, 2014.
23. Lederhos, J.P., Long, J.P., Sum, A., Christiansen, R.L., Sloan, E.D. Effective kinetic inhibitors for natural gas hydrates. *Chem. Eng. Sci.* **1996**, 51, 1221–1229.
24. Liang, S., Kusalik, P.G. Explorations of gas hydrate crystal growth by molecular simulations. *Chem. Phys. Lett.* **2010**, 494, 123–133.
25. Liu, Y., Chen, B., Chen, Y., Zhang, S., Guo, W., Cai, Y., Tan, B., Wang, W. Methane Storage in a Hydrated Form as Promoted by Leucines for Possible Application to Natural Gas Transportation and Storage. *Energy Technol.* **2015**, 3, 815–819.
26. Mak, T.C.W., McMullan, R.K. Polyhedral clathrate hydrates. X. Structure of the double

- hydrate of tetrahydrofuran and hydrogen sulfide. *J. Chem. Phys.* **1965**, 42, 2732–2737.
27. McDonald, S.M., Brady, J.W., Clancy, P. Molecular dynamics simulations of a winter flounder “antifreeze” polypeptide in aqueous solution. *Biopolymers* **1993**, 33, 1481–503.
28. Moon, C., Hawtin, R.W., Rodger, P.M. Nucleation and control of clathrate hydrates: insights from simulation. *Faraday Discuss.* **2007**, 136, 367–382.
29. Naeiji, P., Arjomandi, A., Varaminian, F. Amino acids as kinetic inhibitors for tetrahydrofuran hydrate formation: Experimental study and kinetic modeling. *J. Nat. Gas Sci. Eng.* **2014**, 21, 64–70.
30. Nosé, S. A unified formulation of the constant temperature molecular dynamics methods. *J. Chem. Phys.* **1984**, 81, 511–519.
31. Ohno A, Ano T, Shoda M. Production of a lipopeptide antibiotic, surfactin, by recombinant *Bacillus subtilis* in solid state fermentation. *Biotechnology and bioengineering*, **1995**, 47, 209-214.
32. Ohno, H., Susilo, R., Gordienko, R., Ripmeester, J., Walker, V.K. Interaction of antifreeze proteins with hydrocarbon hydrates. *Chemistry* **2010**, 16, 10409–17.
33. Oluwunmi, P.A., Finney, A.R., Rodger, P.M. Molecular dynamics screening for new kinetic inhibitors of methane hydrate. *Can. J. Chem.* **2015**, 93, 1043–1049.
34. Parrinello, M., Rahman, A. Polymorphic transitions in single crystals: A new molecular dynamics method. *J. Appl. Phys.* **1981**, 52, 7182–7190.
35. Perfeltdt, C.M., Chua, P.C., Daraboina, N., Friis, D., Kristiansen, E., Ramløv, H., Woodley, J.M., Kelland, M.A., von Solms, N. Inhibition of Gas Hydrate Nucleation and Growth: Efficacy of an Antifreeze Protein from the Longhorn Beetle *Rhagium mordax*. *Energy Fuels* **2014**, 28, 3666–3672.

36. Perrin, A., Musa, O.M., Steed, J.W. The chemistry of low dosage clathrate hydrate inhibitors. *Chem. Soc. Rev.* **2013**, 42, 1996–2015.
37. Rogers RE, Kothapalli C, Lee MS, Woolsey JR. Catalysis of Gas Hydrates by Biosurfactants in Seawater-Saturated Sand/Clay. *Can. J. Chem. Eng.* **2003**, 81, 973–980.
38. Roosta, H., Dashti, A., Mazloumi, S.H., Varaminian, F. Inhibition properties of new amino acids for prevention of hydrate formation in carbon dioxide–water system: Experimental and modeling investigations. *J. Mol. Liq.* **2016**, 215, 656–663.
39. Sa, J.-H., Kwak, G.-H., Han, K., Ahn, D., Lee, K.-H. Gas hydrate inhibition by perturbation of liquid water structure. *Sci. Rep.* **2015**, 5, 11526.
40. Sa, J.-H., Kwak, G.-H., Lee, B.R., Park, D.-H., Han, K., Lee, K.-H. Hydrophobic amino acids as a new class of kinetic inhibitors for gas hydrate formation. *Sci. Rep.* **2013**, 3:2428.
41. Sa, J.-H., Lee, B.R., Park, D.-H., Han, K., Chun, H.D., Lee, K.-H. Amino acids as natural inhibitors for hydrate formation in CO₂ sequestration. *Environ. Sci. Technol.* **2011**, 45, 5885–91.
42. Vanommeslaeghe, K., Hatcher, E., Acharya, C., Kundu, S., Zhong, S., Shim, J., Darian, E., Guvench, O., Lopes, P., Vorobyov, I., Mackerell, A.D. CHARMM general force field: A force field for drug-like molecules compatible with the CHARMM all-atom additive biological force fields. *J. Comput. Chem.* **2010**, 31, 671–690.
43. Vatamanu, J., Kusalik, P.G. Unusual crystalline and polycrystalline structures in methane hydrates. *J. Am. Chem. Soc.* **2006**, 128, 15588–9.

-
44. Vater, J., Kablitz, B., Wilde, C., Franke, P., Mehta, N., Cameotra, S.S. Matrix-assisted laser desorption ionization-time of flight mass spectrometry of lipopeptide biosurfactants in whole cells and culture filtrates of *Bacillus subtilis* C-1 isolated from petroleum sludge. *Appl. Environ. Microbiol.* **2002**, 68, 6210-6219.
45. Walsh, M.R., Koh, C.A., Sloan, E.D., Sum, A.K., Wu, D.T. Microsecond simulations of spontaneous methane hydrate nucleation and growth. *Science* **2009**, 326, 1095–1098.
46. Yagasaki, T., Matsumoto, M., Tanaka, H. Adsorption mechanism of inhibitor and guest molecules on the surface of gas hydrates. *J. Am. Chem. Soc.* **2015**, 137, 12079–12085.
47. Yeh, Y., Feeney, R.E. Antifreeze proteins: structures and mechanisms of function. *Chem. Rev.* **1996**, 96, 601–618.

Chapter 5

CH₄-CO₂ gas separation using clathrate hydrate formation in presence of selective hydrate promoters

5. CH₄-CO₂ gas separation using clathrate hydrate formation in presence of selective hydrate promoters

In the current chapter, the separation of a CO₂-CH₄ gas mixture using clathrate hydrate formation has been investigated and discussed.

5.1. Introduction

Natural gas which is widely acknowledged as the cleanest burning fuel owing to the relatively low production of carbon dioxide as compared to coal and oil on combustion has, particularly in recent times, widely found its rightful place within the energy nexus. However, akin to all the other non-renewable energy sources, conventional natural gas too is riding a set clock with the proven reserves left on the earth estimated to only be sufficient for approximately the next 55 years at the current level of global consumption (B.P., 2016). This has led to the rise of a number of unconventional, renewable sources of natural gas such as biogas and landfill gas. These unconventional sources of natural gas contain a large amount of CO₂ (15-60%) as well as other trace impurities such as H₂S (Fan et.al, 2016; Di Profio et.al, 2017). In order to utilize the methane present in biogas or landfill gas as an energy source, one must separate CO₂ from the gas mixture. Such separation has proved to be quite difficult in the past. The conventional gas separation techniques such as chemical scrubbing, pressure swing adsorption, membrane separation and solid adsorption have all been studied for CO₂-CH₄ separation and the studies are well documented in literature. These processes however all pose their specific limitations with the major drawback being the requirement of a large amount of energy for most of these processes which greatly reduces the energy efficiency of the system or process (Rufford et.al, 2012; Yeo et.al, 2012; Kohl and Nielsen, 1997; Sun et.al, 2015; Ryckebosch et.al, 2011). This has led to efforts to either, improve the energy efficiency of the conventional gas separation processes or identify unconventional gas separation processes which may allow efficient separation of CO₂-CH₄ gas mixtures. The hydrate based gas separation (HBGS) process (discussed in chapter 2) has thus been suggested as one of the novel/ unconventional processes to affect the separation of CO₂ and CH₄ in biogas and other unconventional sources of natural gas (Seo et.al, 2000; Seo et.al, 2001; Uchida et.al, 2005; Golombok et.al,2009; Van Denderen et.al, 2009; Herri et.al, 2011; Ricaurte et.al, 2012; Tomita et.al, 2015; Xia et.al, 2016; Fan et.al, 2016; Long et.al, 2016).

A reasonable amount of study has already been done on the separation of a CO₂-CH₄ gas mixture using gas hydrate formation. From prior knowledge of the hydrate formation systems of various gases and the literature of hydrate formation with CO₂-CH₄ gas mixtures, the major limitation that arises with this particular application of the HBGS process is the relatively similar size of CO₂ and CH₄ and hence the similar hydrate equilibrium conditions for the two gas molecules (it is known that the hydrate equilibrium pressure at a given temperature increases with decrease in the size of the guest molecule). For example, at a hydrate formation temperature of say 274 K, the equilibrium hydrate formation pressure for CO₂ is 1.509 MPa whereas that for CH₄ is 3.0 MPa. This rather small difference in the hydrate equilibrium pressures at a given temperature makes the preferential enclathration and hence separation of these two molecules from each other quite difficult (Sloan and Koh, 2008). At the current level of understanding one expects that the gas separation for a CO₂-CH₄ gas mixture is dynamic which basically means different rates of gas uptake for CO₂ and CH₄, i.e. one of the gases, CO₂ / CH₄ may well be participating in gas hydrate formation at much faster rates compared to the other (CH₄ / CO₂). Few studies suggest that hydrates formed from CO₂-CH₄ gas mixtures show preferential enclathration of CO₂ (Seo et.al, 2000; Seo et.al, 2001; Uchida et.al, 2005; Golombok et.al,2009; Van Denderen et.al, 2009; Herri et.al, 2011; Di Profio et.al, 2016)

A possible way of getting a better separation factor for CO₂-CH₄ separation is the use of various chemical additives known as hydrate promoters. Various thermodynamic and kinetic promoters such as Tetrahydrofuran (THF) and sodium dodecylsulfate (SDS) respectively have been individually used in the past specifically for CO₂-CH₄ separation using gas hydrate formation (Daniel-David et.al, 2015; Zhong et.al, 2015a; Ricaurte et.al, 2012; Ricaurte et.al, 2014). In addition, combinations of thermodynamic and kinetic promoters (THF and SDS) have also been studied. Although on using just the kinetic promoter SDS, there was no impact on the kinetics of hydrate formation, which is unexpected, on using the kinetic (SDS) and thermodynamic (THF) promoters together, relatively faster kinetics of hydrate formation and greater final gas uptake was observed. However, unfortunately neither system was able to show any real impact on the separation efficiency of the system (Ricaurte et.al, 2012). The impact of overpressure, i.e. increasing the driving force for hydrate formation has also been investigated, both in the absence and presence of thermodynamic and kinetic promoters. It was observed that the separation efficiency of the system decreased with increase in the driving force for hydrate formation while

the presence of THF and SDS in the system did lead to faster kinetics of hydrate growth but at the cost of hydrate selectivity for CO₂ (Zhong et.al, 2015b). These results indicate that conventional hydrate promoters may not be the ideal additives to be used for gas separation from a CO₂-CH₄ gas mixture. In addition, there is always the everlasting disadvantage of foam formation when using surfactants such as SDS which has already been discussed in great detail in the previous chapter.

A different approach that may be adopted to increase the separation efficiency of the HBGS process for CO₂-CH₄ separation is to play with the solubility of these two gases in water. Carbon dioxide has a much higher solubility in water than methane and this factor may be exploited to enhance gas separation using hydrate formation as it has been proven in the past that greater the solubility of a gas in water, faster is the kinetics of hydrate formation (Bhattacharjee et.al, 2017). There are certain chemical compounds or additives which may be used to selectively increase the solubility of carbon dioxide in water and further increase the gap in between the solubility and hence concentration of carbon dioxide and methane in the aqueous phase prior to hydrate formation.

If selectivity between gases is the area being targeted, one may also look at enhancing the hydrate selectivity for CH₄ instead of CO₂ which has been the general idea so far. In Chapter 3, the use of hydrophobic surfaces and hydrophobic additives to enhance the kinetics of methane hydrate formation has been discussed. The same principles may be extended to effect a more selective separation of CO₂-CH₄ gas mixture which sees CH₄ get preferentially enclathrated in the hydrate cages. The most feasible way of carrying out this sort of selective separation is of course by the identification and use of hydrophobic additives which allow for gas enrichment and more local ordering of water molecules in the vicinity of hydrophobic regions (Wang et.al, 2008; Bhattacharjee et.al, 2015; Liu et.al, 2015; Veluswamy et.al, 2016; Cai et.al, 2017; Nguyen et.al, 2017).

As it has been proven in the past that the use of traditional hydrate promoters only hinders the selectivity of the HBGS process for CO₂-CH₄ separation, it is perhaps time to shift to a newer class of additives that would have a selectivity based approach towards gas separation, i.e. work/ (affect the system) in such a way as to promote selective enclathration of a certain molecule in the hydrate phase. This may either be by selectively increasing the solubility of a certain

component of the gas mixture in water or by creating hydrophobic regions which attract the more hydrophobic components in the gas mixture. However, it is very important to note that the selective enclathration should not be achieved at the cost of low hydrate formation kinetics.

The result of these modifications to the system ideally is the rapid formation of hydrates which show selectivity for a particular guest gas thus resulting in high separation efficiencies for the process. In the current work, a number of novel additives have been identified that have previously never been used in gas hydrate formation from CO₂-CH₄ gas mixtures. Instead of thermodynamic or kinetic hydrate promoters, these additives have been christened as “selective hydrate promoters” (SHPs). Polar aprotic solvents, propylene carbonate (PC) and Sulfolane were used to selectively enhance the solubility of CO₂ in liquid water whereas a hydrophobic amino acid, Tryptophan was used to study the possibility of selectively enclathrating CH₄ in the hydrates formed from the CO₂-CH₄ gas mixture (Figures 5.1(a), (b) and (c) show the chemical structures of PC, Sulfolane and Tryptophan respectively. Unlike surfactants, all three additives used in this study do not generate any sort of foam whatsoever which is already a major advantage as far as scale up, handling and economics of the process are concerned. A 50-50 % CO₂-CH₄ gas mixture was used to test the efficacy of these additives on the separation efficiency of the process. Also, 50 % is usually the maximum concentration of CO₂ that is found in unconventional natural gas mixtures such as biogas and having an equimolar distribution of each gas in the mixture will give us a very fair representation of the ability of an additive to separate the two gases. Two different hydrate formation pressures (3.5 MPa and 5.0 MPa) were used to study the effect of overpressure on the separation efficiency of the HBGS process in presence of the newly identified SHPs. A fixed bed reactor setup was used for gas hydrate formation with metallic brass packing used as the fixed bed medium.

5.2. Experimental Section

5.2.1. Materials

A 50% CO₂-50% CH₄ gas mixture was purchased from Inox Gases Pvt. Ltd. Propylene Carbonate and Sulfolane with a minimum purity of 99.7% and 99% respectively were purchased from Sigma Aldrich. Tryptophan with a minimum purity of 99% was purchased from HiMedia

Laboratories Pvt. Ltd. Metallic Brass packing which basically consists of brass was prepared in house (Figure 5.2). Distilled and deionized water was used for all the experiments.

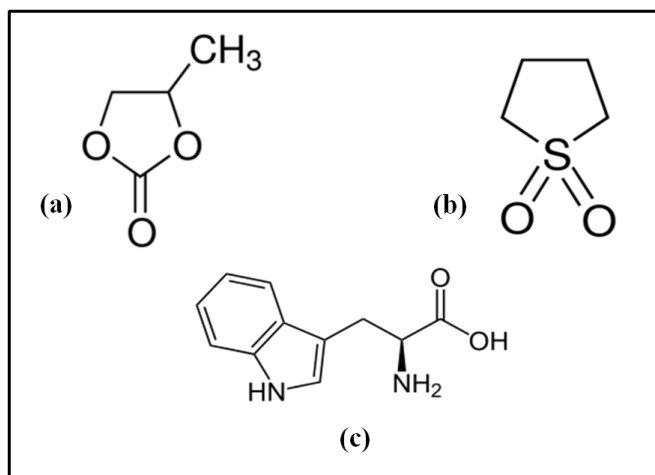


Fig. 5.1: Chemical structures of (a) Propylene Carbonate (PC), (b) Sulfolane and (c) Tryptophan.

5.2.2. Apparatus used and procedure followed for hydrate formation

The apparatus used in this study was a fixed bed reactor (FBR). Metallic brass packing with a water retention capacity of 0.3 gram of water per gram of packing was used as the fixed bed medium owing to its high thermal conductivity. Given below is the procedure used for the hydrate formation experiments which in the process also gives a detailed description of the FBR setup used:

The FBR used in the present study (schematic shown in Figure 5.2) had a total volume of 410 cm³. First the desired weight of the fixed bed medium to be used (brass packing) was weighed out. 100 grams of the brass packing was used for each experiment. The packing medium was then saturated with water up to the desired level. In this study, a 75 % water saturation of the packing medium was maintained to allow space for gas diffusion. This comes out to be 22.5 cm³ of water keeping with the water retention capacity of the brass packing (0.3 g/g). Once the packing medium was satisfactorily saturated with water, the entire mixture was carefully transferred to the 410 cm³ stainless steel crystallizer (CR; Berghoff make) in the process creating an even fixed bed. The CR was then firmly sealed and placed inside a temperature controlled water bath in order to attain the desired experimental temperature (274 K). The vessel was flushed with the 50% CO₂-50% CH₄ gas mixture (hydrate forming gas) using a supply vessel by repeating rapid

pressurization (~ 0.5 MPa) and depressurization cycles. Next, the CR was pressurized with the hydrate forming gas up to a pre-determined experimental pressure. Two different experimental pressures were used in this study, 3.5 MPa and 5.0 MPa in order to study the effect of overpressure on hydrate formation kinetics and separation efficiency in presence of the newly identified additives; the hydrate equilibrium pressure at 274K for the 50% CO_2 -50% CH_4 gas mixture used is 1.813 MPa according to CSMHyd. Thus sufficient driving force was provided for hydrate formation to take place. At this stage, gas uptake measurements were initiated. Hydrate formation is accompanied with pressure drop inside the vessel as a result of the gas moving from the gas phase into the solid hydrate phase. This drop in pressure, measured employing a pressure transducer (WIKA make; range: 0-25 MPa) was used to calculate the moles of gas participating in the hydrate formation experiment. Temperature and pressure inside the vessel were recorded every five seconds using a data acquisition system (PPI, Mumbai - India) which was connected to a computer. As experiments were conducted entirely in batch mode, the effective driving force for hydrate formation decreased as the reaction proceeded with more and more gas moving from the gas phase to the solid hydrate phase.

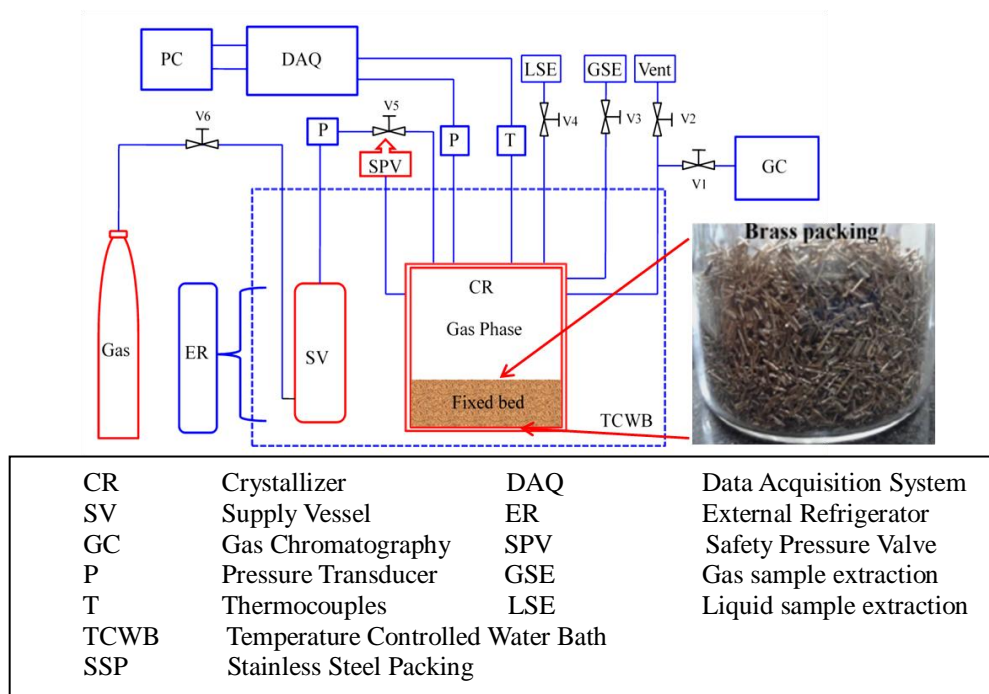


Fig. 5.2: Detailed schematic of the fixed bed reactor setup for hydrate formation.

5.2.3. Procedure used for analyzing the composition of the gas phase

Since the composition of the initial feed gas was already known, for the analysis of the gas phase, the unknown entities that were analysed were the gas phase at the end of every hydrate forming run and the gas phase inside the hydrate which was obtained after completely dissociating the formed hydrates. Once the gas phase samples had been collected (using a Tedler bag), a gas chromatograph instrument (Shimadzu make) was used to determine the compositions of the different gas phase samples. A microlitre syringe was used to transfer the gas samples from the Tedler bag to the gas chromatograph instrument.

5.2.4. Calculation of the amount of gas consumed during hydrate formation

The total number of moles of gas that was consumed in the hydrate formation process at any given time is the difference between the number of moles of gas present in the gas phase of the CR at time $t = 0$ and the number of moles of gas present in the gas phase of the CR at time $t = t$. The same is given by the following equation (Bhattacharjee et.al, 2015):

$$(\Delta n_{H,\downarrow})_t = V_{CR} \left[\frac{P}{zRT} \right]_0 - V_{CR} \left[\frac{P}{zRT} \right]_t \quad (5.1)$$

where z is the compressibility factor calculated by using Pitzer's correlation (Smith et.al, 2004). V_{CR} is the volume of the gas phase inside the crystallizer and P and T are the pressure and temperature of the crystallizer respectively.

5.2.5. Calculation of the rate of hydrate formation

The rate of hydrate formation was calculated by the forward difference method as given below:³⁷

$$\left(\frac{d\Delta n_{H,\downarrow}}{dt} \right)_t = \frac{\Delta n_{H,\downarrow}(t+\Delta t) - \Delta n_{H,\downarrow}(t)}{\Delta t}; \Delta t=5\text{sec} \quad (5.2)$$

The average of these rates was calculated for every 20 minutes and reported.

5.2.6. Calculation of the split fraction and separation factor from gas phase analysis

The split fraction (S.Fr.) of CO₂ in the hydrate phase and the CO₂ separation factor (S.F.) for hydrate formation from the CO₂-CH₄ gas mixture were calculated as shown below (Bhattacharjee et.al, 2017):

$$CO_2 \text{ Split Fraction (S. Fr. (\%))} = \frac{n_{CO_2}^H}{n_{CO_2}^F} \times 100 \quad (5.3)$$

$$CO_2 \text{ Separation Factor (S.F.)} = \frac{y_{CO_2}^H y_{CH_4}^G}{y_{CO_2}^G y_{CH_4}^H} \quad (5.4)$$

, where $n_{CO_2}^H$ and $n_{CO_2}^F$ are the total number of moles of carbon dioxide present in the hydrate gas and feed gas streams respectively, $y_{CO_2}^H$ and $y_{CO_2}^G$ are the mole fractions of carbon dioxide in the hydrate gas and residual gas streams respectively and $y_{CH_4}^H$ and $y_{CH_4}^G$ are the mole fractions of methane in the hydrate gas and residual gas streams respectively. $n_{CO_2}^H$ and $n_{CO_2}^F$ were calculated as follows:

$$n_{CO_2}^H = y_{CO_2}^H n^H \quad (5.5)$$

$$n_{CO_2}^F = y_{CO_2}^F n^F \quad (5.6)$$

, where n^H and n^F are the total number of moles of the hydrate and feed gases respectively which was calculated from the pressure drop data. The total number of moles of feed gas was the initial number of moles present in the system before the start of hydrate formation, i.e. induction and the total number of moles of hydrate gas was the total number of moles of gas that had participated in the formation of hydrate as calculated using equation 5.1 (total number of moles of feed gas minus the total number of moles of residual gas).

The split fraction (S.Fr.) of CH₄ in the hydrate phase and the CH₄ separation factor (S.F.) for hydrate formation from the CMM gas mixture were calculated as shown below (Bhattacharjee et.al, 2017):

$$CH_4 \text{ Split Fraction (S. Fr. (\%))} = \frac{n_{CH_4}^H}{n_{CH_4}^F} \times 100 \quad (5.7)$$

$$CH_4 \text{ Separation Factor (S.F.)} = \frac{y_{CH_4}^H y_{CO_2}^G}{y_{CH_4}^G y_{CO_2}^H} \quad (5.8)$$

, where $n_{CH_4}^H$ and $n_{CH_4}^F$ are the total number of moles of methane present in the hydrate gas and feed gas streams respectively, $y_{CH_4}^H$ and $y_{CH_4}^G$ are the mole fractions of methane in the hydrate gas and residual gas streams respectively and $y_{CO_2}^H$ and $y_{CO_2}^G$ are the mole fractions of carbon dioxide in the hydrate gas and residual gas streams respectively. $n_{CH_4}^H$ and $n_{CH_4}^F$ were calculated as follows:

$$n_{CH_4}^H = y_{CH_4}^H n^H \quad (5.9)$$

$$n_{CH_4}^F = y_{CH_4}^F n^F \quad (5.10)$$

, where n^H and n^F are the total number of moles of the hydrate and feed gases respectively which was calculated from the pressure drop data. The total number of moles of feed gas was the initial number of moles present in the system before the start of hydrate formation, i.e. induction and the total number of moles of hydrate gas was the total number of moles of gas that had participated in the formation of hydrate as calculated using equation 5.1 (total number of moles of feed gas minus the total number of moles of residual gas).

5.3. Results and Discussions

Table 5.1 gives a summary of all the experiments performed in the course of this study. Relevant data such as the sample state, initial hydrate formation pressure, run time of each experiment, amount of gas consumed at the end of each experiment (mol of gas consumed/ mol of water), water to hydrate conversion at the end of each experiment (mol %) and the induction time for hydrate formation in each experiment have been reported.

5.3.1. Hydrate formation in fixed bed reactor using Brass packing and in the presence of various additives

As has been mentioned in the introduction section, the major limitation of the HBGS process for CO₂-CH₄ separation is the low separation efficiency of hydrate formation. Further, the inherently slow kinetics of hydrate formation poses an additional challenge. Therefore there is a need to identify additives that would a) significantly enhance the kinetics of hydrate formation and gas uptake and b) improve the separation efficiency of the system. Figures 5.3 and 5.4 compare the

kinetics of gas uptake in presence of the different additives and at different initial pressures. While Figure 5.3 plots the gas uptake (moles of gas consumed per mole of water) with different additives, Figure 5.4 plots the water to hydrate conversion for the same. In both figures, averages of the different parameters for the fresh runs of hydrate formation have been shown. Time zero in the figures correspond to induction/ nucleation for hydrate formation which means all the gas uptake and corresponding water to hydrate conversion that has been shown in Figures 5.3 and 5.4 are due to hydrate formation. As can be seen in the figures, the kinetics of hydrate formation with the CO₂-CH₄ gas mixture is greatly dependent on the additives used. While hydrate formation kinetics are tremendously enhanced when 1 wt % of the amino acid Tryptophan is introduced into the system, with the other two additives used, no enhancement in hydrate formation kinetics can be observed. At 5.0 MPa initial pressure, while with pure water, only approximately 40 % of the water could be converted to hydrate, with the 1 wt % Tryptophan system, the water to hydrate conversion exceeded 60% in the first fifteen minutes of hydrate formation itself. When the initial hydrate formation pressure was 3.5 MPa initial pressure, pure water showed much faster hydrate formation kinetics as compared to when it was 5.0 MPa which may be a result of faster migration of CO₂ into the hydrate phase. Even then, only approximately 55 % of the water could be converted to hydrate with the pure water system, whereas with the 1 wt % Tryptophan system, the water to hydrate conversion once again reached 60% in the first fifteen to twenty minutes of hydrate formation itself. This enhancement in kinetics of hydrate formation observed when using Tryptophan and at such a small concentration, is remarkable especially when considering the fact that conventional kinetic hydrate promoters such as SDS have not been able to work at all for CO₂-CH₄ gas mixtures as the hydrate forming gas and usually require the help of thermodynamic promoter such as THF to bolster the kinetics of hydrate formation. A significant increase in hydrate formation kinetics in presence of Tryptophan may be due to its high hydrophobicity. Tryptophan is a hydrophobic amino acid as has been mentioned earlier in the introduction section. As discussed in Chapter 3, the presence of hydrophobic surfaces is extremely conducive to hydrate formation as they lead to the creation a gas enriched layer and increase local water ordering in their vicinity. It is quite possible therefore, that when tryptophan is present in the system, it draws the methane molecules in the gas mixture towards itself closely followed by the CO₂ molecules leading to rapid growth of hydrates. It is also expected that the hydrate formed in presence of Tryptophan would preferentially enclathrate methane instead of CO₂ which was the

whole idea behind using this material as an additive for this particular gas separation process. It is also expected that this separation would be more pronounced at the higher pressure of 5.0 MPa which is lowest general overpressure used to form pure methane hydrates at 274K.

In the case of the other two additives, PC and Sulfolane, however, the rate of hydrate formation kinetics could not be enhanced and in fact, hydrate formation kinetics was found to be inhibited as compared to pure water for these systems. However, it can be seen from Figure 5.5 which compares the final gas uptake after ten hours of hydrate formation for all the different studied, that although the kinetics of hydrate formation were decreased in presence of PC and Sulfolane as compared to pure water, the final gas uptake obtained with these additives was actually greater than that for pure water. Even though the kinetics of gas hydrate formation with the two polar aprotic solvents are not as high as one would have liked, there is still some merit in studying the hydrate formation in presence of these additives as they were specifically selected to increase the solubility of CO₂ in water and hence increase the selectivity of CO₂ in the hydrates being formed.

Figure 5.6 compares the rate of hydrate formation (mole of gas consumed/ mole of water/h) for the different systems studied. The rates for the first five hours of hydrate formation subsequent to nucleation have been plotted in Figure 5.6. As expected from the gas uptake profiles, the initial rates of hydrate formation are exorbitantly high for the 1 wt % Tryptophan systems as compared to the others which augur well for the use of this additive in the HBGS process for separation of CO₂-CH₄ gas mixtures.

Figures A7 and A8 in Appendix A show the linear fits of the gas uptake data for the first 10 minutes and 20 minutes of hydrate growth respectively for the different systems studied. The average initial apparent rates of hydrate formation for the different systems obtained as a result of the linear fitting are reported in Table A5, Appendix A.

Table 5.1: Summary of all the experiments conducted in this study-50% CO₂-50 % CH₄ gas mixture was used for all the experiments. Relevant data such as the sample state, initial hydrate formation pressure, run time of each experiment, amount of gas consumed at the end of each experiment (mol of gas consumed/ mol of water), water to hydrate conversion (mol %) at the end of each experiment and the induction time (h) for hydrate formation in each experiment have been reported. The hydrate formation temperature was kept constant (274 K) for all the systems.

System	Reactor Configuration	Exp No.	Sample State	Initial Pressure (MPa)	Run Time (h)	Gas Uptake (mol of gas cons/ mol of water)	Water to hydrate conversion (mol %)	Induction Time (min)
Pure Water	FBR	1	Fresh	5.0 MPa	10	0.095	54.633	3.000
		2	Fresh	5.0 MPa	10	0.061	35.202	4.979
		3	Fresh	3.5 MPa	10	0.107	61.476	0.509
		4	Fresh	3.5 MPa	10	0.104	59.585	0.776
1 wt % PC	FBR	5	Fresh	5.0 MPa	10	0.099	57.086	*CND
		6	Fresh	5.0 MPa	10	0.109	62.846	CND
		7	Fresh	3.5 MPa	10	0.062	35.788	CND
		8	Fresh	3.5 MPa	10	0.076	43.506	CND
1 wt % Sulfolane	FBR	9	Fresh	5.0 MPa	10	0.076	43.654	CND
		10	Fresh	5.0 MPa	10	0.090	51.880	CND
		11	Fresh	3.5 MPa	10	0.053	30.677	CND
		12	Fresh	3.5 MPa	10	0.0389	22.352	CND
1 wt % Tryptophan	FBR	13	Fresh	5.0 MPa	10	0.126	72.313	0
		14	Fresh	5.0 MPa	10	0.125	71.671	0
		15	Fresh	3.5 MPa	10	0.119	68.391	0.033
		16	Fresh	3.5 MPa	10	0.115	66.235	0

*CND: Could not be determined.

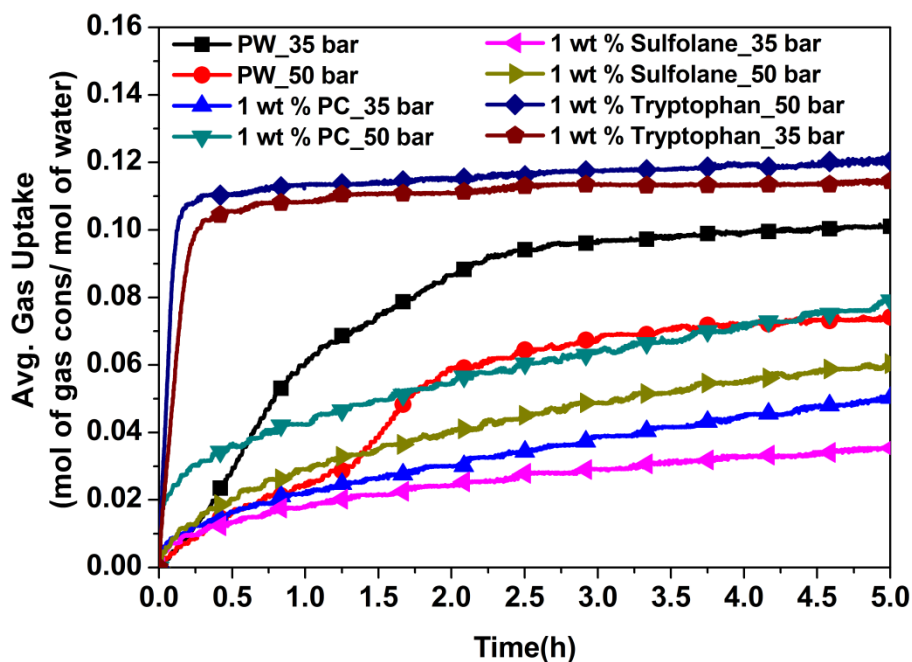


Fig. 5.3: Comparison of the average gas uptake (moles of gas consumed/ mole of water) for the different systems studied (fresh runs).

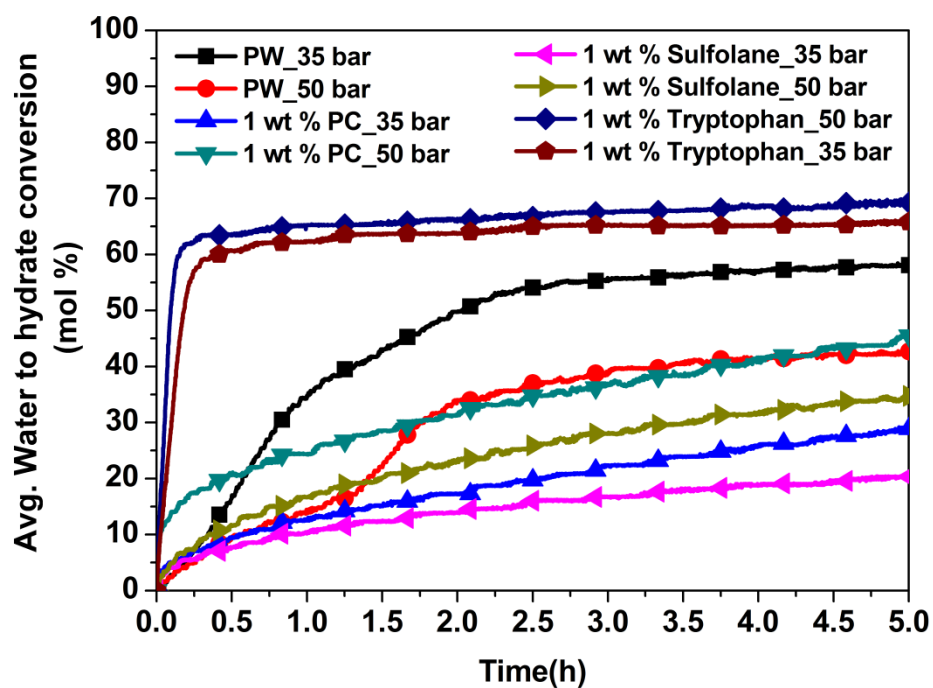


Fig. 5.4: Comparison of the average water to hydrate conversion (mole %) for the different systems studied (fresh runs).

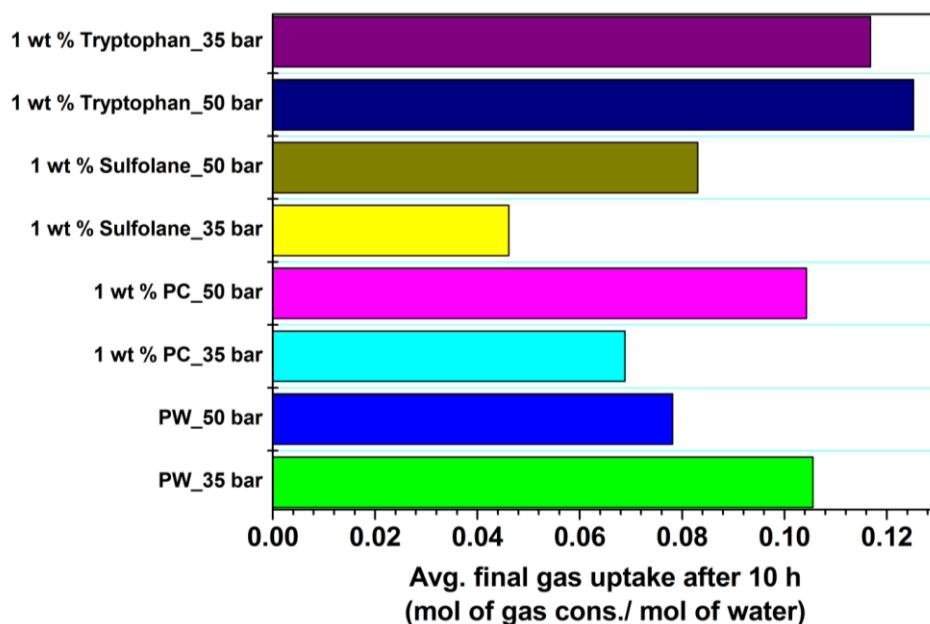


Fig. 5.5: Comparison of the average final gas consumption (moles of gas consumed/ mol of water) after 10 hours of hydrate formation for the different systems studied (fresh runs).

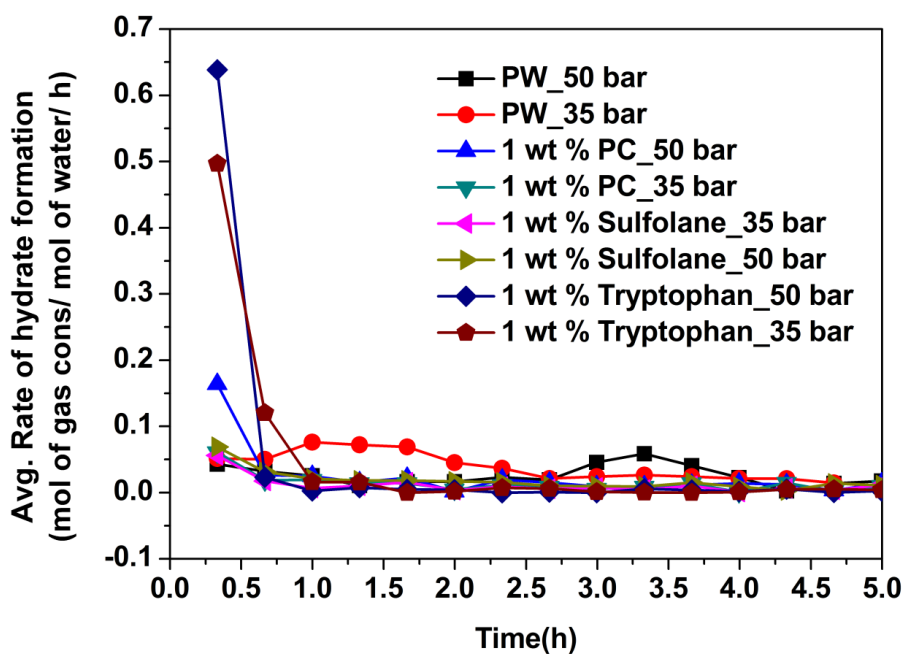


Fig. 5.6: Comparison of the average rates of gas uptake (moles of gas consumed/ mole of water/ hour) for the different systems studied (fresh runs).

5.3.2. Induction time for hydrate formation from a 50% CO₂-50% CH₄ gas mixture in the presence of additives:

Figure 5.7 compares the induction times for hydrate formation in presence of the different additives and different overpressures studied. As can be seen in Figure 5.7, the induction time in presence of Tryptophan is greatly reduced as compared to pure water for both hydrate formation pressures used. In fact for all but one of the runs with Tryptophan, hydrate nucleation began immediately after pressurization such that the induction times for these runs were effectively zero. The same can be seen in Table 5.1. The ultrafast nucleation of gas hydrates in the presence of Tryptophan is probably due to the phenomenon discussed for the first time in the previous chapter to explain the low induction times experienced when using the silicone based surfactant/antifoam as an additive for methane hydrate formation. It was hypothesized that the development of interfacial gas enrichment at the hydrophobic surface and the greater local water ordering in the vicinity of the same, in particular lend their weight to reducing the nucleation/induction time for hydrate formation and the same should hold true for hydrate formation from the CO₂-CH₄ gas mixture (containing hydrophobic CH₄) in the presence of hydrophobic additive Tryptophan.

In Figure 5.7 the other systems studied (PC and Sulfolane) are conspicuous by their absence. This is because, the kinetics of hydrate formation for these systems was so slow that no discernible induction/ nucleation point could be found for these systems, either from a sudden significant drop in the pressure profile or an abrupt spike in the temperature profile.

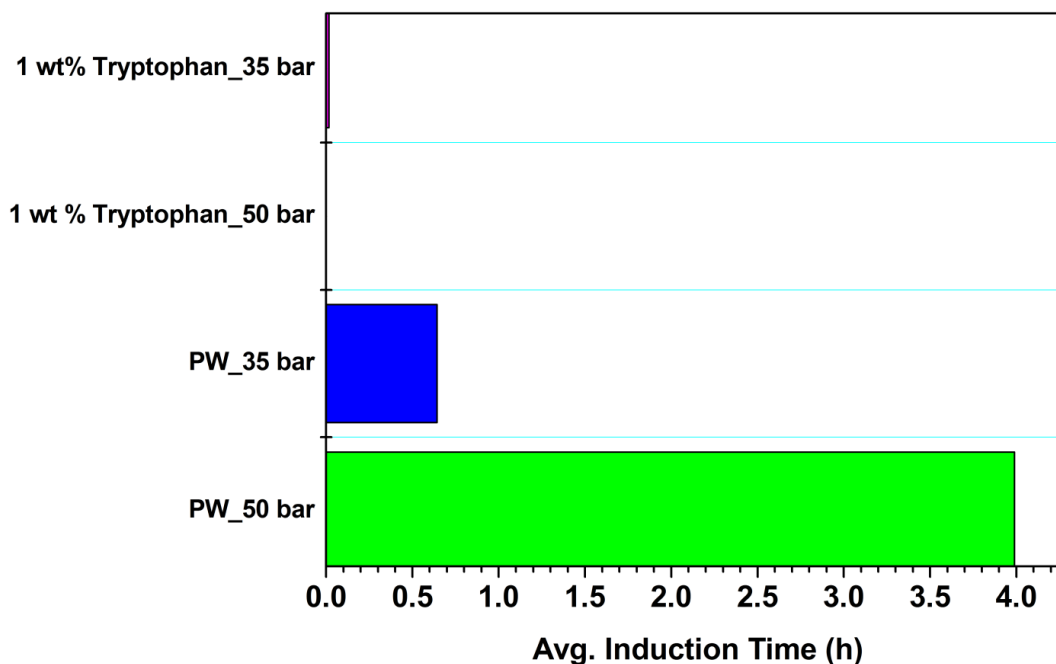


Fig. 5.7: Comparison of the average induction times for the different systems studied (fresh runs). The induction times for the PC and Sulfolane systems could not be plotted here as no discernible nucleation point could be identified for these systems owing to the exceedingly slow hydrate formation kinetics.

5.3.3. Gas separation analysis

The gas phase analysis is an indispensable part of any gas separation efficiency as this tells us about the separation efficiency of the process being studied. With a CO₂-CH₄ gas mixture, it is known that the hydrates formed will be of Structure I and hence both CO₂ and CH₄ will vie to occupy both small and large cages thus making the separation of this gas mixture particularly difficult. One of the objectives of the present study was to identify additives which would facilitate the incorporation of only a certain gas molecule into the hydrate cages thus in the process achieving better separation of the gas mixture. In this regard, three different additives were identified, termed as “selective hydrate promoters (SHPs)”. While the first two (PC and Sulfolane) were identified to increase the solubility of CO₂ in water and thus allow the forming hydrates to selectively capture CO₂ from the solution, the third additive, Tryptophan, owing to its hydrophobic nature, was identified to make possible favourable selection of CH₄ in the forming hydrates. Table 5.2 given below lists the values of the various parameters required to be studied

using the gas phase analysis for all the different systems considered. These parameters include the mole fractions of CO₂ and CH₄ in the hydrate phase, the CO₂ and CH₄ split fractions and the CO₂ and CH₄ separation factors. The calculations for each of these entities have been provided earlier in Section 5.2.6. From the experimental data in Table 5.2, it can be seen that the different additives used work exactly as expected. As compared to pure water, the two polar aprotic solvents increased the mole fraction of CO₂ in the hydrate phase whereas the hydrophobic amino acid Tryptophan clearly increased the mole fraction of CH₄ in the hydrate phase. However, even though the gas mixture could be separated to a certain extent using the additives, the separation factor for either CO₂ or CH₄ could not be increased as significantly as one would have hoped as compared to pure water. The highest separation factor for CO₂ was 1.9 using 1 wt % of PC at 50 bar which was only an approximately 16 % increase as compared to pure water while the highest separation factor for CH₄ was 0.8 with 1 wt % of Tryptophan at 50 bar which was an approximately 22 % increase as compared to pure water. The split fractions obtained are basically ratios of the number of moles of each gas present in the system at the start of hydrate formation to the number of moles of each gas present in the hydrate phase at the end of hydrate formation which explains why, even though the 50 bar systems exhibited faster hydrate formation kinetics and greater final gas uptake than the 35 bar systems, the split fractions of CO₂ and CH₄ achieved in the hydrate gas were lower for the 50 bar systems as compared to the 35 bar systems.

Although the separation efficiency of the process could not be greatly enhanced even on using the additives, the results obtained still hold good value for further research on this subject. It has been proven that these additives at least to a certain extent, improve the selectivity of the gases going into the hydrate phase from the feed gas mixture. This opens up a plethora of options for future work using additives to enhance the separation efficiency of the HBGS process for CO₂-CH₄ separation. In the current study, the additives were used in very small concentrations (1 wt %). If adjusted properly, maybe the concentration of the additives in the system can have a huge impact on the specific gas separation factors. Other additives that would potentially work on similar lines may also be identified and used for this separation process. However, all of these approaches would require considerable experimental work in order to perfect and reach the levels of efficiency desired when attempting the HBGS process for separation of CO₂-CH₄ gas mixtures.

A comparison of the separation efficiency of the HBGS process for the separation of a CO₂-CH₄ gas mixture with those for other conventional (adsorbent based, membrane based) gas separation processes for the same gas mixture has been carried out by defining a parameter termed as the CO₂/CH₄ selectivity or CO₂ partition coefficient and the same has been given in Appendix B.

Table 5.2: Mole fractions of CO₂ and CH₄ in hydrate phase, Split Fraction (%) of CO₂ and CH₄ in hydrate phase and CO₂ and CH₄ Separation Factors obtained via gas phase analysis.

System	Mole Fr. of CO ₂ in hydrate	Mole Fr. of CH ₄ in hydrate	CO ₂ Split Fraction	CH ₄ Split Fraction	CO ₂ Separation Factor	CH ₄ Separation Factor
PW_50 bar	0.60	0.40	18.250	12.421	1.591	0.628
PW_35 bar	0.60	0.40	28.831	19.987	1.637	0.610
1 wt % PC_50 bar	0.63	0.37	27.848	16.450	1.900	0.527
1 wt % PC_35 bar	0.60	0.40	26.073	18.038	1.585	0.630
1 wt % Sulf_50 bar	0.63	0.36	23.833	14.000	1.883	0.531
1 wt % Sulf_35 bar	0.59	0.41	25.015	17.764	1.574	0.635
1 wt% Trypt_50 bar	0.57	0.45	21.883	17.590	1.251	0.800
1 wt% Trypt_35 bar	0.58	0.42	31.400	23.357	1.480	0.677

5.4. Conclusions

The HBGS process for separation of CO₂-CH₄ gas mixtures has been plagued by problems of low gas hydrate formation kinetics and low separation efficiencies. In the present study, three new additives were identified to resolve these issues. The additives were identified such that they would modify the system to preferentially allow the enclathration of only one of the two gases in the mixture into the hydrate phase. These additives, christened as selective hydrate promoters, were expected to a) enhance the kinetics of hydrate formation and b) enhance the separation

efficiency of the HBGS process. While two of the additives identified were polar aprotic solvents (propylene carbonate and sulfolane); expected to enhance the solubility of CO₂ in water and hence its hydrate selectivity, the third, an amino acid Tryptophan, was expected to enhance the hydrate selectivity of CH₄ by virtue of its hydrophobic nature. Furthermore, these additives are non-foaming thus doing away with the problem of foam generation usually experienced with surfactants, the conventional hydrate formation promoters. A 50 % CO₂-50 % CH₄ gas mixture was used as the hydrate forming gas. Hydrate formation was studied at two different initial pressures, 3.5 MPa and 5.0 MPa to study the effect of overpressure on the kinetics of hydrate formation and the separation efficiency of the process. From the hydrate formation studies, it was clear that the presence of the additives significantly affected the kinetics of hydrate formation. While the two polar solvents could not enhance hydrate formation kinetics as compared to pure water, the hydrophobic amino acid Tryptophan was found to increase the same enormously. In fact, in the presence of 1 wt % Tryptophan in the system, more than sixty percent water to hydrate formation was observed within the first fifteen minutes of hydrate formation itself which could not be reached with any other system even after 10 hours of hydrate formation. The gas phase analysis showed that the additives used behaved exactly as expected. As compared to pure water, the two polar aprotic solvents increased the mole fraction of CO₂ in the hydrate phase whereas the hydrophobic amino acid Tryptophan clearly increased the mole fraction of CH₄ in the hydrate phase. However, the increase in mole fractions of specific gases that was observed in the presence of the additives was not enough to satisfactorily overcome the limitation of low separation efficiency. The maximum separation factor that could be achieved for CO₂ was 1.9 (1 wt % of Propylene Carbonate at 50 bar); only an approximately 16 % increase as compared to pure water while the highest separation factor that could be achieved for CH₄ was 0.8 (1 wt % of Tryptophan at 50 bar); an approximately 22 % increase as compared to pure water.

Although the separation efficiency of the process could not be greatly enhanced even on using the additives, the results obtained from this study still hold good value for further research on this subject. The problem of low hydrate formation kinetics could be resolved using the amino acid Tryptophan. Even at a very small concentration of this additive (1 wt %), extraordinarily fast kinetics of hydrate formation with the CO₂-CH₄ gas mixture was observed. It was also proven that these additives at least to a certain extent, improve the selectivity of the gases going into the hydrate phase from the feed gas mixture. This opens up a plethora of options for future work

using additives to enhance the separation efficiency of the HBGS process for CO₂-CH₄ separation. In the current study, the additives were used in very small concentrations (1 wt %). If adjusted properly, maybe the concentration of the additives in the system can have a huge impact on the specific gas separation factors. Other additives that would potentially work on similar lines may also be identified and used for this separation process while various mixtures of additives can also be tried out. However, all of these approaches would require considerable experimental work in order to perfect and reach the levels of efficiency desired when attempting the HBGS process for separation of CO₂-CH₄ gas mixtures.

5.5. References

1. BP Statistical Review of World Energy; British Petroleum: United Kingdom, 2016
2. Fan, S.; Long, X.; Lang, X.; Wang, Y.; Chen, J. CO₂ Capture from CH₄/CO₂ Mixture Gas with Tetra-n-butylammonium Bromide Semi-clathrate Hydrate through a Pressure Recovery Method. *Energy Fuels*, **2016**, 30, 8529-8534.
3. Di Profio, P.; Canale, V.; D'Alessandro, N.; Germani, R.; Di Crescenzo, A.; Fontana, A. Separation of CO₂ and CH₄ from biogas by formation of clathrate hydrates: importance of the driving force and kinetic promoters. *ACS Sustain. Chem. Eng.* **2017**, 5, 1990-1997.
4. Rufford, T. E.; Smart, S.; Watson, G. C.; Graham, B. F.; Boxall, J.; Da Costa, J. D.; May, E. F. The removal of CO₂ and N₂ from natural gas: a review of conventional and emerging process technologies. *J. Petro. Sci. Eng.* **2012**, 94, 123-154.
5. Yeo, Z. Y.; Chew, T. L.; Zhu, P. W.; Mohamed, A. R.; Chai, S. P. Conventional processes and membrane technology for carbon dioxide removal from natural gas: a review. *J. Nat. Gas Chem.* **2012**, 21, 282-298.
6. Kohl, A. L.; Nielsen, R. B. Gas Purification; Gulf Professional Publishing: Texas, 1997.
7. Sun, Q.; Li, H.; Yan, J.; Liu, L.; Yu, Z.; Yu, X. Selection of appropriate biogas upgrading technology-a review of biogas cleaning, upgrading and utilisation. *Renew. Sustainable Energy Rev.* **2015**, 51, 521-532.
8. Ryckebosch, E.; Drouillon, M.; Vervaeren, H. Techniques for transformation of biogas to biomethane. *Biomass Bioenergy* **2011**, 35, 1633-1645.

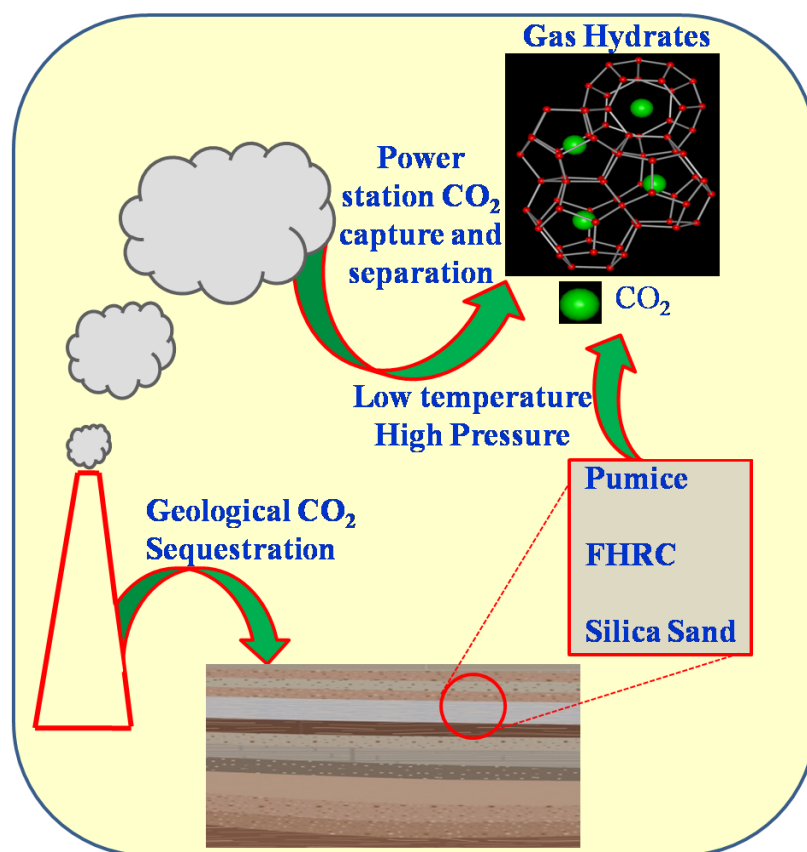
9. Seo, Y. T.; Kang, S. P.; Lee, H.; Lee, C. S.; Sung, W. M. Hydrate phase equilibria for gas mixtures containing carbon dioxide: a proof-of-concept to carbon dioxide recovery from multicomponent gas stream. *Korean J. Chem. Eng.* **2000**, *17*, 659-667.
10. Seo, Y. T.; Lee, H.; Yoon, J. H. Hydrate phase equilibria of the carbon dioxide, methane, and water system. *J. Chem. Eng. Data* **2001**, *46*, 381-384.
11. Uchida, T.; Ikeda, I. Y.; Takeya, S.; Kamata, Y.; Ohmura, R.; Nagao, J.; Zatsepina, O.Y.; Buffett, B. A. Kinetics and Stability of CH₄-CO₂ Mixed Gas Hydrates during Formation and Long-Term Storage. *ChemPhysChem* **2005**, *6*, 646-654.
12. Golombok, M.; Ineke, E.; Luzardo, J. C. R.; He, Y. Y.; Zitha, P. Resolving CO₂ and methane hydrate formation kinetics. *Environ. Chem. Lett.* **2009**, *7*, 325.
13. van Denderen, M.; Ineke, E.; Golombok, M. CO₂ removal from contaminated natural gas mixtures by hydrate formation. *Ind. Eng. Chem. Res.* **2009**, *48*, 5802-5807.
14. Herri, J. M.; Bouchemoua, A.; Kwaterski, M.; Fezoua, A.; Ouabbas, Y.; Cameirao, A. Gas hydrate equilibria for CO₂-N₂ and CO₂-CH₄ gas mixtures—Experimental studies and thermodynamic modelling. *Fluid Phase Equilib.* **2011**, *301*, 171-190.
15. Ricaurte, M.; Dicharry, C.; Broseta, D.; Renaud, X.; Torr , J. P. CO₂ removal from a CO₂-CH₄ gas mixture by clathrate hydrate formation using THF and SDS as water-soluble hydrate promoters. *Ind. Eng. Chem. Res.* **2012**, *52*, 899-910.
16. Tomita, S.; Akatsu, S.; Ohmura, R. Experiments and thermodynamic simulations for continuous separation of CO₂ from CH₄+ CO₂ gas mixture utilizing hydrate formation. *Appl. Energy* **2015**, *146*, 104-110.
17. Xia, Z. M.; Li, X. S.; Chen, Z. Y.; Li, G.; Yan, K. F.; Xu, C. G.; Lv, Q.N.; Cai, J. Hydrate-based CO₂ capture and CH₄ purification from simulated biogas with synergic additives based on gas solvent. *Appl. Energy* **2016**, *162*, 1153-1159.

18. Long, X.; Wang, Y.; Lang, X.; Fan, S.; Chen, J. Hydrate Equilibrium Measurements for CH₄, CO₂, and CH₄+ CO₂ in the Presence of Tetra-n-butyl Ammonium Bromide. *J. Chem. Eng. Data* **2016**, 61, 3897-3901.
19. Sloan, E. D., Koh, C. A. Clathrate hydrates of natural gases; CRC press: New York, 2008.
20. Daniel-David, D.; Guerton, F.; Dicharry, C.; Torr , J. P.; Broseta, D. Hydrate growth at the interface between water and pure or mixed CO₂/CH₄ gases: Influence of pressure, temperature, gas composition and water-soluble surfactants. *Chem. Eng. Sci.* **2015**, 132, 118-127.
21. Ricaurte, M.; Dicharry, C.; Renaud, X.; Torr , J. P. Combination of surfactants and organic compounds for boosting CO₂ separation from natural gas by clathrate hydrate formation. *Fuel* **2014**, 122, 206-217.
22. Zhong, D. L.; Li, Z.; Lu, Y. Y.; Wang, J. L.; Yan, J.; Qing, S. L. Investigation of CO₂ capture from a CO₂+ CH₄ gas mixture by gas hydrate formation in the fixed bed of a molecular sieve. *Ind. Eng. Chem. Res.* **2015a**, 55, 7973-7980.
23. Zhong, D. L.; Li, Z.; Lu, Y. Y.; Wang, J. L.; Yan, J. Evaluation of CO₂ removal from a CO₂+ CH₄ gas mixture using gas hydrate formation in liquid water and THF solutions. *Appl. Energy* **2015b**, 158, 133-141.
24. Bhattacharjee, G.; Kushwaha, O. S.; Kumar, A.; Khan, M. Y.; Patel, J. N.; Kumar, R. Effects of Micellization on Growth Kinetics of Methane Hydrate. *Ind. Eng. Chem. Res.* **2017**, 56, 3687-3698.
25. Wang, W.; Bray, C. L.; Adams, D. J.; Cooper, A. I. Methane storage in dry water gas hydrates. *J. Am. Chem. Soc.* **2008**, 130, 11608-11609.

-
26. Bhattacharjee, G.; Choudhary, N.; Kumar, A.; Chakrabarty, S.; Kumar, R. Effect of the amino acid l-histidine on methane hydrate growth kinetics. *J. Nat. Gas. Sci. Eng.* **2016**, *35*, 1453-1462.
 27. Liu, Y.; Chen, B.; Chen, Y.; Zhang, S.; Guo, W.; Cai, Y.; Tan, B.; Wang, W. Methane storage in a hydrated form as promoted by leucines for possible application to natural gas transportation and storage. *Energy Technol.* **2015**, *3*, 815-819.
 28. Veluswamy, H. P.; Hong, Q. W.; Linga, P. Morphology study of methane hydrate formation and dissociation in the presence of amino acid. *Cryst. Growth Des.* **2016**, *16*, 5932-5945.
 29. Cai, Y.; Chen, Y.; Li, Q.; Li, L.; Huang, H.; Wang, S.; Wang, W. CO₂ Hydrate Formation Promoted by a Natural Amino Acid l-Methionine for Possible Application to CO₂ Capture and Storage. *Energy Technol.* 2017, DOI: 10.1002/ente.201600731
 30. Nguyen, N. N.; Nguyen, A. V.; Steel, K. M.; Dang, L. X.; Galib, M. Interfacial gas enrichment at hydrophobic surfaces and the origin of promotion of gas hydrate formation by hydrophobic solid particles. *J. Phys. Chem. C.* **2017**, *121*, 3830-3840.
 31. Smith, J.M.; Van Ness, H.C.; Abbott, M.M. Introduction to chemical engineering thermodynamics; McGraw-Hill: New York, 2004.

Chapter 6

Carbon Dioxide Sequestration in simulated sub sea sediment



6. Carbon Dioxide Sequestration in simulated sub sea sediment⁶

⁶A version of this chapter has been published

Bhattacharjee, G., Kumar, A., Sakpal, T., Kumar, R. Carbon Dioxide Sequestration: Influence of Porous Media on Hydrate Formation Kinetics. *ACS Sustain. Chem. Eng.* **2015**, 3, 1205–1214.

6.1. Introduction

In the previous few chapters, the use of gas hydrate based technology for applications such as methane storage and separation has been discussed. It has also been mentioned a few times in the preceding chapters that carbon dioxide sequestration is one of the applications that gas hydrates hold potential in. Therefore in the current chapter, carbon dioxide sequestration through hydrate formation will be explored in detail. For this application, naturally occurring porous sediments were considered as fixed bed media for hydrate formation. Carbon dioxide, a major greenhouse gas is an undesirable byproduct of energy related activities such as electricity generation from fossil fuel combustion (Kumar et.al, 2009; Lasfof and Ahuja, 1999; Karl and Trenberth, 2003). Efficient capture and storage of CO₂ is pegged as a short to medium term solution to contain the anthropogenic release of CO₂ into the atmosphere. CO₂ capture and separation from a gas mixture can be achieved through several approaches. These include, conventional approaches like ethanol amine based chemical absorption process, pressure and temperature swing adsorption process, membrane separation and Soloxol / Rectisol based physical absorption process. Some unconventional processes for CO₂ capture (which are still in development stage) are use of metal organic frameworks and ionic liquids for preferential CO₂ adsorption through weak chemical forces. Hydrate based gas separation (HBGS) process is one such technology which can preferentially adsorb CO₂ through enclathration of CO₂ in ice like cages (D'Alessandro et.al, 2010; Aaron and Tsouris, 2005; Miller et.al, 2009).

Carbon dioxide sequestration is defined as storage of anthropogenic CO₂ in geological formations either permanently or for geologically significant time periods (Bickle, 2009; Bachu, 2000; Haszeldine, 2009; Holloway, 2005; Figueroa et.al, 2008; Koide et.al, 1992). Depleted oil and gas reservoirs, saline aquifers, unmineable coal beds and deep sea beds are geological formations that can be used for long-term CO₂ sequestration. Another option of deep ocean storage is plagued by environmental concerns such as ocean acidification and eutrophication (Leung et.al, 2014). In

Canada, about 5 Mt of acid gasses (CO₂ and H₂S) were safely stored into depleted gas reservoirs. The Sleipner West gas field in the North Sea is another example of underground CO₂ storage in porous sediment (Bachu, 2000; Haszeldine, 2009; Holloway, 2005). The above studies all refer to CO₂ storage in the fluid phase. Site selection for CO₂ storage needs addressing of various factors such as appropriate porosity and permeability of the reservoir rock, temperature, pressure and the availability of a stable geological environment (Leung et.al, 2014). CO₂ storage in the form of solid hydrates in underground reservoirs is promising as 1m³ of CO₂ hydrate can store 120-160 m³ of CO₂ gas at STP (Sun and Englezos, 2014; Bachu, 2000; Cote and Wright, 2013). Sun and Englezos mimicked the conditions of the depleted gas reservoir at Northern Alberta, Canada. The objective was to assess the potential of the site in question to serve as a host for CO₂ storage in the form of solid hydrates (Sun and Englezos, 2014).

India has a complex and diverse geology. Much of the geology of present day India is a result of volcanic eruptions dating back to prehistoric eras. The Indian subcontinent is mantled with the remnants of at least five continental flood basalt provinces that occurred between the middle proterozoic to the late cretaceous-early tertiary eras (Mahoney, 1988). The geographical land area of India can be divided into three parts: The Deccan Trap (youngest of the five continental flood basalt provinces), Gondwana and Vindhayan (Medlicott and Blanford, 2011). The Deccan Trap is acknowledged to be one of the largest volcanic features on Earth. It presently occupies around half a million square kilometers of western and central India and southernmost Pakistan (Mahoney, 1988). To simulate such lithography in a laboratory setup for studying CO₂ hydrate formation kinetics, we have chosen pumice and fire hardened red clay (FHRC) with suitable water saturation. Hydrate formation kinetics are studied in these two media and the results are compared with those obtained using silica sand and quartz. Pumice and FHRC are both highly siliceous materials with much higher porosities as compared to silica sand and quartz. Silica sand and quartz are porous sediments found in depleted oil and gas reservoirs. Unfortunately India does not have many depleted oil and gas reserves. Thus a comparison study on CO₂ hydrate formation kinetics using siliceous volcanic materials such as pumice and FHRC (a model material), which are available in plenty in the Indian subcontinent, is going to be valuable in assessing the feasibility of sequestering CO₂ in the form of hydrates for the same.

Pumice is a volcanic rock with an unusual foamy configuration that is created when super-heated, highly pressurized rock is violently ejected from a volcano (McPhie et.al, 1993; Thomas et.al, 1994). On land, it can be found anywhere in the vicinity of a volcano. It can also be found floating in the sea, attributable to underwater volcanoes ejecting molten lava and volcanic gases well above sea level. When the molten lava comes in contact with cold seawater, it hardens to form pumice. FHRC which is used in the construction industry is used as a model material in this work as it closely mimics the nature of siliceous volcanic deposits. Pumice and FHRC both mainly consist of SiO_2 and Al_2O_3 with varying amounts of other materials such as magnesia, iron oxide, lime etc (Venezia et.al, 1992; Weems, 1904; Lourenço et.al, 2010). Like pumice, FHRC is also created at conditions of high pressure and temperature, around 900-1000°C (Herbert, 1994). The conditions of formation of these two materials tell us that these are geologically stable formations. The Deccan Trap abounds with highly siliceous volcanic rocks like pumice (Mahoney, 1988; Subbarao and West, 1999). The Central Indian Basin (CIB) is another volcanic province that consists of layers of ash and pumice (Martín-Barajas and Lallier-Verges, 1993; Iyer and Sudhakar, 1995). The volcanic islands Narcondam and Barren Island in the Andamans are also sources of pumice and similar volcanic rocks (Sheth et.al, 2009)

All the four porous materials discussed above have potential for use as porous geological media for CO_2 storage. In the present work, the effects of these porous materials on hydrate formation kinetics were studied and compared. Three different size fractions were made for a) pumice and b) FHRC. Two types of experiments were conducted: first, the volume of water used was kept constant leading to different bed heights and in second, the bed height was kept constant resulting in different volumes of water used in each case.

6.2. Experimental Section

6.2.1. Materials

Carbon dioxide gas with a certified purity of more than 99.9% was supplied by Vadilal Gases Ltd., India. Silica sand and Quartz used in this study were purchased from Sakalchand & Company, Pune, India. The volume of water required to completely fill the void space between the sand particles and quartz particles was $0.20 \text{ cm}^3/\text{g}$ and $0.16 \text{ cm}^3/\text{g}$ respectively (Kumar et.al, 2015). Pumice and FHRC were purchased from Pune, India. The pumice and FHRC samples

were ground to different size fractions: a) less than 210 micron, b) 210-420 micron and c) more than 420 micron. The volume of water required to completely fill the void interstitial spaces between the particles of different size fractions of pumice and FHRC was calculated as discussed next.

6.2.2. Calculation of water retention capacities of the different materials studied

A porous material was tightly packed into a measuring cylinder up to a known volume (15 cm^3). Weight of the material constituting the known volume of 15 cm^3 was noted to calculate the density of the material. Volume of water required to completely fill the pores of the material was measured (Kumar et.al, 2015) and the ratio of water volume to the bulk volume of the material was considered to be the porosity of the material. These measurements were done thrice for each material. The final average porosities obtained for the different materials along with the corresponding standard deviation values are reported in Table 6.1.

Table 6.1: Volume of water required to completely fill the void spaces between the particles of the different size fractions of porous media used.

Material	Size Fraction (μm)	Volume of water required to completely fill the void spaces (cm^3/g)
Pumice	< 210	0.64
	210-420	0.72
	> 420	0.56
FHRC	< 210	0.30
	210-420	0.46
	> 420	0.44
Silica Sand	30-400	0.20
Quartz	210-1000	0.16

6.2.3. Apparatus and procedure for hydrate formation experiments

A fixed bed reactor setup as shown in Figure 6.1 was used to carry out the experiments in this study. Given below is the procedure used for the hydrate formation experiments which in the process also gives a detailed description of the stirred tank apparatus used:

For each of the four porous media discussed above, two types of experiments were carried out: a) with a constant volume of water (24 cm^3) and varying bed heights (Table 3.2) and b) with a constant bed height (3 cm) and varying corresponding volumes of water (Table 3.3). The water saturation of the porous fixed bed was kept constant at 75% for all the experiments conducted in this study. Distilled and de-ionized water was used. The water saturated packing medium was placed inside a 323 cm^3 SS-316 crystallizer (Parr make) which was then firmly sealed and placed inside a temperature controlled water bath in order to attain the desired experimental temperature (274 K). The vessel was flushed with pure CO_2 gas using a supply vessel by repeating rapid pressurization ($\sim 0.5 \text{ MPa}$) and depressurization cycles. Next, the crystallizer was pressurized with pure CO_2 gas up to a pre-determined experimental pressure of 3.0 MPa (equilibrium hydrate formation pressure for pure CO_2 gas at 274 K is 1.509 MPa) (Sloan and Koh, 2008) thus providing sufficient driving force for the hydrate formation reaction. At this stage, gas uptake measurements were initiated which were all performed in batch mode with pure CO_2 gas at a constant temperature of 274 K. Hydrate formation is accompanied with pressure drop inside the vessel as a result of the gas moving from the gas phase into the solid hydrate phase. This drop in pressure, measured employing a pressure transducer (WIKA make; range: 0-25 MPa) was used to calculate the moles of gas participating in the hydrate formation experiment. Temperature and pressure inside the vessel were recorded every five seconds using a data acquisition system (PPI, Mumbai - India). As entire experiments were conducted in batch mode, the effective driving force for hydrate formation decreased as the reaction proceeded with more and more CO_2 gas moving from the gas phase to the solid hydrate phase.

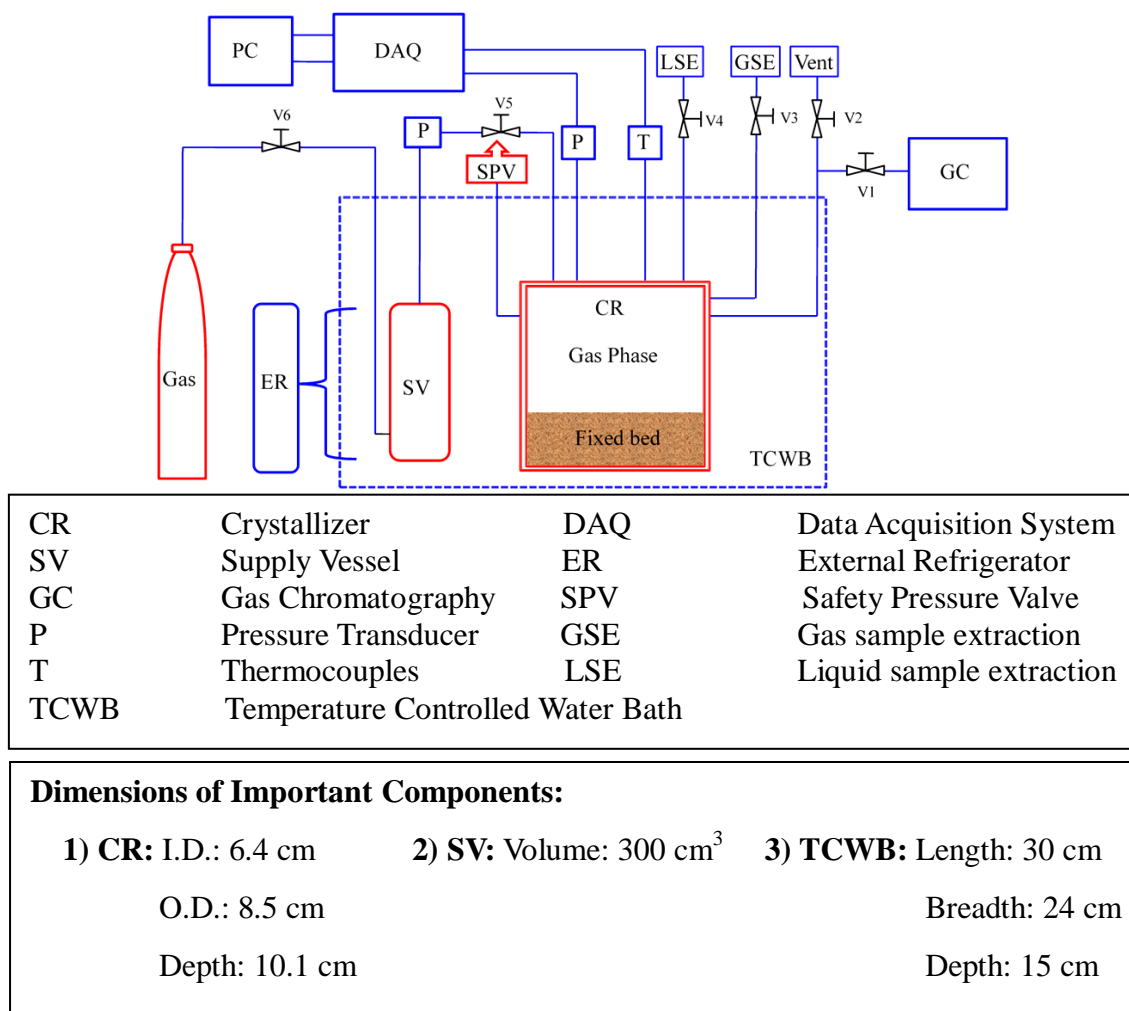


Fig. 6.1: Schematic of the experimental apparatus

6.2.4. Calculation of the amount of gas consumed during the hydrate formation experiments

At any given time, the total number of moles of gas that was consumed in the hydrate formation process is the difference between the number of moles of gas present in the gas phase of the crystallizer at time $t = 0$ and the number of moles of gas present in the gas phase of the crystallizer at time $t = t$. The same is given by the following equation (Linga et.al, 2012):

$$(\Delta n_{H,\downarrow})_t = V_{CR} \left[\frac{P}{zRT} \right]_0 - V_{CR} \left[\frac{P}{zRT} \right]_t \quad (6.1)$$

, where z is the compressibility factor calculated by Pitzer's correlation (Smith et.al, 2001); V_{CR} is the volume of the gas phase inside the crystallizer. P and T are the pressure and temperature of the crystallizer.

6.2.5. Calculation of the water to hydrate conversion

The amount of water that was converted to hydrate was determined by using the following equation (Linga et.al, 2012):

$$\text{Conversion of water to hydrate (mol\%)} = \frac{\Delta n_{H,\downarrow} \times \text{HydrationNo.}}{n_{H_2O}} \times 100 \quad (6.2)$$

Where $\Delta n_{H,\downarrow}$ is the total number of moles of gas consumed at the end of the hydrate formation process as calculated from the gas uptake measurements and n_{H_2O} is the total number of moles of water in the system. The hydration number used for the above calculations is 5.75 (Sloan and Koh, 2008).

6.2.6. Calculation of the CO₂ to hydrate conversion

The amount of gas (CO₂) that was converted to hydrate was determined by using the following equation (Yang et.al, 2014):

$$\text{Conversion of CO}_2 \text{ to hydrate (mol\%)} = \frac{(\Delta n_{H,\downarrow})}{(n_{start} - n_{eqbm})} \times 100 \quad (6.3)$$

Where $\Delta n_{H,\downarrow}$ is the total number of moles of gas consumed at the end of the hydrate formation process as calculated from the gas uptake measurements, n_{start} is the number of moles of gas present in the gas phase of the system at the start of the experiment and n_{eqbm} is the number of moles of gas present in the gas phase of the system at equilibrium (P and T).

6.2.7. Calculation of the hydrate saturation

The CO₂ hydrate saturation was calculated using the following equation (Sun and Englezos, 2014):

$$\text{Hydrate Saturation (\%)} = (\text{Initial water saturation} \times \text{Water to hydrate conversion} \times 1.1) \quad (6.4)$$

The density of CO₂ hydrate being less than that of water, when water is converted into hydrate,

the volume of the hydrate phase is taken to be 1.1 times that of the originally existing water (Sun and Englezos, 2014).

6.2.8. Calculation of the rate of hydrate formation

The rate of hydrate formation was calculated by the forward difference method as given below (Linga et.al, 2012):

$$\left(\frac{d\Delta n_{H,\downarrow}}{dt} \right)_t = \frac{\Delta n_{H,\downarrow(t+\Delta t)} - \Delta n_{H,\downarrow(t)}}{\Delta t}; \Delta t=5\text{sec} \quad (6.5)$$

The average of these rates was calculated for every 20 minutes and reported.

6.3. Results and Discussions

Tables 6.2, 6.3 and 6.4 summarize all the relevant information for each experiment conducted during this study. These include the sample state, the volume of water used, the bed height, induction times, the amount of gas consumed, the water to hydrate conversion in mol% and the gas to hydrate conversion in mol%. Hydrate formation was investigated for a fixed time of five hours after nucleation for all the experiments conducted. The reason for choosing five hours as the cut off point for studying hydrate formation is that the overall conclusion would not change even if the study would be extended for another five hours. Figure C1 in Appendix C shows the hydrate formation kinetics for each of the four systems for at least 12 hours from nucleation.

Hydrate formation kinetics are usually discussed through a gas uptake curve. A typical gas uptake curve for hydrate formation can be divided into three parts. First is the dissolution stage during which the gas gets dissolved into the system. The next stage is the hydrate nucleation. The hydrate nucleation phenomenon continues until the formation of critical sized stable hydrate nuclei. Once nucleation occurs, we enter the hydrate growth phase where the formed hydrate nuclei grow as solid hydrate particles (Natarajan et.al, 1994). The average induction times along with standard deviation for the hydrate formation experiments in presence of all the four porous media have been listed in Tables 6.2, 6.3 and 6.4. An illustration of the same has been included in Appendix C as Figure C2.

Table 6.2: Summary of all experiments conducted with constant volume of water (24 ml).

System	Average Porosity (vol%) \pm SD	Vol. of water used (cm ³)	Bed Height (cm)	Exp. No.	Run Type	Gas consumed (mol of gas/ mol of water)	Final water to hydrate conversion (mol %)	Final gas to hydrate conversion (mol %)	Induction time (min)	Average. Induction time \pm SD
Sand: Size: 30 to 400 micron	30.7 \pm 0.8	24.0	3.0	1	Fresh	0.040	23.1	14.5	9.0	18.6 \pm 15.6
				2	Repeat	0.040	23.1	14.9	10.8	
				3	Fresh	0.051	29.3	19.7	5.4	
				4	Repeat	0.064	36.8	25.3	26.0	
				5	Fresh	0.044	25.1	16.1	3.0	
				6	Repeat	0.076	44.1	31.2	31.3	
				7	Repeat	0.067	38.4	24.8	44.5	
Quartz: Size: 200-1000 micron	24.0 \pm 0.7	24.0	4.5	8	Fresh	0.033	19.1	14.1	0.3	7.4 \pm 8.8
				9	Repeat	0.034	19.8	14.4	0.2	
				10	Repeat	0.041	23.0	17.6	6.2	
				11	Fresh	0.031	18.3	13.8	1.1	
				12	Repeat	0.042	24.1	18.3	16.9	
				13	Repeat	0.038	21.9	17.1	19.8	
Pumice: Size: > 420 micron	46.4 \pm 2.0	24.0	2.2	14	Fresh	0.024	13.6	7.4	5.3	32.1 \pm 24.0
				15	Repeat	0.019	10.7	6.5	39.7	
				16	Repeat	0.018	10.4	6.5	51.3	
Pumice Size: 210-420 micron	57.0 \pm 1.8	24.0	2.3	17	Fresh	0.050	29.0	15.9	1.8	10.3 \pm 9.8
				18	Repeat	0.066	37.7	21.1	8.2	
				19	Repeat	0.032	18.5	10.3	21.1	

Pumice Size: < 210 micron	42.3±0.7	24.0	2.7	20	Fresh	0.080	46.0	26.4	10.3	31.6± 21.5
				21	Repeat	0.079	45.1	26.5	48.5	
				22	Repeat	0.082	47.1	27.7	47.8	
				23	Fresh	0.084	48.2	27.2	0.2	
				24	Repeat	0.072	41.3	24.7	49.5	
				25	Fresh	0.074	42.3	24.2	17.1	
FHRC: Size: > 420 micron	31.2±1.7	24.0	3.5	26	Fresh	0.025	14.3	9.3	6.3	71.1±62.9
				27	Repeat	0.022	12.7	8.3	75.0	
				28	Repeat	0.020	11.9	7.9	131.9	
FHRC: Size: 210- 420 micron	49.0±2.9	24.0	2.4	29	Fresh	0.039	22.2	12.6	1.8	93.4±144. 8
				30	Repeat	0.034	19.8	11.3	18.0	
				31	Repeat	0.029	16.6	9.6	260.4	
FHRC: Size: < 210 micron	55.9±2.0	24.0	2.4	32	Fresh	0.065	37.5	21.0	0.2	61.6± 87.9
				33	Repeat	0.061	35.1	20.0	115.0	
				34	Repeat	0.059	34.0	19.5	216.4	
				35	Fresh	0.076	43.7	23.8	0.1	
				36	Repeat	0.062	35.9	20.6	36.4	
				37	Fresh	0.066	37.9	21.4	1.3	

The dependent variables listed are bed height, induction time, the amount of CO₂ gas consumed till the end of the reaction, the water to hydrate conversion and the gas (CO₂) to hydrate conversion. Experimental temperature and pressure were 274K and 3.0 MPa respectively. The gas uptake was measured for a fixed time of 5 hours after induction for all the experiments conducted.

Table 6.3: Summary of all experiments conducted with constant bed height (3 cm).

System	Average Porosity (vol%) ±SD	Volume of water used (cm ³)	Bed Height (cm)	Exp. No	Run Type	Carbon dioxide Consumed (mol of gas/mol of water)	Final water to hydrate conversion (mol%)	Final gas to hydrate conversion (mol%)	Induction time (min)	Average Induction time ± SD
Sand: Size: 30 to 400 micron	30.6±0.8	24.0	3.0	As given in Table 1.						
Quartz: Size: 200-1000 micron	24.0±0.7	16.5	3.0	38	Fresh	0.016	15.4	6.3	0.3	6.2±9.1
				39	Repeat	0.039	22.2	9.4	0.5	
				40	Repeat	0.042	24.2	9.9	0.5	
				41	Fresh	0.027	15.4	6.4	0.2	
				42	Repeat	0.047	26.8	11.2	16.2	
				43	Repeat	0.045	25.6	10.8	19.7	
Pumice: Size: < 210 micron	42.3±0.7	25.5	3.0	44	Fresh	0.084	48.2	31.8	5.5	99.5±199.5
				45	Repeat	0.062	37.7	27.9	39.0	
				46	Repeat	0.060	35.6	26.7	40.5	
				47	Fresh	0.071	41.0	27.8	22.0	
				48	Repeat	0.061	34.7	24.9	28.8	
				49	Repeat	0.062	35.1	26.0	551.0	
				50	Fresh	0.068	38.8	25.8	10.0	
FHRC: Size: < 210 micron	55.9±2.0	28.3	3.0	51	Fresh	0.072	41.6	29.5	0.3	115.1±189.9
				52	Repeat	0.058	33.1	24.9	60.0	
				53	Fresh	0.073	41.7	29.4	0.2	
				54	Repeat	0.057	32.6	24.4	485.0	
				55	Fresh	0.068	39.0	27.4	0.2	
				56	Repeat	0.059	34.0	25.2	145.0	

The dependent variables listed are volume of water used, induction time, the amount of CO₂ gas consumed till the end of the reaction, the water to hydrate conversion and the gas (CO₂) to hydrate conversion. Experimental temperature and pressure were 274K and 3.0 MPa respectively. The gas uptake was measured for a fixed time of 5 hours after induction for all the experiments conducted.

Table 6.4: Pumice: Effect of bed height: Summary of all experiments conducted.

System	Average Porosity (vol%) \pm SD	Volume of water used (cm ³)	Bed Height (cm)	Exp. No	Run Type	Carbon dioxide Consumed (mol of gas/mol of water)	Final gas to hydrate conversion (mol%)	Final gas to hydrate conversion (mol%)	Induction time (min)	Average Induction time \pm SD
Pumice Size: < 210 micron	42.3 \pm 0.7	24.0	2.7	As given in Table 1.						
Pumice Size: < 210 micron		44.1	5.5	57	Fresh	0.045	25.7	41.6	6.5	60.1 \pm 59.8
				58	Repeat	0.040	23.2	39.5	126.6	
				59	Repeat	0.040	23.2	39.9	94.7	
				60	Fresh	0.047	27.2	43.6	1.4	
				61	Repeat	0.041	23.8	40.7	120.2	
				62	Fresh	0.047	26.7	43.7	11.4	

The dependent variables listed are bed height, volume of water used, induction time, the amount of CO₂ gas consumed till the end of the reaction, the water to hydrate conversion and the gas (CO₂) to hydrate conversion. Experimental temperature and pressure were 274K and 3.0 MPa respectively. The gas uptake was measured for a fixed time of 5 hours after induction for all the experiments conducted.

6.3.1. Gas hydrate formation in various porous media with constant volume of water and with constant bed height

Figures 6.2 and 6.3 compare averages of the gas uptake and water to hydrate conversion for the hydrate growth experiments conducted in different porous media (pumice, FHRC, silica sand and quartz). Only the fresh runs have been included in Figures 6.2 and 6.3. Figure 6.2 corresponds to the constant volume of water experiments whereas Figure 6.3 covers the constant bed height experiments. Time zero in the graphs corresponds to the hydrate nucleation point for the experiments. As seen in Figure 6.2, hydrate growth kinetics is the best in case of pumice (~46% in 5 hours) followed by FHRC, silica sand and quartz respectively. This can be attributed to two main reasons: First is the effect of particle size. Hydrate formation kinetics is enhanced with decrease in particle size (Heeschen et.al, 2014; Mekala et.al, 2014). This topic has been discussed in detail later. In the case of both pumice and FHRC, the particle size used is < 210 micron whereas for silica sand and quartz, the particle sizes vary between 30-400 micron and 200-1000 micron respectively. This shows that smaller particle size of pumice and FHRC had positive effect on hydrate formation kinetics. The second cause for pumice showing better hydrate formation kinetics is the higher porosity of pumice bed compared to other media. A highly porous bed ensures that for same amount of water used for hydrate formation, it has a smaller bed height compared to others, resulting in better gas-water contact (Babu et.al, 2014). In the case of the constant bed height experiments which have been highlighted in Figure 6.3, the bed height is the same in all the cases, and thus the volume of water used varies. As expected, pumice and FHRC again show enhanced hydrate formation kinetics as compared to silica sand and quartz. Averages of the gas uptake and water to hydrate conversion for the repeat runs have been shown in Appendix C as Figures C3 and C4 respectively. Rates of gas uptake (mol of gas/mol of water/hour) corresponding to Figures 6.2 and 6.3 have been plotted against time and are given as Figures 6.4 and 6.5. Results follow the same trend for both types of experiments: pumice showing the best kinetics followed by FHRC, silica sand and quartz respectively. Figures A9 and A10 in Appendix A show the linear fits of the first twenty minutes of hydrate formation for the systems represented in Figures 6.2 and 6.3 respectively. The average initial apparent rates of hydrate formation for the first twenty minutes of hydrate growth for these systems obtained as a result of the linear fitting have been reported in Table A6, Appendix A.

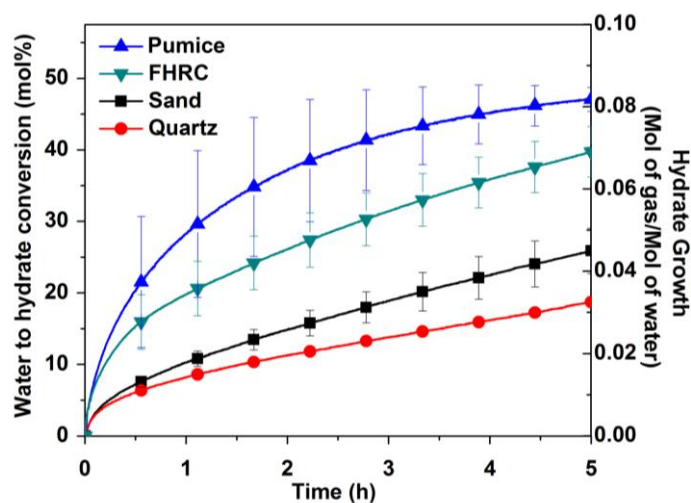


Fig. 6.2: Comparison of the gas uptake and water to hydrate conversion in presence of the different porous media used for the case of the constant volume of water experiments: Sand: Average and standard deviation of experiment numbers 1, 3 and 5, Quartz: Average and standard deviation of experiment numbers 8 and 11, Pumice: Average and standard deviation of experiment numbers 20, 23 and 25 and FHRC: Average and standard deviation of experiment numbers 32, 35 and 37.

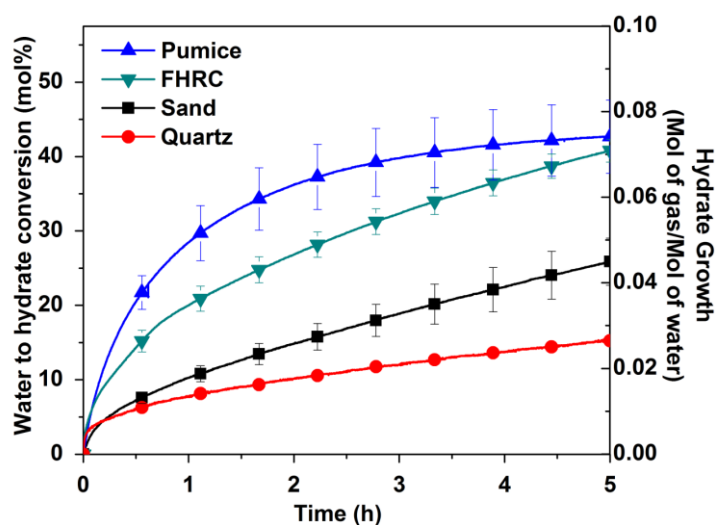


Fig. 6.3: Comparison of the gas uptake and water to hydrate conversion in presence of the different porous media used for the case of the constant bed height experiments: Sand: Average and standard deviation of experiment numbers 1, 3 and 5, Quartz: Average and standard deviation of experiment numbers 38 and 41, Pumice: Average and standard deviation of experiment numbers 44, 47 and 50 and FHRC: Average and standard deviation of experiment numbers 51, 53 and 55.

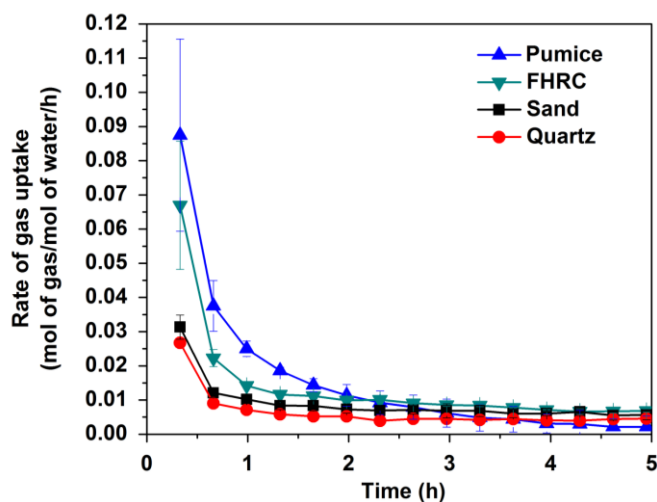


Fig. 6.4: Comparison of the rates of gas uptake and water to hydrate conversion in presence of the different porous media used for the case of the constant volume of water experiments: Sand: Average and standard deviation of experiment numbers 1, 3 and 5, Quartz: Average and standard deviation of experiment numbers 8 and 11, Pumice: Average and standard deviation of experiment numbers 20, 23 and 25 and FHRC: Average and standard deviation of experiment numbers 32, 35 and 37.

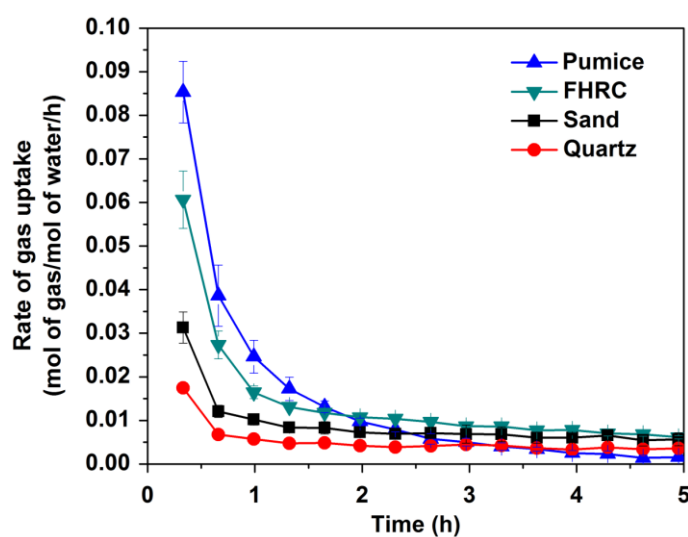


Fig. 6.5: Comparison of the rates of gas uptake and water to hydrate conversion in presence of the different porous media used for the case of the constant bed height experiments: Sand: Average and standard deviation of experiment numbers 1, 3 and 5, Quartz: Average and standard deviation of experiment numbers 38 and 41, Pumice: Average and standard deviation of experiment numbers 44, 47 and 50 and FHRC: Average and standard deviation of experiment numbers 51, 53 and 55.

6.3.2. Effect of particle size and water saturation on gas hydrate formation kinetics

The effect of particle size distribution of the porous medium being used, on hydrate formation kinetics, has not been widely studied. Some studies using CH₄ and CO₂ as the hydrate forming guests have concluded that particle size distribution does affect hydrate formation kinetics (Heeschen et.al, 2014; Mekala et.al, 2014; Siangsai et.al, 2015; Babu et.al, 2013). Figures 6.6 and 6.7 represent the effect of particle size on the hydrate formation kinetics using pumice and FHRC individually as porous media. For the experiments conducted, the figures plot the gas uptake and water to hydrate conversion after nucleation with respect to time. It is to be noted that these experiments were all conducted with a constant volume of water (24 cm³) and varying bed heights. As can be seen from the figures, hydrate formation kinetics is enhanced with decrease in particle size. These observations are in good agreement with those made by some earlier studies. Heeschen et.al reported a kinetic promoting effect of finer grain sizes of quartz sand on methane hydrate formation in methane-sand-water and methane-sand-seawater systems (Heeschen et.al, 2014). Mekala et.al studied the effect of particle size on CO₂ hydrate formation kinetics with a view on CO₂ sequestration using silica sand as the porous medium in the presence of both pure water and seawater (Mekala et.al, 2014). They observed that decrease in particle size enhances hydrate formation kinetics. Siangsai et.al investigated the effect of particle sizes of activated carbon on methane hydrate formation and dissociation. They speculated that compared to a system having only quiescent water, the presence of activated carbon particles increases the gas-water interfacial area by allowing the gas to pass through the carbon bed by making use of interstitial spaces present in the bed (Siangsai et.al, 2015). Babu et.al studied methane hydrate formation in the presence of porous media (activated carbon and silica sand). Their results showed that pore space and its corresponding interconnectivity play an important role in hydrate formation (Babu et.al, 2013). A smaller grain size ideally leads to a more regular packing and thus results in more interconnectivity of the pores and greater surface area for gas-water contact (Siangsai et.al, 2015; Babu et.al, 2013). With the help of glass micromodels, Tohidi et.al observed the difference in mechanisms of formation of gas hydrates in sediments having different particle size fractions. Hydrate formation in the interstitial spaces between grains in the sediment, occurs at the center of the pores rather than on the surface of the grains (Tohidi et.al, 2001; Kuhs et.al, 2014). This is mainly due to the preferential wetting of the particle surfaces with water rather than gas. However, Tohidi et.al observed that this holds true mainly for large grain sizes (0.313 mm) whereas for the smaller grain sizes (0.070 mm), the hydrates form

large masses almost completely encompassing the grains. This has been represented in the form of a well detailed schematic as Figure 6.8. We can thus conclude that decrease in particle size increases the surface area for gas-water contact. A larger surface area for gas-water contact means an increased number of nucleating sites thus resulting in accelerated hydrate growth (Heeschen et.al, 2014). The observation made in this study (enhancement in hydrate formation kinetics in the presence of small particle size fractions) is probably a combination of all these factors.

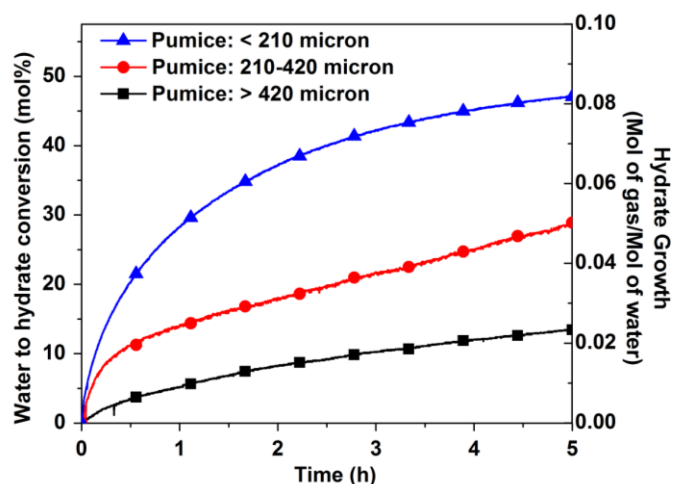


Fig. 6.6: Effect of particle size of Pumice on hydrate formation kinetics. Pumice: > 420 micron: Experiment number 14, Pumice: 210-420 micron: Experiment number 17, Pumice: < 210 micron: Average of experiment numbers 20, 23 and 25.

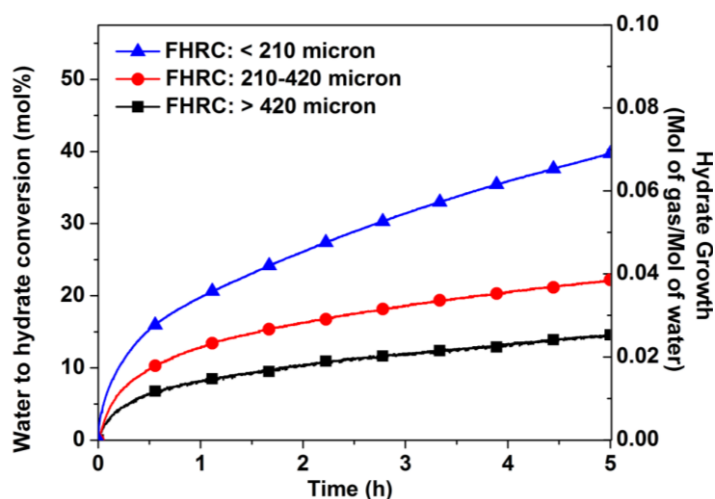


Fig. 6.7: Effect of particle size of FHRC on hydrate formation kinetics. FHRC: > 420 micron: Experiment number 26, FHRC: 210-420 micron: Experiment number 29, FHRC: < 210 micron: Average of experiment numbers 32, 35 and 37.

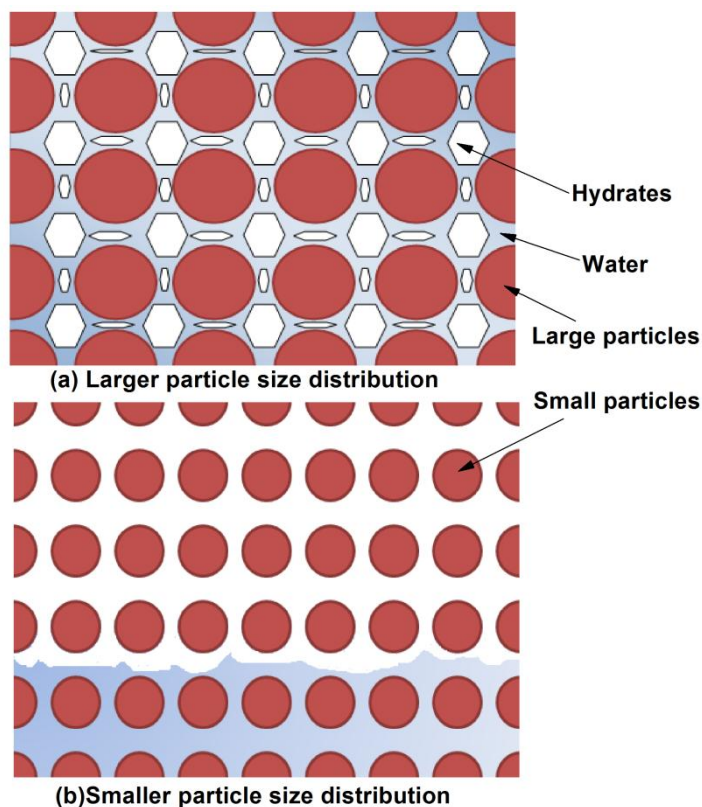


Fig. 6.8: Mechanism of hydrate formation in systems having different particle size fractions (a) Large particle size fraction: no interaction between the hydrates and the surface of the particles. (b) Small particle size fraction: hydrates form in large masses almost completely enveloping the particles themselves. (Maroon: Sediment particles/grains, Blue:Water, White:Hydrates)

Gas-water interfacial area is an important aspect of hydrate formation kinetics and can be affected by a number of other factors too. The water saturation of the bed is one such dynamic that affects the contact area between gas and water. There are two scenarios, first when the pores are completely filled with water and it cannot be replaced / moved by CO_2 pressure. Under this scenario, hydrate formation will proceed through dissolution of gas into the water. In the second scenario, the pores are partially filled with water and thus under CO_2 pressure, these interconnected pores will have higher interfacial area of contact by creating a dedicated gas channel within the pores. This aspect of gas diffusion is further explored when conducting experiments with different bed heights. Averages of the gas uptake and the water to hydrate conversion for the repeat runs have been included separately in Appendix C as Figures C5 and C6 respectively. The rates of gas uptake corresponding to Figures 6.6 and 6.7 have been

plotted against time and are given as Figures 6.9 and 6.10. As expected, the rate of gas uptake is the maximum for the smallest particle size fraction in the case of both pumice and FHRC.

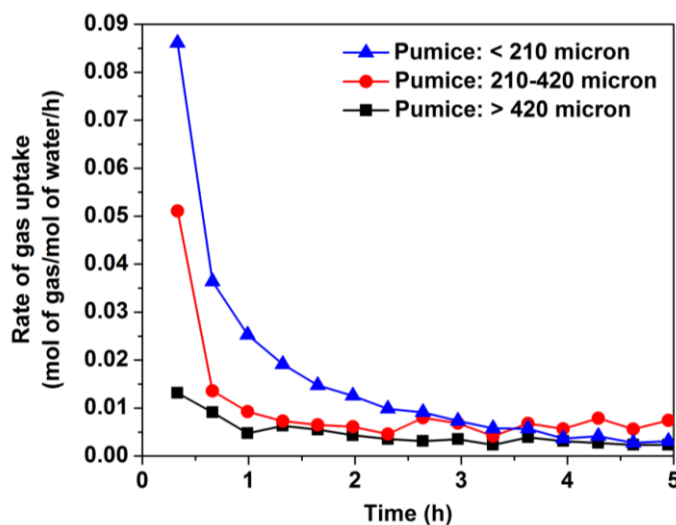


Fig. 6.9: Comparison of the rates of gas uptake for the different particle size fractions of pumice: Pumice: > 420 micron: Experiment number 14, Pumice: 210-420 micron: Experiment number 17, Pumice: < 210 micron: Average of experiment numbers 20, 23 and 25.

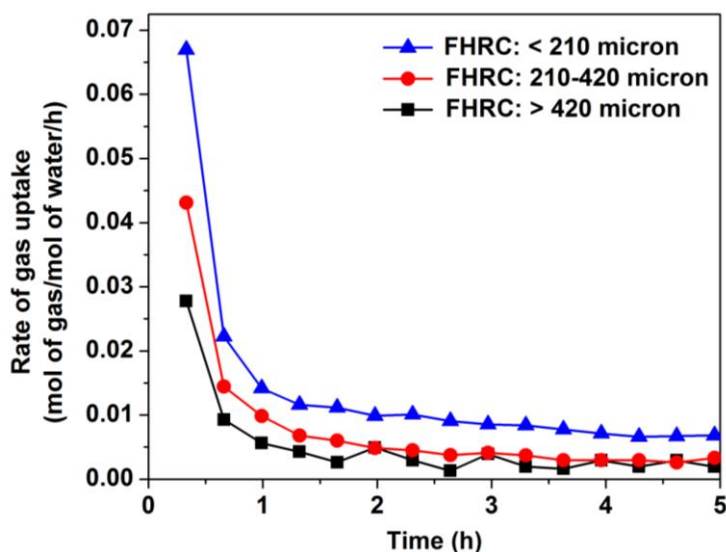


Fig. 6.10: Comparison of the rates of gas uptake for the different particle size fractions of FHRC: FHRC: > 420 micron: Experiment number 26, FHRC: 210-420 micron: Experiment number 29, FHRC: < 210 micron: Average of experiment numbers 32, 35 and 37.

Figures A11 and A12 in Appendix A show the linear fits of the first twenty minutes of hydrate formation for the systems represented in Figures 6.6 and 6.7 respectively. The average initial apparent rates of hydrate formation for the first twenty minutes of hydrate growth for these systems obtained as a result of the linear fitting have been reported in Table A6, Appendix A.

6.3.3. Effect of bed height on gas hydrate formation kinetics

Figure 6.11 shows the effect of bed height on gas uptake and water to hydrate conversion for the hydrate formation experiments using pumice as the porous medium. Only the fresh runs have been included in Figure 6.11. Two different bed heights were taken: 2.7 cm and 5.5 cm. In the first case (2.7 cm), the volume of water used was 24 cm³ whereas in the second case (5.5 cm), the volume of water used was 44.1 cm³ (75% saturation in both cases). Further details are given in Table 6.4. A smaller bed height ensures efficient transfer of hydrate forming gases to the bottom of the reactor and thus enhanced rate of hydrate formation. It can be seen in Figure 6.11, that with increase in the bed height, water to hydrate conversion decreases as does the total gas uptake. This is probably due to the limited diffusion / migration of gas molecules deep inside the porous bed. This leads to the conclusion that bed height indeed affects the availability of sufficient gas to the water dispersed in the bed for hydrate formation. Extrapolating these results to real world systems can give us important conclusions regarding the challenges to be faced when applying these schemes on a pilot/field scale. In a real world system, there will always be enough bed height present, i.e. the porous geological formation would always limit the migration of gas molecules deep inside the bed. The results obtained in this study point to the fact that CO₂ sequestration in porous geological formations would be at a relatively lesser rate than those obtained through experiments performed in the laboratory. Averages of the water to hydrate conversion and the gas uptake for the repeat runs are given in the Appendix C as Figure C7. The rates of gas uptake corresponding to Figure 6.11 have been plotted against time and are displayed in Figure 6.12. The system with the smaller bed height shows faster uptake of the gas. Figure A13 in Appendix A shows the linear fits of the first twenty minutes of hydrate formation for the systems represented in Figure 6.11. The average initial apparent rates of hydrate formation for the first twenty minutes of hydrate growth for these systems obtained as a result of the linear fitting have been reported in Table A6, Appendix A.

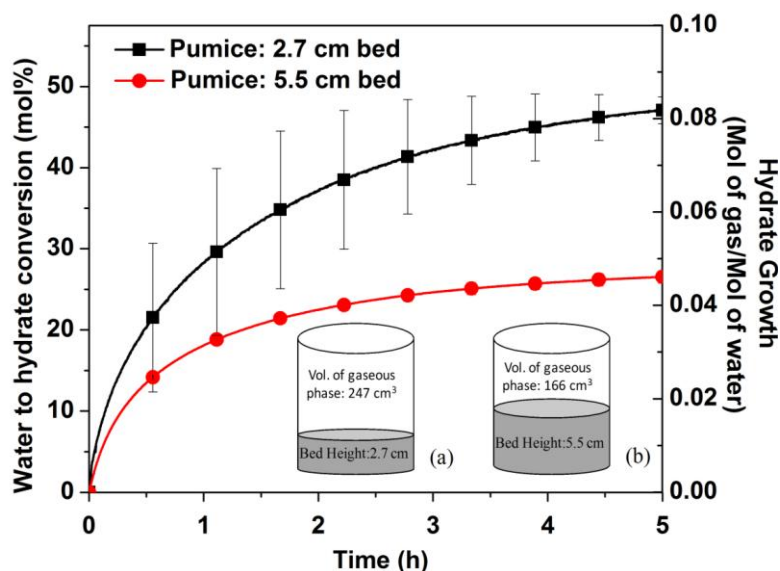


Fig. 6.11: Effect of bed height on hydrate formation kinetics using Pumice as the porous medium: Pumice: 2.7 cm bed: Average and standard deviation of experiment numbers 20, 23 and 25 and Pumice: 5.5 cm bed: Average and standard deviation of experiment numbers 57, 60 and 62.

Inset: The different bed heights considered for the study and the corresponding change in volume of the gaseous phase; (a) Bed height: 2.7 cm and (b) Bed height: 5.5 cm.

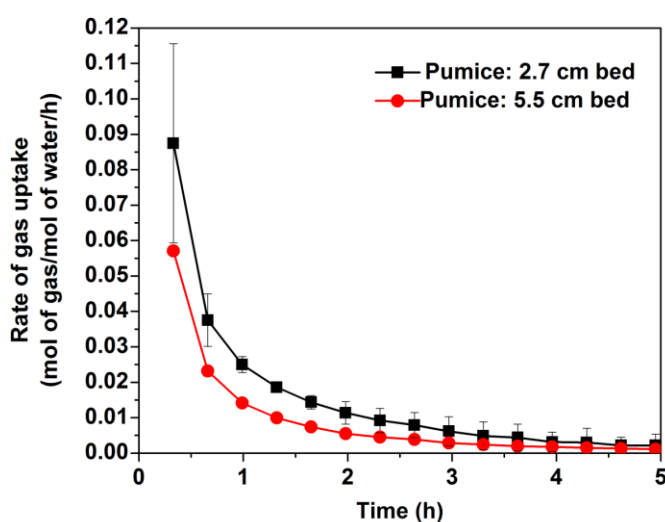


Fig. 6.12: Comparison of rates of gas uptake for the two bed heights considered for pumice: Pumice: 2.7 cm bed: Average and standard deviation of experiment numbers 20, 23 and 25 and Pumice: 5.5 cm bed: Average and standard deviation of experiment numbers 57, 60 and 62.

6.3.4. Hydrate Saturation

Average hydrate saturation (%) obtained for different porous media (pumice and FHRC) are given in Table 6.5. Hydrate saturation has been calculated only for the fresh runs. Hydrate saturation for our study ranges from 21.9 % (pumice system with 44.1 cm³ water and 5.5 cm bed height) to 37.5 % (pumice system with 24 cm³ water and 2.7 cm bed height). The hydrate saturation also decreases with increase in bed height. Sun and Englezos reported hydrate saturation for a silica sand system with water saturation of 25%. They performed two types of experiments: injection of CO₂ in a gas cap and injection of CO₂ in a spiral tube mode. The water to hydrate conversion (mol%) for these experiments ranged from 38% to 55% for 24 hour runs and was thus comparable with those obtained in the present study. The hydrate saturation for Sun and Englezos' study ranged from 10.7 % to 15.2 % whereas in the present study it is observed to vary from 21.9% to 37.5%. The reason for this is the high initial water saturation level used in the present work (75%) compared to that in Sun and Englezos' study (Sun and Englezos, 2014). Based on these results, we can conclude that the initial water saturation level too has a major role to play at least on the final hydrate saturation.

Table 6.5: Average hydrate saturation for different systems studied (Pumice and FHRC).

System	Exp. Nos.	Volume of water used (cm ³)	Bed Height (cm)	Initial water saturation	Average water to hydrate conversion (mol%)	Average Hydrate saturation (%)
Pumice Size: < 210 μm	20, 23 and 25	24.0	2.7	0.75	45.5	37.5
FHRC: Size: < 210 μm	32, 35 and 37	24.0	2.4	0.75	39.7	32.7
Pumice: Size: < 210 μm	44, 47 and 50	25.5	3.0	0.75	42.7	35.2
FHRC: Size: < 210 μm	51, 53 and 55	28.3	3.0	0.75	40.8	33.7
Pumice Size: < 210 μm	57, 60 and 62	44.1	5.5	0.75	26.6	21.9

The average hydrate saturation varies from **21.9%** to **37.5%**.

6.4. Conclusions

Hydrate formation experiments were carried out in a fixed bed apparatus with a CO₂-water system and various porous media with a focus on geological storage of CO₂ in the form of gas hydrates. Four types of porous media were used: pumice, FHRC, silica sand and quartz. Two different types of experiments were carried out keeping a) the volume of water used constant and b) the height of the fixed bed constant. In both types of experiments, hydrate formation kinetics were found to be the most enhanced when pumice was used as the porous medium. The effect of particle size on hydrate formation kinetics was looked into. Pumice and FHRC were each divided into three size fractions. Kinetics was found to be enhanced greatly with decrease in particle size in the case of both pumice and FHRC. The effect of bed height on hydrate formation kinetics was also studied using pumice as the porous medium. Two different bed heights were chosen: 2.7 cm and 5.5 cm to study the effect of gas diffusion / migration on hydrate formation kinetics. Rate of hydrate formation decreases with increase in bed height as a result of reduced gas diffusion / migration. Pumice and FHRC, used in this study seems to be as good as silica sand or quartz in terms of kinetics of CO₂ hydrate formation as well as the water to hydrate conversion. Pumice and FHRC are typical volcanic sediments which are available in India and both these materials provide us with an option for geological storage of CO₂ in the form of gas hydrates.

6.5. References

1. Kumar, R., Linga, P., Ripmeester, J. A., Englezos, P. Two-Stage Clathrate Hydrate/Membrane Process for Precombustion Capture of Carbon Dioxide and Hydrogen. *J. Environ. Eng.* **2009**, 135, 411-417.
2. Lashof, D. A., Ahuja, D. R. Relative contributions of greenhouse gas emissions to global warming. *Nature* **1999**, 344, 529–531.
3. Karl, T. R., Trenberth K. E. Modern global climate change. *Science* **2003**, 302, 1719–1723.
4. D'Alessandro, D. M., Smit, B., Long, J. R. Carbon dioxide capture: prospects for new materials. *Angew. Chem. Int. Ed.* **2010**, 49, 6058–6082.
5. Aaron, D., Tsouris, C. Separation of CO₂ from Flue Gas: A Review. *Sep. Sci. Technol.* **2005**, 40, 321-348.
6. Miller, M. B., Chen, D. L., Xie, H. B., Luebke, D. R., Johnson, J. K., Enick, R. M. Solubility of CO₂ in CO₂-philic oligomers; COSMOtherm predictions and experimental results. *Fluid Phase Equilibria* **2009**, 287, 26-32.
7. Sloan, E. D., Koh, C. A. Clathrate hydrates of natural gases; CRC press: New York, 2008.
8. Babu, P., Kumar, R., Linga, P. Unusual behavior of propane as a co-guest during hydrate formation in silica sand: Potential application to seawater desalination and carbon dioxide capture. *Chem. Eng. Sci.* **2014**, 117, 342-351.
9. Sun, D., Englezos, P. Storage of CO₂ in a partially water saturated porous medium at gas hydrate formation conditions. *Int. J. Greenh. Gas Con.* **2014**, 25, 1–8.
10. Bickle, M. J. Geological carbon storage. *Nat. Geosci.* **2009**, 2, 815–818.

11. Bachu, S. Sequestration of CO₂ in geological media: criteria and approach for site selection in response to climate change. *Energ. Convers. Manage.* **2000**, 41, 953-970.
12. Haszeldine, R. S. Carbon capture and storage: how green can black be? *Science* **2009**, 325, 1647–1652.
13. Holloway, S. Underground sequestration of carbon dioxide—a viable green-house gas mitigation option. *Energy* **2005**, 30, 2318–2333.
14. Figueroa, J. D., Fout, T., Plasynski, S., McIlvried, H., Srivastava, R. D. Advances in CO₂ capture technology—the US Department of Energy's Carbon Sequestration Program. *Int. J. Greenh. Gas Con.* **2008**, 2, 9-20.
15. Koide, H., Tazaki, Y., Noguchi, Y., Nakayama, S., Iijima, M., Ito, K., Shindo, Y. (1992). Subterranean containment and long-term storage of carbon dioxide in unused aquifers and in depleted natural gas reservoirs. *Energ. Convers. Manage.* **1992**, 33, 619-626.
16. Leung, D. Y. C., Caramanna, G., Valer, M. M. M. An overview of current status of carbon dioxide capture and storage technologies. *Renewable Sustainable Energy Rev.* **2014**, 39, 426–443.
17. Côté, M. M., Wright, J. F. Preliminary assessment of the geological potential for sequestration of CO₂ as gas hydrate in the Alberta portion of the Western Canada Sedimentary Basin. Natural Resources Canada **2013**, open file 6582, 57p, Doi: <http://dx.doi.org/10.4095/292515>.
18. Mahoney, J. J. Deccan traps. In *Continental Flood Basalts*; Macdougall, J.D., Ed; Springer Science and Business Media: The Netherlands, 1988.
19. Medlicott, H. B., Blanford, W. T. *A Manual of the Geology of India: Chiefly Compiled from the Observations of the Geological Survey*. Oldham, R.D., Ed.; Cambridge University Press: New York, 2011.

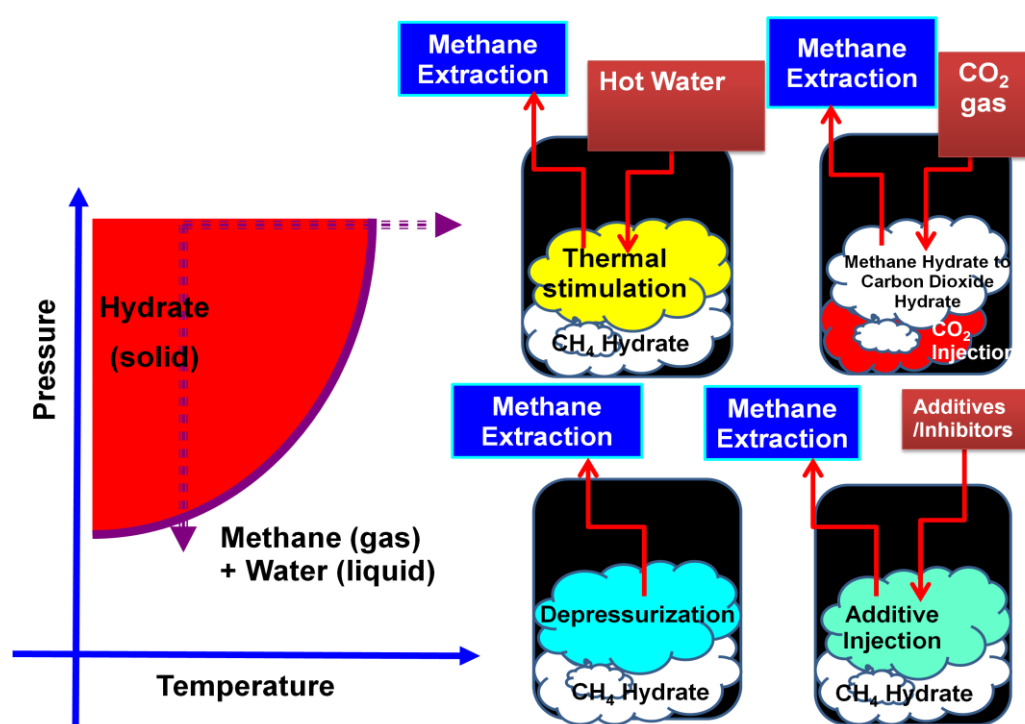
-
20. Subbarao, K. V., West, W. D. Deccan volcanic province (Vol. 2), Geological Society of India, 1999.
 21. McPhie, J., Doyle, M., Allen, R. L. *Volcanic textures: A guide to the interpretation of textures in volcanic rocks*; CODES, University of Tasmania, 1993.
 22. Thomas, N., Jaupart, C., Vergnolle, S. On the vesicularity of pumice. *J. Geophys. Res.* **1994**, 99, 15633–15644.
 23. Venezia, A. M., Floriano, M. A., Deganello, G., Rossi, A. Structure of pumice: An XPS and ^{27}Al MAS NMR study. *Surf. Interface Anal.* **1992**, 18, 532–538.
 24. Weems, J. B. Chemistry of clays. *Iowa Geological Survey Annual Report* **1904**, 14, 319-346.
 25. Lourenço, P. B., Fernandes, F. M., Castro, F. Handmade clay bricks: Chemical, physical and mechanical properties. *Int. J. Archit. Herit.* **2010**, 4, 38-58.
 26. Herbert, J. A skill to build on: the brick-maker's art. CERES no. 145, 50 p, 1994.
 27. Martín-Barajas, A., Lallier-Verges, E. Ash layers and pumice in the central Indian Basin: relationship to the formation of manganese nodules. *Mar. geol.* **1993**, 115, 307-329.
 28. Iyer, S. D., Sudhakar, M. Evidences for a volcanic province in the Central Indian Basin. *J. Geol. Soc. India.* **1995**, 46, 353-358.
 29. Sheth, H. C., Ray, J. S., Bhutani, R., Kumar, A., Smitha, R. S. Volcanology and eruptive styles of Barren Island: an active mafic stratovolcano in the Andaman Sea, NE Indian Ocean. *Bull. Volcanol.* **2009**, 71, 1021-1039.

-
30. Kumar, A., Sakpal, T., Roy, S., Kumar, R. Methane hydrate formation in a test sediment of sand and clay at various level of water saturation. *Can. J. Chem.* **2015**, 93, 874-881. DOI: 10.1139/cjc-2014-0537.
31. Kumar, A., Sakpal, T., Linga, P., Kumar, R. Enhanced carbon dioxide hydrate formation kinetics in a fixed bed reactor filled with metallic packing. *Chem. Eng. Sci.* **2015**, 122, 78-85.
32. Linga, P., Daraboina, N., Ripmeester, J. A., Englezos, P. Enhanced rate of gas hydrate formation in a fixed bed column filled with sand compared to a stirred vessel. *Chem. Eng. Sci.* **2012**, 68, 617–623.
33. Smith, J. M., Van Ness, H. C., Abbott, M. M. *Introduction to Chemical Engineering Thermodynamics*; McGraw-Hill Inc.: New York, 2001.
34. Yang, S. H. B., Babu, P., Chua, S. F. S., Linga, P. Carbon dioxide hydrate kinetics in porous media with and without salts. *Appl. Energ.* **2014**, 162, 1131-1140.
35. Natarajan, V., Bishnoi, P. R., Kalogerakis, N. Induction phenomena in gas hydrate nucleation. *Chem. Eng. Sci.* **1994**, 49, 2075–2087.
36. Heeschen, K., Schicks, J. M., Oeltzschner, G. The influence of sediment and fluid properties on methane hydrate formation. In: Proceedings of the 8th International Conference on Gas Hydrates, Beijing, China, **2014**.
37. Mekala, P., Busch, M., Mech, D., Patel, R. S., Sangwai, J. S. Effect of silica sand size on the formation kinetics of CO₂ hydrate in porous media in the presence of pure water and seawater relevant for CO₂ sequestration. *J. Petrol. Sci. Eng.* **2014**, 122, 1-9.
38. Siangsai, A., Rangsunvigit, P., Kitiyanan, B., Kulprathipanja, S., Linga, P. Investigation on the roles of activated carbon particle sizes on methane hydrate formation and dissociation. *Chem. Eng. Sci.* **2015**, 126, 383-389.

39. Babu, P., Yee, D., Linga, P., Palmer, A., Khoo, B. C., Tan, T. S., Rangsunvigit, P. Morphology of methane hydrate formation in porous media. *Energy Fuels*. **2013**, 27, 3364-3372.
40. Tohidi, B., Anderson, R., Clennell, M. B., Burgass, R. W., Biderkab, A. B. Visual observation of gas-hydrate formation and dissociation in synthetic porous media by means of glass micromodels. *Geology* **2001**, 29, 867-870.
41. Kuhs, W. F., Chaouachi, M., Falenty, A., Sell, K., Schwarz, J. O., Wolf, M., Enzmann, F., Kersten, M., Haberthür, D. In-situ micro-structural studies of gas hydrate formation in sedimentary matrices. In: Proceedings of the 8th International Conference on Gas Hydrates, Beijing, China, **2014**.

Chapter 7

Enhancement of hydrate dissociation kinetics using benign additives in low concentrations



A hybrid combination of two or more basic hydrate dissociation processes may also be employed

7. Enhancement of hydrate dissociation kinetics using benign additives in low concentrations⁷

⁶A version of this chapter has been published as a patent

Kumar, R.; Roy, S.; Bhattacharjee, G., Choudhary, N.; Kumar, A.; Kashyap, R.K.; Chugh, P.; Pandey, N.K.WO2017125954. A process for dissociation of hydrates in presence of additives or hydrate dissociation promoters, 2017.

7.1. Introduction

The three basic methods employed to dissociate methane hydrates and generate the stored methane gas, namely thermal stimulation, depressurization and chemical inhibitor injection have been described briefly in Chapter 1. It has also been mentioned that the way forward as far as methane recovery from gas hydrate reserves is concerned is a hybrid process combining at least two or all three of these processes. In the current chapter, the three major processes for dissociation of gas hydrates will first be looked at in much greater detail and will be followed by the introduction of and subsequent detailed discussion on a new process for dissociation of methane hydrates employing a combination of the depressurization and thermal stimulation approaches in presence of benign additives in low concentrations.

7.1.1. Hydrate dissociation by depressurization

The depressurization method involves reducing the bottomhole pressure using a vacuum pump installed in the down-hole thus reducing the pressure of the reservoir to create hydrate instability in order to induce hydrate decomposition as shown in Figure 7.1. The reservoir pressure in the vicinity of the well decreases first on reducing the bottomhole pressure of a well below the three phase equilibrium pressure resulting in the decomposition of hydrate zone. Along with the dissociation of the hydrate, the saturation of hydrate also decreases due to flow of water resulting in an increase in the effective permeability to the fluids. This now allows the low pressure to be more easily transferred to the regions away from the well bore creating a virtuous cycle of low pressure transfer-hydrate dissociation-increase in permeability- low pressure transfer to more distant areas and so forth. Thus the area and quantity of gas produced is enhanced with respect to time. This process however does not guarantee dissociation of all the hydrate contained in the low pressure region. Hydrate dissociation being an endothermic process, the reservoir temperature decreases with dissociation; the time scale of heat transfer from the adjoining area is not the same and thus

when the reservoir temperature reaches the three phase equilibrium temperature corresponding to the already reduced reservoir pressure, hydrate dissociation stops. The same has been shown in Figure 7.2. The methane recovery from a hydrate reservoir by depressurization depends largely on reservoir characteristics and is predicted to be up to about 60% (Sloan and Koh, 2008; Kurihara et.al, 2011; Li et.al, 2014).

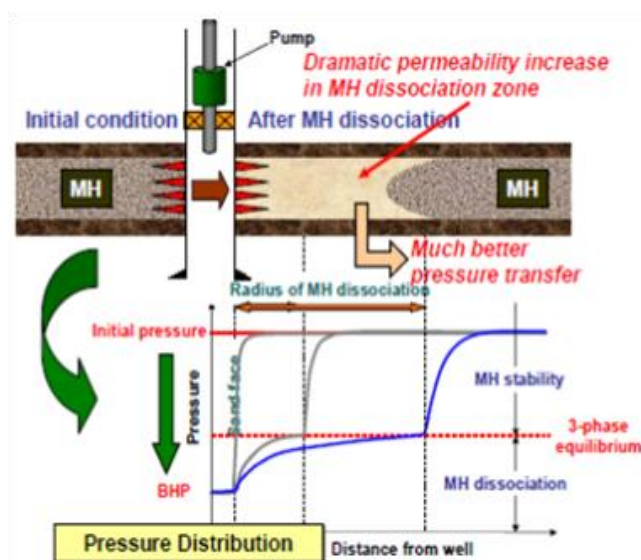


Fig. 7.1: Concept of pressure reduction and methane hydrate dissociation induced by depressurisation method (adopted from Kurihara et al., 2011).

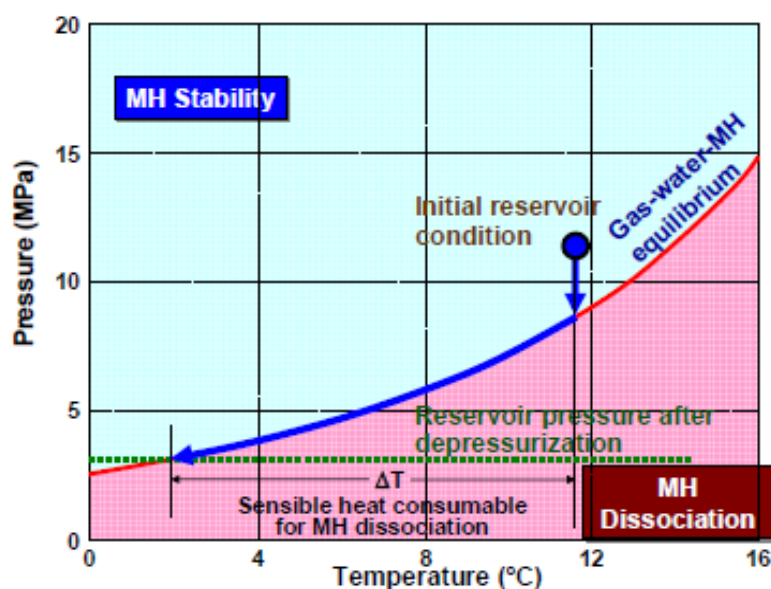


Fig. 7.2: Temperature reduction due to methane hydrate dissociation by the depressurisation method (adopted from Kurihara et al., 2011).

7.1.2. Hydrate dissociation by thermal stimulation

Thermal stimulation quite simply refers to the method of increasing the reservoir temperature in order to dissociate the hydrate. The thermal stimulation method aims to increase the temperature around the vicinity of the well which can be achieved in a number of ways including hot water circulation into a wellbore to increase bottomhole temperature, installing heaters in the bottomhole to increase the temperature of the area surrounding the wellbore and the hot water huff'n'puff method in which hot water is injected into the reservoir from a well which acts as both an injection and a production well. The first method which is thermal flooding involves injecting hot water into the reservoir through an injection well which floods the entire reservoir sediment slowly seeping up to the areas far away from the injection well. As a consequence of this hot water flooding, the temperature of reservoir is increased thus resulting in dissociation of the hydrate which results in production of gas from the production well/s (different patterns of arrangement of injection and production wells have been tested in bench scale setups including using single and multiple production wells). Unlike the thermal flooding method, in the huff and puff method, first hot water is injected (huff) through a well, then the well is shut-in for a certain period of time (shut-in or soaking period) and finally after sufficient transfer of heat from the injected hot water to the reservoir sediment, gas and water are produced from the same well (puff).

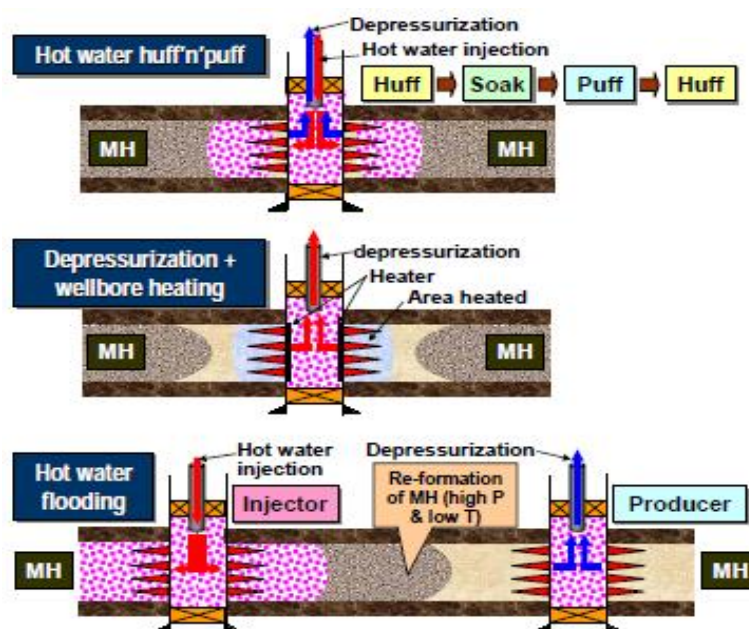


Fig. 7.3: Overview of variety of thermal methods (adopted from Kurihara et al., 2011).

During the thermal stimulation approach for gas hydrate dissociation, the temperature of the reservoir increases and ultimately becomes greater than the three phase equilibrium temperature which sparks the dissociation of hydrate and the hydrate dissociates, the pressure of the reservoir increases due to gas generation. Hydrate dissociation terminates at the region where the reservoir pressure becomes identical to the three phase equilibrium pressure. However, even after hydrate dissociation stops, the continuous supply of heat due to the hot water flooding or wellbore heating through installation of heaters ensures that the reservoir temperature increases beyond the new three phase equilibrium temperature which allows complete dissociation of the hydrate located in the region. Since the heat is transferred through thermal conduction, the expansion of the high temperature region is extremely slow.

It is suggested that in the methods related to injecting hot water into a reservoir such as hot water huff'n'puff and hot water flooding, much faster propagation of the heat and hence much faster expansion of the hydrate dissociation area is expected, if the hot water can be injected smoothly. The effective permeability to hot water is very low in the initial stages of the process because of high hydrate saturation restricting the flow of hot water to the areas further away from the injection well. Furthermore, in hot water flooding, the gas generated due to dissociation of hydrates near the injection well gets cooled again in the course of the advancement towards the production well and secondary hydrate formation takes place between the wells, resulting in the reduction of the permeability and preventing further smooth propagation of hot water. Therefore, it is proposed to use the hot water injection method as a secondary recovery method after dissociation of hydrates to some extent by depressurization and creating pathways for water movement. By applying hot water circulation, only a few percent of methane recovery is expected, since the bottomhole pressure should be kept higher than the initial reservoir pressure to circulate water in a wellbore. In the other thermal methods, ideally, combining the depressurization method, almost 100% of methane recovery is expected by the synergistic effect of depressurization and heating. However, since the energy supplied in these methods is quite large, the applicability of the thermal methods is disputed from the viewpoint of energy efficiency (Sloan and Koh, 2008; Wang et.al, 2014; Kurihara et.al, 2011).

7.1.3. Hydrate dissociation by inhibitor injection method

This method, which has widely been discredited in recent times involves the injection of certain additives into the system which have the ability to shift the three phase equilibrium

conditions to more drastic pressure and temperature sides and hence move a reservoir to unstable hydrate condition which in turn dissociates the hydrate. The inhibitors that may be used in this process are usually highly toxic in nature and required in large quantities thus highly reducing the process' feasibility. Furthermore, since the magnitude of this shift is limited, significant dissociation is not expected by solely applying this method. Another major disadvantage of this process is that it would be difficult to inject an inhibitor smoothly into a reservoir due to very low initial effective permeability (a result of high hydrate saturation). Therefore, it is proposed to inject benign additives along with hot water in order to improve the energy efficiency of the thermal stimulation methods (something that has been discussed in detail later in this chapter (Sloan and Koh, 2008; Li et.al, 2007).

7.2. Methane Recovery using benign additives

In order to increase gas production from a hydrate reservoir, it is proposed to combine multiple methods from the already existing ones and/or to apply horizontal wells and hydraulic fracturing, which are widely used in conventional oil/gas development (Feng et.al, 2015a; Feng et.al, 2015b). The other approach that may be followed is the identification of benign additives which when used even in sparingly small concentrations may enhance the kinetics of hydrate dissociation.

7.2.1. Identification of benign additives

This is one of the biggest objectives among all the work undertaken and reported in this thesis and one in which significant strides have been made in the right direction. The additives that have been identified have been done so keeping in mind that first and foremost, they should be benign (environment friendly) and can be considered bio-degradable.

7.2.1.1. Preliminary identification of additives

Apart from the fact that they should be environment friendly, the preliminary selection of additives was done based on a number of individual criteria and hypotheses. Any additive selected for use as a hydrate dissociation promoter should be able to fulfil the following three objectives:

- **Enhance hydrate dissociation kinetics**
- **Have good feasibility for scale up operations**
- **Can achieve desired effects even when used in incredibly small doses.**

After an extensive literature search, our understanding has led us to believe that for an additive to significantly enhance hydrate dissociation kinetics, it has to work through one of the following mechanisms:

- **Should be capable of forming hydrogen bonds with water molecules** thus disrupting their ability to form cages and enclathrate guest molecules. Cage defects may be created as a result of the difference in number of hydrogen bonds formed between the specific compound and water compared to typical water-water interactions (McLaurin et.al, 2014).
- **May be zwitterionic.** Some additives may exist as zwitterions. It is known that around electric charges, water molecules tend to become less ice like. The electric charges present on the molecules will enable them to interact more freely with water with water molecules having a special tendency to favor the negative charge (Scheu et.al, 2014).
- **May change the thermodynamic phase equilibria boundary of methane or natural gas hydrates.** Some additives may change the thermodynamic phase equilibria boundary of methane or natural gas hydrates, not allowing hydrates to remain stable at their inherent equilibrium conditions (Koh, 2002; Cha et.al, 2013; Perrin et.al, 2013).

The various classes of additives that have the ability to work through the mechanisms described above and thus exhibit potential to act as hydrate dissociation promoters are as follows:

- **Hydrophilic, Hydrophobic and Charged amino acids**
- **Zwitterionic compounds**
- **Betaines**
- **Polysaccharides**
- **Silicone oils**
- **Other hydrogen bond formers like Alcohols**

Table 7.1 given lists the additives that had been identified for this study. The additives have been listed along with their respective class, the gas used for forming hydrates and the concentration of additive used.

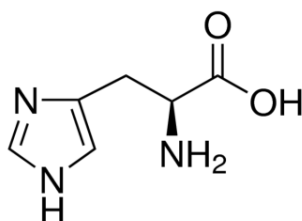
Table 7.1: List of the additives identified for use as hydrate dissociation promoters in the present study

Sr. No.	Additive	Class of Compound	Gas used for forming hydrates	Conc. of additive used
1.	L-histidine	Hydrophilic Amino Acid	Pure Methane	0.1, 1 wt %
2.	L-proline	Hydrophobic Amino Acid	Pure Methane	0.1, 1 wt %
3.	Bicine	Zwitterionic Compound	Pure Methane	0.1, 1 wt %
4.	Gum Arabic	Natural gum (mixture of glycoproteins and polysaccharides)	Pure Methane	1 wt %
5.	Gellan Gum	Long Chain Polysaccharide	Pure Methane	1 wt %
6.	L-tryptophan	Hydrophobic Amino Acid	Pure Methane	0.1, 1 wt %
5.	Ethylene Glycol*	Alcohol (thermodynamic inhibitor)	Pure Methane	1 wt %

*a description of this additive is not given in the upcoming section as this is not one of the novel additives identified in this study but was rather used for the purpose of comparison.

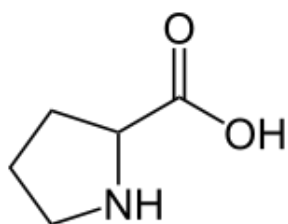
7.2.1.2. Brief individual description of the different additives studied

1. L-histidine: A number of hydrophobic amino acids that might be useful for this work have been identified. These are essential compounds to sustain life (environment friendly) in addition to being zwitterionic in nature and having a large number of hydrogen bond forming moieties in their structures thus satisfying all the criteria for identifying the additives discussed in the previous section. Histidine is an amino acid having a hydrophathy index of -3.2 and an imidazole functional group. The different functional groups present in the compound capable of forming hydrogen bonds with water molecules are expected to facilitate dissociation of methane hydrates by a) hindering the capability of water molecules to arrange themselves in ice like structures and b) by creating defects in the crystal lattice of formed gas hydrate molecules.



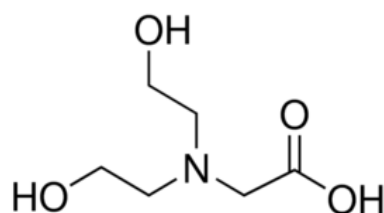
Structure of L-Histidine

2. L-proline: Proline is a non-polar amino acid that is usually used in the biosynthesis of proteins. Like every other amino acid, proline contains a carboxylic group and an amino group which are supposed to facilitate the dissociation of gas hydrates by forming hydrogen bonds with the water molecules thus disrupting the hydrogen bonded water cages. Being non-polar, it is also expected to enhance the diffusion of non-polar methane. The structure of Proline is given below.



Structure of Proline

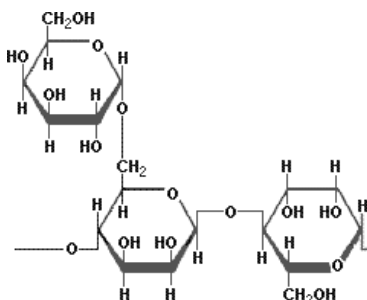
3. Bicine: Formed through the reaction of glycine with ethylene oxide and hydrolysis of the resultant ketone. This is a zwitterionic compound that is expected to work on the principle of perturbation. The electric charges present on this compound enable it to interact with water through strong electrostatic interactions. It is also a known fact that around electric charges, water molecules tend to become less ice like. In addition, the –OH bonds present are expected to compete with other molecules so as to form hydrogen bonds thus hindering the ability of water molecules to form labile clusters. The –OH groups are also expected to form hydrogen bonds with water molecules present on the crystal lattice of the hydrates thus creating defects in the hydrate crystals and facilitating recovery of methane gas.



Structure of Bicine

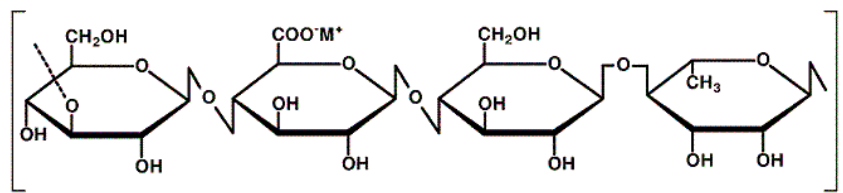
4. Gum Arabic: This is a natural gum made up of the hardened sap of two species of the acacia tree, gum arabic is a complex mixture of glycoproteins and polysaccharides. It has a

variety of hydrophilic functional groups attached to its hydrocarbon chains thus rendering it highly capable of interacting and forming hydrogen bonds with water.



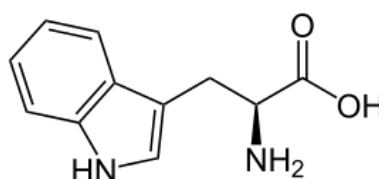
Structure of Gum Arabic

- 5. Gellan gum:** This is an anionic polysaccharide produced from the bacterium *Sphingomonas elodea*. Gellan gum is widely used in the food and cosmetic industry as a thickener, emulsifier and stabilizer. It is also used as a gelling agent alternative to Agar in microbial culture. The repeating unit of the polymer is a tetrasaccharide, which consists of two residues of D-glucose and one of residue each of L-rhamnose and D-glucuronic acid. This compound contains a large number of hydrogen bond formers (functional groups) that are expected to facilitate decomposition of methane hydrates.



Structure of Gellan Gum

- 6. Tryptophan:** Tryptophan is a non-polar aromatic amino acid having an indole group in addition to the customary carboxylic and amino groups. This is expected to work on similar lines to Proline, i.e. forming hydrogen bonds with water molecules thus disrupting hydrogen bonded water cages and facilitating the diffusion of non-polar methane.



Structure of Tryptophan

7.3. Enhanced hydrate dissociation kinetics in presence of low concentrations of benign additives

7.3.1. Experimental Setups

Two different experimental setups were used for this study. The first was a dedicated setup for additive selection which is a stirred tank reactor setup and the second was a bench scale (2350 ml) high pressure continuous circulating loop large scale methane recovery setup. Both these setups have been discussed in detail in the following paragraphs.

Figure 7.4 below shows the Dedicated Reactor Setup for Additive Selection. This setup was designed at CSIR-NCL and fabricated by ALPRO EQUIPMENTS PVT. LTD., Pune that was be used as a dedicated tool for screening criteria for additive selection. Additives that enhance hydrate dissociation kinetics, identified using this setup were subsequently studied further in the “Continuous Circulating Loop Large Scale Methane Recovery Apparatus.”

The “Dedicated Reactor Setup for Additive Selection” has a volume of $\sim 252 \text{ cm}^3$ with design pressure of 150 bar. A magnetic drive enabled overhead stirrer capable of operating under requisite experimental pressure is installed on the head of the setup and has a range of 0-1000 rpm. The vessel is also provided with 1 inch transparent windows (made up of submarine glass) on either side which are used to observe the morphology of the hydrate formation and dissociation processes as shown in Figure 7.4. A circulating fluid jacket with a design pressure of 5 bar is built around the crystallizer in order to maintain the temperature of the system. A Pt-100 type RTD with range -199.9 to $600 \text{ }^\circ\text{C}$ and $\pm 0.25\%$ accuracy immersed in the crystallizer is used to measure and monitor the temperature of the crystallizer. Any change in the pressure in the crystallizer is measured by a WIKA make pressure transducer with a range of 0-250 bar and accuracy of 0.075% of the span. Both the RTD and pressure transducer are connected to a data acquisition system (DAQ) which logs the readings at 5 second intervals.

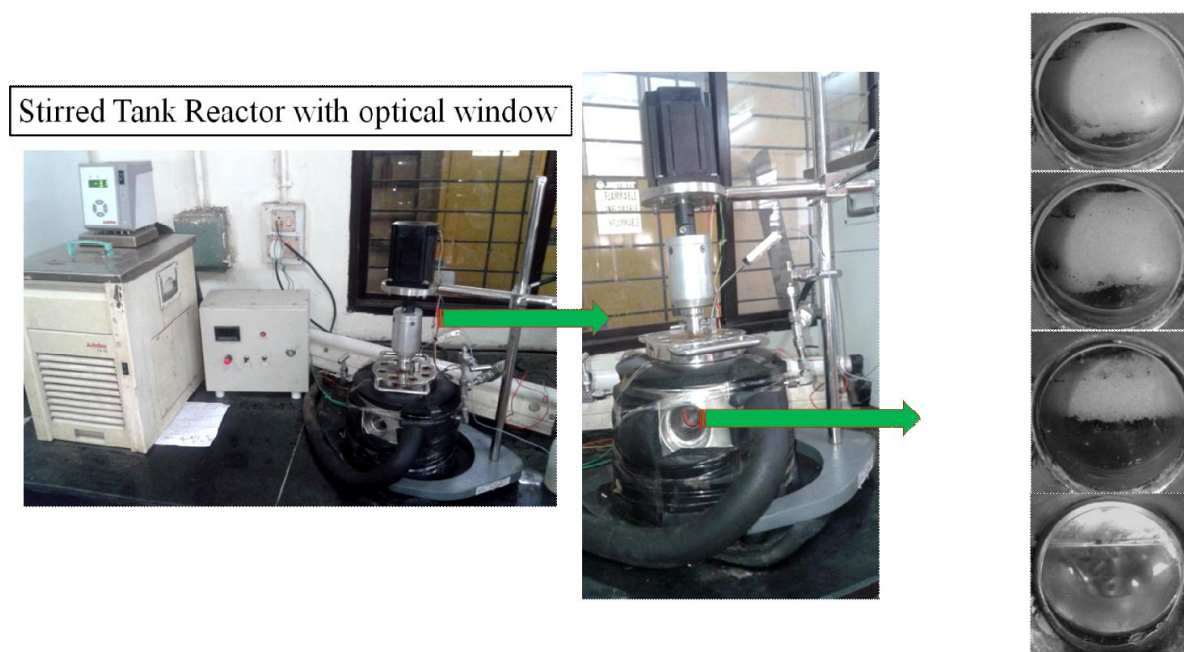


Fig. 7.4: Stirred tank reactor setup with optical window for additive selection.

Figure 7.5 shows the schematic diagram of the Continuous Circulating Loop Large Scale Methane Recovery Setup whereas Figure 7.6 shows the actual image of the same. It was designed at CSIR-NCL and fabricated by AMAR Equipment's Pvt. Ltd., Mumbai. It consists of a 2.35 L SS-316 high pressure hydrate crystallizer (CR) having a design pressure of 200 bar and is equipped with a cooling jacket connected to an external refrigerator (ER1) to maintain the CR at desired temperature. The CR is provided with a rupture disk in adherence with safety regulations. Seven RTDs Pt-100 type with range -199.9 to 600 °C and $\pm 0.25\%$, ± 1 LSD accuracy are present within the CR at various depths inside the hydrate forming sediment to measure the temperature as shown in the figures. Gas from the supply vessel (SV) which is also connected to ER1 is immersed in the crystallizer at the experimental temperature and pressure. A mass flow controller (MFC) Brooks instruments make with a maximum flow rate of 0-500ml/min at calibrated inlet pressure of 70 bar is attached to the outlet of the CR and inlet of the reservoir whose main function is to act as a back pressure regulator. The pressure inside CR at the time=0 during dissociation of gas hydrate is the set point of MFC. During dissociation, pressure of the CR rises due to decomposition of gas hydrates. As the pressure of the CR rises, the valve connected to the MFC opens up and the amount of excess gas prior to dissociation generated in the CR is collected in the reservoir tank. Flow rate and volume of gas generated during decomposition is measured and logged via a totalizer which is connected to the MFC. An ECOM make high pressure liquid circulation pump (HPLC) with flow-rate range of 0-100 ml/min is connected to the CR. The

inlet of the pump is connected to a temperature controlled water tank in which additive solution is stocked and this additive solution is injected into the crystallizer via the HPLC pump during the additive injection experiments. ER2 (the second external chiller) is connected to the water tank and the reservoir to control their respective temperatures. Any change in the pressure in the CR, reservoir and water tank is measured using a WIKA make pressure transducer with a range of 0-250 bar and accuracy of 0.075% of the span. Software based SCADA system is used to log and monitor the data obtained during experiments. The detailed operation and working of the Continuous Circulating Loop Large Scale Methane Recovery Setup is explained in one of the upcoming sections.

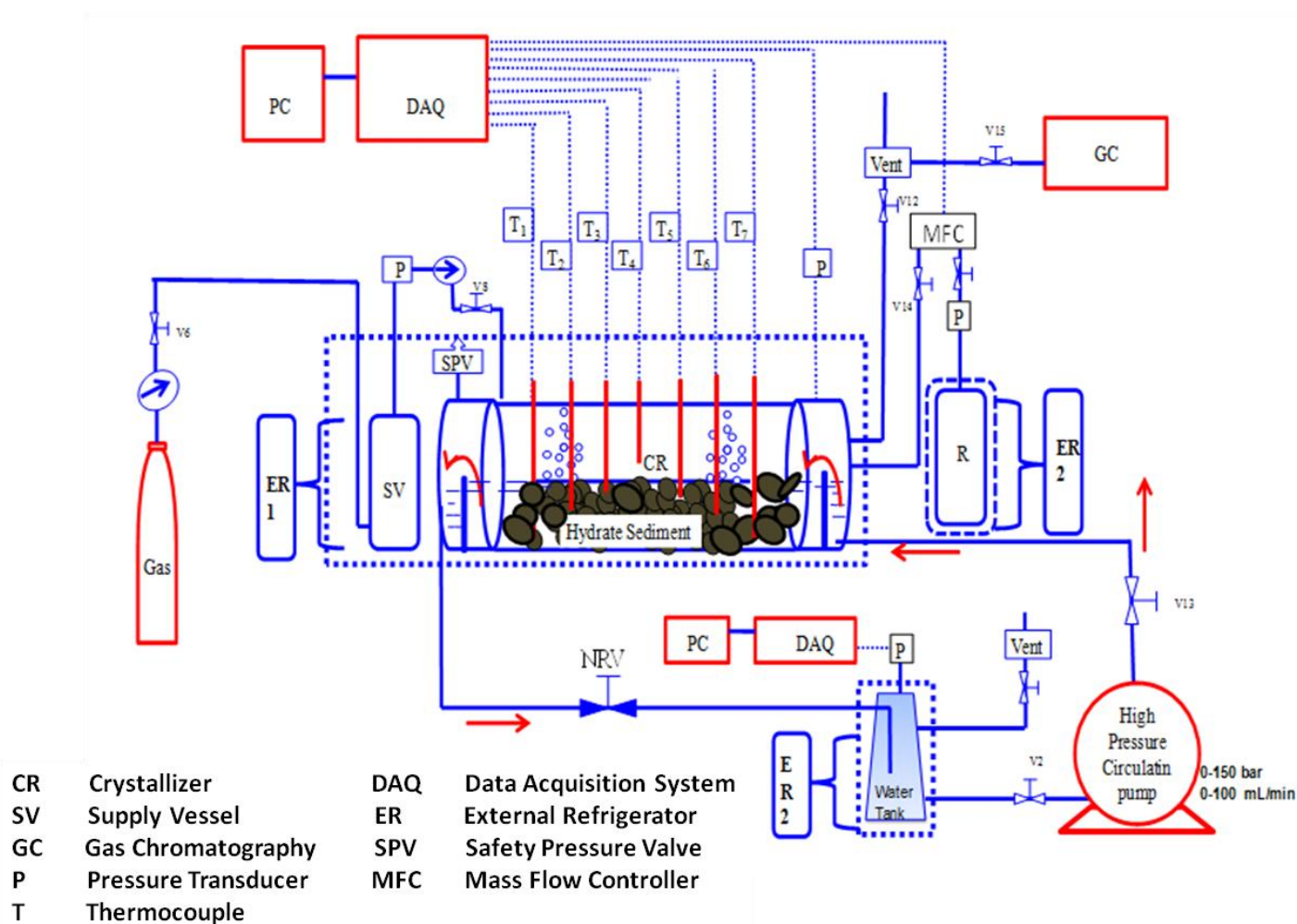


Fig. 7.5: Schematic of the bench scale methane recovery setup.

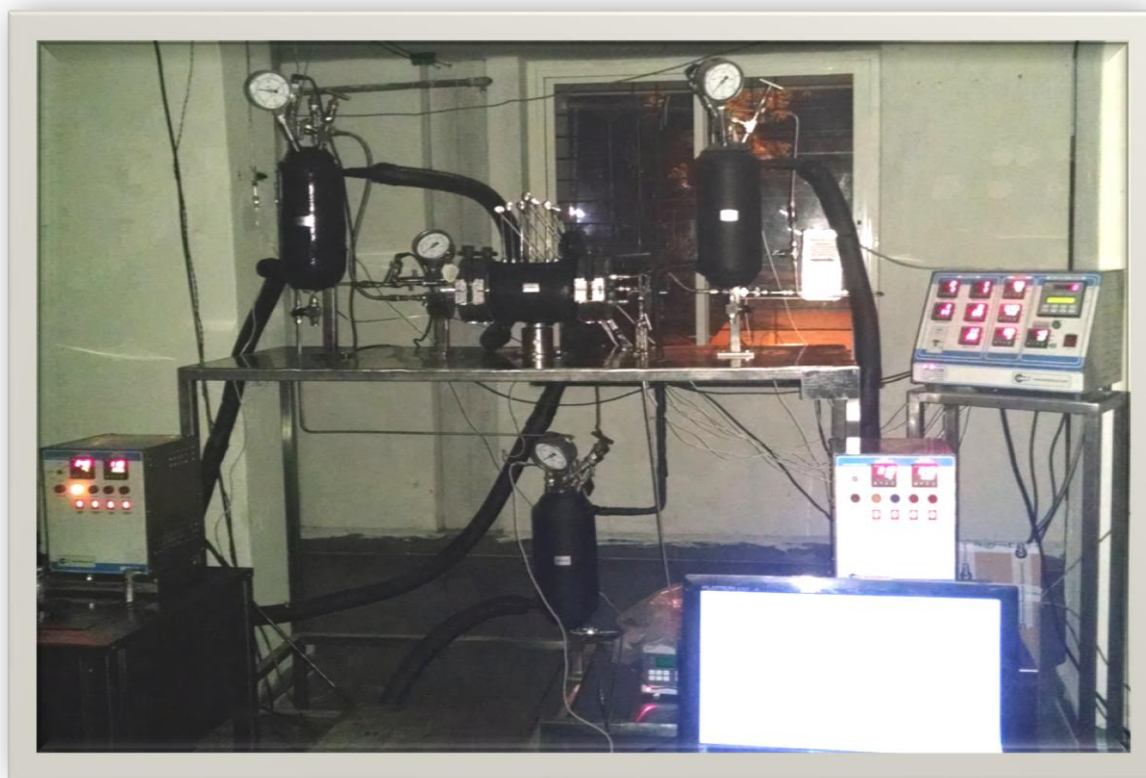


Fig. 7.6: High pressure continuous setup for studying methane hydrate decomposition kinetics in sub-sea environments

7.3.2. Testing of additives in the dedicated reactor setup for additive selection

As mentioned earlier, the additives identified were first tested in a lab scale stirred tank reactor setup (volume ~250 ml) christened “the dedicated setup for additive selection”. The reactor is fitted with two transparent windows made out of submarine glass on each side which are used to study the morphology of hydrate formation. A jacket enveloping the reactor is connected to an external circulating water bath in order to maintain the desired temperature for hydrate formation.

As a result of there being no external influence on the system, the dedicated reactor setup for additive selection is a perfect system to purely test the efficacy of the additives in enhancing hydrate dissociation kinetics. All experiments were conducted at 274 K temperature and 5.0 MPa pressure using pure methane gas. In these experiments, the additives were included in the system from the beginning of the experiments. First methane hydrates were formed in the presence of the additives and then the dissociation kinetics were studied. Dissociation was studied at two different temperatures, 283 K and 293 K. The concentration of all the additives

used was kept constant at 1 wt %. 80 ml water was used for all the experiments thus leaving a volume of 172 ml for the gaseous phase.

Figure 7.7 given below plots the normalised moles of gas released during dissociation at 293 K for the fresh runs for all the different additives studied and compares them with that obtained using pure water. As can be seen from the figure, all the additives used considerably enhance the kinetics of methane hydrate dissociation at 293 K. Figure 7.8 shows the methane recovery after 18 minutes in the presence of these additives and at 293 K and compares it with that obtained from pure water. From Figures 7.8 and 7.9, it becomes clear that the additives selected by us indeed have a potential to enhance hydrate dissociation kinetics. Representatives of all the different classes of additives studied; “Gum Arabic” for “long chain polysaccharides”, “Bicine” for zwitterionic compounds and L-histidine for “amino acids” respectively really stand out as suitable choices even in the big picture scheme of things.

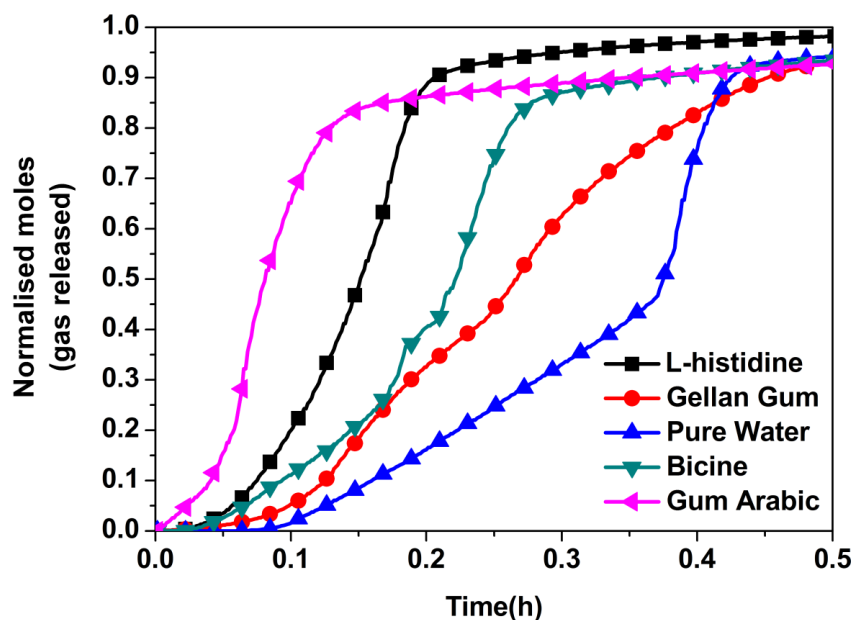


Fig. 7.7: Normalised moles of gas released vs. Time (h) for all the additives studied: Dissociation at 293 K. Fresh runs. Concentration of all the additives: 1 wt %.

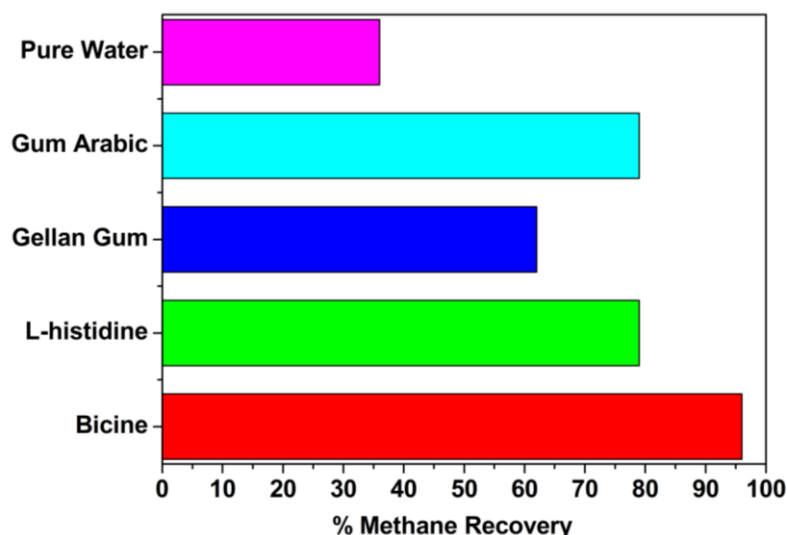


Fig. 7.8: Dissociation of methane hydrates in presence of different additives at 293 K: % Methane recovery after 18 minutes.

Figure 7.9 given below plots the normalised moles released during dissociation at 283 K for the fresh runs for all the different additives studied and compares them with that obtained using pure water at a) 283 K and b) 293 K. Once again, all the additives used considerably enhance the kinetics of methane hydrate dissociation at 283 K. However what is interesting is that the presence of a number of the additives such as Gum Arabic, Bicine and L-histidine in the system returns much enhanced kinetics even at 283 K when compared to that with pure water at 293 K. Figure 7.10 shows the methane recovery after 18 minutes in the presence of these additives and at 283 K and compares it with that obtained with pure water at a) 283 K and b) 293K. The main take away from this figure is that almost all the additives used show higher methane recovery after 18 minutes when hydrate dissociation is carried out at 283 K as compared to that obtained with pure water at 293 K. The information garnered from Figures 7.9 and 7.10 is extremely important as this can have major implications when recovering natural gas from hydrates on a commercial scale. A difference of 10 degrees achieved at lab scale can translate into a major economic advantage at field scale.

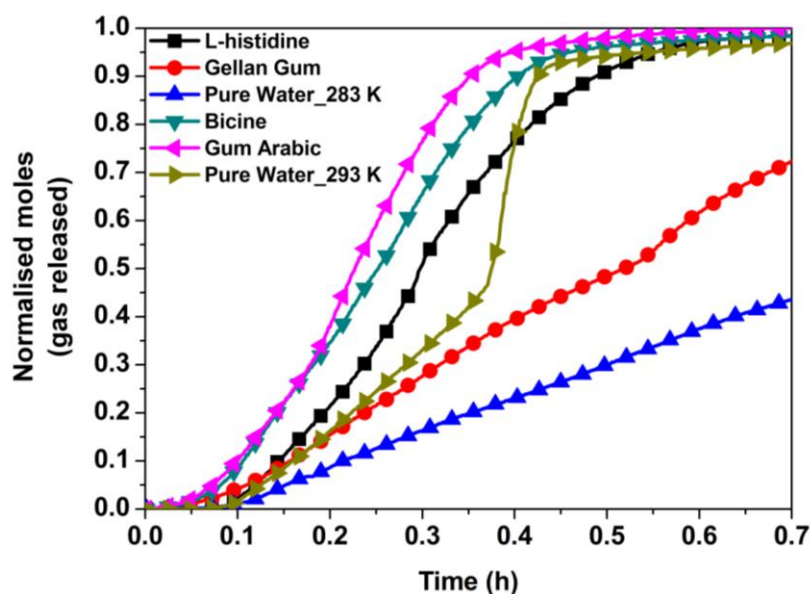


Fig. 7.9: Normalised moles of gas released vs. Time (h) for all the additives studied: Dissociation at 283 K. Fresh runs. Concentration of all the additives: 1 wt %.

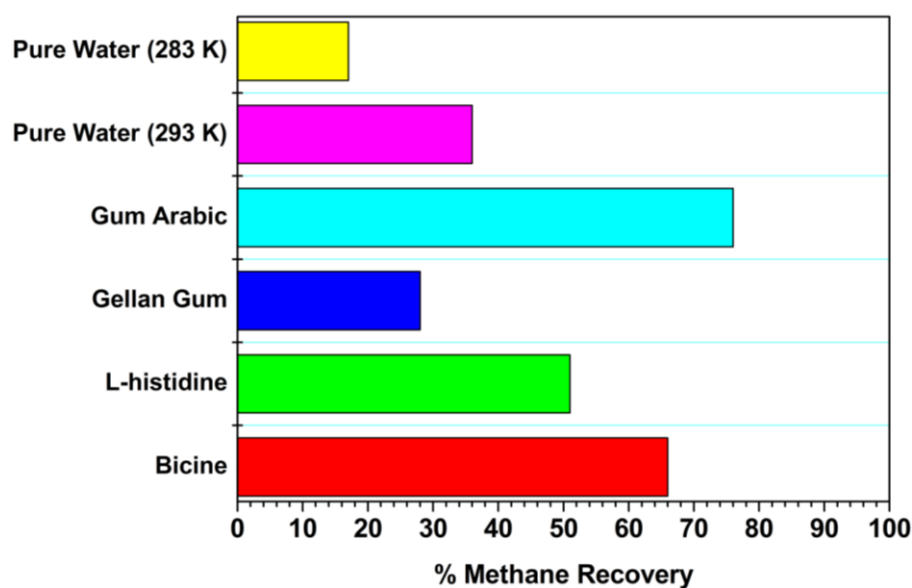


Fig. 7.10: Dissociation of methane hydrates in presence of different additives at 283 K: % Methane recovery after 18 minutes.

Figure 7.11 shows the normalised moles obtained during dissociation at 293K for the memory runs of the hydrate formation experiments. Hydrate dissociation kinetics for the memory runs in presence of additives has been compared with that for the fresh run of pure water. This is to show the repeatability of these compounds even they are used in small concentrations (1 wt % in this case). It can be clearly seen from the figure that all the additives studied exhibit credible repeatability as far as hydrate dissociation is concerned. Compared to the fresh run

with pure water, with the exception of Gellan Gum, all the additives studied show superior dissociation kinetics even during their respective memory runs.

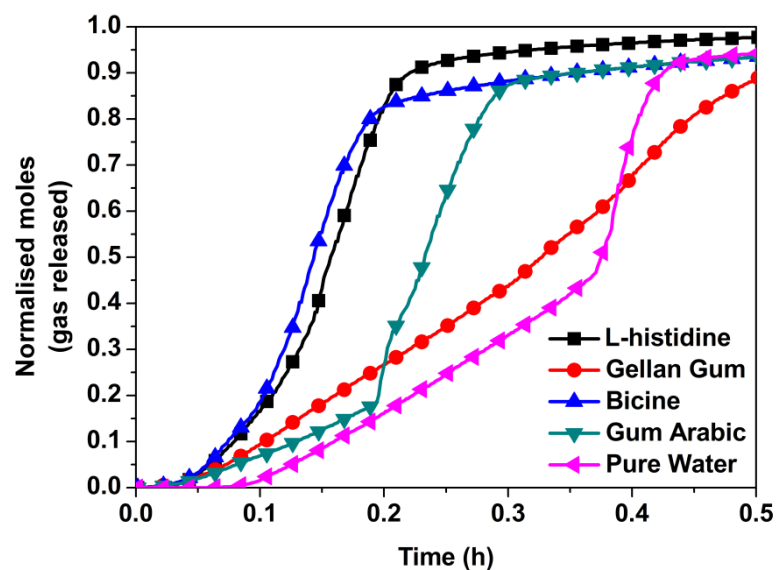


Fig. 7.11: Normalised moles of gas released vs. Time (h) for all the additives studied: Dissociation at 293 K. Memory runs. Concentration of all the additives: 1 wt %.

7.3.3. Injection of additives to enhance hydrate dissociation kinetics: Continuous flow loop circulating apparatus

Based on the results obtained from the experiments carried out in the dedicated reactor setup for additive selection and the feasibility of conducting the experiments on a larger scale (especially injecting the additives into the system through the water stream, a number of additives were selected for use in the continuous flow loop circulating apparatus. The experimental procedure used for these set of experiments is as follows. 700 gm of the sediment mixture was loaded into the 2.35 litre crystallizer vessel. The sediment mixture had a water saturation of 75% (~110 ml) and was made up of sand and clay mixed in a 75:25 ratio by weight. The crystallizer was then brought down to the experimental temperature (274K) with the help of an external circulating water bath. Once the desired temperature was reached, methane gas was introduced into the system at the desired experimental pressure (~50 bar) leading to the formation of pure methane gas hydrates. Methane hydrates were allowed to form overnight and dissociated after saturation was reached in the growth phase. Dissociation was achieved by injecting a water-additive mixture stream into the system with the help of a high pressure circulating pump. Additives were used in low concentrations (0.1 wt %-1 wt %) and the water-additive mixture was injected to the system in a continuous stream for 1 hour

following which the supply of water to the system was stopped. The mass flow controller attached to the crystallizer was opened at the same time at which pumping was started and the MFC was set at the initial crystallizer pressure at the beginning of the dissociation process. This ensures that only the gas released due to dissociation of methane hydrates passes through the MFC and gets collected in the reservoir. After the pumping of the water-additive mixture was stopped, the system was left as it is for thirty minutes. Following this, the temperature of the crystallizer was brought up to room temperature (298K) to finish the hydrate dissociation process.

Figure 7.12 shown below gives an idea of the conditions inside the crystallizer both at the start and end of the hydrate formation-dissociation experiment. While Figure 7.13(a) shows the hydrate formation sediment prior to the start of the experiment, Figure 7.13(b) shows the hydrate bearing sediment after water flooding. Figure 7.13(c) shows the formation of bubbles on top of the water flooded sediment which clearly indicates the released gas as a result of the dissociating gas hydrates.

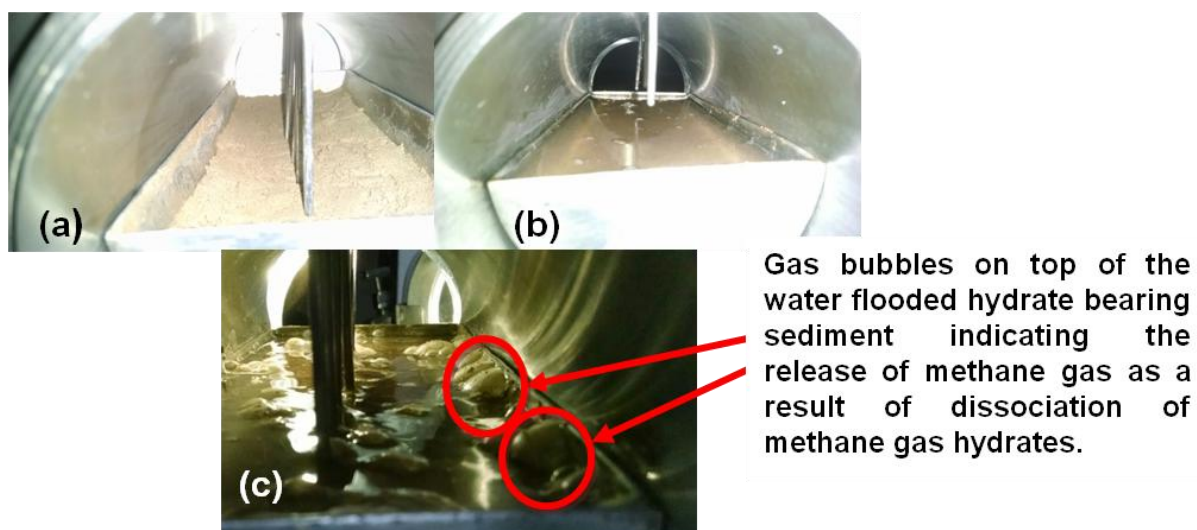


Figure 7.12: Hydrate bearing sediment before formation and after dissociation of methane hydrates:

- (a) Hydrate formation sediment prior to the start of the experiment.
- (b) Hydrate bearing sediment after water flooding.
- (c) Presence of gas bubbles indicating release of gas as a result of dissociation of gas hydrates.

Figure 7.13 which follows, plots the methane recovery obtained using the continuous apparatus for the pure water system and in the presence of a number of benign additives identified by us. The flow rate of the injected solution was kept constant at 10 ml/min for all

the experiments conducted and all the additives were used in the same concentration (0.1 wt %). Methane recovery has been shown for the first thirty minutes of hydrate dissociation. As can be seen in Figure 7.13, out of all the novel benign additives tested, L-histidine (a polar amino acid) serves our purpose the best by considerably speeding up the hydrate dissociation process as compared to pure water with Bicine (a zwitterionic molecule) not far behind. On the other hand, the hydrophobic amino acids L-proline and L-tryptophan fail to adequately enhance the kinetics of methane hydrate dissociation with L-proline in fact showing a slight inhibition in the same. The latter two results notwithstanding, it is still extremely promising to see the superb enhancement in methane hydrate dissociation kinetics observed with an extremely low concentration (0.1 wt %) of the additives L-histidine and Bicine as compared to pure water. It can also be seen from Figure 7.13 that the presence of ethylene glycol (0.1 wt %) affects the hydrate dissociation kinetics more favourably than all the novel benign additives studied so far. This is more or less expected as ethylene glycol is a thermodynamic inhibitor and its presence in the system shifts the hydrate equilibrium conditions to more drastic conditions rendering the hydrates unstable, which is something that does not happen in the case of L-histidine or Bicine. However, this does not necessarily make ethylene glycol the additive better suited for our purpose. It needs to be kept in mind that the additives being discussed here are supposed to be injected into a natural environment and hence first and foremost should be benign and environment friendly. Sadly ethylene glycol does not serve this purpose which makes the use of ethylene glycol in hydrate dissociation highly unlikely. Compounds like L-histidine and Bicine however are benign and don't need to be used in very large doses thus making them great candidates for use as additives to enhance hydrate decomposition kinetics.

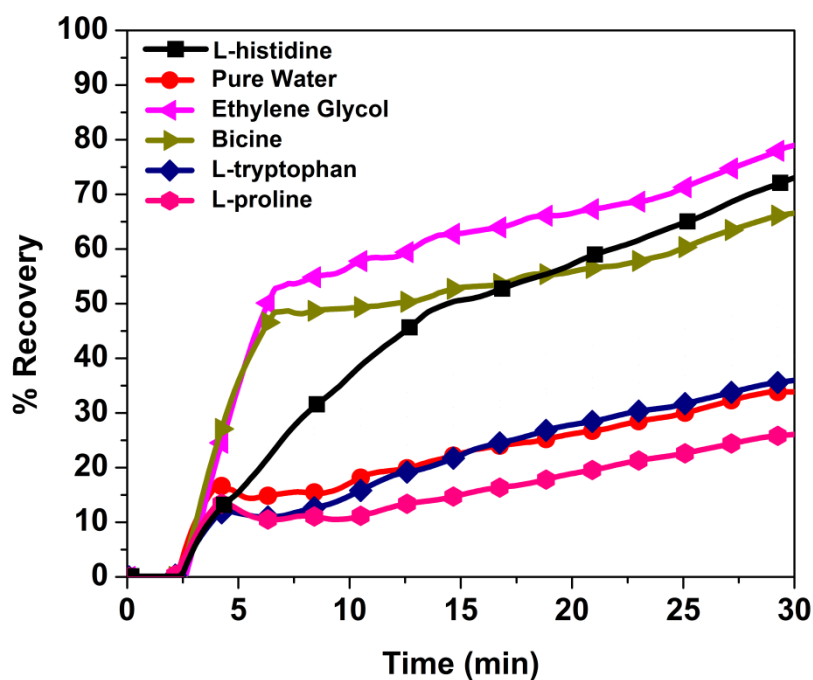


Fig. 7.13: % Methane recovery vs. time (min) for hydrate dissociation effected by the injection of benign additive-water mixtures into the large scale continuous apparatus (0.1 wt % and 10 ml/ min).

Figure 7.14 plots the methane recovery obtained using the flow loop apparatus and a few of the benign additives identified to enhance hydrate dissociation kinetics. Here the flow rate of the injected solution was maintained at 30 ml/min while the concentration of the additives used was kept constant at 0.1 wt %. The two best benign additives at 0.1 wt % and 10 ml/ min (L-histidine and Bicine) were chosen for this study along with the thermodynamic inhibitor Ethylene Glycol. Such a diverse group of additives was selected to effectively study the effect of injection flow rate on methane hydrate dissociation kinetics. From Figure 7.14, it can be seen that all the benign additives show a marked improvement in hydrate dissociation kinetics as compared to pure water injected at 30 ml/ min. L-histidine achieves the maximum kinetic enhancement as compared to pure water and is closely followed by Bicine while both in fact, show better hydrate dissociation kinetics as compared to Ethylene Glycol, the thermodynamic inhibitor. This is a very important result from our point of view as the use of a higher injection flow rate can be seen to have a very positive effect on hydrate dissociation kinetics while also increasing the effectiveness of our novel benign additives as a result of faster delivery to the hydrate containing sediment.

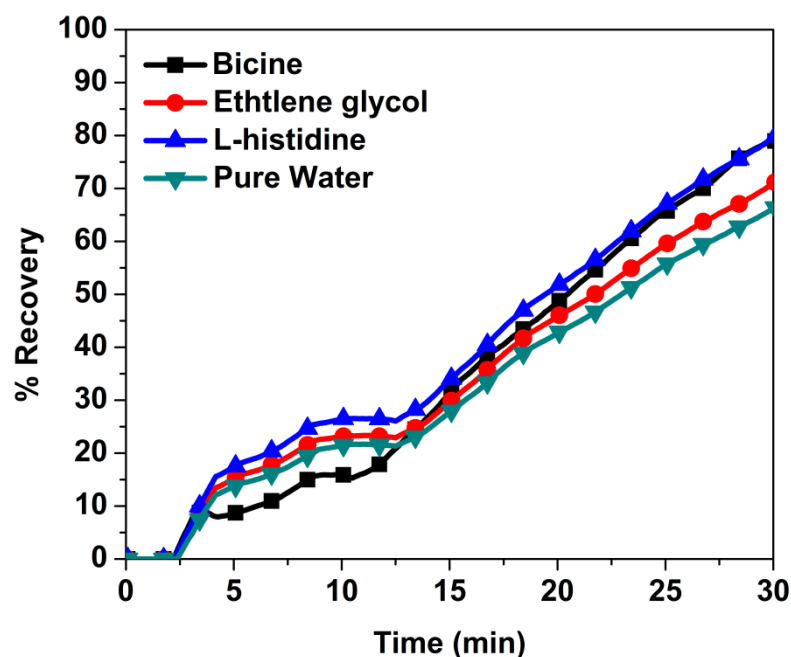


Fig. 7.14: % Methane recovery vs. time (min) for hydrate dissociation effected by the injection of benign additive-water mixtures into the large scale continuous apparatus (0.1 wt % and 30 ml/ min).

Figure 7.15 plots the methane recovery obtained using the flow loop apparatus and a few of the benign additives identified to enhance hydrate dissociation kinetics. Here the flow rate of the injected solution was maintained at 30 ml/min while the concentration of the additives used was kept constant at 1 wt %. L-histidine and Bicine were both chosen for this study as was the hydrophobic amino acid L-tryptophan which hadn't performed all that well at 10 ml/min and 0.1 wt %. Ethylene Glycol wasn't used for this study due to the obvious toxic nature of Ethylene Glycol and the fact that now the additives were being used at higher concentrations. As can be seen from Figure 7.15, at 30 ml/min, Bicine leads the pack in terms of enhancing hydrate dissociation kinetics and is closely followed by L-histidine. L-tryptophan doesn't fare too well here either with only a slight improvement over pure water injected at 30 ml/min. The other additives however show remarkable improvement in hydrate dissociation kinetics as compared to pure water.

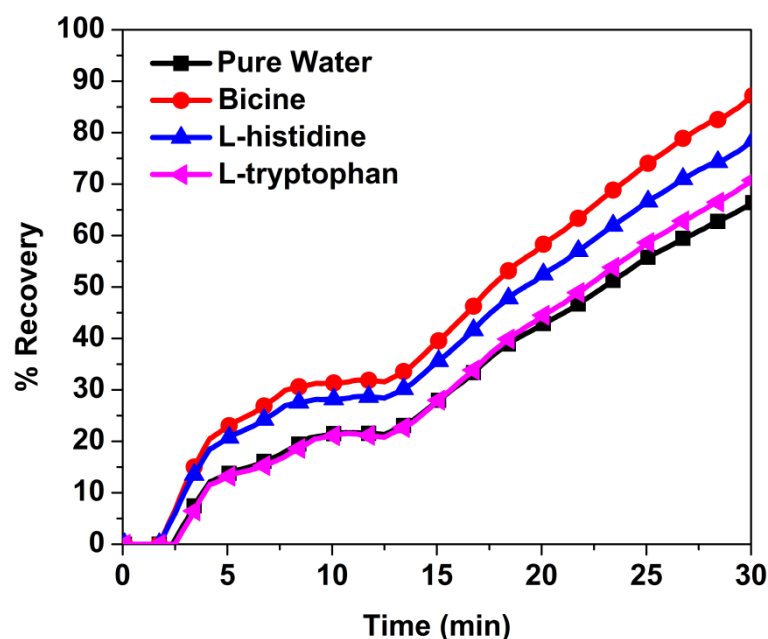


Fig. 7.15: % Methane recovery vs. time (min) for hydrate dissociation effected by the injection of benign additive-water mixtures into the large scale continuous apparatus (1 wt % and 30 ml/ min).

7.3.4: Energy and Efficiency Analysis in the presence of low concentrations of additives (injection)

Energy ratio and thermal efficiency are the two common parameters used to evaluate the efficiency of gas production from a hydrate reservoir and the same was calculated for the hydrate dissociation process in presence of additives employed here.

Energy ratio is the ratio of the total combustion heat of the produced methane gas to the total input energy and is given by the following formula:

$$\eta = \frac{G_p M_{gas}}{C_w m_w (T_{inj} - T_{env}) + W_{pump}} \quad (7.1)$$

G_p is the cumulative amount of the produced gas (mol), M_{gas} is the combustion heat of methane (890.3 kJ/ mol), C_w is the specific heat of water (4.2 kJ kg⁻¹ K⁻¹), m_w is the total mass of injected water, T_{inj} is the temperature of injected water (298K), T_{env} is the temperature of the reservoir during hydrate formation and W_{pump} is the total work done by the metering pump in pumping the injection solution at a particular flow rate.

The total work done by the pump can be calculated as:

$$Pump\ Work = Shaft\ Power \times Time\ for\ which\ pump\ was\ operated \quad (7.2)$$

Shaft Power can be calculated as:

$$\text{Shaft Power} = \frac{\text{Hydraulic Power}}{\text{Efficiency of Pump}} \quad (7.3)$$

where the efficiency of the pump is 70 % as specified by the manufacturer.

Hydraulic Power of the pump can be calculated as:

$$\text{Hydraulic Power} = \text{Pressure head } (\Delta P) \times \text{Flow rate of injection solution} \quad (7.4)$$

The flow rate of the injection solution varies according to the experiment in question (10 ml/min and 30 ml/min).

The thermal efficiency on the other hand is an indicator of the proportion of the total amount of heat used to dissociate the formed hydrate to the total injected heat. Thermal efficiency can be given by the following equation:

$$\zeta = \frac{N_h \Delta H_h}{C_w m_w (T_{inj} - T_{env})} \quad (7.5)$$

Where N_h is the number of moles of dissociated hydrate, ΔH_h is the decomposition heat of hydrate (52.9 kJ/mol at 274.15K).

Energy ratio is a parameter which evaluates the effectiveness of a hydrate dissociation process from the perspective of energy output. A higher energy ratio signifies greater energy output for the same amount of input energy. Thermal efficiency however speaks from the viewpoint of energy use. A higher thermal efficiency means more amount of the injected heat is used in dissociating the hydrate, that is to say the hydrate dissociation process is more energy efficient.

The energy ratios and thermal efficiencies for the various systems (different additive concentrations and injection flow rates) with respect to time were calculated for the first thirty minutes of hydrate dissociation and the maximum energy ratio and thermal efficiency obtained for each system has been reported in Table 7.2.

Table 7.2: Energy and efficiency analysis for the various systems studied (injection of additives)

Additive concentration and Flow Rate	Additive	Maximum Energy Ratio Obtained	Maximum Thermal Efficiency Obtained
0.1 wt % and 10 ml/min	Pure Water	1.0	0.06
	L-histidine	4.7	0.28
	Ethylene Glycol	2.2	0.13
	Bicine	4.5	0.26
	L-tryptophan	2.5	0.15
	L-proline	1.5	0.08
0.1 wt % and 30 ml/min	Pure Water	3.0	0.18
	Bicine	3.2	0.20
	L-histidine	3.7	0.24
	Ethylene Glycol	3.1	0.19
1 wt % and 30 ml/min	Pure Water	2.8	0.18
	Bicine	3.5	0.23
	L-histidine	3.0	0.20
	L-tryptophan	3.0	0.20

It can be seen from Table 7.2 that the energy and efficiency analysis in general follows the same trend as the gas release profiles that is to say that the systems which show higher methane recovery also exhibit higher values for the energy ratios and thermal efficiencies.

When the flow rate of the injected additive stream is increased while keeping the concentration of injected additive constant, it can be observed that the values of energy ratio and thermal efficiency for the pure water and ethylene glycol systems increase whereas those for Bicine and L-histidine decrease. The reason for this is that when the flow rate of the additive stream is increased, the systems like pure water and ethylene glycol now receive an extra driving force to aid in the dissociation process which results in faster release of gas from the formed hydrate and hence a higher energy ratio. For the L-histidine and Bicine systems, the additives used were already providing the extra driving force (so to say) when the flow rate of the additive stream was low (10 ml/min) and hence when the flow rate of the additive stream was increased to 30 ml/min, since the concentration of the additives in the additive stream remained constant, the systems returned a lower energy ratio than the earlier case as a result of the pump doing more work to maintain the higher flow rate. There is no real improvement in the values of the energy ratios and thermal efficiencies obtained when the concentration of

injected additive is increased while keeping the flow rate of the additive stream constant thus indicating that a very small amount of additive is enough to satisfactorily enhance the energy ratio and thermal efficiency of the system.

For all the additive systems studied, a higher energy ratio and thermal efficiency is observed as compared to pure water which not only highlights the positive effect of the novel benign additives on methane hydrate dissociation kinetics but also goes a long way in strengthening the feasibility of the additive injection based hydrate dissociation based process.

7.4. Conclusions

- The way forward with regards to gas hydrate dissociation is a hybrid process combining the depressurization and thermal stimulation methods. Some benign additives may be used in small concentrations to increase the energy efficiency of the thermal stimulation process.
- Ability of additives to interact with water molecules and modify/ break hydrogen bonds is one of main reasons behind the enhancement in dissociation of methane hydrates in presence of additives.
- Trend observed (effectiveness of additives to enhance hydrate dissociation) using STR was followed in experiments using the large scale continuous reactor.
- All the additives used were found to enhance the energy ratio and thermal efficiency of the process as compared to pure water.
- High flow rate is required to enhance the energy ratio and thermal efficiency for just the pure water system whereas for the systems containing L-histidine and Bicine, only a small concentration of additive in solvent stream and low flow rate of the same is required to obtain satisfactorily high energy efficiency. In the latter case, higher flow rate actually decreases the energy ratio and thermal efficiency of the system as higher flow rate signifies more work done by the pump and hence higher energy input into the system.
- The hybrid hydrate dissociation approach developed in this study, combining the depressurization and hot water flooding methods while also employing benign additives such as amino acids thus indeed hold great promise for the future, environmentally, economically and commercially.

7.5. References

1. Sloan, E. D.; Koh, C. A. Clathrate hydrates of natural gases; CRC press: New York, 2008.
2. Kurihara, M., Ouchi, H., Narita, H., Masuda, Y. Gas production from methane hydrate reservoirs. In: Proceedings of the 7th International Conference on Gas Hydrates (ICGH), Edinburgh, UK, 2011.
3. Li, B., Li, X. S., Li, G., Feng, J. C., Wang, Y. Depressurization induced gas production from hydrate deposits with low gas saturation in a pilot-scale hydrate simulator. *Appl. Energy* **2014**, 129, 274-286.
4. Wang, Y., Li, X. S., Li, G., Huang, N. S., Feng, J. C. Experimental study on the hydrate dissociation in porous media by five-spot thermal huff and puff method. *Fuel* **2014**, 117, 688-696.
5. Li, G., Li, X. S., Tang, L. G., Zhang, Y. Experimental investigation of production behavior of methane hydrate under ethylene glycol injection in unconsolidated sediment. *Energy Fuels* **2007**, 21, 3388-3393.
6. Feng, J. C., Wang, Y., Li, X. S., Li, G., Chen, Z. Y. Production behaviors and heat transfer characteristics of methane hydrate dissociation by depressurization in conjunction with warm water stimulation with dual horizontal wells. *Energy* **2015a**, 79, 315-324.
7. Feng, J. C., Wang, Y., Li, X. S., Li, G., Zhang, Y., Chen, Z. Y. Effect of horizontal and vertical well patterns on methane hydrate dissociation behaviors in pilot-scale hydrate simulator. *Appl. Energy* **2015b**, 145, 69-79.
8. McLaurin, G., Shin, K., Alavi, S., Ripmeester, J. A. Antifreezes act as catalysts for methane hydrate formation from ice. *Angew. Chem.* **2014**, 126, 10597-10601.

-
9. Scheu, R., Rankin, B.M., Chen, Y., Jena, K.C., Ben-Amotz, D., Roke, S. Charge asymmetry at aqueous hydrophobic interfaces and hydration shells. *Angew. Chem. Int. Ed.* **2014**, 53, 9560-9563.
 10. Koh, C. A. Towards a fundamental understanding of natural gas hydrates. *Chem. Soc. Rev.* **2002**, 31, 157-167.
 11. Cha, M., Shin, K., Kim, J., Chang, D., Seo, Y., Lee, H., Kang, S. P. Thermodynamic and kinetic hydrate inhibition performance of aqueous ethylene glycol solutions for natural gas. *Chem. Eng. Sci.* **2013**, 99, 184-190.
 12. Perrin, A., Musa, O. M., Steed, J. W. The chemistry of low dosage clathrate hydrate inhibitors. *Chem. Soc. Rev.* **2013**, 42, 1996-2015.

Chapter 8

Summary of Conclusions, Contribution to Knowledge and Recommendations for Future Work

8. Summary of Conclusions, Contribution to Knowledge and Recommendations for Future Work

The technological applications of gas hydrates such as gas storage and separation all require rapid hydrate formation and dissociation kinetics to be relevant on an industrial scale. When viewed as an energy source, the recovery of natural gas from gas hydrate reserves requires rapid hydrate dissociation kinetics as does the dissociation of hydrate plugs that get formed in trans-continental oil and gas pipelines preventing smooth flow of hydrocarbons and resulting in losses to the oil and gas industry. The current thesis explores the use of additives in small concentrations to enhance gas hydrate formation and dissociation kinetics with a view on improving the feasibility of the various technological applications of gas hydrates in addition to their potential as a recoverable future energy source.

8.1. Conclusions

Surfactants being the most common form of kinetic hydrate promoters, the much debated surfactant micelle hypothesis was tested by synthesizing surfactant micelles at hydrate forming temperature (275 K) using a combination of anionic surfactant SDS and zwitterionic surfactant CAPB. Hydrate forming experiments were performed using pure methane as well as a low concentration coal mine gas mixture (30% CH₄ and 70% N₂). For both gas systems studied, efficient promotion of hydrate formation kinetics was observed in the presence of surfactant micelles as compared to pure water and micelle-less surfactant systems.

The biosurfactant Surfactin was used as a kinetic hydrate promoter and its efficacy for methane hydrate promotion was compared to that for SDS, a synthetic surfactant and the most commonly used kinetic hydrate promoter. It was observed that the promotion effected with Surfactin was slightly greater than that with SDS. This is a very important piece of finding as we suggest a benign, environment friendly additive for use as kinetic promoters in gas hydrate based applications such as methane separation, storage and transport.

Although surfactants have been extensively used as kinetic hydrate promoters and the presence of small concentrations of these additives provide significant promotion of hydrate formation kinetics as compared to pure water, the scalability of operations employing surfactants remains a major issue due to the problem of excessive foam generation that is frequently encountered when using the same. To deal with the problem of foam generation, different additives were identified that when used by themselves or in conjunction with

surfactants as kinetics hydrate promoters expel the generation of any kind of foam during the hydrate formation process. With regards to this, the amino acid L-histidine was studied at two different concentrations, 0.1 wt % and 1 wt %. For both the concentrations of L-histidine used, methane hydrate formation kinetics was observed to be enhanced in comparison to pure water. The final gas consumption for hydrate formation with 1 wt % L-histidine was found to be comparable with that for 1 wt % SDS. Moreover, no foam generation was observed during hydrate dissociation in presence of L-histidine as a kinetic hydrate promoter. The absence of foam generation with L-histidine and it being a benign substance, in addition to the similar final gas uptakes for methane hydrate formation observed between L-histidine and SDS, render this study vital. However, from an economical point of view we further tested antifoams along with known surfactants to tide over the issue of foam generation during hydrate dissociation.

A hydrophobic silicone surfactant (Antifoam-A) was identified to act as an antifoam which when mixed with SDS would suppress the foam generated by the surfactant thus making the system easy to handle and scale up. SDS-Silicone complexes were prepared by mixing the two additives which were then used in methane hydrate formation runs. From the gas uptake studies, it was concluded that the 1 wt % SDS + 0.5 wt % Antifoam-A system was the best in terms of promoting the kinetics of hydrate formation. There was no loss whatsoever in the kinetic promotion property of SDS at this ratio of the two additives. The use of the silicone antifoam was also found to significantly reduce the induction time for hydrate formation as a result of its high hydrophobicity. The absence of foam formation when using the silicone antifoam greatly enhances the feasibility of commercializing the hydrate based methane storage technology. Moreover, since it is being used in conjunction with a traditional kinetic hydrate promoter such as SDS, there is no compromise on the kinetics of methane hydrate formation either.

The hydrate based gas separation process for the separation of CO₂ and CH₄ gas mixtures was studied using an equimolar mixture of the same. Three different additives were identified to enhance the kinetics of hydrate formation and increase the selectivity of one particular gas from the gas mixture to occupy the hydrate cages. Out of the three additives studied, the hydrophobic amino acid Tryptophan was identified to be the most effective in enhancing the kinetics of hydrate formation. All three additives were found to increase the selectivity of a specific gas, either CO₂ or CH₄ to occupy the hydrate cages although the separation factors obtained in the presence of the additives were not much enhanced as compared to the pure

water systems. While the addition of a small amount of Tryptophan to the system easily solves the problem of low kinetics of hydrate formation and low gas uptake, a significant amount of research is still required to realize the desired separation efficiency of the process.

Carbon dioxide sequestration in porous geological media using hydrate formation was studied, especially keeping in mind the geology of the Indian subcontinent. Four types of porous media with diverse porosities were used: silica sand, quartz, pumice and fire hardened red clay (FHRC) and two different kinds of experiments were performed: a) keeping the volume of water constant and b) keeping the bed height constant. For both types of experiments, pumice was observed to be the fixed bed medium that led to maximum enhancement in hydrate formation kinetics. Decrease in particle size was found to greatly enhance hydrate formation kinetics while the same was found to be inhibited on increasing the bed height. Pumice and FHRC, used in this study, which are typical volcanic sediments abounding in the Indian subcontinent seem to be as good as silica sand or quartz in terms of kinetics of CO₂ hydrate formation as well as the water to hydrate conversion and both these materials provide us with a very realistic option for geological storage of CO₂ in the form of gas hydrates.

Last but not the least, the use of additives to enhance the kinetics of hydrate dissociation was investigated. It is very important that the additives employed here should be benign and must be used in very small concentrations as they are to be injected into the marine environment (hydrate reservoir) along with the hot water stream. A number of additives to serve this purpose were thus identified using hydrate formation experiments in a stirred tank reactor and the most promising ones were then used in a fixed bed setup that was designed to mimic marine hydrate reservoir conditions. These additives such as amino acids mainly work on their ability to interact with water molecules and modify/ break hydrogen bonds thus creating defects in the hydrate cages and facilitating the dissociation of the formed hydrates. In addition to enhancing the kinetics of hydrate dissociation, these additives were also found to enhance the energy ratio and thermal efficiency of the process as compared to pure water. The concentration of additive in the system was found to be more important than the flow rate with regards to increasing the energy efficiency of the system. Finally, the hydrate dissociation process proposed in this study which combines the depressurization and hot water flooding approaches while also employing benign additives in low concentrations looks to be a very promising future option as far as recovery of natural gas from marine gas hydrates is concerned.

8.2. Contribution to Knowledge

This thesis provides a number of new insights on the use of additives to enhance gas hydrate formation and dissociation kinetics. The contributions to knowledge are as follows:

- 1) The surfactant micelle hypothesis is one of the most widely debated topics pertaining to the use of surfactants as kinetic hydrate promoters. In our study, it has been conclusively proven for the first time that the presence of surfactant micelles in the system indeed promotes the kinetics of hydrate formation.
- 2) The biosurfactant Surfactin has been shown to be slightly more efficient than the synthetic surfactant SDS with regards to promoting the kinetics of methane hydrate formation. This puts the feasibility of using both biosurfactants and synthetic surfactants into perspective as in spite of their benign nature and the slight enhancement in hydrate formation kinetics observed with Surfactin as compared to SDS, biosurfactants however are more expensive than their synthetic counterparts.
- 3) The major issue encountered when using surfactants as kinetic hydrate promoters; that of foam generation, has been adequately resolved in this thesis. Additives such as the amino acid L-histidine and a silicone based surfactant/antifoam have been used either individually or in conjunction with conventional kinetic hydrate promoters such as SDS (surfactant) to counter the problem of foam generation. The silicone based antifoam, when used in combination with SDS is particularly effective as foam generation could be effectively suppressed while also preserving the inherent promotion effect of the surfactant.
- 4) A handful of additives have been identified to act as selective hydrate promoters (SHPs) particularly for the HBGS process to effect CO₂-CH₄ gas separation. Ideally, the additives should enhance the kinetics of hydrate formation as well as improve the separation efficiency of the process. The addition of 1 wt % of the hydrophobic amino acid Tryptophan to the system brings about extraordinary enhancement in the kinetics of hydrate formation from a 50 % CO₂-50 % CH₄ gas mixture as compared to pure water.
- 5) Pumice and Fire Hardened Red Clay (FHRC) have been identified as typical porous, siliceous volcanic sediments that abound in the Indian subcontinent and which can be used as viable media for geological sequestration of carbon dioxide in the form of gas hydrates. As expected it was observed that decrease in particle size distribution

enhances the kinetics of hydrate formation while increase in bed height inhibits the same.

- 6) A number of benign additives have been recognized which when used in very small concentrations greatly enhance the kinetics of methane hydrate dissociation. These additives also improve the energy ratio and thermal efficiency of the system. A new process for hydrate dissociation has been suggested combining the depressurization and thermal stimulation (hot water flooding) approaches while also using benign additives in low concentrations.

8.3. Recommendations for Future Work

The following recommendations are proposed for future work

- 1) Biosurfactants are attractive substitutes to synthetic surfactants like SDS for use as kinetic hydrate promoters. Apart from Surfatin, there are a number of other biosurfactants such as Iturin and Fengycin that may be tested as kinetic hydrate promoters. Additionally, cost-efficiency analysis needs to be done in order to understand the feasibility of using biourfactants as compared to their synthetic counterparts.
- 2) Functionalized nanoparticles containing both hydrophilic and hydrophobic parts and properties, such as Janus spheres may be used to mimic surfactant micelles in solution and hence enhance the kinetics of hydrate formation without the requirement of external stirring energy (the vibrating nanoparticles may be used as inbuilt nano-stirrers) and without the problem of foam generation encountered when using surfactants.
- 3) With regards to scale up of hydrate based technological applications, it is widely agreed that fixed bed reactors are the way to go. The non foaming additives that were identified in this thesis using a stirred tank reactor need to be used in a fixed bed setup using a metallic packing such as brass or stainless steel as the fixed bed medium to get a more realistic idea of how these additives would behave if used in an industrial scale hydrate based gas storage or separation process that requires rapid hydrate formation kinetics.
- 4) CO₂ sequestration studies were done on Pumice and FHRC samples in a fixed bed configuration; these materials mimic the geological formations which can be a potential target for CO₂ sequestration in Indian subcontinent. However, the hydrate

formation studies need to be carried out in authentic underwater samples of pumice and other readily available volcanic rocks in order to gather more knowledge and build a better understanding of these systems before attempting to actually turn this practice into reality. CO₂ soluble additives may also be identified to further enhance the kinetics of carbon dioxide hydrate formation in these porous geological media.

- 5) The hydrate dissociation study reported in this thesis has so far only been performed on a bench scale (2.35 litres). The same needs to be performed on different larger scales in order to better understand the effect of the identified additives on methane hydrate dissociation kinetics. Proper scaling criteria also need to be developed to predict with a certain amount of accuracy the expected promotion effect of the inject additives on hydrate dissociation when working on a commercial/ industrial scale.

APPENDIX A

This appendix contains linear fits of the first 20 minutes of hydrate growth for the different systems studied throughout the course of this thesis. The slopes of these fits have been taken to be the initial apparent rate of hydrate formation with the unit (moles of gas consumed/h). The initial apparent rates of hydrate formation thus calculated for each system studied have been reported in a tabular form, segregated chapter wise.

Chapter 2: Effects of Micellization on Growth Kinetics of Methane Hydrate

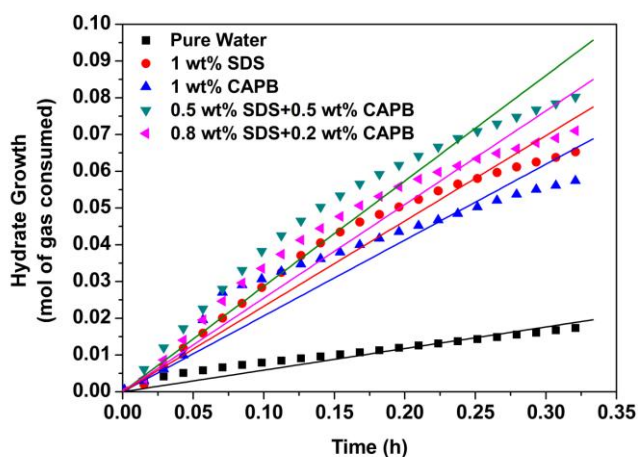


Fig. A1: Linear fit of the first 20 minutes (0.334h) of hydrate growth for pure methane gas with different surfactant solutions and pure water. STR configuration was used.

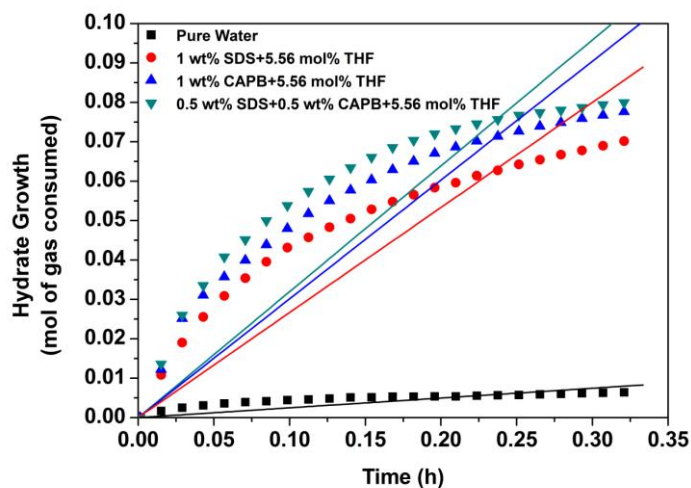


Fig. A2: Linear fit of the first 20 minutes (0.334h) of hydrate growth for CBM gas mixture with different surfactant solutions in conjunction with THF and with pure water (without the presence of any additives in the system). STR Configuration was used.

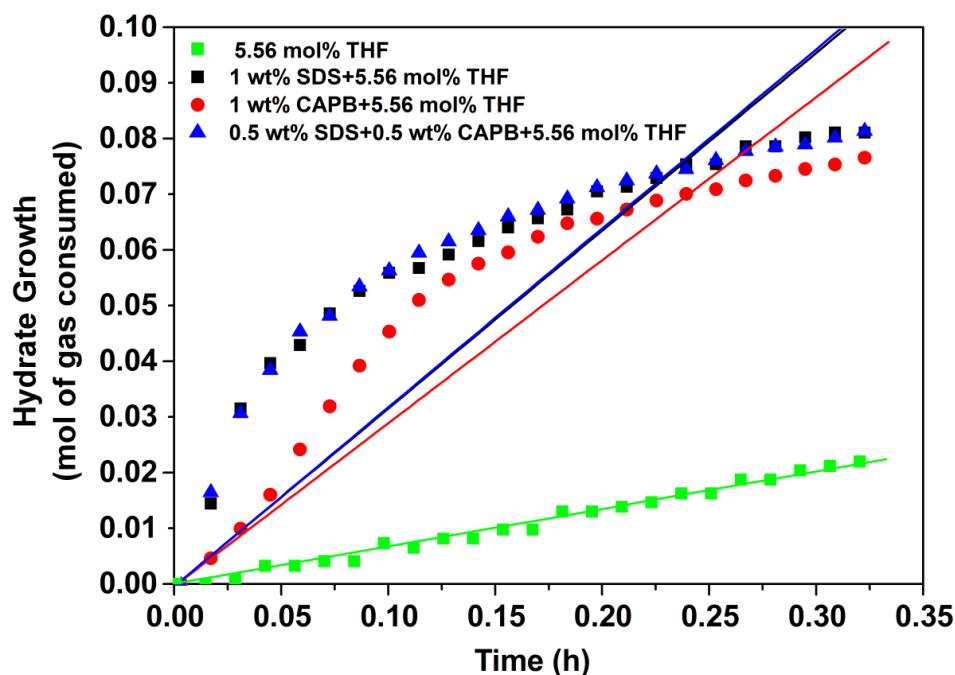


Fig. A3: Linear fit of the first 20 minutes (0.334h) of hydrate growth for CBM gas mixture with different surfactant solutions in conjunction with THF and with only THF. FBR Configuration was used.

Table A1: Initial apparent rates of hydrate formation (mol of gas consumed/h) for the different systems considered during the course of the work reported in Chapter 2 of the thesis.

System	Average rate of hydrate formation for first 20 minutes (gas uptake) (mol of gas / h) \pm SD
Pure Water/CH ₄ /STR	0.059 \pm 0.0005
Pure Water/CMM/STR	0.025 \pm 0.0005
1 wt % SDS/CH ₄ /STR	0.232 \pm 0.0020
1 wt % SDS/CMM/STR	0.267 \pm 0.0040
1 wt % SDS/CMM/FBR	0.319 \pm 0.0080
1 wt % CAPB/CH ₄ /STR	0.206 \pm 0.0020
1 wt % CAPB/CMM/STR	0.301 \pm 0.0050
1 wt % CAPB/CMM/FBR	0.293 \pm 0.0050
0.5 wt % SDS + 0.5 wt % CAPB/CH ₄ /STR	0.287 \pm 0.0020
0.5 wt % SDS + 0.5 wt % CAPB/CMM/STR	0.320 \pm 0.0050
0.5 wt % SDS + 0.5 wt % CAPB/CMM/FBR	0.322 \pm 0.0080
0.8 wt % SDS + 0.2 wt % CAPB/CH ₄ /STR	0.255 \pm 0.0020

Chapter 3: Kinetic promotion of methane hydrate formation by combining anionic and silicone surfactants: scalability promise of methane storage due to prevention of foam formation

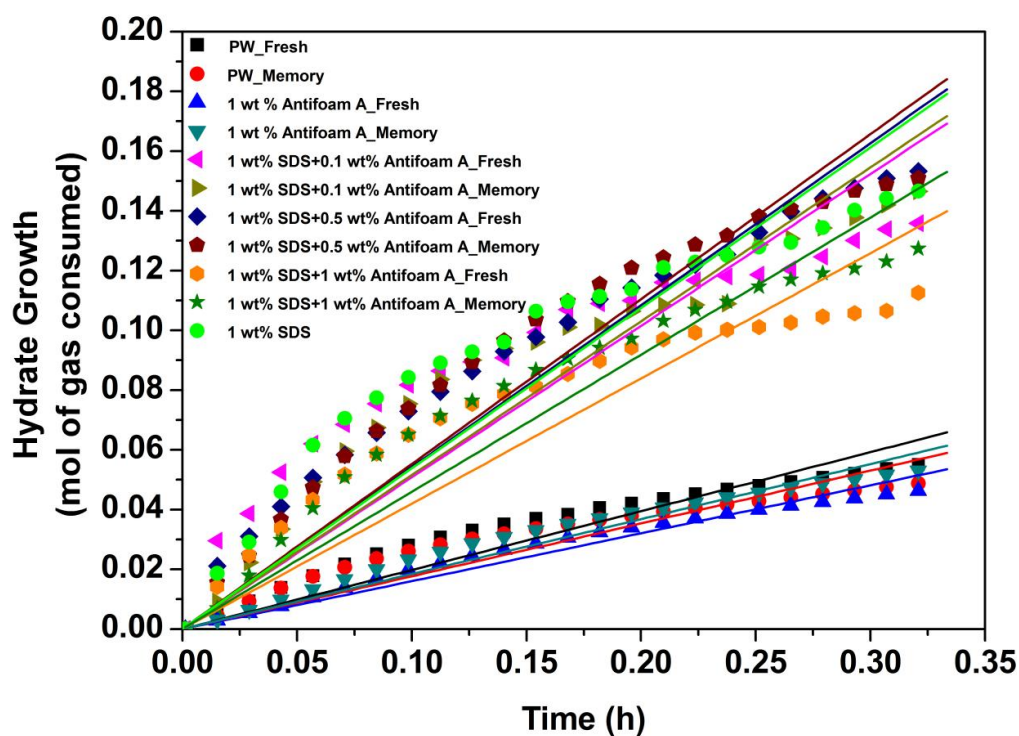


Fig. A4: Linear fit of the first 20 minutes (0.334h) of hydrate growth (both fresh and memory runs) for pure methane gas with different surfactant/surfactant-antifoam solutions and pure water.

Table A2: Initial apparent rates of hydrate formation (mol of gas consumed/h) for the different systems considered during the course of the work reported in Chapter 3 of the thesis.

System	Average rate of hydrate formation for first 20 minutes (gas uptake) (mol of gas / h) \pm SD
Pure Water_Fresh	0.197 \pm 0.0020
Pure Water_Memory	0.177 \pm 0.0020
1 wt % Antifoam A_Fresh	0.160 \pm 0.0010
1 wt % Antifoam A_Memory	0.184 \pm 0.0010
1 wt % SDS + 0.1 wt % Antifoam A_Fresh	0.508 \pm 0.0070
1 wt % SDS + 0.1 wt % Antifoam A_Memory	0.515 \pm 0.0050
1 wt % SDS + 0.5 wt % Antifoam A_Fresh	0.542 \pm 0.0040
1 wt % SDS + 0.5 wt % Antifoam A_Memory	0.552 \pm 0.0050
1 wt % SDS + 1 wt % Antifoam A_Fresh	0.420 \pm 0.0050
1 wt % SDS + 1 wt % Antifoam A_Memory	0.460 \pm 0.0040
1 wt % SDS	0.537 \pm 0.0070

Chapter 4: Bio based additives as kinetic promoters for methane hydrate formation

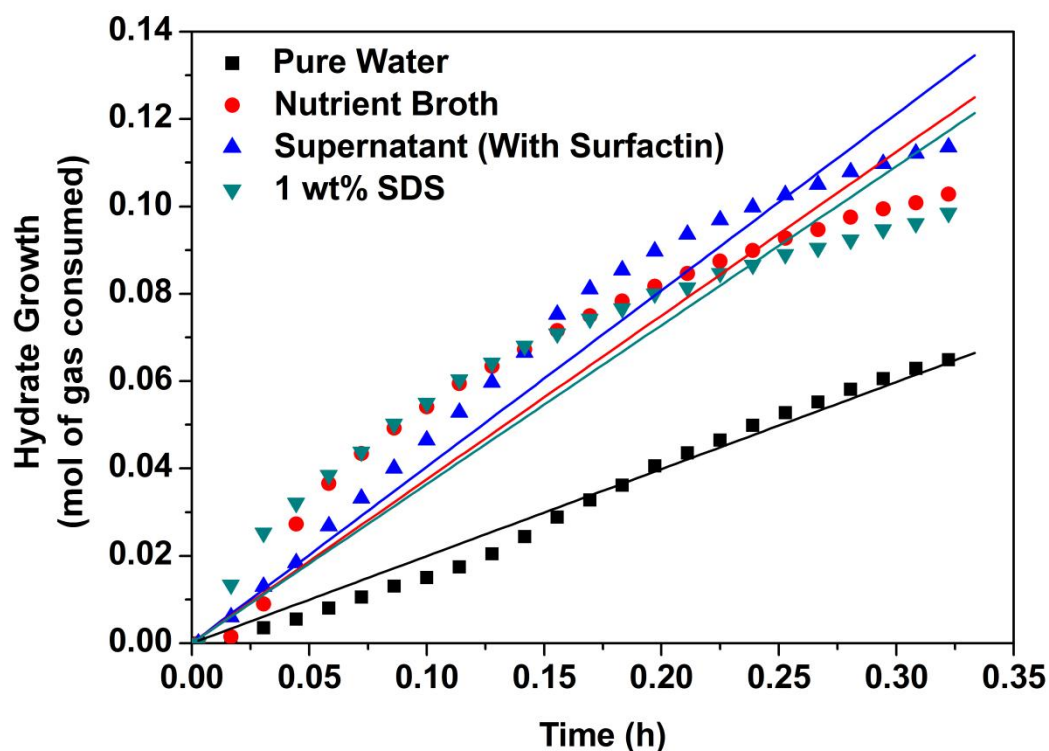


Fig. A5: Linear fit of the first 20 minutes (0.334h) of hydrate growth for pure methane gas with different surfactant solutions (Bio-Surfactant/ Synthetic Surfactant) and pure water.

Table A3: Initial apparent rates of hydrate formation (mol of gas consumed/h) for the different systems considered during the course of the first study reported in Chapter 4 of the thesis.

System	Average rate of hydrate formation for first 20 minutes (gas uptake) (mol of gas / h) \pm SD
Pure Water	0.199 \pm 0.0010
Nutrient Broth	0.375 \pm 0.0050
Supernatant (With Surfactin)	0.404 \pm 0.0040
1 wt % SDS	0.364 \pm 0.0060

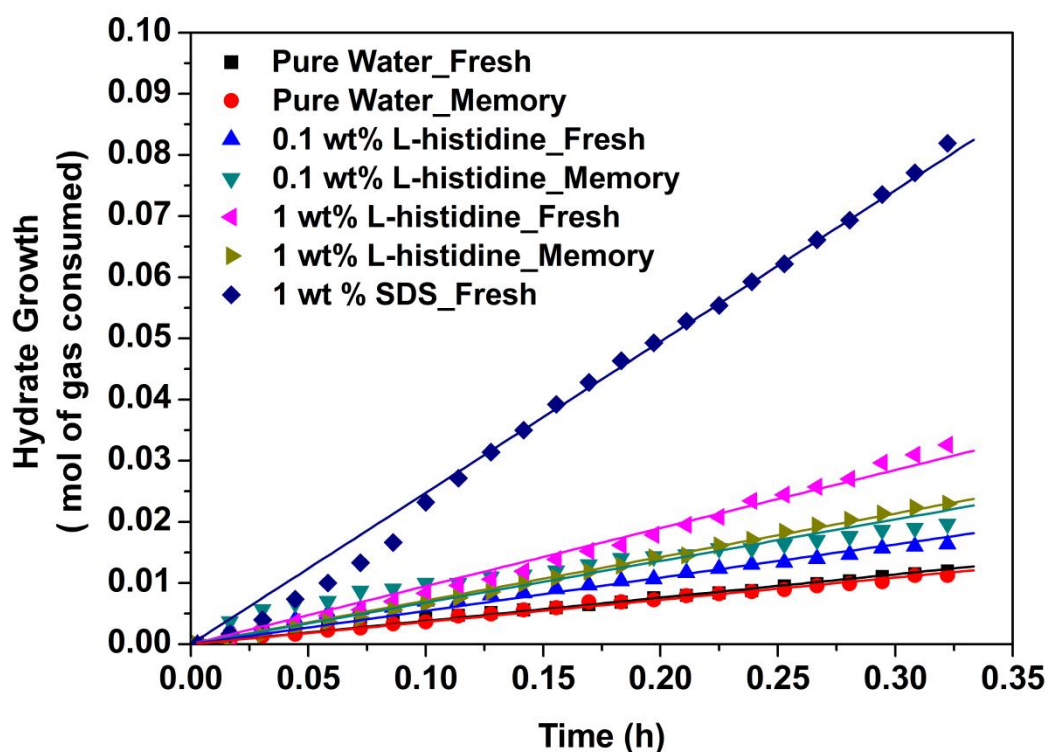


Fig. A6: Linear fit of the first 20 minutes (0.334h) of hydrate growth (both fresh and memory runs) for pure methane with the various amino acid/ surfactant systems studied.

Table A4: Initial apparent rates of hydrate formation (mol of gas consumed/h) for the different systems considered during the course of the second study reported in Chapter 4 of the thesis.

System	Average rate of hydrate formation for first 20 minutes (gas uptake) (mol of gas / h) \pm SD
Pure Water_Fresh	0.035 \pm 0.00003
Pure Water_Memory	0.036 \pm 0.0001
0.1 wt % L-Histidine_Fresh	0.046 \pm 0.0004
0.1 wt % L-Histidine_Memory	0.068 \pm 0.0010
1 wt % L-Histidine_Fresh	0.101 \pm 0.0007
1 wt % L-Histidine_Memory	0.071 \pm 0.0002
1 wt % SDS_Fresh	0.247 \pm 0.0010

Chapter 5: CH₄-CO₂ gas separation using clathrate hydrate formation in presence of selective hydrate promoters

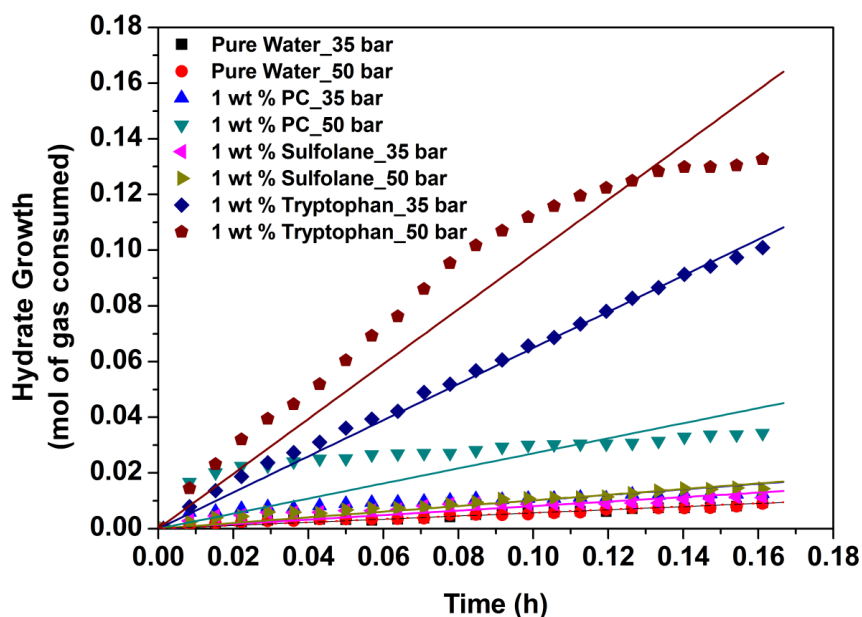


Fig. A7: Linear fit of the first 10 minutes (0.167h) of hydrate formation for an equimolar CO₂-CH₄ gas mixture in presence of the different selective hydrate promoters and varying hydrate formation pressures.

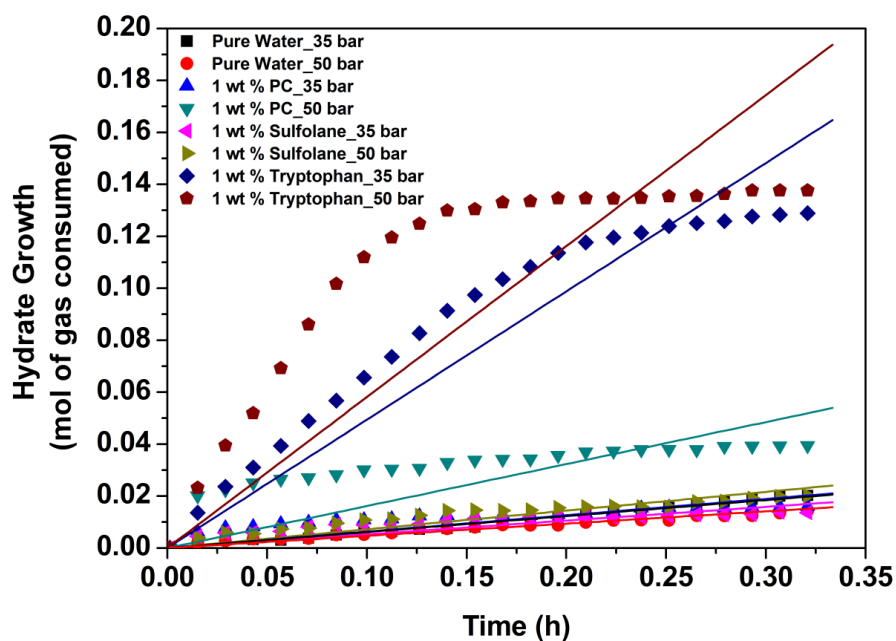


Fig. A8: Linear fit of the first 20 minutes (0.334h) of hydrate formation for an equimolar CO₂-CH₄ gas mixture in presence of the different selective hydrate promoters and varying hydrate formation pressures.

Table A5: Initial apparent rates of hydrate formation (mol of gas consumed/h) for the different systems considered during the course of the work reported in Chapter 5 of the thesis.

System	Average rate of hydrate formation for first 10 minutes (gas uptake) (mol of gas / h) \pm SD	Average rate of hydrate formation for first 20 minutes (gas uptake) (mol of gas / h) \pm SD
Pure Water_35 bar	0.057 \pm 0.0007	0.062 \pm 0.0002
Pure Water_50 bar	0.057 \pm 0.0006	0.047 \pm 0.0003
1 wt % Propylene Carbonate_35 bar	0.099 \pm 0.003	0.063 \pm 0.0010
1 wt % Propylene Carbonate_50 bar	0.270 \pm 0.009	0.162 \pm 0.0040
1 wt % Sulfolane_35 bar	0.081 \pm 0.002	0.053 \pm 0.0009
1 wt % Sulfolane_50 bar	0.102 \pm 0.001	0.072 \pm 0.0009
1 wt % Tryptophan_35 bar	0.649 \pm 0.002	0.494 \pm 0.0050
1 wt % Tryptophan_50 bar	0.985 \pm 0.013	0.581 \pm 0.0120

Chapter 6: Carbon Dioxide Sequestration in simulated sub sea sediment

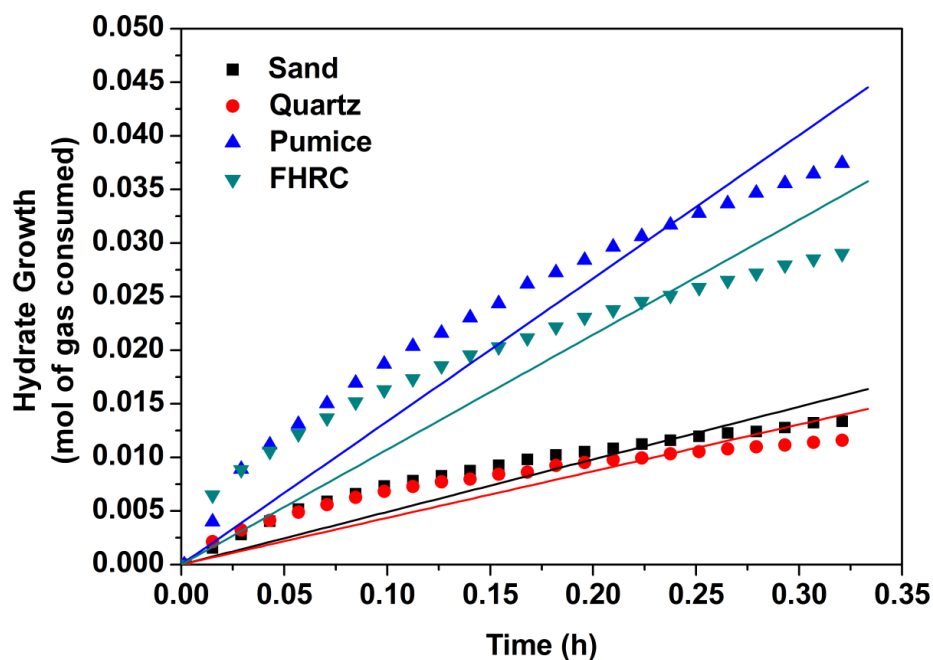


Fig. A9: Linear fit of the first 20 minutes (0.334h) of hydrate formation for pure CO₂ gas in presence of the different porous media used for the case of the constant volume of water experiments.

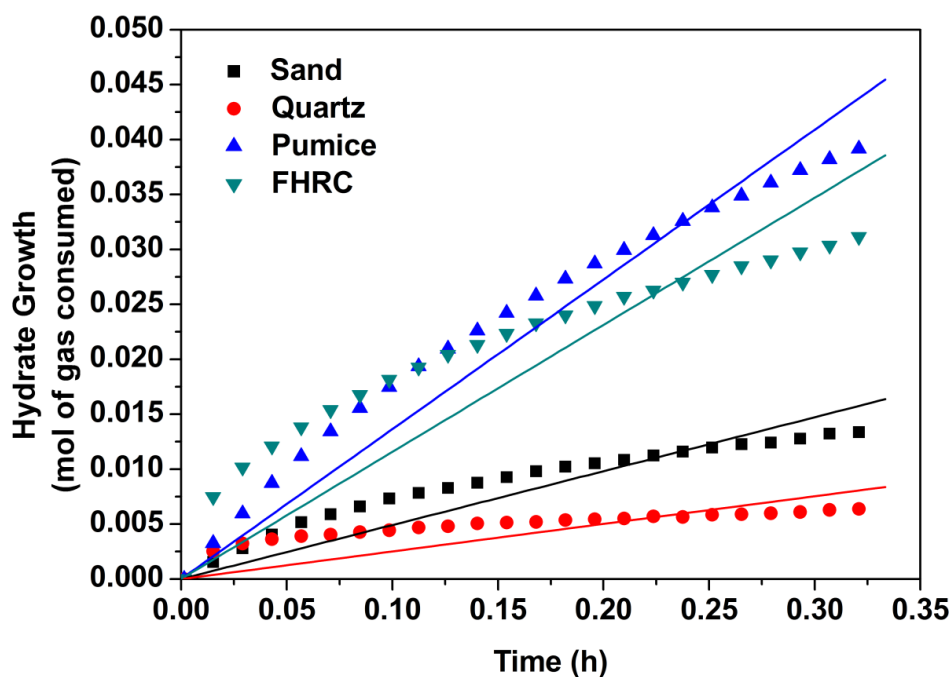


Fig. A10: Linear fit of the first 20 minutes (0.334h) of hydrate formation for pure CO₂ gas in presence of the different porous media used for the case of the constant bed height experiments.

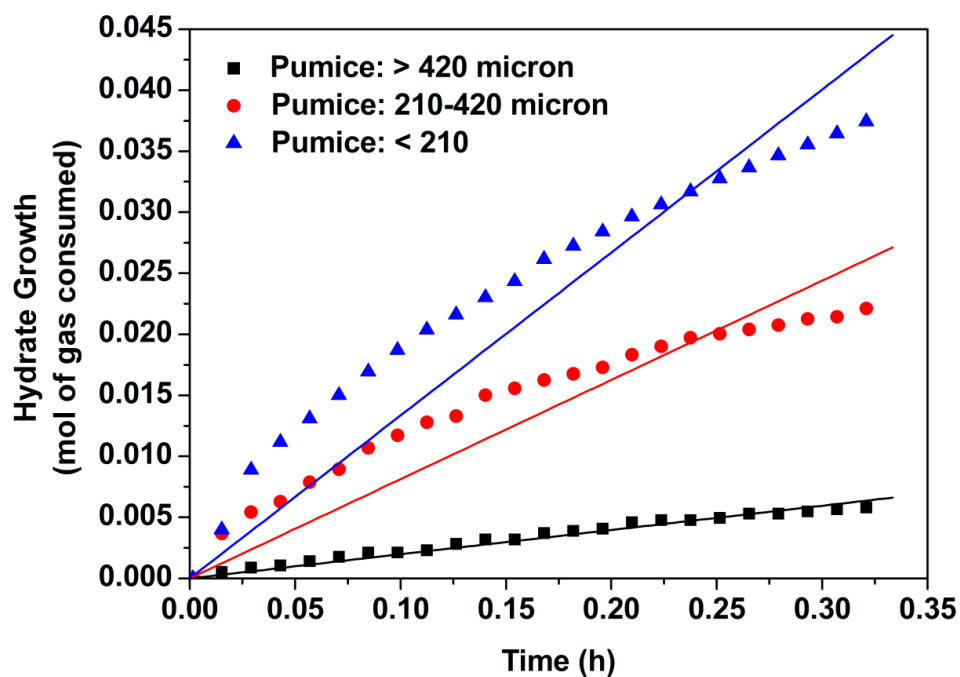


Fig. A11: Linear fit of the first 20 minutes (0.334h) of hydrate formation for pure CO₂ gas using different particle size fractions of pumice as the porous medium.

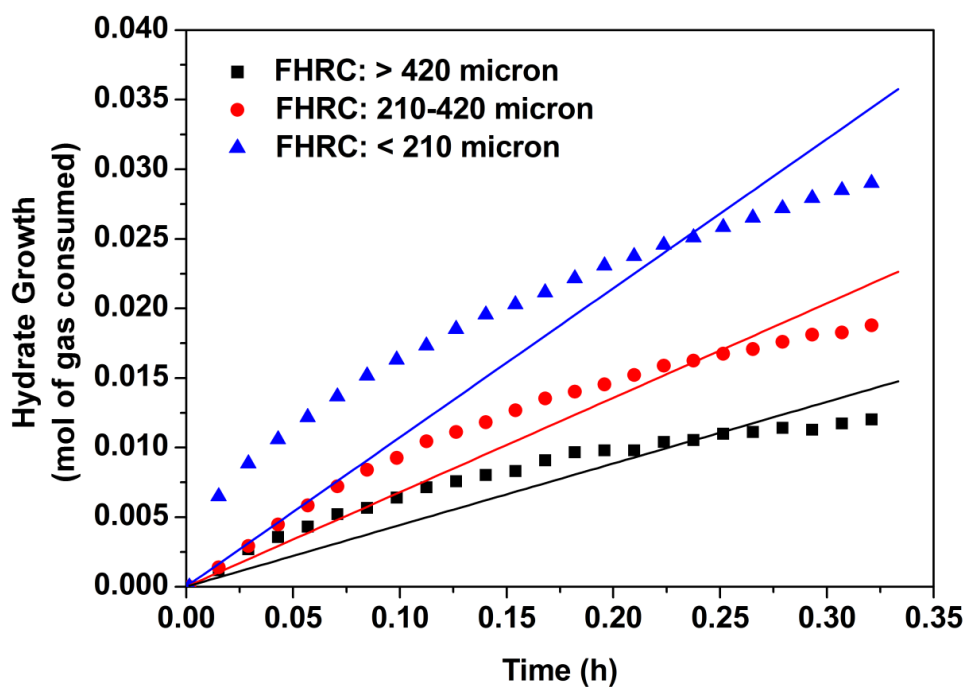


Fig. A12: Linear fit of the first 20 minutes (0.334h) of hydrate formation for pure CO₂ gas using different particle size fractions of FHRC as the porous medium.

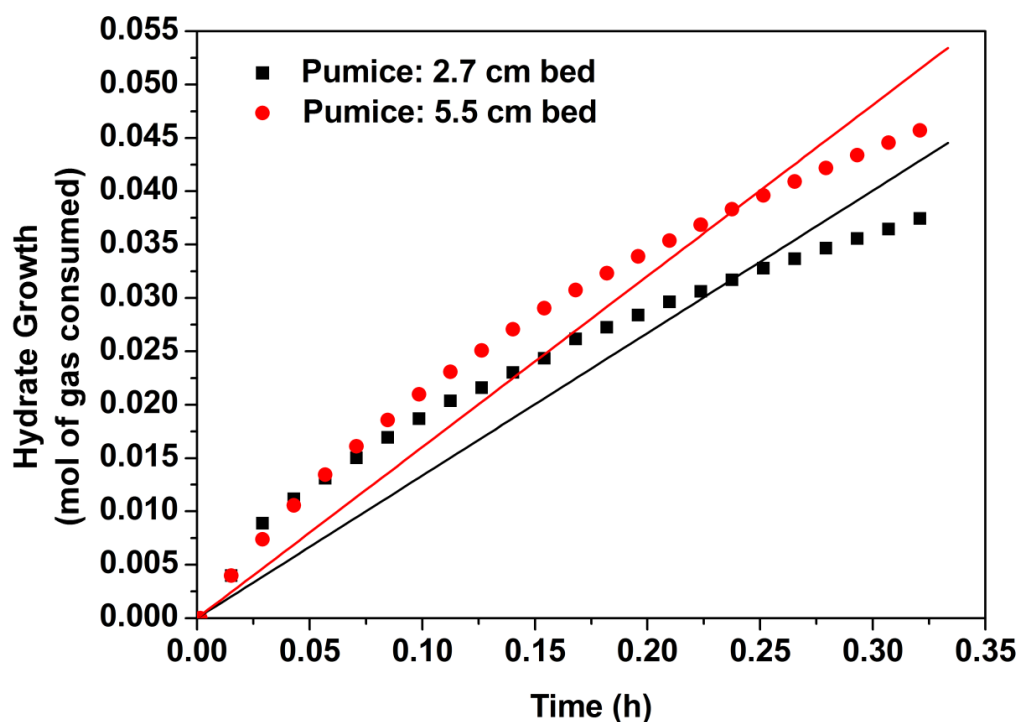


Fig. A13: Linear fit of the first 20 minutes (0.334h) of hydrate formation for pure CO₂ gas using pumice (particle size < 210 micron) as the porous medium and varying the bed height.

Table A6: Initial apparent rates of hydrate formation (mol of gas consumed/h) for the different systems considered during the course of the work reported in Chapter 6 of the thesis.

System	Average rate of hydrate formation for first 20 minutes (gas uptake) (mol of gas / h) \pm SD
Constant Volume of Water Experiments (24 ml)	
Sand	0.049 \pm 0.0006
Quartz	0.044 \pm 0.0006
Pumice: > 420 micron	0.020 \pm 0.0001
Pumice: 210-420 micron	0.081 \pm 0.0009
Pumice: < 210 micron	0.134 \pm 0.0014
FHRC: > 420 micron	0.044 \pm 0.0005
FHRC: 210-420 micron	0.068 \pm 0.0006
FHRC: < 210 micron	0.107 \pm 0.0014
Constant Bed Height Experiments (3 cm)	
Sand	0.049 \pm 0.0006
Quartz	0.025 \pm 0.0005
Pumice: < 210 micron	0.136 \pm 0.0010
FHRC: < 210 micron	0.116 \pm 0.0017
Pumice: <210 micron (5.5 cm bed height)	0.160\pm0.0013

APPENDIX B

The current appendix deals with comparing the efficiency of the hydrate based gas separation (HBGS) process for the separation of a CO₂-CH₄ gas mixture with those for other conventional (adsorbent based, membrane based) gas separation processes for the same gas mixture.

The parameter that has been used to compare the separation efficiencies of these gas separation processes can be termed either as the CO₂/CH₄ selectivity for a particular process or the CO₂ partition coefficient for that process. The parameter to be calculated is given by the following formula:

$$\text{CO}_2 / \text{CH}_4 \text{ Selectivity or CO}_2 \text{ Partition Coefficient} = \frac{(x_{\text{CO}_2} / x_{\text{CH}_4})}{(y_{\text{CO}_2} / y_{\text{CH}_4})} \quad (\text{B1})$$

, where, x_{CO_2} and x_{CH_4} are the mole fractions of CO₂ and CH₄ respectively in the adsorbed or hydrate gas phase and y_{CO_2} and y_{CH_4} are the mole fractions of CO₂ and CH₄ in the feed gas.

A general representation of this formula assuming there are two individual gas species in a gas mixture, say i and j , would be:

$$\text{Specie } i / \text{Specie } j \text{ Selectivity or Specie } i \text{ Partition Coefficient} = \frac{(x_i / x_j)}{(y_i / y_j)} \quad (\text{B2})$$

, where x_i and x_j are the mole fractions of species i and j respectively in the adsorbed or hydrate phase and y_i and y_j are the mole fractions of species i and j respectively in the gas phase.

Table B1 reports the best CO₂/CH₄ selectivity or CO₂ partition coefficient obtained out of the various hydrate based gas separation experiments carried out in the presence of different selective hydrate promoters in the course of the present study and compares it with the best reported values of the same parameter for the representative studies of other conventional and hydrate based gas separation processes dealing with the same gas mixture. The representative studies were chosen such that similar to the current study, the individual feed gases used in them were either also equimolar (50%-50%) mixtures of CO₂ and CH₄ or at least one very close to being an equimolar mixture of the two components. In addition to the CO₂/CH₄ selectivity or CO₂ partition coefficient, for each representative study, other relevant details such as the material used as an adsorbent or a membrane or a promoter; the latter only in the

case of HBGS, the process used to achieve the gas separation and the operating temperature and pressure conditions have also been included in Table B1. For the sake of comparison, the table also contains all these details for representative studies of the HBGS process for various other gas mixtures.

Table B1: Comparison of the separation efficiencies of the HBGS process and other conventional gas separation processes for the separation of a CO₂-CH₄ gas mixture. The determining factor here is the CO₂/CH₄ selectivity or CO₂ partition coefficient as given by equation C1. Additionally, for the sake of comparison, the separation efficiency of the HBGS process for other gas mixtures has also been given using some representative studies.

	Gas separation method								
	Solvent/Adsorbent based		Membrane based		Hydrate based		Hydrate based process for separating other gas mixtures		
	Belmabkhout et.al, 2009	Alvarez-Gutierrez et.al, 2016	Sandstrom et.al, 2011	Venna and Carreon, 2010	Di Profio et.al, 2017	Chapter 5- This Thesis	(Chapter 2- This Thesis) 30% CH₄-70% N₂ mixture	(Kumar et.al, 2014) 16% CO₂-84% N₂ mixture	(Linga et.al, 2007) 40% CO₂-60% H₂ mixture
Material/Process used	Ordered MCM-41 silica/PSA	CS-H ₂ O/PSA	High flux MFI membrane	8 layered ZIF membrane	No additive/HBGS	PC/HBGS	CAPB/HBGS	THF/Fly Ash/HBGS	HBGS
CO ₂ mole fraction in feed gas	0.5	0.5	0.5	0.5	0.4	0.5	-	0.16	0.4
Operating Temp (K)	298	303	277	295	274	274	275	274.5	273.6
Operating Pressure (MPa)	0.200	1.000	1.000	1.395	4.000	5.000	3.500	3.750	7.500
CO ₂ /CH ₄ selectivity or CO ₂ Partition Coefficient	5.000	4.390	4.500	7.000	7.100	1.900	CH₄/N₂ Selectivity or CH₄ Partition Coefficient- 3.034	CO₂/N₂ selectivity or CO₂ Partition Coefficient- 16.06	CO₂/N₂ selectivity or CO₂ Partition Coefficient- 98.7

Full forms of abbreviations mentioned in Table B1:

Ordered MCM-41 Silica: Ordered Mobil Composition of Matter No. 41 Silica

CS-H₂O: Cherry Stones-H₂O; Cherry Stones-based activated carbon

High flux MFI membrane: High flux Modernite Framework Inverted membrane

8 layered ZIF membrane: 8 layered Zeolite Imidazolate Framework membrane

PC: Propylene Carbonate

PSA: Pressure Swing adsorption

CAPB: Cocoamidopropyl Betaine

HBGS: Hydrate Based Gas Separation

THF: Tetrahydrofuran

The CO₂/CH₄ selectivity or CO₂ partition coefficient as seen in Table B1 is higher for the conventional gas separation processes than the hydrate based gas separation process. However, this does not necessarily mean that such processes are very feasible for the separation of a CO₂-CH₄ gas mixture as these processes are all carried out at very low gas pressures. This coupled with the low selectivity (although more than HBGS) observed for the conventional gas separation techniques directly translate to low scalability potential. Additionally, regeneration of the membrane or adsorbent required for the conventional gas separation techniques poses an additional challenge to researchers with regards to commercialization.

References:

1. Belmabkhout, Y.; Sayari, A. Adsorption of CO₂ from dry gases on MCM-41 silica at ambient temperature and high pressure. 2: Adsorption of CO₂/N₂, CO₂/CH₄ and CO₂/H₂ binary mixtures. *Chem. Eng. Sci.* **2009**, 64, 3729-3735.
2. Álvarez-Gutiérrez, N.; Gil, M. V.; Rubiera, F.; Pevida, C. Adsorption performance indicators for the CO₂/CH₄ separation: Application to biomass-based activated carbons. *Fuel Process. Technol.* **2016**, 142, 361-369.
3. Sandström, L.; Sjöberg, E.; Hedlund, J. Very high flux MFI membrane for CO₂ separation. *J. Membr. Sci.* **2011**, 380, 232-240.
4. Venna, S. R.; Carreon, M. A. Highly permeable zeolite imidazolate framework-8 membranes for CO₂/CH₄ separation. *J. Am. Chem. Soc.* **2009**, 132, 76-78.
5. Di Profio, P.; Canale, V.; D'Alessandro, N.; Germani, R.; Di Crescenzo, A.; Fontana, A. Separation of CO₂ and CH₄ from biogas by formation of clathrate hydrates: importance of the driving force and kinetic promoters. *ACS Sustain. Chem. Eng.* **2017**, 5, 1990-1997.
6. Kumar, A.; Sakpal, T.; Linga, P.; Kumar, R. Impact of fly ash impurity on the hydrate-based gas separation process for carbon dioxide capture from a flue gas mixture. *Ind. Eng. Chem. Res.* **2015**, 53, 9849-9859.
7. Linga, P.; Kumar, R.; Englezos, P. Gas hydrate formation from hydrogen/carbon dioxide and nitrogen/carbon dioxide gas mixtures. *Chem. Eng. Sci.* **2007**, 62, 4268-4276.

APPENDIX C

This appendix contains valuable additional data related to the study reported in Chapter 6 on CO₂ sequestration in porous media using gas hydrate formation. The information provided here includes figures plotting the average induction times in presence of the different porous media studied and the averages of the gas uptake and water to hydrate conversion for the repeat hydrate formation runs conducted.

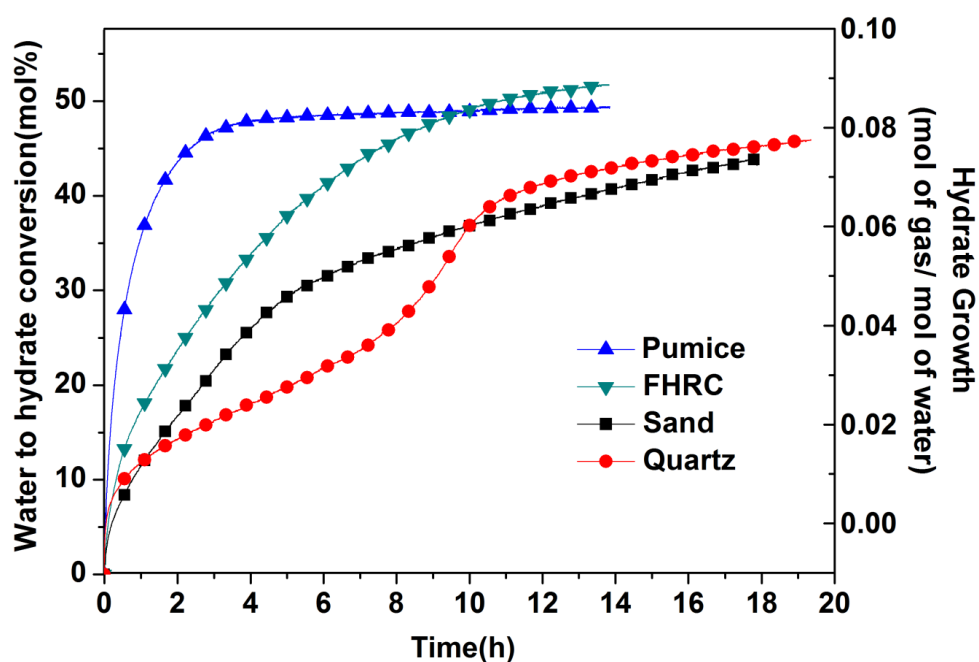


Fig. C1: Comparison of the gas uptake and water to hydrate conversion in presence of the different porous media used for the case of the constant volume of water experiments. Sand: Experiment number 3, Quartz: Experiment number 9, Pumice: Experiment number 23 and FHRC: Experiment number 37. Gas uptake has been shown for the entire duration of the experiments.

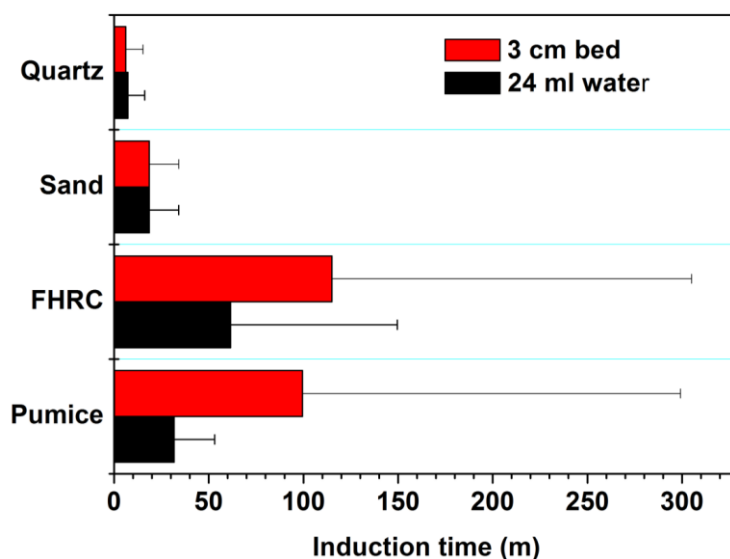


Fig. C2: Comparison of the average induction times along with standard deviation for the different porous media used.

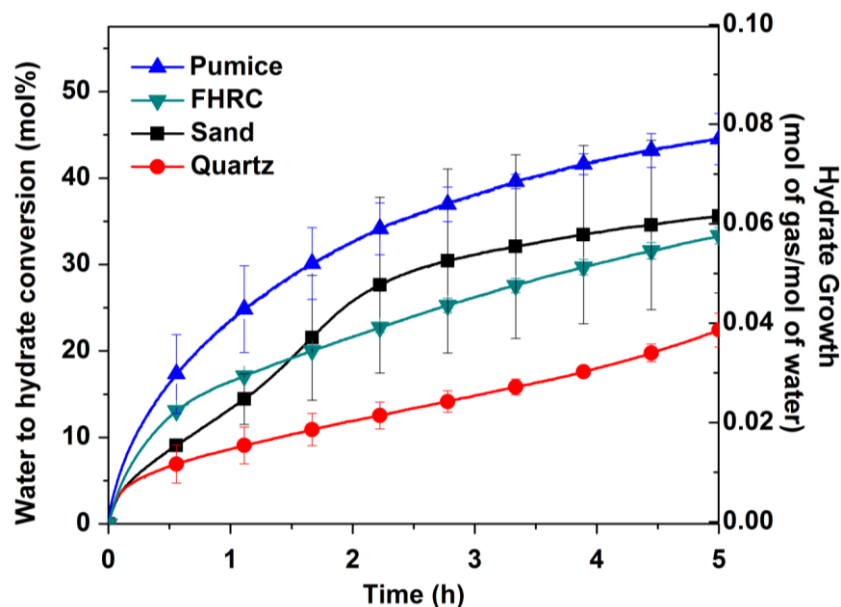


Fig. C3: Comparison of the gas uptake and water to hydrate conversion in presence of the different porous media used for the case of the constant volume of water experiments: Sand: Average and standard deviation of experiment numbers 2, 4, 6 and 7, Quartz: Average and standard deviation of experiment numbers 9, 10, 12 and 13, Pumice: Average and standard deviation of experiment numbers 21, 22 and 24 and FHRC: Average and standard deviation of experiment numbers 33, 34 and 36.

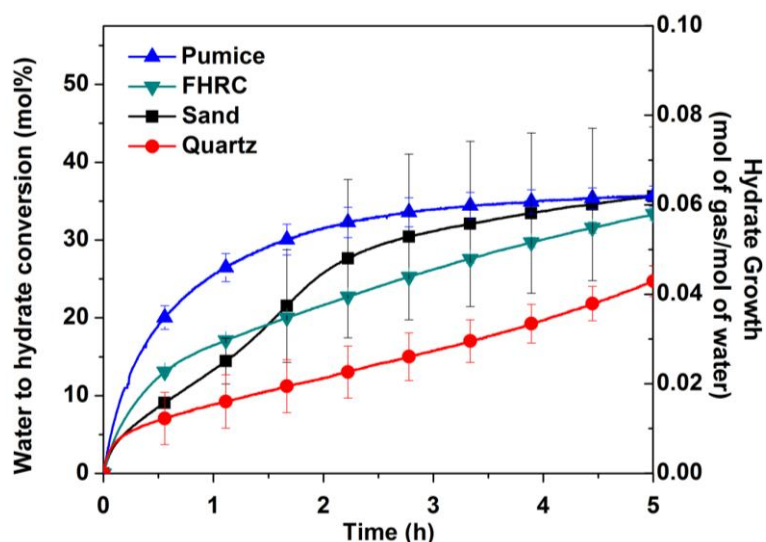


Fig. C4: Comparison of the gas uptake and water to hydrate conversion in presence of the different porous media used for the case of the constant bed height experiments: Sand: Average and standard deviation of experiment numbers 2, 4, 6 and 7, Quartz: Average and standard deviation of experiment numbers 39, 40, 42 and 43, Pumice: Average and standard deviation of experiment numbers 45, 46, 48 and 49 and FHRC: Average and standard deviation of experiment numbers 52, 54 and 56.

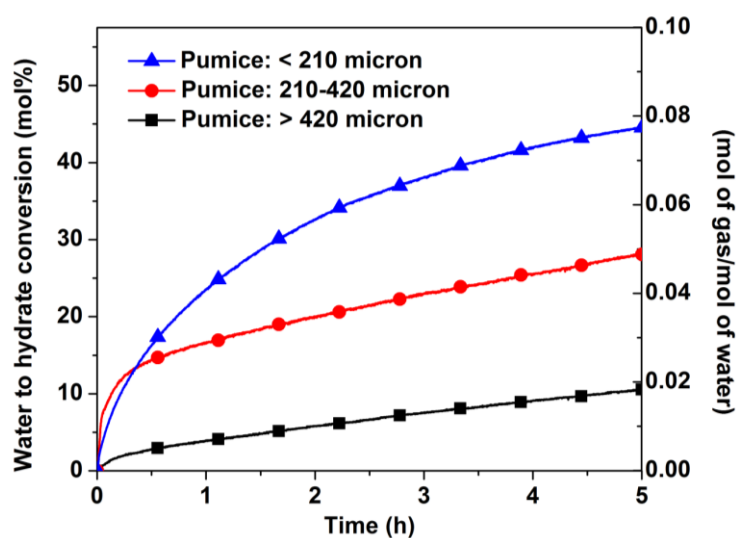


Fig. C5: Effect of particle size of pumice on hydrate formation kinetics: Pumice: > 420 micron: Average of experiment numbers 15 and 16, Pumice: 210-420 micron: Average of experiment numbers 18 and 19, Pumice: < 210 micron: Average of experiment numbers 21, 22 and 24.

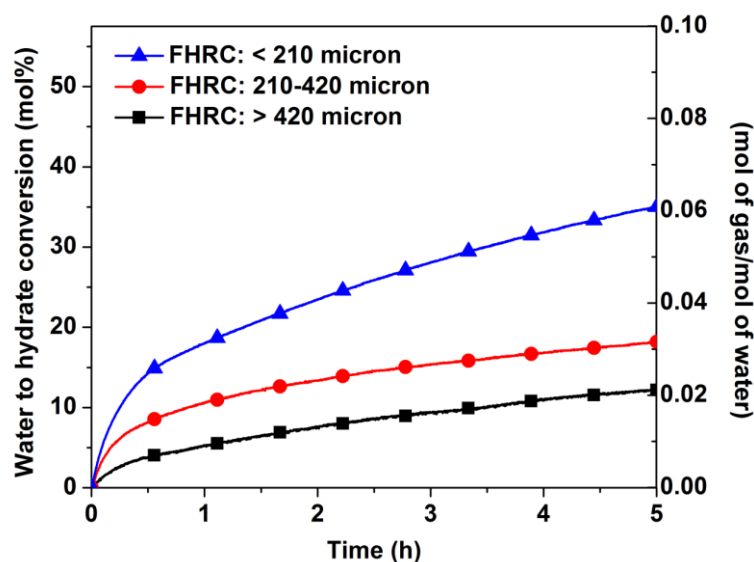


Fig. C6: Effect of particle size of FHRC on hydrate formation kinetics: FHRC: > 420 micron: Average of experiment numbers 27 and 28, FHRC: 210-420 micron: Average of experiment numbers 30 and 31, FHRC: < 210 micron: Average of experiment numbers 33, 34 and 36.

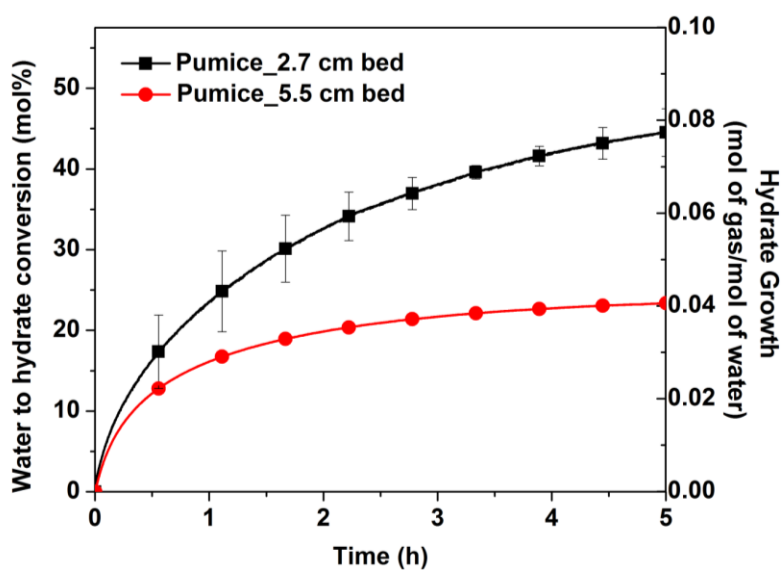


Fig. C7: Effect of bed height on gas hydrate formation kinetics using pumice as the fixed bed medium: Pumice: 2.7 cm bed: Average and standard deviation of experiment numbers 21, 22 and 24 and Pumice: 5.5 cm bed: Average and standard deviation of experiment numbers 58, 59 and 61.